

The impact of interferometric noise on the performance of optical communication networks

Thesis presented for the degree of PhD

by

Peter Jonathon Legg MA

Optoelectronics Division

Department of Electronic and Electrical Engineering

University of Strathclyde

204 George Street

Glasgow G1 1XW

Scotland

September 1995

Declaration

The copyright of this thesis belongs to the author under the terms of the United Kingdom Copyright Acts as qualified by University of Strathclyde Regulation 4.49. Due acknowledgement must always be made of the use of any material contained in, or derived from, this thesis.

Acknowledgements

Two individuals have been outstanding in their encouragement, guidance and overall contribution towards the success of this work - Ivan Andonovic (University of Strathclyde) and Moshe Tur (Tel Aviv University). Ivan has given support of all kinds, with good humour, encouraging and financing my collaborative work and conferences. Moshe has been an inspiration; never before have I witnessed work more brilliant than that undertaken in those two weeks together at BT Labs. I thank you both.

This work has been undertaken under contract with BT Laboratories, comprising financial support and use of their facilities for all the experimental work reported herein. Special thanks go to Pete Barnsley, Mohammed Shabeer, Dave Spirit and Steve Pycock.

Last, but not least, the Opto Group deserve credit for distracting me from my work to play football and drink ale. Gareth will be remembered for his lasagne and pizza, Tim for his white water aerobatics, Grumpy and Iain for their arm wrestling, Gordon for being himself, Kevin for his left foot, and DKH for his collapsing chair. Thanks also to Ail, Carol and to Brian whose willing and flexible response brought me to Strathclyde in the first place.

Abstract

Interferometric noise, arising on the interference of data and parasitic crosstalk and common to many current and proposed fibre optic communication networks, may induce unacceptable power penalties and bit-error-rate floors. This work addresses key aspects of this problem via experiment and theoretical analysis: the origin and characteristics of the noise, the resultant performance degradation of optical networks, and solution paths.

The study of a single crosstalk interferer generates a classification of all interferometric noise forms and reveals the key properties of probability density function and power spectrum. Performance degradation from theory and experiment agree closely.

The aggregation of multiple crosstalk terms is analysed and the validity of Gaussian statistics, predicted by the Central Limit Theorem, is demonstrated. It is predicted that the total crosstalk level of noise generating terms should be held below -25 dB for a penalty of less than 1 dB - a further 2 to 4 dB may lead to network failure. Optical TDM switching networks, constructed from discrete lithium niobate directional couplers of -15 dB isolation, and delay lines, illustrate the importance of interferometric noise. Larger networks are modelled on a computer simulator (XHatch) that tracks all crosstalk waveforms, calculates both interferometric and amplifier noise, and thus the bit-error-rate.

A bilateral approach is proposed to manage interferometric noise; crosstalk power is minimised and noise owing to the residual crosstalk is RF rejected. Several methods are critically discussed. A novel technique, exploiting intra-bit frequency evolution of directly modulated DFB lasers in response to injection heating, is introduced and critically assessed.

Table of contents

Chapter 1: Introduction

1.1 The role of fibre optics in the information age	1
1.2 Performance limitations of fibre optic networks due to interferometric noise	2
1.3 Objectives of the thesis	3
1.4 Outline of the thesis	4
1.5 References	4

Chapter 2: Interferometric noise

2.1 Introduction	6
2.2 The origin of interferometric noise	
2.2.1 Phase noise in single frequency semiconductor lasers	6
2.2.2 A classification of interferometric noise	7
2.3 Systems limited by interferometric noise	11
2.3.1 Generalised networks	11
2.3.2 Multiple reflections	15
2.3.3 Rayleigh backscatter	18
2.3.4 Subcarrier-multiplexed networks	22
2.3.5 Recirculating fibre loops	24
2.3.6 Space switches	27
2.3.7 WDM transport networks	27
2.3.8 Optical TDM switching nodes	30
2.4 Proposed methods for achieving suppression of interferometric noise	31
2.5 Conclusions	34
2.6 References	37

Chapter 3: Theoretical modelling: single interferer

3.1 Introduction	42
3.2 Properties of interferometric noise from CW waveforms	43
3.2.1 Probability density function (pdf)	44
3.2.2 Autocorrelation of the interferometric noise	45

3.2.3 Interferometric noise power spectrum	45
3.2.4 Signal-to-interferometric-noise-ratio (SINR)	47
3.3 Properties of interferometric noise from ASK externally modulated waveforms	50
3.3.1 Probability density function (pdf)	51
3.3.2 Autocorrelation of the interferometric noise	51
3.3.3 Interferometric noise power spectrum	51
3.3.4 Signal-to-interferometric-noise-ratio (SINR)	53
3.4 Properties of interferometric noise from ASK directly modulated waveforms	54
3.5 Estimation of BER, power penalty and error floor	56
3.5.1 Preliminaries	56
3.5.2 BER calculation employing bounded pdf	60
3.5.3 BER calculation employing a Gaussian interferometric noise pdf	64
3.5.4 BER for incoherent noise-free crosstalk	67
3.5.5 Optical power penalties	70
3.5.6 Error floors	70
3.5.7 Performance with finite modulation depth	76
3.6 Partial coherence	77
3.7 Conclusions	78
3.8 References	79

Chapter 4: Theoretical modelling: multiple interferers

4.1 Introduction	83
4.2 General formulation of optical mixing at the photodetector	84
4.3 Conditions for statistical independence of beating terms	85
4.3.1 Identification of beating terms according to the crosstalk classification	85
4.3.2 Statistical independence	86
4.3.3 Interferometric noise variance for independent beating terms	88
4.4 BER calculation for independent terms by the convolution method	89
4.5 BER calculation for independent terms by the Central Limit Theorem	94
4.5.1 Conditions for the application of the Central Limit Theorem	94
4.5.2 Application of the Central Limit Theorem	94

4.5.3 BER calculation	95
4.6 Application of the Central Limit Theorem: statistical model	97
4.7 Conclusions	98
4.8 References	99
 Chapter 5 Experimental investigation	
5.1 Introduction	100
5.2 Single interferer	101
5.2.1 Incoherent noise-free crosstalk	101
5.2.2 Coherent crosstalk	104
5.2.3 Incoherent beat noise crosstalk - direct modulation	107
5.2.4 Incoherent beat noise crosstalk - external modulation	110
5.3 Multiple interferers	112
5.3.1 Case-study optical TDM switching networks	112
5.3.2 Recirculating delay line	117
5.4 Conclusions	122
5.5 References	124
 Chapter 6: Network modelling by the XHatch computer simulator	
6.1 Introduction	125
6.2 Comparative magnitude of different beating terms in optical TDM switching networks	126
6.3 Simulation of optical TDM switching networks	132
6.4 Conclusions	135
6.5 References	136
 Chapter 7: Interferometric noise suppression through intra-bit frequency evolution of directly modulated lasers	
7.1 Introduction	137
7.2 Experimental characterisation	138
7.2.1 Initial investigation	138
7.2.2 Further investigation	143
7.3 Theoretical model for a single interferer	146
7.4 Theoretical model for multiple interferers	152

7.5 Discussion	153
7.6 Conclusions	154
7.7 References	155

Chapter 8: Solution paths to combat crosstalk and interferometric noise

8.1 Introduction	157
8.2 Minimisation of crosstalk power	157
8.3 Suppression of interferometric noise	163
8.4 Conclusions	168
8.5 References	169

Chapter 9: Conclusions and further work

9.1 Conclusions	171
9.2 Further work	174
9.2.1 Experimental	174
9.2.2 Theoretical	176
9.3 References	176

Publications resulting from this work	178
---------------------------------------	-----

Chapter 1

Introduction

1.1 The role of fibre optics in the Information Age

As the twenty-first century approaches, dramatic changes are occurring in the telecommunications industry. The forthcoming 'Information Age' [1] will see new high bandwidth services on offer to business and domestic customers alike. This presents a considerable challenge to the industry; the existing networks, only recently upgraded to 'digital' status, must grow in capacity and operate in an increasingly competitive and diverse market. Naturally, there is considerable debate on how this may be achieved, but it is generally assumed that fibre optic technology will play a key role in network evolution [2].

In the telecommunications network of today, optical fibre is principally employed as a low cost high bandwidth pipe, interlinking the switching centres of the trunk network. In other potential applications, for example, in the switching nodes, or in the local loop, the penetration of optical technology is modest, and electronics predominates. This will change in the future - the unique advantages of optics, particularly the high bandwidth, immunity to EMI, transparency to data format and bit rate, and the possibility of multiplexing in the wavelength, as well as the time domain, will ultimately result in a performance/unit cost advantage [3].

Research activity into optically multiplexed networks, including the construction of demonstrators, is growing rapidly around the globe. Networks employing wavelength division multiplexing, as typified by the RACE MWTN and MUNDI projects [4], are likely to see the first deployment in the field. Before this occurs many difficulties remain to be resolved- much new effort is currently directed towards topics such as power level equalisation in amplifier cascades [5], non-linear interactions and dispersion in long fibre links [6], and to the impact of crosstalk, and its associated interferometric noise; the latter shall be addressed in this work.

1.2 Performance limitations of fibre optic networks due to interferometric noise

In a typical optical network data is digitally encoded onto the optical medium by switching a laser on and off, and is then routed to the destination where (direct) photodetection takes place. The recovered information may be corrupted by:

- crosstalk and inter-symbol interference (ISI)
- electronic noise¹ generated at the receiver - shot noise and thermal noise
- noise of optical origin - source intensity noise, spontaneous emission, and interferometric noise

Interferometric noise arises from the optical interference, or beating, of the desired data waveform with unwanted crosstalk waveforms derived from other data channels, or indeed from the very same data channel, and square-law envelope detection at the receiver. This is illustrated in Fig. 1.1 below for the latter scenario.

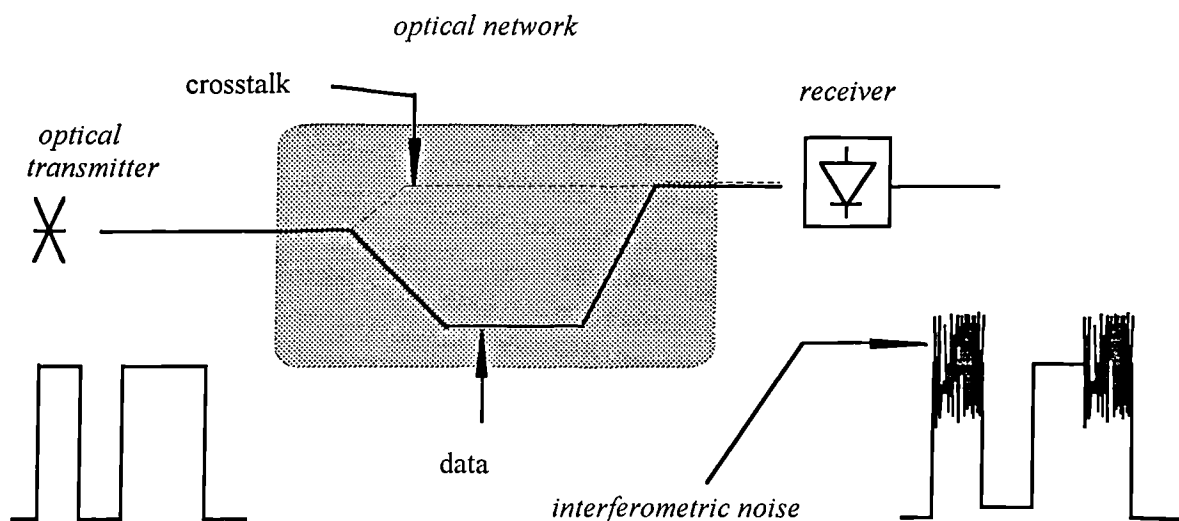


Figure 1.1. Generation of interferometric noise on the interference of data and crosstalk from the same optical source.

Square-law detection implies that the photocurrent attributed to the interferometric noise is much greater than that attributed to the incident optical power of the crosstalk signal, giving more severe performance degradation than would be expected. Indeed, interferometric noise has been reported to cause significant degradation,

¹noise is taken to be random in nature, unlike crosstalk which may, in principle, be predicted.

characterised by large power penalties or unrecoverable error floors, in many optical network configurations, both in transmission and in switching [7,8,9]. The move towards greater 'transparency' in optical networks, whereby signals are routed via intermediate nodes without regeneration, through optical amplification, further exacerbates these effects.

This work advances the understanding of interferometric noise in a number of ways - the identification of the problem in crosstalk corrupted TDM switching networks has been established, and a crosstalk classification has been proposed; a new theoretical analysis of multiple interferers has been devised and applied to generate guidelines for the construction of future optical networks; new strategies for management of crosstalk and noise have been developed, including a novel (patented) invention that employs commercially available laser sources.

1.3 Objectives of the thesis

The objective of this work was to address the importance of interferometric noise in optical networks. The following aspects of this task have been met-

- explanation of the nature and origin of interferometric noise.
- theoretical calculation of the performance degradation due to a single noise generating interferer.
- development of a theoretical description of interferometric noise due to multiple interferers, thereby generating a guideline for maximum permissible crosstalk level.
- experimental characterisation of the impact of interferometric noise from a single interferer.
- experimental characterisation of the impact of crosstalk-derived interferometric noise on small TDM switching networks, comprising up to four 2x2 crosspoints.
- prediction of the performance of TDM switching networks in the presence of crosstalk-derived interferometric noise using a network simulator (XHatch [10]) programmed with the aforementioned theoretical analysis.
- development of strategies for combating interferometric noise.
- experimental investigation of a novel interferometric noise suppression technique exploiting injection heating in directly modulated laser sources.

1.4 Outline of the thesis

Within Chapter 2 the nature and origin of interferometric noise is carefully explained, and examples of interferometric noise in a number of different network scenarios are discussed. Additionally, proposed techniques for noise suppression are scrutinised.

In Chapter 3, a theoretical analysis of the performance degradation due to interferometric noise from a single interferer is described, followed by a Central Limit Theorem approach to multiple interferers (Chapter 4).

An experimental study of interferometric noise, addressing both single interferers and small case-study TDM switching fabrics, is summarised in Chapter 5. A recirculating delay line configuration that generates multiple interferers from a single 2x2 crosspoint is also included. Comparison with the theory of the previous chapter is made where appropriate.

Results from the XHatch computer simulator, when configured to model a number of optical TDM crossconnects, are shown in Chapter 6.

The following two chapters consider methods for managing crosstalk and interferometric noise. In Chapter 7, an experimental demonstration of interferometric noise suppression that exploits, in a novel way, the injection heating within directly modulated laser sources, is described. Chapter 8 presents a critical appraisal of crosstalk reduction and interferometric noise suppression techniques.

Conclusions and proposals for future work are presented in the final chapter.

1.5 References

1. Proceedings of Mediacomm '95, 'The information Age', Southampton, UK, 11-12 April 1995.
2. P. Cochrane, R. Heckingbottom and D.J.T. Heatley, "Optical transparency a new paradigm for telecommunications", *OSA Optics and Photonics News*, 5(8), pp. 15-19, 1994.
3. J.E. Midwinter, "The threat of optical communications", *IEE Electronics and Communication Eng. J.*, 6(1), pp. 33-38, 1994.

4. P.J. Chidgey, "Multi-wavelength transport networks", *IEEE Comms. Mag.*, 32(12), pp. 28-35, 1994.
5. L. Eskildsen, E.L. Goldstein, V. Dasilva, M. Andrejco and Y. Silberberg, "Optical power equalisation for multi-wavelength fiber-amplifier cascades using periodic inhomogeneous broadening", *IEEE Photon. Tech. Lett.*, 5(10), pp. 1188-1190, 1993.
6. R. Chraplyvy, "Limitations on lightwave communications imposed by fiber non-linearities", *J. Lightwave Technol.*, 8(10), pp. 1548-1557, 1990.
7. J.L. Gimlett and N.K. Cheung, "Effects of phase-to-intensity noise conversion by multiple reflections on gigabit-per-second DFB laser transmission systems", *J. Lightwave Technol.*, 7(6), pp. 888-895, 1989.
8. R.K. Staubli, P. Gysel and R.U. Hofstetter, "Power penalties due to multiple Rayleigh backscattering in coherent transmission systems using in-line optical amplifiers", *IEEE Photon. Tech. Lett.*, 2(12), pp. 872-874, 1990.
9. N.K. Shankaranarayanan, S.D. Elby and K.Y. Lau, "WDMA/subcarrier FDMA lightwave networks: limitations due to beat interference", *J. Lightwave Technol.*, 9(7), pp. 931-943, 1991.
10. T.H. Gilfedder, P.J. Legg, D.K. Hunter, I. Andonovic and M. Shabeer, "Modelling of the performance of optical TDM switching networks in the presence of interferometric noise due to inter-channel crosstalk", Proceedings of *Advanced Networks and Services*, vol. 2450, European Optical Society, Amsterdam, March 1995.

Chapter 2

Interferometric noise

2.1 Introduction

This review begins with a detailed description of the origin of interferometric noise. It is assumed that the optical source comprises a single frequency laser, for example, a distributed-feedback (DFB) laser, sources which will find common application in future networks. Other optical sources, the LED and the multi-longitudinal mode Fabry-Perot laser, suffer less from interferometric noise and are considered briefly in Section 2.4. A four element classification is introduced to describe the possible outcomes from the interference of data and crosstalk waveforms.

The literature review highlights the importance of interferometric noise in a wide range of different networks. Emphasis is placed upon the measurement of bit-error-rate (BER) degradation. Proposed noise suppression techniques are also summarised.

2.2 The origin of interferometric noise

2.2.1 Phase noise in single frequency semiconductor lasers

The output of a single frequency semiconductor laser is affected in two ways by the presence of quantum noise. Firstly, the amplitude is found to fluctuate. However, this so called *laser intensity noise* is very small except in the region close to threshold. Secondly, the phase contains a random time component, termed *phase noise*, arising from spontaneous emission events, following a random-walk type diffusion characterised by a Gaussian probability density function (pdf) and a white frequency spectrum (Weiner -Levy random process [1,2]). The spontaneous emission also perturbs the carrier density away from the steady state value but the system recovers in a short series of *relaxation oscillations* [2]. However, these carrier density fluctuations induce refractive index and therefore phase fluctuations of the lasing medium at the relaxation frequency, typically 1-10 GHz, adding additional phase

noise. Relaxation oscillations have been neglected in this work although they have been found to be significant in coherent mixing [3].

The optical CW waveform of centre frequency ω_0 and phase noise $\phi(t)$ is given in the complex representation by

$$E(t) = A \exp j(\omega_0 t + \phi(t)) \quad (2.1)$$

with the (random) phase change over a time τ defined by

$$\Phi(t, \tau) = \phi(t) - \phi(t - \tau) \quad (2.2)$$

governed by a Gaussian distributed pdf of

$$P(\Phi) = \frac{\exp\left(-\Phi^2 / 2\sigma^2(\tau)\right)}{\sqrt{2\pi\sigma^2(\tau)}} \quad (2.3)$$

where $\sigma^2(\tau) = 2\pi \Delta\nu \tau$

$\Delta\nu = 3$ dB laser linewidth.

Note the greater the delay τ the broader the pdf becomes until ultimately $\sigma \gg \pi$ and $P(\Phi)$ is essentially uniformly distributed over $(-\pi, \pi)$. The linear relationship between the phase noise variance $\sigma^2(\tau)$ and the delay τ is a consequence of the assumed white frequency spectrum, and implies a Lorentzian lineshape (this may be simply demonstrated by taking a Fourier Transform of the autocorrelation of $E(t)$). If the laser spectrum is non-Lorentzian, for example, because of relaxation oscillations, the phase variance can be easily measured and provides a more accurate measure of the noise magnitude than $\Delta\nu$ [1].

2.2.2 A classification of interferometric noise

Consider the mixing of two CW optical waveforms representing the *data* and *crosstalk*, having frequency ω_d and ω_x , phase noise $\phi_d(t)$ and $\phi_x(t)$, optical power P_d and P_x , polarisation \underline{p}_d and \underline{p}_x , respectively.

$$E(t) = E_d(t) + E_x(t) \\ \propto \sqrt{P_d} \exp j(\omega_d t + \phi_d(t)) \underline{p}_d + \sqrt{P_x} \exp j(\omega_x t + \phi_x(t)) \underline{p}_x \quad (2.4)$$

Following square-law envelope detection the photocurrent i is given by:

$$i \propto E(t)E^*(t) \\ \propto P_d + P_x + 2\sqrt{P_d P_x} \cos\{\text{relative phase}\} \underline{p}_d \cdot \underline{p}_x \\ = P_d + P_x + 2\sqrt{P_d P_x} \cos\{(\omega_d - \omega_x)t + \phi_d(t) - \phi_x(t)\} \underline{p}_d \cdot \underline{p}_x \quad (2.5) \\ \text{data} \quad \text{crosstalk} \quad \text{interferometric noise}$$

The data can be seen to be corrupted not only by the additive crosstalk P_x , as would be predicted by a sum of intensities approach, but also by the mixing term that exhibits a cosinusoidal dependence on the relative phase of the data and crosstalk. When this relative phase fluctuates randomly (mechanisms for this will be discussed shortly) *interferometric noise* arises. The (dimensionless) crosstalk level, ξ , is defined as P_x/P_d . Eqn. 2.5 highlights several important properties of this interferometric noise:

- the photocurrent due to the interferometric noise is far greater than that due to the additive crosstalk. For example, if $P_d=10$ (arbitrary units) and $P_x=1$, representing a crosstalk level ξ of -10 dB, the interferometric noise spans ± 6.3 (Fig. 2.1).
- the interferometric noise magnitude is dependent upon the relative polarisations of data and crosstalk. When they are orthogonally polarised there is no interferometric noise.
- the noise magnitude relative to the signal is independent of the signal level itself. Consequently, this optical noise may dominate over the detector thermal noise and lead to error flooring.

Interferometric noise may be classified as follows (Fig. 2.2):

a) data and crosstalk arise from the same laser source, with coherence time τ_c and phase noise $\phi(t)$, and suffer a differential delay between source and detector of τ .

$$\text{relative phase} = \omega_0 \tau + \phi(t) - \phi(t - \tau) \\ = \omega_0 \tau + \Phi(t, \tau) \quad (2.6)$$

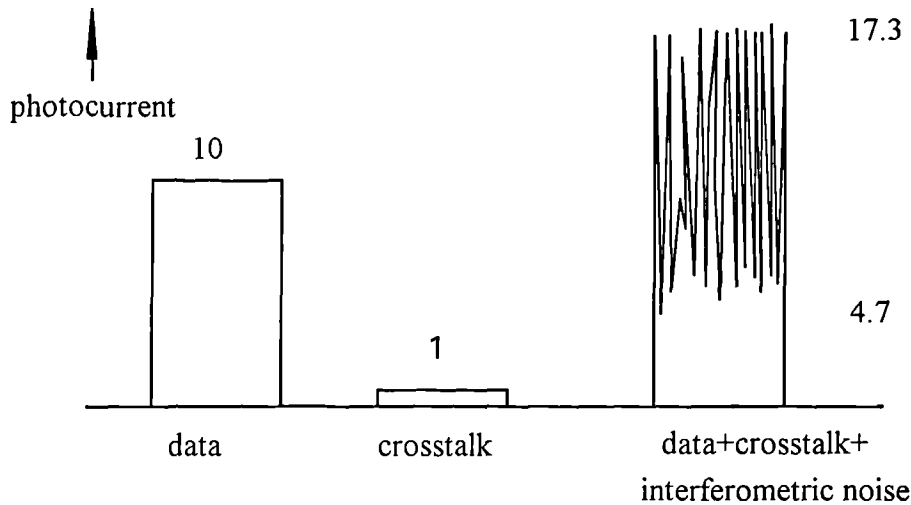


Figure 2.1. Photocurrent fluctuation due to interferometric noise.

coherent crosstalk - τ is much smaller than τ_c , resulting in an interference very close to the coherent limit ($\tau=0$), characterised by an absence of phase noise (variance of $\Phi(t,\tau) \ll 2\pi$) [2,4]. However, it has been appreciated for the first time that significant interferometric noise will arise if τ itself is not constant. Indeed τ has been found to fluctuate slowly (sub kHz frequencies, cf. Section 5.2.2), but with sufficient amplitude to induce $\omega\tau$ variations exceeding 2π , because of temperature fluctuations and phonon excitations in silica optical fibre [5]¹. If τ is constant, the interferometric term in Eqn. 2.5 is static and may be determined, its value depending on $\omega\tau$.

incoherent beat noise crosstalk (also often called phase-induced intensity noise, PIIN) - τ is much greater than τ_c , resulting in an interference at the so-called 'incoherent limit', such that the variance of $\Phi(t,\tau) \gg 2\pi$ [2,4]. Here the phase noise of the laser is converted into intensity noise by the optical mixing. In the case of a directly modulated DFB laser the incoherent limit is attained with path length differences of a few metres (τ being tens of ns). Phase fluctuations due to $\omega\tau$ do not influence the intensity noise because the phase change fluctuation Φ is much faster (\approx laser linewidth).

partially coherent crosstalk - this class falls between the two extremes of coherent and incoherent beat noise crosstalk. The resulting noise is very difficult to analyse, its properties depending on the exact value of $\omega\tau$. The

¹ This is the environmental interferometer drift that has been frequently noted in fibre sensors.

reader is referred to [2] and Section 3.6.

b) data and crosstalk arise from distinct laser sources, giving:

$$\text{relative phase} = \{(\omega_d - \omega_x)t + \phi_d(t) - \phi_x(t)\} \quad (2.7)$$

incoherent noise-free crosstalk - if the beat frequency of the two lasers, $(\omega_d - \omega_x)/2\pi$, exceeds the receiver bandwidth, B, then the intensity noise is removed by electronic filtering following detection, and only additive crosstalk components remain [6].

incoherent beat noise crosstalk - if the beat frequency of the two lasers, $(\omega_d - \omega_x)/2\pi$, is smaller than the receiver bandwidth then the cyclic variation in phase due to $(\omega_d - \omega_x)t$, and the random variation due to the phase noise elements, generate interferometric noise. This is also called *incoherent beat noise crosstalk* because the mixing is incoherent [6].

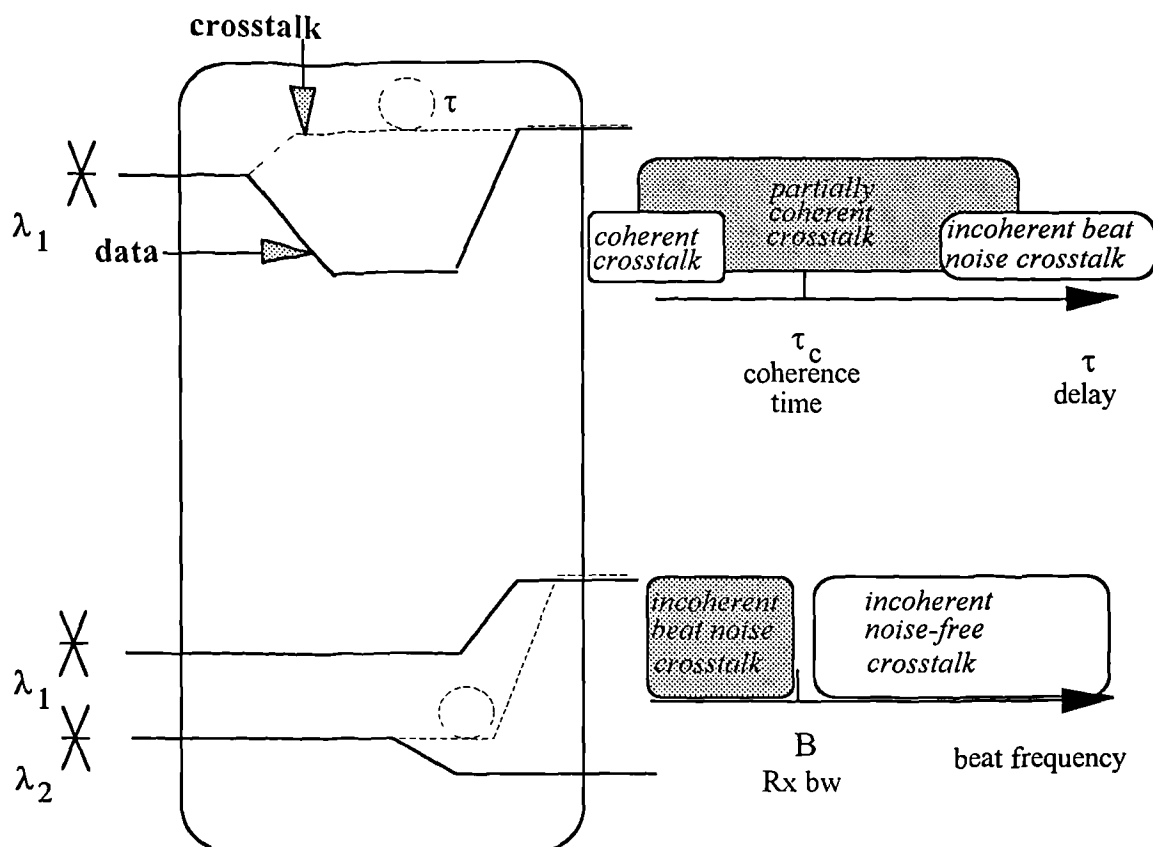


Figure 2.2. Classification of interferometric noise, from a single source (upper) and from separate sources (lower).

2.3 Systems limited by interferometric noise

Table 2.1 summarises the principal network configurations, employing ASK modulation and direct detection, where interferometric noise has been reported to degrade the BER performance.

NETWORK	CAUSE OF INTERFEROMETRIC NOISE	REFERENCE
general	non-specific	[7-11]
transport via cascaded optical components	multiple discrete reflections	[6,12-15]
transport via fibre	Rayleigh backscatter	[16-20]
WDMA/subcarrier FDMA broadcast and select	beating between subcarrier channels at the same λ	[21-24]
fibre loop buffers and signal processors	crosstalk addition at the loop coupler	[25-33]
space switches	switch crosstalk	[30]
WDM transport network	switch crosstalk filter crosstalk	[34-36]
optical TDM switching node	switch crosstalk	[37]

Table 2.1. Systems exhibiting interferometric noise.

2.3.1 Generalised networks

An excellent understanding of interferometric noise may be gained from a number of references [7-10]. The first BER characterisations of phase-to-intensity-noise conversion were reported in 1988 [7]. Two directly modulated optical sources were employed in turn to feed a recirculating delay line interferometer: a multilongitudinal-mode laser and a DFB laser (Fig. 2.3). In both cases polarisation-sensitive error floors were observed; the floor for the DFB laser being higher (Fig. 2.4). This may be understood by noting that in multi-mode lasers only beating between modes at the same centre optical frequency will generate noise within the electrical bandwidth of the receiver (cf. Section 3.6), other beating components being filtered.

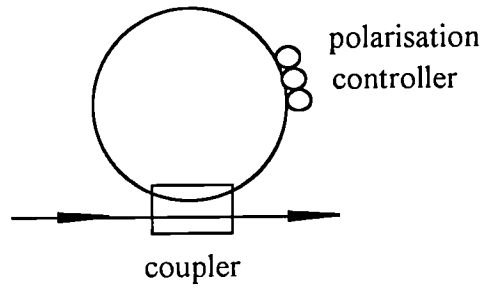


Figure 2.3. Recirculating delay line interferometer.

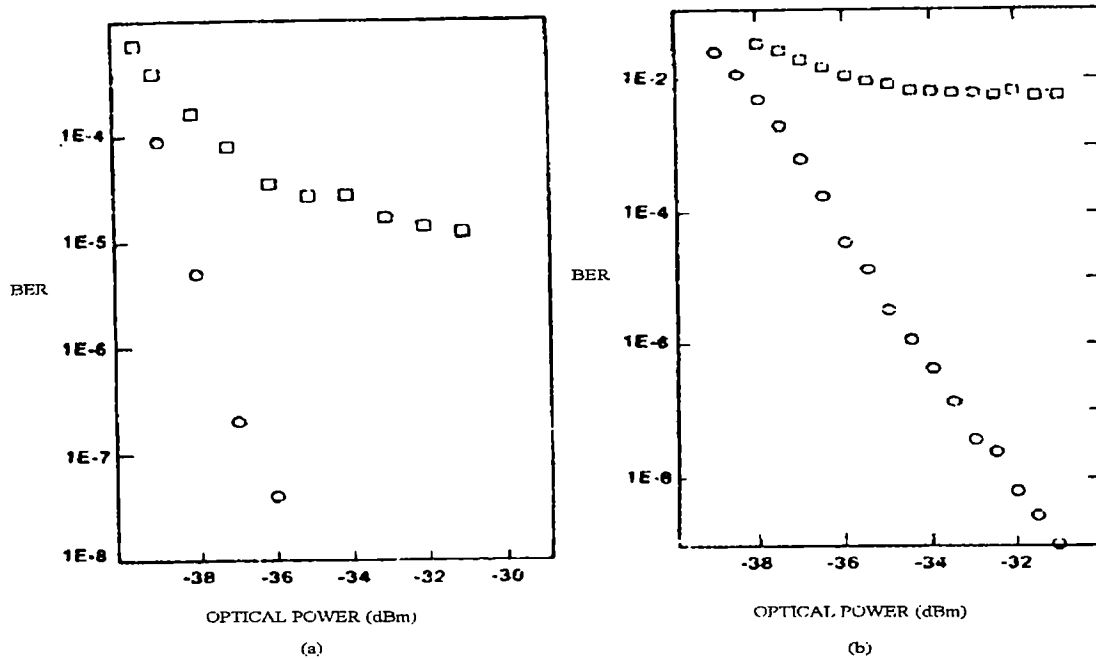


Figure 2.4. BER curves for recirculating fibre loop driven by (a) a 1.3 μm multilongitudinal-mode laser (loop delay = 13 ns) and (b) a 1.55 μm DFB laser (loop delay = 11 ns). Circles and squares represent, respectively, orthogonal and parallel polarisations. Both lasers have coherence times much smaller than the loop delay, and the bit-rate was 44.7 Mb/s (from [7]).

A theoretical and experimental analysis of noise due to a single interferer [8] highlighted the importance of noise statistics. The electrical signal-to-noise-ratio (SNR) for a BER=10⁻⁹ was found to vary from 22dB for pure Gaussian noise to only 9.1 dB for pure interferometric noise with its more tightly bound 'two-pronged' probability density function (cf. Section 3.2.1). The analysis of the intermediate states of noise forms the basis of theoretical work in Chapter 3.

A single interferer experiment was also performed with an externally modulated DFB source feeding an interferometer with a 2 km imbalance to ensure mixing at the

incoherent limit [9]. Comparison of the power penalty for $BER=10^{-9}$ (all power penalties quoted in this thesis are optical power penalties at $BER=10^{-9}$) with several theoretical models, one assuming Gaussian statistics and the others addressing closure of the received eye, was undertaken (Fig. 2.5).

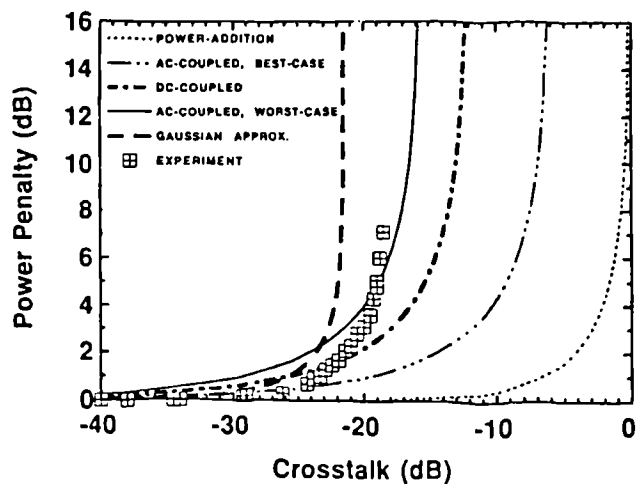


Figure 2.5. Power penalty versus component crosstalk (ξ) for systems corrupted by a single crosstalk generator (from [9])

It may be seen that none of the theoretical curves accurately predicts the experiment; nevertheless, it was concluded that crosstalk between -10 and -20 dB is required. The models were extended, with several simplifications, to address multiple (N) interferers of crosstalk ξ arising from component imperfection (Fig. 2.6): the photocurrent noise scales as $N\sqrt{\xi}$, the photocurrent variance a $N\xi$.

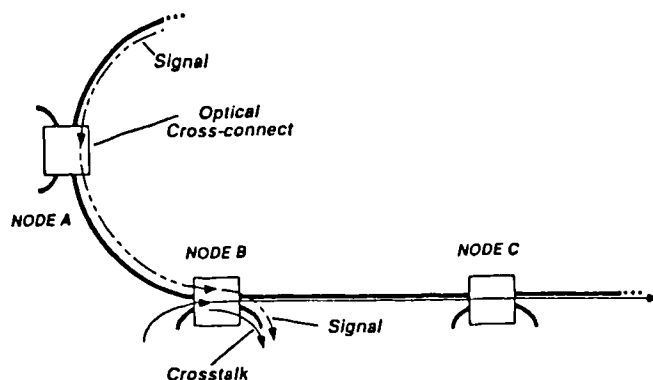


Figure 2.6. Network portion exhibiting crosstalk due to component imperfection (from [9])

The initial work was extended to an experiment with eight interferers [10], demonstrating excellent agreement with the analytic expression:

$$\text{power penalty} = -5 \log[1 - 139.2 N 10^{\xi(\text{dB})/10}] \quad (2.8)$$

derived assuming Gaussian statistics (Fig. 2.7). This Gaussian approximation is central to much of the analysis presented in this work. Increasing crosstalk may be accommodated by increasing the optical power (to offset the penalty), but dramatic communication failure will ultimately occur at the asymptote (error floor with $\text{BER} > 10^{-9}$).

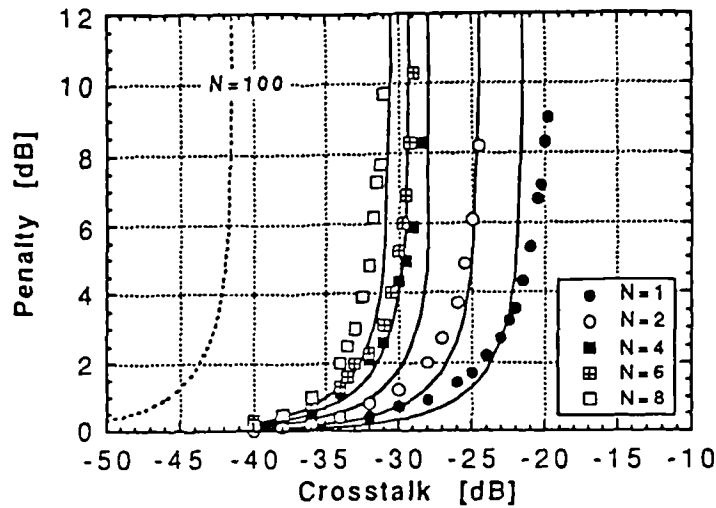


Figure 2.7. Crosstalk-induced penalty versus component crosstalk, ϵ , plotted for various number, N , of crosstalk paths. The curves are theoretical predictions of Eqn. 2.8 (from [10])

Li et al. have considered the influence of adjacent channel crosstalk in a dense single-mode waveguide array, i.e. the case of two interferers [6]. Three distinct cases were considered:

- each channel has a separate laser source of different wavelength. The penalty was found to fall with increasing wavelength separation to an asymptotic value necessitating (total) crosstalk $\xi < -12\text{dB}$ (penalty=1 dB); this limit is *incoherent noise-free crosstalk* using the classification of Section 2.2.2.
- each channel has a separate laser injection-locked to a weak reference line, or all channels are derived from a master laser but interfere incoherently - this is *incoherent beat noise crosstalk* in the classification of Section 2.2.2. The penalty in this case decreased with an increase in the laser linewidth because of greater filtering (of the noise) by the receiver. An accurate estimate of the crosstalk requirements was unrealisable because of the assumption of Gaussian statistics which is invalid for only two interferers.

- all channels derive from a master laser and have a fixed phase relationship - this is similar to *coherent crosstalk* (cf. Section 2.2.2) although no noise is present. The required crosstalk level was found to be dependent on the (fixed) relative phases, equalling -25 dB in the worst case.

The authors also investigated further deterioration in the above performance when the decision threshold was not optimised.

A novel approach to the treatment of the effects of multiple interferers has been reported by O'Reilly [11]. The range and variance of the all beating terms, not only those between the data and crosstalk but also those between crosstalk and crosstalk, are determined. Although simplifying assumptions unlikely to exist in practise are made, an upper bound to the error probability is obtained by a method attributed to Graves [39]. This technique is more accurate than taking the inner eye closure technique [40] when the range and standard deviation of the noise differ significantly, as will occur with many interferers. Error floors are also predicted. Further extension of this work should produce network design guidelines of great value.

2.3.2 Multiple reflections

In a transmission link interferometric noise results from multiple reflections at splices and connectors (Fig. 2.8).

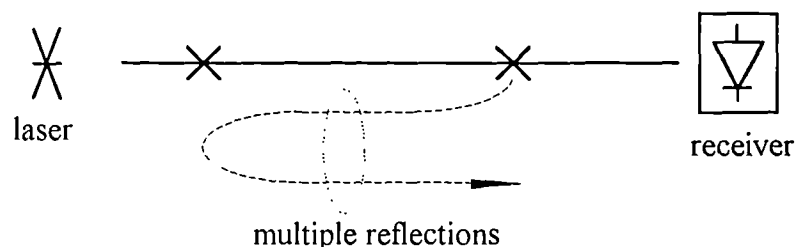


Figure 2.8. Interferometric noise due to multiple reflections.

This problem has been studied extensively. Gimlett and Cheung derived the noise RF spectrum and relative-intensity-noise parameters for the example of a single interferer (two reflection points), considering coherent, partially coherent and incoherent regimes [4]. However, in the subsequent analysis they assumed the incoherent limit (appropriate for directly modulated lasers) and no filtering of the interferometric noise. Power penalties were calculated assuming firstly, Gaussian, and secondly, bounded non-Gaussian ('two-pronged') statistics; values determined by experiment

employing a directly modulated DFB source (threshold choice unstated) (Fig. 2.9,2.10), were better than the former, but worse than the latter. The effective reflection coefficient R is $\propto \sqrt{R_1 R_2}$, where α is the (single pass) intensity transmittance and R_1 and R_2 are the reflection coefficients at the two discontinuities. It is analogous to $\sqrt{\text{crosstalk level } \xi}$.

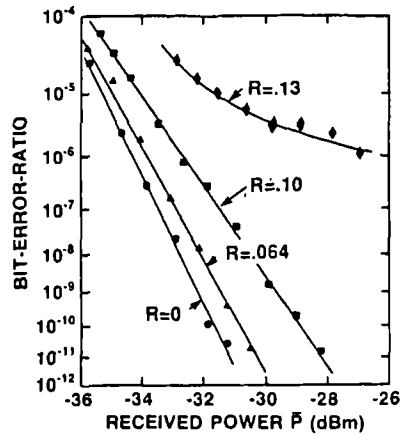


Figure 2.9. Measured BER curves versus effective reflection coefficient R (equivalent to $\sqrt{\text{crosstalk } \xi}$) at 1 Gb/s for two reflection points (from [4]).

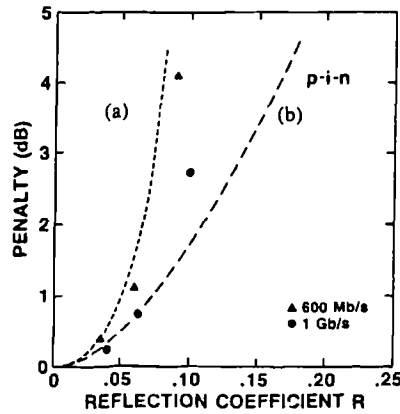


Figure 2.10. Power penalties versus R for two reflection points: (a) theory using Gaussian pdf; (b) theory using actual pdf (from [4]).

The penalty (dB) at $\text{BER}=10^{-9}$ assuming Gaussian statistics, aligned polarisations, a midway threshold choice, and no filtering of the noise, is:

$$\text{penalty} = -5 \log[1 - 139.2 R^2] \quad (2.9)$$

When there are N reflection points the number of interferers grows as N^2 .

Elrefaie et al. [12] computed the performance in the presence of a single interferer using the noise-driven single-mode rate equations for a directly modulated DFB laser, as developed by Marcuse [40]. They concluded that both NRZ and RZ systems have approximately the same penalty if the round-trip time delay between the two connectors is an exact integer number of bits. If this is not the case the RZ penalty is significantly reduced - this results from the decrease in probability of the coincidence of optical pulses. The predicted penalty under the assumption of bounded interferometric noise is smaller than that reported in [4], attributed to the broadening of the laser linewidth, owing to chirp, that is included within their analysis.

Transmission of analog CATV over fibre has been addressed [13]. Measurements of the RIN (relative-intensity-noise) spectrum indicate a noise reduction with increasing (direct) modulation index of the DFB laser - again this is attributed to chirp. If a highly coherent source is employed, e.g. an externally modulated Nd:YAG, the phase noise change $\ll \pi$ and interferometric noise is no longer problematic. When amplifiers are added to the system, without isolation, the performance degrades markedly because the reflections transit twice through the gain block whilst the signal only passes once. For N reflection points and gain G , the RIN grows as G^2N^2 . A RIN of -135 dB/Hz @2.4 Gb/s is required for satisfactory performance [14] - this goal may be satisfied by three -20 dB return loss connectors.

Further study has considered both single frequency and multi-modal lasers via the multi-mode rate equations [15]. In the presence of optical feedback (reflection) into an unisolated DFB, the frequency spectrum of the source is broadened, and therefore the penalty is reduced (noise filtered at the receiver). Measurement of the BER under optimised threshold choice for isolated DFBs showed no error flooring and thus no asymptote in the power penalty characteristic (Fig. 2.11). The penalty for the multi-mode source is strongly dependent upon the delay, bias and the spectral width, and is less than that for the DFB.

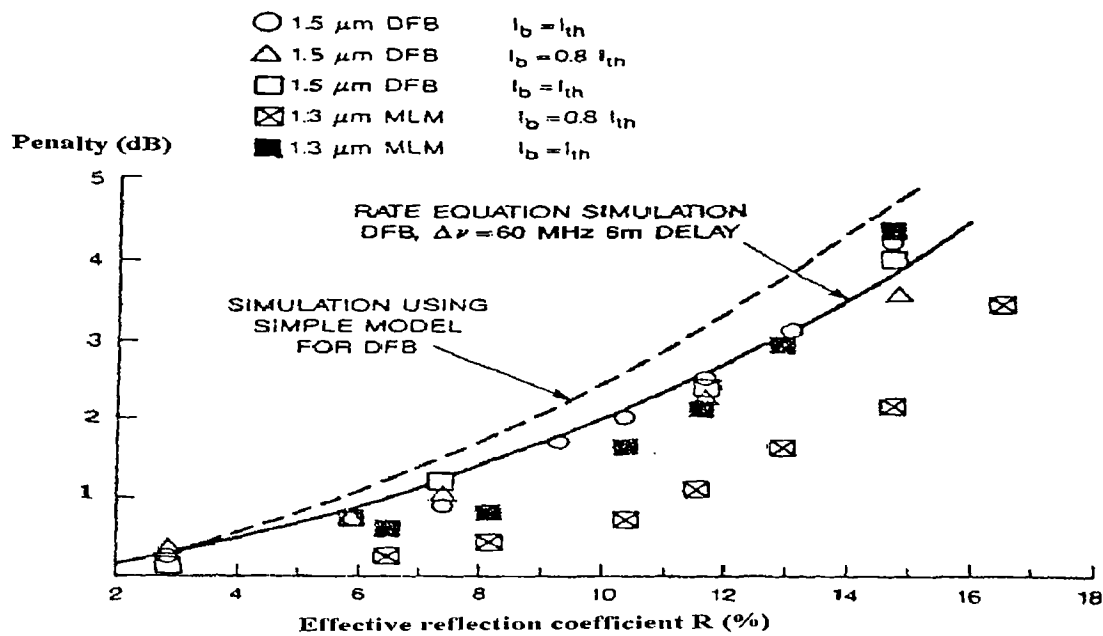


Figure 2.11. Experimental results of power penalty @BER=3x10⁻¹¹ for two reflecting points, for single and multifrequency lasers based systems operating at 1.7 Gb/s under optimised decision threshold choice (from [15]).

For N reflective points, assuming zero transmission loss between discontinuities, with effective reflection coefficient R , and eye margin M in the absence of interferometric noise, the power penalty (dB) for any bit-rate is:

$$\text{power penalty} = 10 \log \left[1 - \frac{N(N-1)R}{M} \right] \quad (2.10)$$

2.3.3 Rayleigh backscatter

It is possible to minimise the optical return loss from connections and splices to better than -55 dB by appropriate design; e.g. semiconductor amplifier facets may be angled. However, there remains the reflections resulting from Rayleigh backscatter; this *distributed* reflection occurs along the complete length of the silica fibre. Given a long length of fibre, the fraction of power that is Rayleigh backscattered, commonly called the backscatter reflectance R_B , is approximately -32 dB at 1.55 μm [16].

In conventional unidirectional transmission (Fig. 2.12a) degradation derives from backscattered light which is subsequently scattered itself into the path of the signal - this is called double Rayleigh backscatter; in bidirectional systems (Fig. 2.12b), a single backscatter will generate interferometric noise. The penalty in the latter case depends upon the relative wavelengths of the up-stream and downstream lasers, being greatest when the wavelengths are equal - this arises when a reflective MQW modulator is employed at the receiver to permit both down-stream detection and upstream transmission, Fig. 2.12c.

In analysis, Rayleigh backscatter is considered to arise from a finite number of discrete reflections suitably located along the fibre length. In analogy with the discrete reflection scenario (cf. Section 2.3.2), the performance penalty is increased by the addition of amplifiers to an unidirectional link, and may be reduced by employing in-line isolators.

Interferometric noise due to Rayleigh backscatter was first reported in 1988 [17]. The experiment employed a nearly single mode laser and a multiple quantum well (MQW) reflective modulator in a bidirectional system (Fig. 2.12c). The backscatter of the downstream light was treated as deriving from a single discrete reflector located at an effective distance on the fibre such that the interference with the upstream signal fell into the incoherent limit.

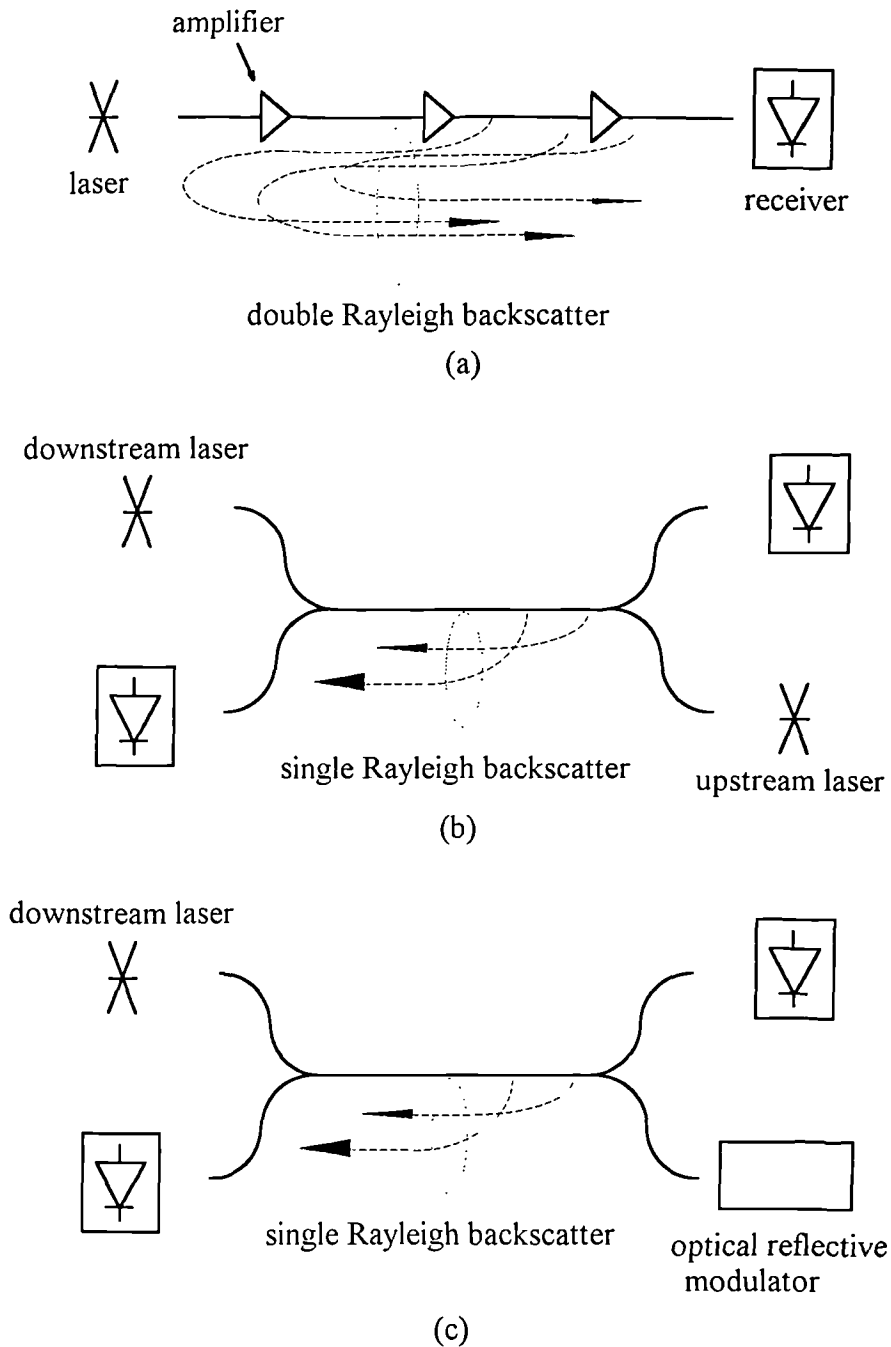


Figure 2.12. Interferometric noise due to Rayleigh backscatter. (a) unidirectional transmission. (b) bidirectional transmission with two sources. (c) bidirectional transmission with a single source.

Measurements of the RF noise spectrum gave a Lorentzian profile (Fig. 2.13a), identical to that from a self-homodyne interferometer, expected at the incoherent limit. If light was allowed to reflect back into the laser cavity from a discrete reflector at approximately 1.5m, peaks in the spectrum were observed (Fig. 2.13b), attributed

to mode hopping of the laser over the longitudinal modes of the parasitic 1.5m Fabry-Perot cavity [41]. On the interference of light from different modes, the noise generated is translated from baseband by an amount equal to the beat frequency of the two modes - this may equal all integral multiples of the modal spacing, 66 MHz. This effect has been highlighted because similar observations were made in the experiments described in Section 5.2.3.

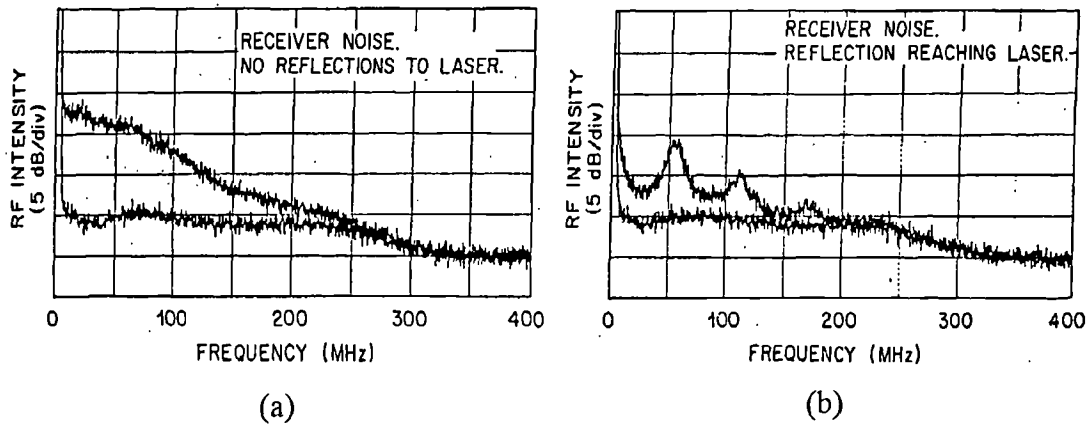


Figure 2.13. Noise spectra with (a) no reflections into laser cavity, and (b) reflections into laser cavity. Upper and lower traces represent receiver noise with and without Rayleigh backscatter, respectively (from [17]).

Rayleigh backscatter in an optical amplifier cascade (Fig. 2.12a) has also been considered [16]. In an experiment employing a CW DFB source, a single fibre amplifier and 140 km of fibre, a Lorentzian noise spectrum was again observed - the incoherent limit applied. The RIN was found to increase as the square of the amplifier gain in agreement with the theory presented. Under the assumptions of Gaussian statistics (Central Limit Theorem) for the noise, depolarised light, a receiver bandwidth B very much greater than the source linewidth $\Delta\nu$, and a decision threshold midway between zeros and ones, the power penalty (dB) at $BER=10^{-9}$ for a single amplifier of gain G is :

$$\text{power penalty} = -5\log\left[1 - 72 G^2 R_B^2\right] \tag{2.11}$$

A penalty of less than 1 dB requires a $G < 20.6$ dB.

Other treatments [18] consider the backscatter from every fibre link to be generated from a single discrete reflector of reflectivity R_B . The power penalty at $BER=10^{-9}$ was determined for N_A amplifiers by a similar analysis, and assumptions, to that of Gimlett et al. [16]:

$$\text{power penalty} = -5 \log \left[1 - 72 G^2 R_B^2 \frac{N_A (N_A - 1)}{2} \right] \quad (2.12)$$

This relation is displayed graphically in Fig. 2.14 for $G=10$ dB.

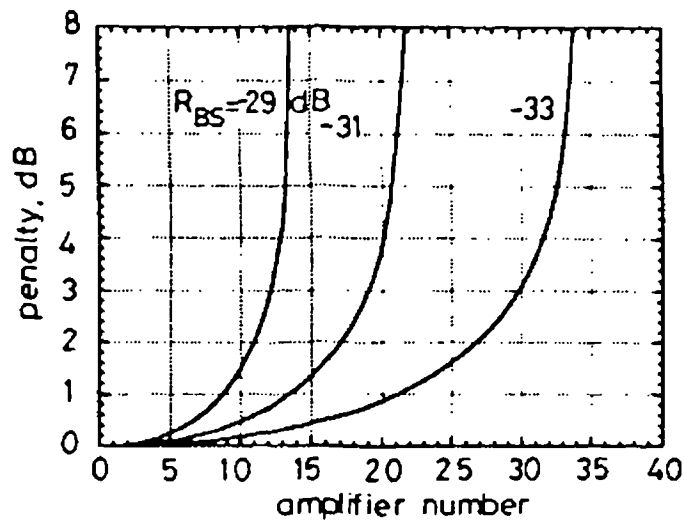


Figure 2.14. Calculated power penalty against number of amplifiers in the cascade for three typical values of Rayleigh backscatter (from [18]).

Theory and experiment were found to agree closely for a six-amplifier cascade given an externally modulated source. If the laser was directly modulated, however, the penalty was much smaller - this was attributed to spectral broadening (chirp), (Fig. 2.15) although a different explanation is proposed in Chapter 3.

In conclusion, with an amplifier gain of 10 dB the number of amplifiers is limited to ~10-30.

A study of the degradation due to Rayleigh backscatter when RF filtering of the interferometric noise takes place at the receiver, i.e. when the linewidth $\Delta\nu$ is not much smaller than the receiver bandwidth, has been undertaken [19]. The method is an extension of the above analysis [16] with the assumption that the noise is Gaussian with a white power spectrum. The penalty for depolarised light and a bit period T is:

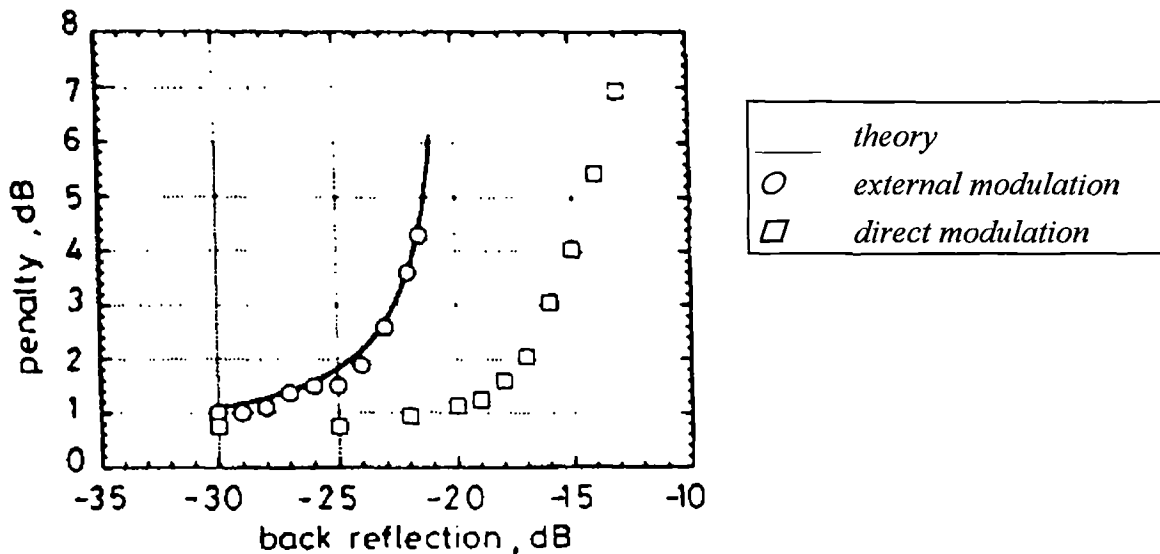


Figure 2.15. Measured power penalties due to interferometric noise with both external and direct modulation of transmitter laser (from [18]).

$$\text{power penalty} = -5 \log \left[1 - 72 G^2 R_B^2 \frac{2}{\pi \Delta \nu T} \right] \quad \text{for } \Delta \nu \gg \frac{1}{T} \quad (2.13)$$

The power penalty falls with increasing linewidth given a fixed bit-rate. It is suggested that this expression is applicable to chirped direct modulation; however, the validity of substituting the measured linewidth of a chirped laser into a formula derived assuming CW operation is questionable and will be discussed further in Section 3.4.

In other treatments [20] a complete analysis of the probability density function of the noise in a bidirectional system is presented. The BER is determined and is found to agree well with an experimental two source configuration.

2.3.4 Subcarrier-multiplexed networks

Microwave subcarrier-multiplexing may be used to distribute broadcast and point-to-point services within the local loop. For example, in CATV many 5 MHz analog video signals modulate different microwave subcarriers (separated in frequency by 5 MHz) which are then combined before modulating a single optical carrier. This signal is then broadcast via a passive optical branch network to all subscribers. In

bidirectional networks the customer may communicate to the head-end by single subcarrier modulation at a unique RF frequency of its own laser source.

Interferometric noise will arise in this upstream transmission when the lasers located at the customer's premises are close in wavelength [21,22]. At the head end receiver many waveforms of similar power arrive simultaneously and generate not only the required information (the head-end tunes its electronic receiver to the subcarrier frequency, i.e. customer, of his choice) but also the beating components. The ratio of signal power to in-band interferometric noise power (SIR) has been calculated for two simultaneous transmitters assuming a 5 MHz signal bandwidth and a laser source of much greater linewidth [21] (Fig. 2.16).

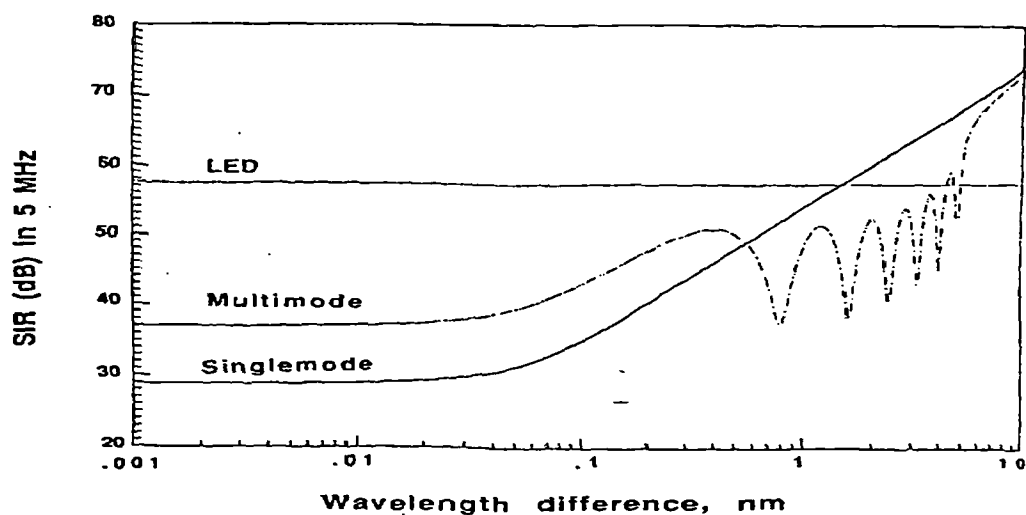


Figure 2.16. The variation of SIR as a function of the wavelength separation of the optical sources. The LED has a linewidth of 40 nm, and the two laser sources have longitudinal modes with linewidths of 10 GHz. The multimode source has seven longitudinal modes with spacing of 0.8 nm (from [21]).

At zero wavelength separation the single mode source has the smallest SIR since its optical spectrum, and therefore its interferometric noise spectrum, is the narrowest. Performance improves with increasing wavelength separation because the interferometric noise spectrum becomes centred further and further away from the microwave subcarrier frequency to which the receiver is tuned. In the case of the LED, the noise spectrum is extremely broad (~80 nm) giving a large SIR that varies little with the change in wavelength separation. The troughs for the multimode source occur when the modal positions of the two lasers coincide (this occurs every 0.8nm, the value of the modal separation). The performance improves when there are

more longitudinal modes (within the same spectral width). An experimental investigation with two multimode lasers indicated the predominance of interferometric noise over thermal noise, and highlighted the need for care in estimation of the noise spectrum under modulation [22]. Preliminary studies [21] indicate that the number of customers could be limited to 16 if broadcast quality FM video was to be transmitted with multimode lasers.

A theoretical analysis has addressed the influence of interferometric noise on the ultimate capacity of WDMA(Wavelength Division Multiple Access)-Subcarrier-FDMA(Frequency Division Multiple Access) lightwave networks [23]. Users are linked via a passive star and are allocated a unique wavelength-subcarrier frequency pair. At the receiver the required channel is selected by tuneable optical and electrical bandpass filters. Interferometric noise arises from the beating of waveforms that are transmitted by the optical filter. The probability of channel outage is determined and it is found that as more subcarrier channels are added, the network capacity increases sub-linearly and eventually saturates.

In an experiment employing four DFB lasers, each modulated by a FSK-pseudorandom signal translated onto a subcarrier, error floors at $BER=10^{-9}$ were found when two lasers were temperature tuned to the same wavelength [24]. The error floors were eliminated by increasing the modulation index, and therefore the laser chirp, from 0.8 to 1.8. Measurements of the SNR supported the effective modelling of the beating as a white Gaussian noise process.

2.3.5 Recirculating fibre loops

Fibre loops are employed in two distinct ways: in the first, the loop is continuously illuminated and light is shed after each circulation giving an output optical field that is the sum of a large number of terms. When the loop delay is made much greater than the optical source coherence length - an incoherent recirculating structure - RF notch filters and bit-rate limiters may be realised. In the second scenario, the loop acts as a buffer for storing an optical cell which circulates until required.

The bit-rate limiter (Fig. 2.17) is severely compromised by intensity noise arising from phase-to-intensity noise conversion [25]. The theory is presented in [25-27], whilst experimental measurements are reported in [28] (Fig. 2.4).

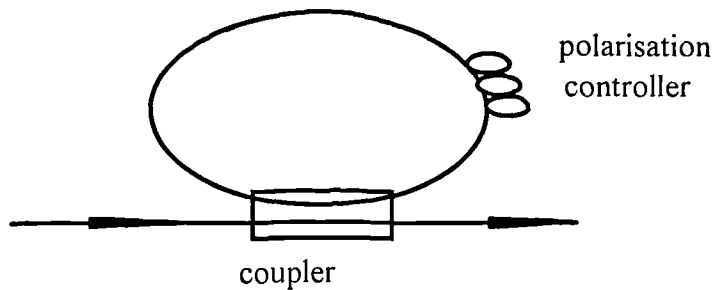


Figure 2.17. Bit-rate limiter

Fibre loops are also under consideration for use as buffer elements in optical ATM and packet switching systems [29]. The corruption of a buffered cell due to spontaneous emission from the amplifier element placed within the loop to compensate for power losses, and from crosstalk arising from other cells, has been analysed [31]. In the experiment a 312-bit cell was launched into a fibre loop and allowed to circulate (Fig. 2.18). The SLA1 gate was immediately closed but a controllable amount of crosstalk was permitted to enter the loop and the BER was measured after each circulation by monitoring the output of the coupler. The BER is plotted against the contrast ratio of SLA1 for 10, 15 and 23 circulations in Fig. 2.19.

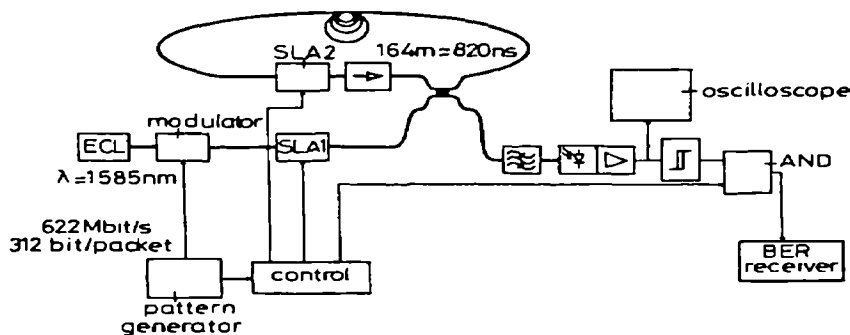


Figure 2.18. Experimental configuration of fibre-loop (from [31])

Comparison with a theoretical analysis [30] indicates excellent agreement for 23 circulations. In the analysis, the phases of all the crosstalk terms are considered to be random and uncorrelated, and the photocurrent noise is assumed to be Gaussian distributed - i.e. they employ the Central Limit Theorem which becomes more accurate with more terms. An expected BER following averaging over all parameters - phase and bit offset - is derived.

The nature of the crosstalk here falls into the coherent class since the laser source has a coherence time much greater than the loop delay. When many crosstalk terms are

simultaneously corrupting the data the fibre phase noise, although certainly much slower than the bit-rate, will not induce detectable BER variations with time; the changes are simply averaged out as observed in their experiment.

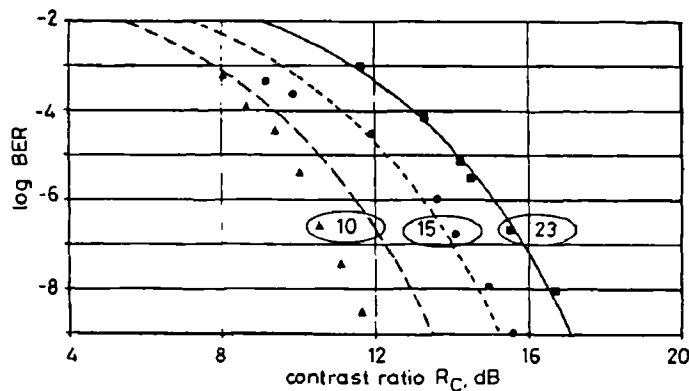


Figure 2.19. Experimental and theoretical results of BER against contrast ratio R_c of gate SLA1 for different numbers of circulations (from [31]).

Multiple cells may be stored in a single fibre loop buffer by assigning a different wavelength to each [32,33] (Fig. 2.20). The cell is stored in the buffer (i.e. continues to circulate) until the SOA dedicated to its wavelength is switched off. The configuration offers multiple paths for every wavelength around the loop, only one of which is desired; thus *two* filters for every wavelength are included in the loop to minimise the interferometric noise.

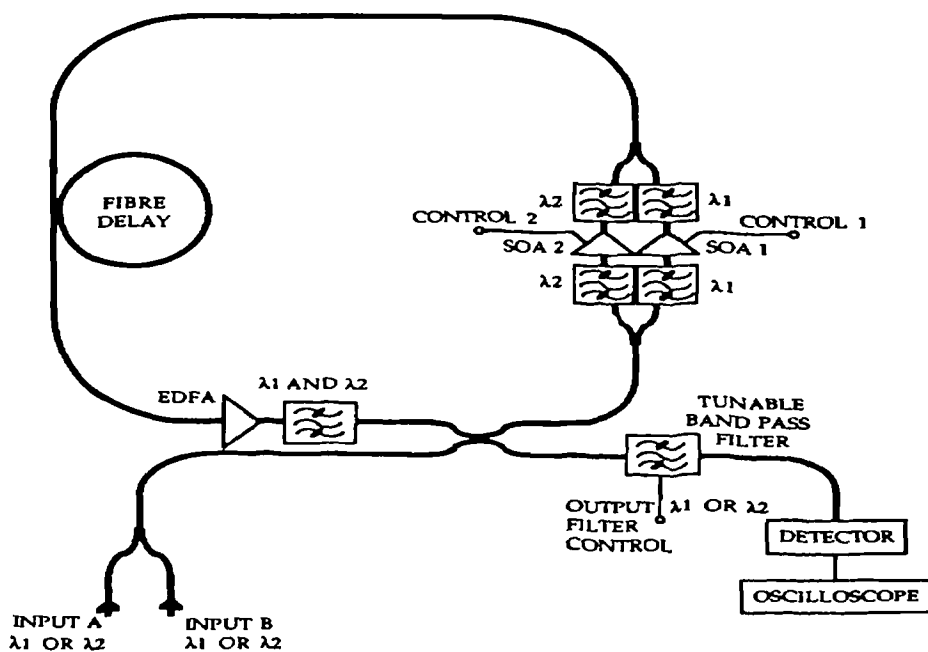


Figure 2.20. Two-wavelength fibre loop-memory testbed (from [32]).

2.3.6 Space switches

In the great wealth of literature concerning integrated optical space switches (for a review see [42]) very little attention has been paid to the difficulties of interferometric noise due to crosstalk. The path lengths from input ports to output ports are short, and therefore the transit time difference between signal and crosstalk is also small, of the order of ps, or less. If a single frequency laser is employed the phase noise due to both the laser and the waveguide material will be negligible, resulting in a time independent, i.e. noise-free, aggregate photocurrent when crosstalk and signal, derived from the same laser, add together. However, degradation will still result from the (static) interference term (cf. Eqn. 2.5), the magnitude being dependent on the relative phases of signal and crosstalk. Interferometric *noise* will arise if the crosstalk and signal arise from separate sources that are closely wavelength-matched.

Eiselt et al. have addressed noise in a cascade of 2x2 semiconductor amplifier switches [30] (see Section 2.3.5). Other workers, for example Burke et al. [43], have ignored it.

2.3.7 WDM transport networks

The use of multiple wavelengths in the optical communications network, offering increased capacity in the trunk network and, additionally, service discrimination in the local-loop, will be implemented in the near future. Here two network demonstrator studies undertaken within the RACE II research program, MWTN (trunk) and MUNDI (local-loop), shall be highlighted concentrating on the effect of interferometric noise.

The MWTN (Multi-wavelength Transport Node) network node [34] is placed within the optical network layer of the trunk network, and overlays the digital network layer that comprises electronic (SDH(Synchronous Digital Hierarchy) crossconnects.

The example node (Fig. 2.21) has three inputs, each carrying four wavelengths, $\lambda_1 \dots \lambda_4$; these 12 channels may be routed to the 12 output channels, and in addition there exists an add/drop facility to the digital network layer below. The first 4x4 space switch routes traffic at λ_1 , the second at λ_2 , etc.; the unwanted wavelengths are attenuated by optical filters placed before the space switch inputs.

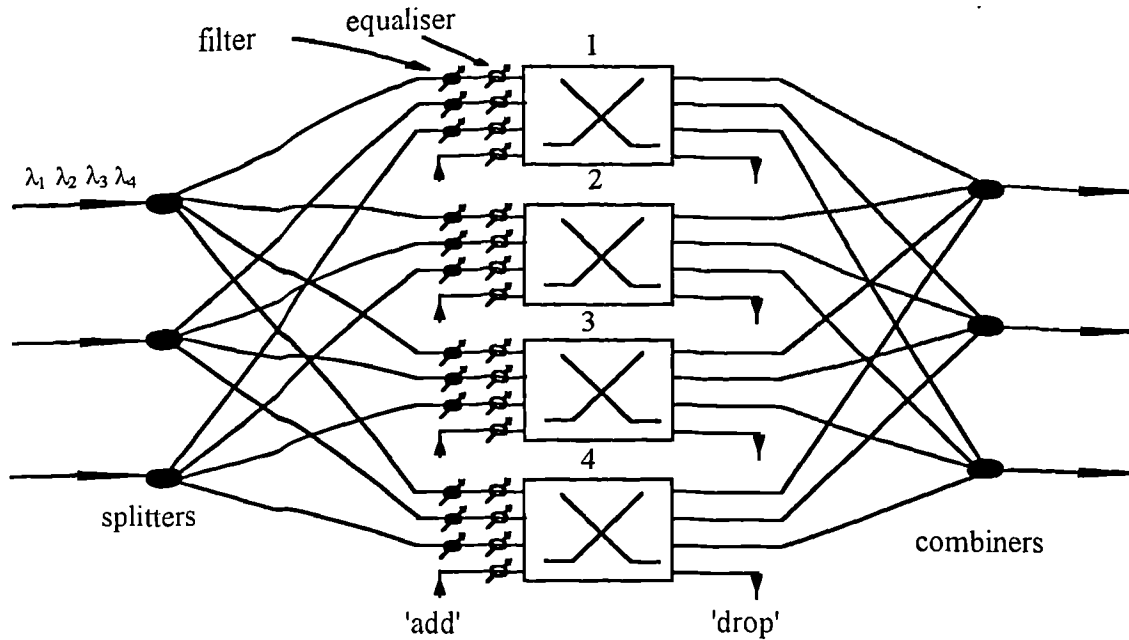


Figure 2.21. MWTN node architecture.

Since there is no wavelength conversion blocking may occur: for example, if the channels at λ_1 at inputs 1 and 2 both want to exit at output 3. Since the wavelengths are likely to be spaced a few nms apart, interferometric noise may only result when crosstalk at the same wavelength adds to the signal. Two mechanisms are relevant:

1. crosstalk addition within the space switch
2. crosstalk leakage of the same wavelength (as the data) through the optical filters prior to the space switches that handle the other wavelengths, subsequently routed to the passive combiners.

In the MWTN demonstrator a time-varying BER and error flooring were observed [34], attributed to interferometric noise visible on the oscilloscope. The WDM node under-development within the ONTC (Optical Networks Technology Consortium) has also experienced similar problems [35].

The MUNDI (Multiplexed Network for Distributive and Interactive Services) project addresses the integrated delivery of narrowband telephony and ISDN together with broadband broadcast (e.g. CATV) and interactive services (e.g. video-on-demand) in the access network [36]. In the demonstrator a narrowband 1300 nm passive optical network (PON) is upgraded by the addition of high density WDM (HDWDM) in the 1500 nm window (Fig. 2.22).

The wavelengths are accurately held (to better than 0.1 nm) at specified wavelengths,

separated by 1 nm, by a distributed wavelength reference comb. Therefore, when crosstalk adds to the data at the same nominal wavelength, the interferometric noise spectrum will lie at baseband and a significant fraction will fall within the receiver bandwidth. Such crosstalk arises principally from the imperfect wavelength MUX/DMUX components (the central space switch is opto-mechanical and adds little crosstalk). Interferometric noise occurs when the signal wavelength is poorly rejected by the DMUX, and is switched to the same MUX as the main signal, where further poor crosstalk couples it back into the same path [44].

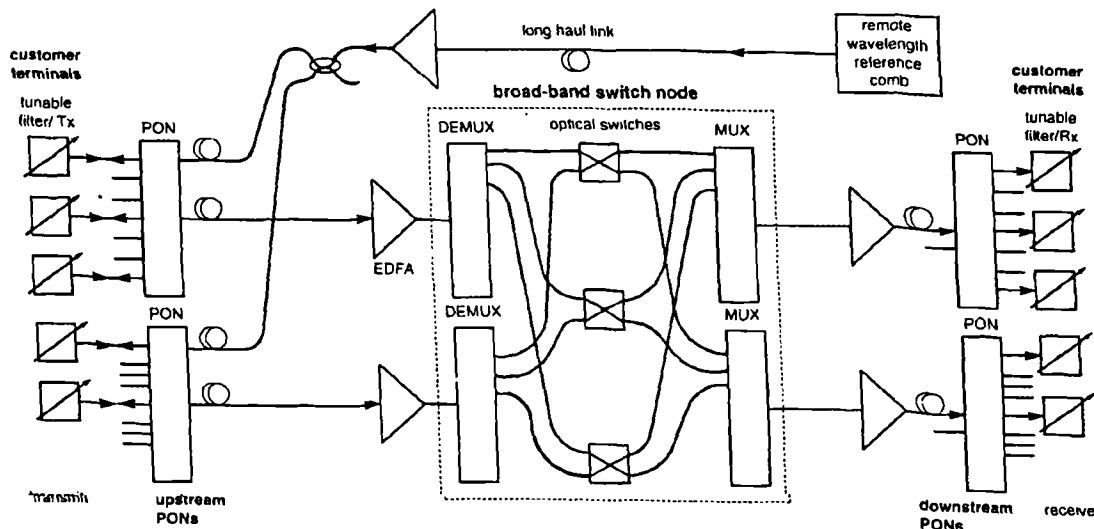


Figure 2.22. The MUNDI broadband interactive demonstrator (from [36]).

The receiver sensitivity penalty was measured for PIIN due to a single interferer (Fig. 2.23) [36,44]. The experimentally measured power penalty asymptote lies at a crosstalk level of approximately -7 dB. Inexplicably, this is unaffected by the choice of decision threshold, whether optimised or not.

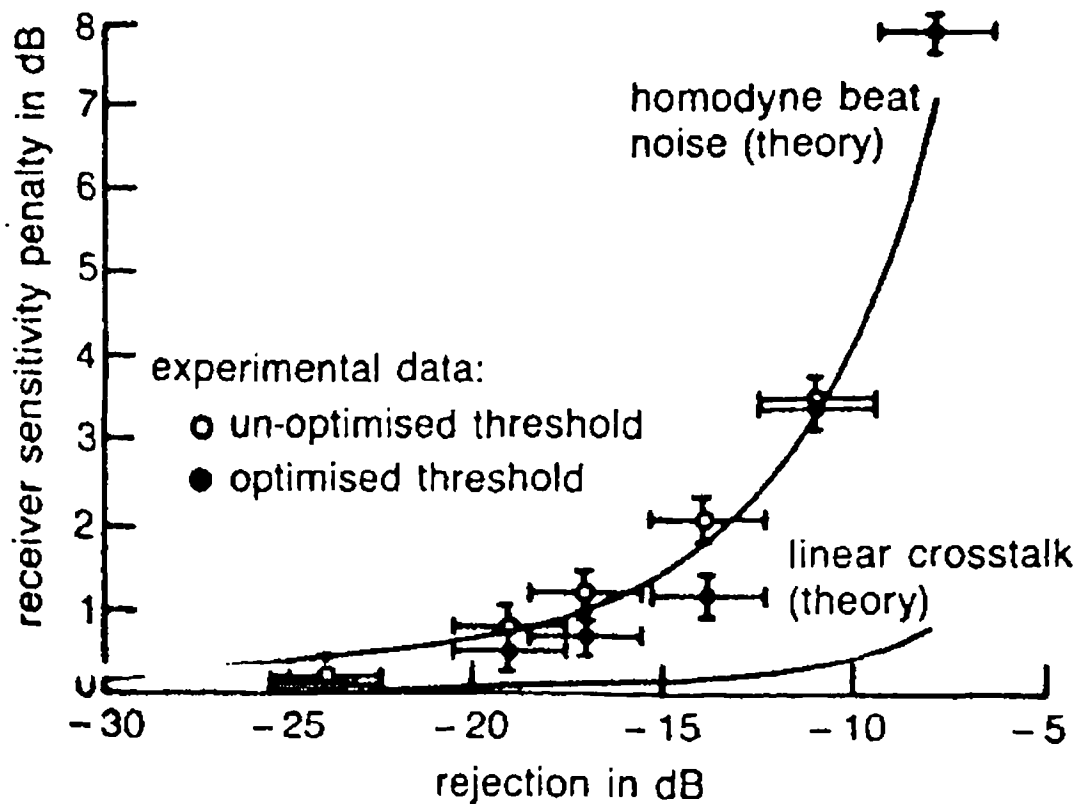


Figure 2.23. Receiver penalty due to self-homodyne beat-noise (from [36]).

2.3.8 Optical TDM switching nodes

Network capacity may also be upgraded via optical TDM techniques. This approach is an extension of the current digital network technology, alleviating the speed limitations imposed by electronics, by transmitting at 10's of Gb/s. An optical network layer is required overlaying the electronic network layer; this is analogous to MWTN but the crossconnects now switch in space and time. Suitable optical TDM switching networks for this task, formed from 2x2 integrated optical crosspoints interlinked by single mode fibre delay lines, have been extensively studied [45-47] (Fig. 2.24). In these networks the crosspoint switching time may be relaxed by employing block multiplexing of the data. The delay lines are accurately cut to integral multiples of the block period.

Crosstalk is added to the data signal at every (imperfectly-isolated) crosspoint in the switch fabric, and because of the delay lines the complete 'spectrum' of interferometric

noise classes may be generated. This will be elaborated upon in subsequent chapters of the thesis.

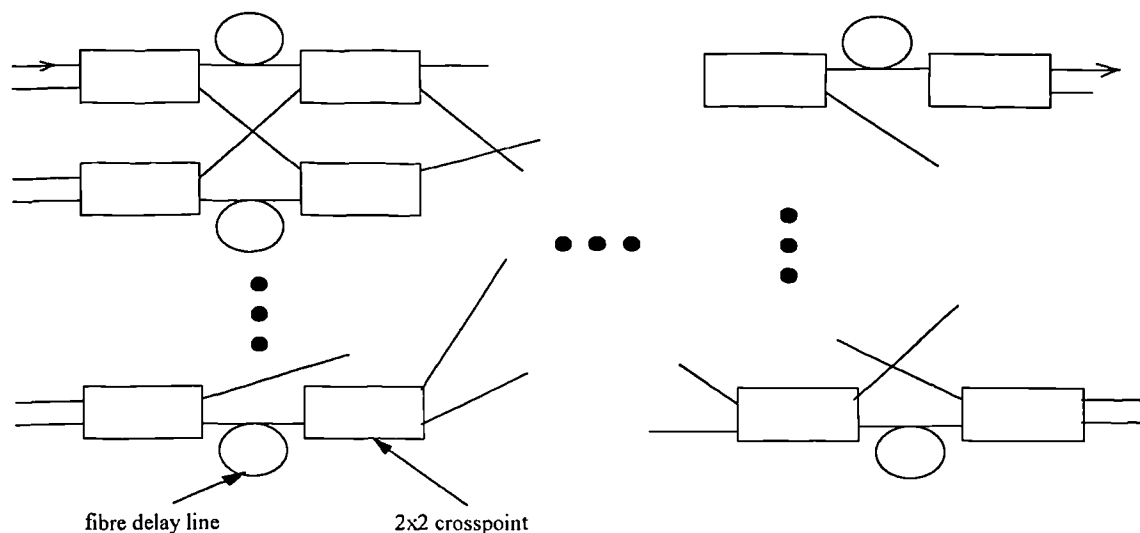


Figure 2.24. A schematic illustration of an optical TDM switching network.

2.4 Proposed methods for achieving suppression of interferometric noise

Methods to suppress interferometric noise attempt to realise a noise spectrum that is either far broader than the data bandwidth, or is translated from baseband, thereby reducing the fraction of noise which falls within the receiver bandwidth. It has long been known that interferometric noise may be reduced by employing low coherence sources like multi-mode laser diodes [48] and LEDs [21]. In the former case all beating components between modes at different wavelengths lie outside the baseband and are low-pass filtered [2]; in the latter case the noise spectrum is simply extremely broad (1000's of GHz). Directly-modulated single frequency lasers may have their coherence upset by application of a large modulation depth that increases the transient chirp¹ [24], or by the addition of a current dither [49]. Direct modulation has been found to improve noise performance with respect to external modulation [18]. Self-pulsating lasers exhibiting multi-longitudinal mode operation with broad linewidths [50] have been proposed as suitable sources for interferometric noise affected systems [2].

¹a different mechanism is proposed in Chapter 7.

Another technique for single mode lasers superposes a single tone phase modulation and an amplitude modulation (that carries the data) onto the optical carrier; the phase modulation is deep (modulation index >2) and at a higher frequency ($>3\times$) than the data bandwidth [51,52]. The phase modulation may be imparted externally or by direct modulation. The mechanism involves a redistribution of the noise from baseband to multiple harmonics of the phase modulation frequency. Noise is suppressed except when the modulation frequency and the reciprocal of the data-crosstalk differential delay are related by integer multiples. This situation is avoided if modulation is applied with multiple tones, or a bandpass filtered Gaussian noise source whose bandwidth is larger than the reciprocal of the shortest differential delay in the network is used [51].

An intuitive description of this technique considers the frequency spectrum of the optical field [53]. This comprises a series of terms separated by the modulation frequency. Since the modulation frequency exceeds the receiver bandwidth only beating between data and crosstalk terms at the same optical frequency (i.e. identically numbered terms in the series) will generate noise. Hence, the noise reduction improves with increasing modulation index since the optical spectrum spans more significant terms (this is the same mechanism for the reduction in noise with the number of modes in a multi-mode laser). Measurement of the noise spectrum from a 1.8 GHz sine-wave phase modulated CW-running DFB demonstrated a $\times 5$ reduction for an index of 2 [53]. The phase modulation technique is being employed successfully in CATV transmission [54].

An alternative approach that does not influence the noise spectrum, but instead reduces the likelihood of data and crosstalk bits being simultaneously high, has been proposed [55]. The raw data is sampled m bits at a time and is then transmitted as a 2^m symbol 'word' containing only a single high symbol. For example, in the pre-coding scheme for $m=2$, 00 is transmitted as 0001, 01 as 0010, etc. (Fig. 2.25). The redundancy is equal to $2^m / m$.

It can be seen that given a single interferer the probability of a symbol being a 'one' with noise (i.e. the crosstalk symbol is also a 'one') is reduced from $1/4$ (no pre-coding) to $1/16$ ($m=2$). A new analysis [56] of this scheme for many crosstalk terms indicates that the mean number of units of interferometric noise afflicting the 'one' symbol in the transmitted word is inversely proportional to the redundancy. This is illustrated for 100 crosstalk noise-generating terms in Fig. 2.26.

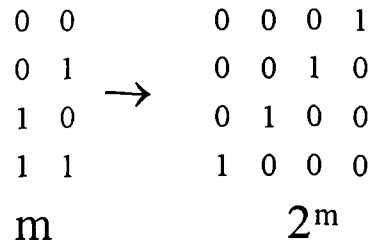


Figure 2.25. Data pre-coding for $m=2$.

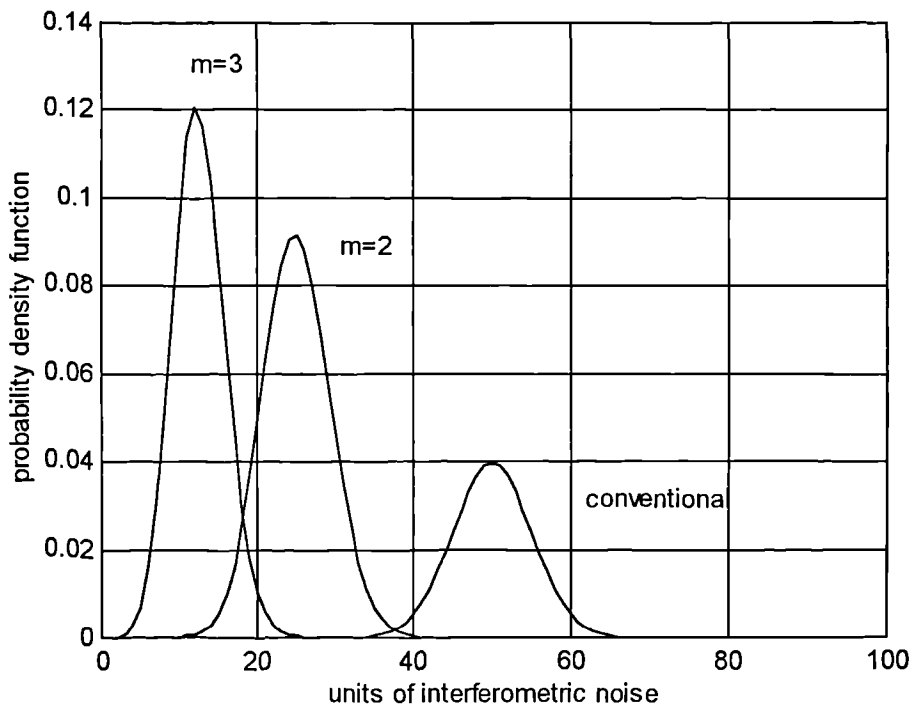


Figure 2.26. Probability density function of the number of units of interferometric noise given 100 crosstalk terms and different amounts of pre-coding.

Performance may not be improved indefinitely by increasing m since a point is reached where the interferometric noise reduction is offset by the increase in thermal noise within the necessarily broader receiver bandwidth. The method requires additional hardware at transmitter and receiver, operating at the symbol rate, and may give rise to additional dispersion penalties.

2.5 Conclusions

In this chapter the importance of interferometric noise in a wide range of optical network topologies has been highlighted (cf. Table 2.1). The subject has been addressed extensively in the literature, for both single and multiple interferers, both experimentally and theoretically; a summary is presented in Tables 2.2 and 2.3. Interest is centred on single-mode lasers, typified by the DFB laser, since they offer excellent all-round performance but are more prone to interferometric noise than multi-mode lasers and LEDs.

In the case of a single interferer the following items are worthy of note:

- interferometric noise induces error floors or , equivalently, the power penalty characteristic displays an asymptote.
- interferometric noise is bounded, hence Gaussian statistics are inappropriate.
- performance improves markedly if the decision threshold is optimised.
- the BER floors at 10^{-9} for crosstalk of -7 dB (threshold optimised)
 -12 to -18 dB (AC-coupled Rx).

For multiple interferers:

- interferometric noise induces error floors, or , equivalently, the power penalty characteristic displays an asymptote.
- analysis employs (almost exclusively) Gaussian statistics and closely follows experiment.
- performance is relatively insensitive to the decision threshold.
- the BER floors at 10^{-9} for a total crosstalk of -21.4 dB.

Interferometric noise may be suppressed by:

- employing low coherence sources (multi-mode laser, LED, chirped DFB, self-pulsating laser)
- high frequency, large index, single tone phase modulation.
- addition of redundancy via sparse pre-coding.

Theory		Experiment		Ref.
	crosstalk ξ (dB) for BER floor at 10^{-9}		crosstalk ξ (dB) for BER floor at 10^{-9}	
AC-coupled Rx. (worst case)	-16	externally modulated DFB	-18	[9]
eye-closure method		AC-coupled Rx.		
unspecified	~ -12			[11]
unspecified	-7	optimised threshold	-7	[36]
AC-coupled, Gaussian statistics	-21.4	directly modulated DFB	-17 to -20	[4]
AC-coupled, bounded statistics	~ -12	Rx unspecified (likely to be AC-coupled)		
no asymptote predicted when threshold optimised				[12]
no asymptote predicted when threshold optimised		threshold optimised, no asymptote found (for crosstalk < -16.5 dB)		[15]

Table 2.2. Summary of interferometric noise owing to a single interferer (single-mode laser, aligned polarisations and no noise filtering assumed).

Scenario	Theory		Experiment	Ref.
	Method	Penalty Formula		
General	Gaussian statistics	$-5 \log(1 - 144 \cdot \text{total crosstalk})$ asymptote at total crosstalk = -21.4dB	external modulation 1-8 crosstalk terms	[9,10]
N reflections of effective reflectivity R	Gaussian statistics	$-5 \log(1 - 72 N(N-1)R^2)$	N=3	[4]
Eye-closure	Eye-closure	$10 \log(1 - N(N-1)R/M)$ M=uncorrupted eye opening	-	[15]
Rayleigh Backscatter (R_B), 1 amp. (G)	Gaussian statistics	$-5 \log(1 - 72 G^2 R_B^2)$ fails if $G > 22.7$ dB	-	[16]
Rayleigh Backscatter (R_B), N_A amps.	Gaussian statistics	$-5 \log(1 - 36 G^2 R_B^2 N_A (N_A - 1))$ $G = 10$ dB, $N_A < 13$	external and direct mod. $N_A = 6$	[19]
Multiple amplifiers	Gaussian statistics	In a cascade of N 2x2 switches the contrast ratio (dB) of amps. increases linearly with $\log(N)$ ($N = 10$ CR > 25dB)	external modulation, recirculating loop	[30]

Table 2.3. Summary of interferometric noise owing to a multiple interferers (single-mode laser, aligned polarisations and no noise filtering assumed).

2.6. References

1. R.W. Tkach and A.R. Chraplyvy, "Phase noise and linewidth in an InGaAsP DFB laser", *J. Lightwave Technol.*, 4(11), pp. 1711-1716, 1986.
2. K. Petermann, *Laser diode modulation and noise*, Kluwer Academic Publishers, New York, 1993.
3. A. Arie and M. Tur, "Phase-induced intensity noise in optical interferometers excited by semiconductor lasers with non-Lorentzian lineshapes", *J. Lightwave Technol.*, 8(1), pp. 1-6, 1990.
4. J.L. Gimlett and N.K. Cheung, "Effects of phase-to-intensity noise conversion by multiple reflections on gigabit-per-second DFB laser transmission systems", *J. Lightwave Technol.*, 7(6), pp. 888-895, 1989.
5. K. Bløtekjær, "Thermal noise in optical fibers and its influence on long-distance coherent communication systems", *J. Lightwave Technol.*, 10(1), pp. 36-41, 1992.
6. C. Li, M. Olsen and D.G. Messerschmitt, "Analysis of crosstalk penalty in dense optical chip interconnects using single-mode waveguides", *J. Lightwave Technol.*, 9(12), pp. 1693-1701, 1991.
7. M. Tur, E.L. Goldstein and C.A. Brackett, "Bit-error-rate limitations due to laser phase noise in single-mode optical fiber systems with multiple paths", *Optical Fiber Communication OFC'88*, paper WQ39, OSA, 1988.
8. M. Tur and E.L. Goldstein, "Dependence of error rate on signal-to-noise-ratio in fiber-optic communication systems with phase-induced intensity noise", *J. Lightwave Technol.*, 7(12), pp. 2055-2058, 1989.
9. E.L. Goldstein, L. Eskildsen and A.F. Elrefaie, "Performance implications of component crosstalk in transparent lightwave networks", *IEEE Photon. Tech. Lett.*, 6(5), pp. 657-660, 1994.
10. L. Eskildsen, E.L. Goldstein, "Scaling limitations in transparent optical networks due to low-level crosstalk", *IEEE Topical Meeting on Optical Networks*, 1994.
11. J.J. O'Reilly and C.J. Appleton, "System performance implications of homodyne beat noise effects in optical fibre networks", *IEE Proc. J*, 142(3), pp. 143-148, 1995.
12. A. Elrefaie, S. Tu and M. Romeiser, "Performance degradations of 2.4 Gbit/s NRZ/RZ lightwave systems due to reflection-induced phase-to-intensity noise conversion", *IEEE Photon. Tech. Lett.*, 1(7), pp. 173-175, 1989.
13. W.I. Way, C. Lin, C.E. Zah, L.C.R. Spicer and W.C. Young, "Multiple-reflection-induced intensity noise studies in a lightwave system for multichannel AM-VSB television signal distribution", *IEEE Photon. Tech. Lett.*, 2(5), pp. 360-362, 1990.

14. M. Shikada and N. Henmi, "Evaluation of power penalty due to beat noise induced by connector reflection", *Elect. Lett.*, 24(18), pp. 1126-1128, 1988.
15. D.A. Fishman, D.G. Duff and J.A. Nagel, "Measurements and simulation of multipath interference for 1.7 Gb/s lightwave transmission systems using single and multifrequency lasers", *J. Lightwave Technol.*, 8(6), pp. 894-905, 1990.
16. J.L. Gimlett, M.Z. Iqbal, N.K. Cheung, A. Righetti, F. Fontana and G. Grasso, "Observation of equivalent Rayleigh scattering mirrors in lightwave systems with optical amplifiers", *IEEE Photon. Tech. Lett.*, 2(3), pp. 211-213, 1990.
17. T.H. Wood, R.A. Linke, B.L. Kasper and E.C. Carr, "Observation of coherent Rayleigh noise in single-source bidirectional optical fiber systems", *J. Lightwave Technol.*, 6(2), pp. 346-351, 1988.
18. L. Eskildsen, E.L. Goldstein, M. Andrejco, L. Curtis, V. Shah, D. Mahoney, C.E. Zah and C. Lin, "Interferometric noise limitations in fiber-amplifier cascades", *Elect. Lett.*, 29(23), pp. 2040-2041, 1993.
19. R.K. Staubli, P. Gysel and R.U. Hofstetter, "Power penalties due to multiple Rayleigh backscattering in coherent transmission systems using in-line optical amplifiers", *IEEE Photon. Tech. Lett.*, 2(12), pp. 872-874, 1990.
20. R.K. Staubli and P. Gysel, "Crosstalk penalties due to coherent Rayleigh noise in bidirectional optical communication systems", *J. Lightwave Technol.*, 9(5), pp. 375-380, 1991.
21. C. Desem, "Optical interference in subcarrier multiplexed systems with multiple optical carriers", *IEEE J. Selected Areas Commun.*, 8(7), pp. 1290-1295, 1990.
22. C. Desem, "Measurement of optical interference due to multiple optical carriers in subcarrier multiplexing", *IEEE Photon. Tech. Lett.*, 3(4), pp. 387-389, 1991.
23. N.K. Shankaranayanan, S.D. Elby and K.Y. Lau, "WDMA/subcarrier FDMA lightwave networks: limitations due to beat interference", *J. Lightwave Technol.*, 9(7), pp. 931-943, 1991.
24. T.H. Wood and N.K. Shankaranayanan: "Measurements of the effect of optical beat interference on the bit error rate of a subcarrier-based passive optical network", *Optical Fiber Communication OFC '93*, paper ThM3, OSA/IEEE, San Jose, 1993.
25. M. Tur and B. Moleshi, "Laser phase noise effects in fiber-optic signal processors with recirculating loops", *Optics Letters*, 8(4), pp. 229-231, 1983.
26. M. Tur, B. Moleshi and J.W. Goodman, "Theory of laser phase noise in recirculating fiber-optic delay lines", *J. Lightwave Technol.*, 3(1), pp. 20-35, 1985.
27. E. Shafir and M. Tur, "Phase-induced intensity noise in an incoherent Fabry-Perot interferometer and other recirculating devices", *J. Opt. Soc. Am. A*, 4(1), pp. 77-81, 1987.

28. M. Tur, E.L. Goldstein and C.A. Brackett, "Effect of laser phase noise on a class of bit-rate limiter", *Elect. Lett.*, 24(2), pp. 126-128, 1988.
29. M. Eiselt, G. Großkopf, R. Ludwig, W. Pieper and H.G. Weber, "Photonic ATM switching with semiconductor laser amplifier gates", *Elect. Lett.*, 28(15), pp. 1438-1439, 1992.
30. A. Ehrhardt, M. Eiselt, G. Großkopf, L. Küller, R. Ludwig, W. Pieper, R. Schnabel and H.G. Weber, "Semiconductor laser amplifier as optical switching gate", *J. Lightwave Technol.*, 11(8), pp. 1287-1295, 1993.
31. W. Pieper, M. Eiselt, G. Großkopf, R. Langenhorst, A. Ehrhardt and H.G. Weber, "Investigation of crosstalk interference in a fibre loop optical buffer", *Elect. Lett.*, 30(5), pp. 435-438, 1994.
32. M. Calzavara, P. Gambini, M. Puleo, B. Bostica, P. Cinato and E. Vezzoni, "Simultaneous buffering of ATM packets in a multiwavelength optical-fiber-loop memory", *Optical Fiber Communication OFC'94*, paper ThD2, OSA/IEEE, San Jose, 1994.
33. M. Calzavara, P. Gambini, M. Puleo, P. Cinato, E. Vezzoni, F. Delorme and H. Nakajima, "Resolution of ATM cell contention by multiwavelength fiber loop memory", *20th European Conference on Optical Communication ECOC'94*, pp. 567-570, IIC, 1994.
34. P.J. Chidgey, "Multi-wavelength transport networks", *IEEE Comms. Mag.*, 32(12), pp. 28-35, 1994.
35. C.A. Brackett, "Status and early results of the Optical Network Technology Consortium", *Optical Fiber Communication OFC'94*, paper WD3, OSA/IEEE, San Jose, USA, 1994.
36. A.M. Hill, S. Carter, L. Blair, D.J. Pratt, G. Sherlock, R.A. Harmon, S. Culverhouse, M. Searle, J.J. O'Reilly and C. Appleton, "Broad-band upgrade of optical access networks by HDWDM", *20th European Conference on Optical Communication ECOC'94*, pp. 777-780, IIC, 1994.
37. P.J. Legg, D.K. Hunter, I. Andonovic and P.E. Barnsley, "Inter-channel crosstalk phenomena in optical time division multiplexed switching networks", *IEEE Photon. Tech. Lett.*, 6(5), pp. 661-663, 1994.
38. F.E. Glave, "An upper bound on the error probability due to intersymbol interference for correlated signals", *IEEE Trans. Inf. Theory*, 18(3), pp. 356-363, 1972.
39. A.M. Hill and D.B. Payne, "Linear crosstalk in Wavelength Division Multiplexed optical-fiber transmission systems", *J. Lightwave Technol.*, 3(3), pp. 643-650, 1985.

40. D. Marcuse, "Computer simulation of laser photon fluctuations: theory of a single-cavity laser", *IEEE J. Quantum Electron.*, 20(10), pp. 1139-1148, 1984.
41. L. Goldberg, H.F. Taylor, A. Dandridge, J.F. Weller and R.O. Miles, "Spectral characteristics of semiconductor lasers with optical feedback", *IEEE J. Quantum Electron.*, 18(4), pp. 555-564 1982.
42. A. Selvarajan and J.E. Midwinter, "Photonic switches and arrays on LiNbO₃", *Optical and Quantum Electronics*, 21(1), pp. 1-15, 1989.
43. C. Burke, H. Fujiwara, M. Yamaguchi, H. Nishimoto, and H. Honmou, "128 line photonic switching system using LiNbO₃ switch matrices and semiconductor traveling wave amplifiers", *J. Lightwave Technol.*, 10(5), pp. 610-615, 1992.
44. A.M. Hill, *Personal communication*.
45. D.K. Hunter, P.E. Barnsley, I. Andonovic, and B. Culshaw, "Architectures for optical TDM switching", *OE/Fibers '92*, Paper 1787-18, SPIE, Boston, 1992.
46. D.K. Hunter, I. Andonovic, B. Culshaw, and P.E. Barnsley, "Experimental test bed for optical time-domain switching fabrics", *Optical Fiber Communication OFC/IOOC '93*, paper TuO2, OSA/IEEE, San Jose, 1993.
47. D.K. Hunter, P.J. Legg and I. Andonovic, "Architecture for large dilated optical TDM switching networks", *IEE Proc. J*, 140(5), pp. 337-343, 1993.
48. H. Fujiwara, "Optical cross-connect system using photonic switch matrices", paper ThI2, *Optical Fiber Communication OFC'94*, IEEE/OSA, San Jose, U.S.A., February 1994.
49. T.H. Wood, E.C. Carr, B.L. Kasper, R.A. Linke and C.A. Burrus, "Bidirectional fibre-optical transmission using a multiple-quantum-well (MQW) modulator/detector", *Elect. Lett.*, 22(10), pp. 528-529, 1986.
50. S. Yamashita, A. Ohishi, T. Kajimura, M. Inoue and Y. Fukui, "Low-noise AlGaAs lasers grown by organo-metallic vapor phase epitaxy", *IEEE J. Quantum Electron.*, 25(6), pp. 1483-1488, 1989.
51. P.K. Pepeljugoski and K.Y. Lau, "Interferometric noise reduction in fiber-optic links by superposition of high frequency modulation", *J. Lightwave Technol.*, 10(7), pp. 957-963, 1992.
52. A. Yariv, H. Blauvelt and S-W. Wu, "A reduction of interferometric phase-to-intensity conversion noise in fiber links by large index phase modulation of the optical beam", *J. Lightwave Technol.*, 10(7), pp. 978-981, 1992.
53. F.W. Willems and W. Muys, "Suppression of interferometric noise in externally modulated lightwave AM-CATV systems by phase modulation", *Elect. Lett.*, 19(23), pp. 2062-2063, 1993.
54. A. Yariv, *Personal communication*.

55. C-J.L. Van Driel and A.N. Sinha, "How to beat the beat-noise in an SCMA-PON", *20th European Conference on Optical Communication ECOC '94*, pp. 809-812, 1994.
56. P.J. Legg, *unpublished*.

Chapter 3

Theoretical modelling: single interferer

3.1 Introduction

A theoretical understanding of interferometric noise is essential to rationalise the complex behaviour observed on the experimental test-bed and to predict the performance of proposed optical networks. This chapter is devoted to a study of the case of a single interferer. Although not directly applicable to the performance evaluation of real networks, where many noise generating crosstalk terms are likely to exist (see Chapter 4), many of the characteristics derived, such as the noise spectrum, are of relevance. Great insight into the nature of interferometric noise may be gained without the unnecessary complexity of multiple beat components. Furthermore, direct comparison may be made with simple experiments requiring only a single Mach-Zehnder fibre interferometer (this will be undertaken in Chapter 5).

It is assumed that the optical sources are single-mode lasers, e.g. DFB lasers, the polarisations are equal (worst-case), and that the interferometric noise lies at the coherent or incoherent limits. Incoherent noise-free crosstalk is also considered as a special case. Many important properties of interferometric noise- the probability density function (pdf), the power spectral density and the signal-to-interferometric-noise-ratio (SINR)- are derived for the case of a CW waveform corrupted by a single CW crosstalk term. When the waveforms are NRZ ASK externally modulated, the power spectrum is modified by the spectrum of the information; under direct modulation chirp adds further complexity. The bit-error-rate (BER) characteristic, the optical power penalty and the existence of error floors are predicted.

Finally brief remarks are made regarding partial coherence.

3.2 Properties of interferometric noise from CW waveforms

3.2.1 Probability density function (pdf)

The pdf is a required for calculation of the BER

Recall from Chapter 2 that on the mixing of two CW optical waveforms representing the data and crosstalk, having frequency ω_d and ω_x , phase noise $\phi_d(t)$ and $\phi_x(t)$, optical power P_d and P_x , polarisation \underline{p}_d and \underline{p}_x , respectively, the photocurrent i generated by a photodiode of responsivity \mathcal{R} is given by:

$$i / \mathcal{R} = \underbrace{P_d}_{\text{data}} + \underbrace{P_x}_{\text{crosstalk}} + \underbrace{2\sqrt{P_d P_x} \cos\{(\omega_d - \omega_x)t + \phi_d(t) - \phi_x(t)\}}_{\text{interferometric noise}} \underline{p}_d \cdot \underline{p}_x \quad (3.1)$$

When data and crosstalk arise from the same source of frequency ω_0 , coherence time τ_c , linewidth $\Delta\nu$ and phase noise $\phi(t)$, and suffer a differential delay between source and detector of τ , the (phase-induced intensity noise, PIIN) photocurrent noise is:

$$\begin{aligned} i_N &= 2\mathcal{R}\sqrt{P_d P_x} \cos\{\omega_0 \tau + \phi(t) - \phi(t - \tau)\} \underline{p}_d \cdot \underline{p}_x \\ &= 2\mathcal{R}\sqrt{P_d P_x} \cos\{\omega_0 \tau + \Phi(t, \tau)\} \underline{p}_d \cdot \underline{p}_x \end{aligned} \quad (3.2)$$

where $\Phi(t, \tau)$ is a Gaussian distributed random variable of variance $2\pi \Delta\nu \tau$. The statistics of $\omega_0 \tau + \Phi(t, \tau)$ determine the statistics of i_N . In the coherent limit the phase noise $\Phi(t, \tau)$ is negligible but the environmental variation in $\omega_0 \tau$ ensures a uniform distribution $\omega_0 \tau + \Phi(t, \tau)$ over $(-\pi, \pi)$. In the incoherent limit $2\pi \Delta\nu \tau \gg 1$, and again $\omega_0 \tau + \Phi(t, \tau)$ becomes uniformly distributed over $(-\pi, \pi)$. In both cases the pdf of i_N , $p(i_N)$, may be simply calculated since cosine is monotonic in $(0, \pi)$ and even [1]. For aligned polarisations $\underline{p}_d \cdot \underline{p}_x = 1$,

$$p(i_N) = \frac{1}{\pi \sqrt{4\mathcal{R}^2 P_d P_x - i_N^2}} \quad (3.3)$$

This is plotted in Fig. 3.1.

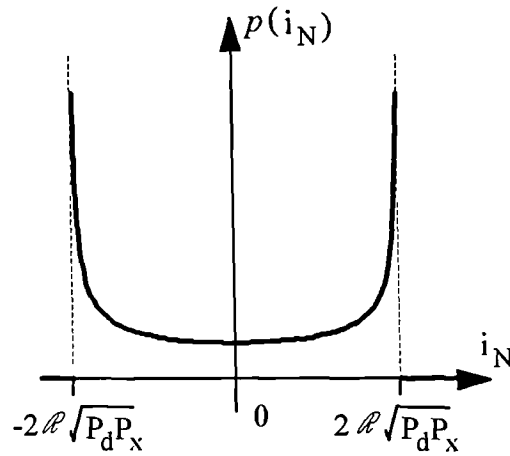


Figure 3.1. Probability density function of interferometric noise at the coherent and incoherent limits.

If the data and crosstalk derive from different lasers whose wavelengths are closely matched the pdf of the phase difference, the argument of the cosine in Eqn. 3.1, is uniform over $(-\pi, \pi)$ and the pdf of i_N is once more given by Eqn. 3.3 (assuming aligned polarisations).

Several mechanisms may induce deviation from this ideal response in real systems-

1. *partial coherence*- this tends to asymmetrise the response which becomes dependent on the phase $\omega_0\tau$ [2].
2. *thermal noise*- the net pdf in the presence of thermal detector noise is formed by convolving the pdf above with the Gaussian pdf of the thermal noise, and is consequently smoother being finite at $\pm 2\Re\sqrt{P_dP_x}$ and non-zero beyond these points (cf. Section 3.5).
3. *receiver bandwidth*- if the receiver bandwidth results in significant filtering of the interferometric noise the averaging process smears out the distribution towards a Gaussian-like shape [2].
4. *multiple paths*- the superposition of multiple crosstalk terms will result in the convolution of many such bounded pdfs, giving a net Gaussian pdf for very many terms (cf. Chapter 4).

3.2.2 Autocorrelation of the interferometric noise

To calculate the power spectrum of the interferometric noise the Fourier Transform is taken of the appropriate autocorrelation function given by the Weiner-Khinchin Theorem [3]:

$$R_N(t) = \langle R_N(t_1+t, t_1) \rangle \quad (3.4)$$

where $R_N(t_1+t, t_1)$ is the statistical ensemble autocorrelation

$$= \overline{i_N(t_1, \tau) i_N(t_1+t, \tau)} \quad \text{and}$$

$\langle \dots \rangle$ and $\overline{\dots}$ denote time and statistical averaging respectively

For a stationary process [3] the statistical autocorrelation is a function of t alone (not t_1) and time averaging is not required. For PIIN with aligned polarisations [4,5]:

$$R_N(t, \tau) = 2\Re^2 P_d P_x \begin{cases} (\cos(2\omega_0 \tau) + 1) \exp(-\sigma^2(\tau)) & |t| > \tau \\ (\cos(2\omega_0 \tau) \exp(-2\sigma^2(\tau - |t|)) + 1) \exp(-\sigma^2(t)) & |t| < \tau \end{cases} \quad (3.5)$$

$$\sigma^2(y) = 2\pi \Delta\nu y$$

If the data and crosstalk terms arise from distinct sources of linewidths $\Delta\nu_d$ and $\Delta\nu_x$, and frequency difference $\Delta\omega$ [4,5]:

$$R_N(t) = 2\Re^2 P_d P_x \cos(\Delta\omega t) \exp(-\sigma_m^2(t))$$

$$\text{where } \sigma_m^2(t) = 2\pi \Delta\nu_m t \quad (3.6)$$

and $\Delta\nu_m = 1/2 (\Delta\nu_d + \Delta\nu_x)$ is the mean linewidth.

3.2.3 Interferometric noise power spectrum

The power spectral density of i_N , $S_N(f)$, may be determined by multiplication of the Fourier Transform of the above autocorrelation expressions by the load resistance R.

For PIIN the single-sided spectrum with the dc term subtracted [6] is -

$$S_N(f) = \frac{4\Re^2 P_d P_x R}{\pi} \left[\frac{\Delta\nu}{f^2 + \Delta\nu^2} \right] \times \left\{ \begin{array}{l} \sin^2(\omega_0 \tau) [1 + \exp(-4\pi\Delta\nu\tau) - 2\exp(-2\pi\Delta\nu\tau) \cos(2\pi f\tau)] \\ + \cos^2(\omega_0 \tau) \left[1 - \exp(-4\pi\Delta\nu\tau) - 2\exp(-2\pi\Delta\nu\tau) \frac{\Delta\nu}{f} \sin(2\pi f\tau) \right] \end{array} \right\} \quad (3.7)$$

In the incoherent limit $2\pi\Delta\nu\tau \gg 1$ (incoherent beat noise crosstalk) the power spectrum approaches a Lorentzian dependence of HWHM (half-width at half maximum) = $\Delta\nu$ (Fig. 3.2(a)):

$$S_N(f) = \frac{4\Re^2 P_d P_x R}{\pi} \left[\frac{\Delta\nu}{f^2 + \Delta\nu^2} \right] \quad (3.8)$$

The power spectrum due to phase noise in the coherent limit is given by Eqn. (3.7) but in many cases the interferometric noise spectrum will be dominated by environmental phase fluctuations. These result in a narrow spectrum of width < 1 kHz (estimated), the detail of which is not of interest since no filtering of this narrowband noise will occur in practical systems.

In the case of mixing between incoherent signals from two sources the (single-sided) spectrum is again found to be approximately Lorentzian with HWHM = mean of the individual linewidths centred at the beat frequency Δf (Fig. 3.2(b)):

$$S_N(f) = \frac{2\Re^2 P_d P_x R}{\pi} \left[\frac{\Delta\nu_m}{(f - \Delta f)^2 + \Delta\nu_m^2} \right] + \frac{2\Re^2 P_d P_x R}{\pi} \left[\frac{\Delta\nu_m}{(f + \Delta f)^2 + \Delta\nu_m^2} \right] \\ \cong \frac{2\Re^2 P_d P_x R}{\pi} \left[\frac{\Delta\nu_m}{(f - \Delta f)^2 + \Delta\nu_m^2} \right] \quad \text{for } \Delta f \gg \Delta\nu_m \quad (3.9)$$

$\Delta\nu_m = 1/2 (\Delta\nu_d + \Delta\nu_x)$ is the mean linewidth

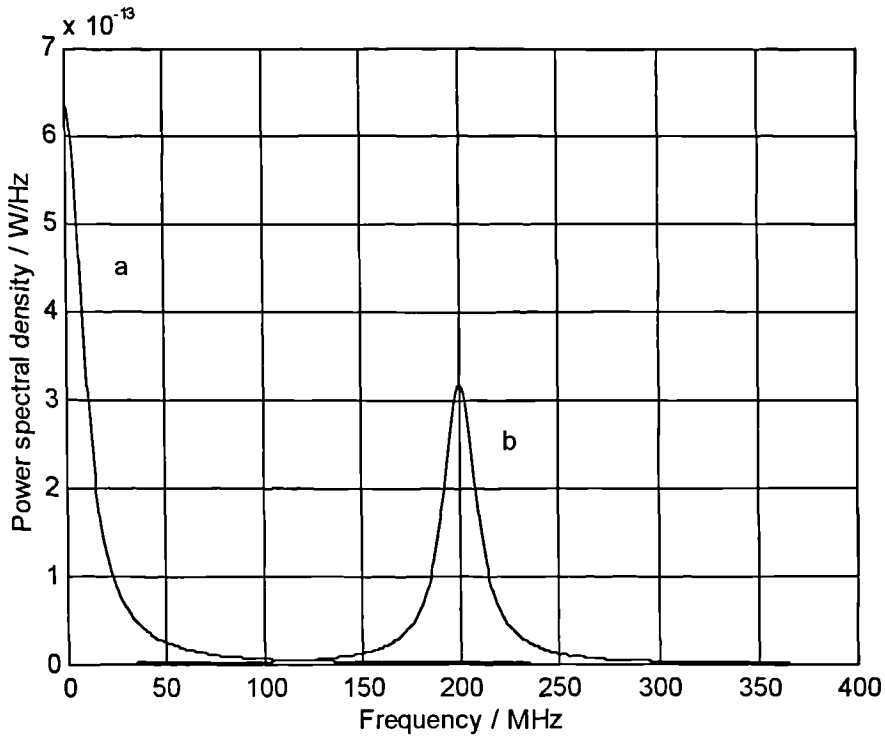


Figure 3.2. Interferometric noise power spectra: (a) a single CW source of linewidth=10 MHz (PIIN), (b) two CW sources of linewidth=10 MHz with beat frequency $\Delta f=200$ MHz. Data power=1mW, crosstalk level=-10dB, responsivity of diode=1A/W, load resistance=50 Ω , and polarisations are equal.

3.2.4 Signal-to-interferometric-noise-ratio (SINR)

The in-band interferometric noise power (electrical), P_N , may be found by integration of the power spectral density over the bandwidth of the receiver, B . The maximum PIIN noise power arises when the $B \gg \Delta\nu$:

$$P_{N,\max} = \int_0^\infty S_N(f)df = \int_0^\infty \frac{4\Re^2 P_d P_x R}{\pi} \left[\frac{\Delta\nu}{f^2 + \Delta\nu^2} \right] df = 2\Re^2 P_d P_x R \quad (3.10)$$

(Alternatively, $R_N(0,\tau)$ can be used to achieve the same result [3]).

The data signal generates a (electrical) power of $\Re^2 P_d^2 R$ (B is chosen to transmit almost all of the data power, maximising the signal to thermal noise ratio). Thus, the minimum SINR is:

$$SINR_{\min} = \frac{\mathfrak{R}^2 P_d^2 R}{2\mathfrak{R}^2 P_d P_x R} = \frac{1}{2 \frac{P_x}{P_d}} = \frac{1}{2 \times \text{crosstalk level } (\xi)} \quad (3.11)$$

The SINR falls as the crosstalk increases. Calculating the rms. intensity noise using Eqn. 3.1, the $SINR_{\text{optical}} = 1/\sqrt{(2\xi)}$ giving a $SINR = 1/(2\xi)$ in agreement with the above calculation. Note that a naive sum of intensities approach would take the $SINR_{\text{optical}} = 1/\xi$, and $SINR = 1/\xi^2$, thus greatly underestimating the noise present. In contrast to the signal to thermal noise ratio (STNR), SINR is independent of the optical power of the data signal.

The general expression for SINR (for PIIN) determined over a bandwidth B is:

$$SINR = \frac{\pi}{2 \tan^{-1}\left(\frac{B}{\Delta\nu}\right)} \left(\frac{1}{2\xi}\right) \quad (3.12)$$

This is plotted in Fig. 3.3. Note:

$$\begin{aligned} \text{If } B = \Delta\nu & \quad SINR = 1/\xi \quad (\text{half of the noise is rejected}) \\ \text{If } B \gg \Delta\nu & \quad SINR = 1/(2\xi) \quad (\text{none of the noise is rejected}) \\ \text{If } B \ll \Delta\nu & \quad SINR = \left(\frac{\pi \Delta\nu}{2B}\right) 1/2\xi \end{aligned}$$

This illustrates a general feature of PIIN, viz. significant noise filtering (and performance improvement) occurs when the noise spectrum is broader than the receiver bandwidth.

When there are two sources (of equal polarisation) integration of the above expression Eqn. (3.9) for the $S_N(f)$ over an infinite bandwidth gives a $SINR = 1/(2\xi)$, equal to that value determined for a single source. If the receiver bandwidth is restricted to B the SINR is given by (Fig. 3.4):

$$SINR = \left(\frac{1}{2\xi}\right) \pi \left/ \left[\tan^{-1}\left(\frac{B+\Delta f}{\Delta\nu}\right) + \tan^{-1}\left(\frac{B-\Delta f}{\Delta\nu}\right) \right] \right. \quad (3.13)$$

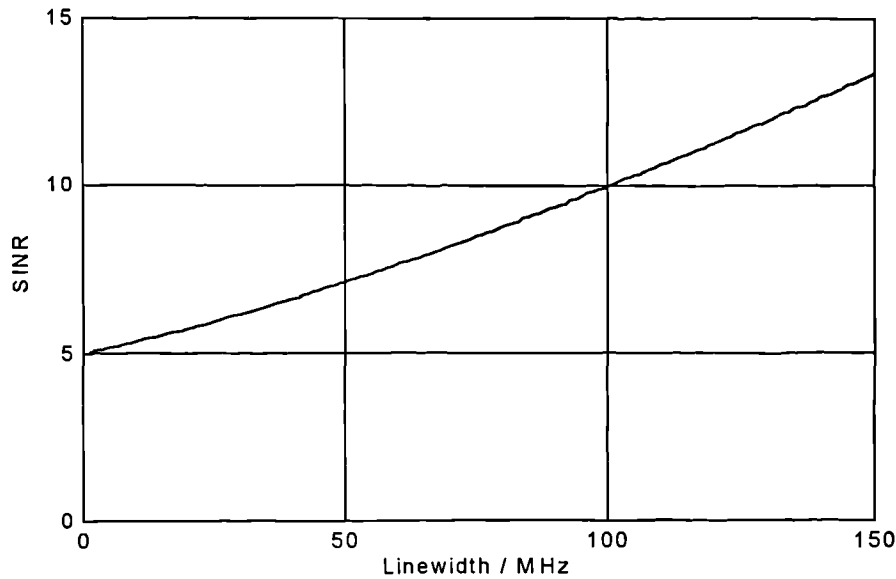


Figure 3.3. Plot of signal-to-interferometric-noise-ratio (SINR) against source linewidth for noise from a single CW source (receiver bandwidth $B=100$ MHz and the crosstalk is -10 dB).

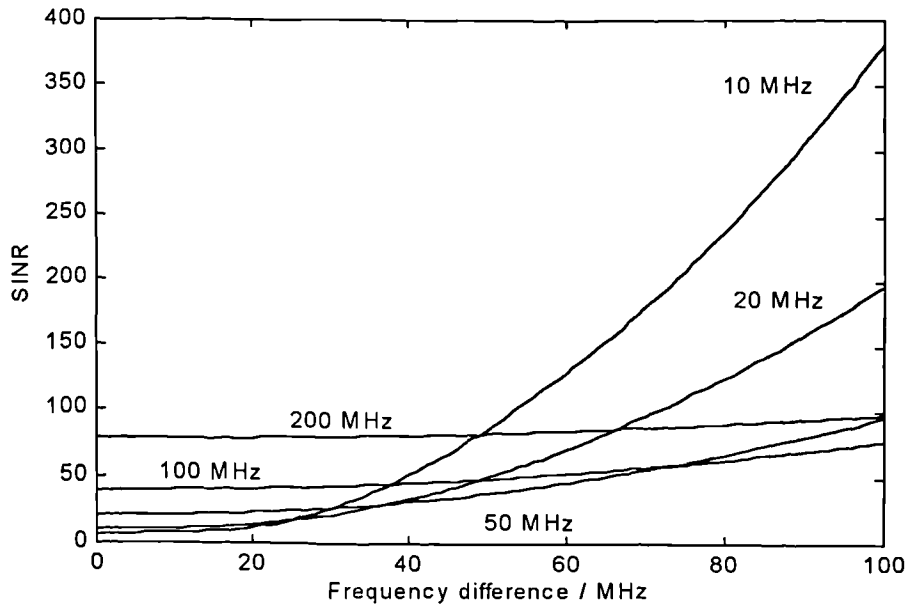


Figure 3.4. Plot of signal-to-interferometric-noise ratio (SINR) for two CW sources separated by Δf for laser linewidths of 10 to 200 MHz. The receiver bandwidth B is 20 MHz, the crosstalk level is -10 dB and the polarisations are equal.

As Δf increases the noise spectrum moves further from baseband and the SINR improves. This explains why, for instance, no interferometric noise is observed on mixing single-mode lasers of 1nm wavelength separation. When $\Delta f < B$, the lasers

with the greatest linewidths give the greatest SINR as was noted in the earlier discussion of a single source. At large Δf the order is reversed - lasers with the smallest linewidths have the smallest overlap of the optical spectra of data and crosstalk, and hence the greatest SINR (cf. Section 3.4).

3.3 Properties of interferometric noise from ASK externally modulated waveforms

Consider the mixing of data and crosstalk waveforms which are NRZ externally amplitude modulated (ASK) by balanced (equal numbers of 'ones' and 'zeros') binary functions $a_d(t)$ and $a_x(t)$ respectively. P_d and P_x are the respective *mean* powers (as before) and it is assumed that the 'zeros' carry no light. This represents the optimum modulation depth of the optical carrier since performance is shown to degrade markedly when the 'zeros' contain light. Telecommunication lasers are typically biased slightly above threshold to reduce the turn-on delay and to damp the turn-on relaxation oscillation; the derived results remain applicable if the power in the 'ones' is much greater (x100 say) than that in the 'zeros' (cf. Section 3.5.7). The external modulation, requiring an integrated-optical modulator, e.g. a lithium niobate Mach Zehnder interferometer, is assumed to be chirp-free implying that the phase of the optical electric field is given by the CW source phase noise as before.

$$E(t) = E_d(t) + E_x(t) \\ \propto \underline{p_d} \sqrt{a_d(t) 2P_d} \exp j(\omega_d t + \phi_d(t)) + \underline{p_x} \sqrt{a_x(t) 2P_x} \exp j(\omega_x t + \phi_x(t)) \quad (3.14)$$

Following square-law envelope detection:

$$i \propto E(t)E^*(t) \\ = 2\Re(\underbrace{P_d a_d(t)}_{\text{data}} + \underbrace{P_x a_x(t)}_{\text{crosstalk}} + 2\sqrt{\underbrace{P_d P_x}_{\text{interferometric noise}} a_d(t) a_x(t)} \cos((\omega_d - \omega_x)t + \phi_d(t) - \phi_x(t))) \underline{p_d} \cdot \underline{p_x} \quad (3.15)$$

The key difference from the CW case is that the noise now depends upon the product of $a_d(t)a_x(t)$, implying that there is only noise when both data and crosstalk are high ('one' bits) - this occurs on average one in every four bits for balanced binary data and crosstalk sequences whose bit boundaries are aligned.

In the case of mixing between waveforms that originate from a single source and suffer a differential delay τ (PIIN) the expression changes to

$$i = 2\Re(P_d a(t) + P_x a(t - \tau) + 2\sqrt{P_d P_x} a(t) a(t - \tau) \cos(\omega_0 \tau + \phi(t) - \phi(t - \tau))) \underline{P_d \cdot P_x} \quad (3.16)$$

3.3.1 Probability density function (pdf)

The pdf of the interferometric noise corrupting the data 'one' bits that suffer crosstalk bits that are also 'one', takes the same bounded form in the coherent and incoherent limits as the CW case (Section 3.3.1):

$$p(i_N) = \frac{1}{\pi \sqrt{16\Re^2 P_d P_x - i_N^2}} \quad (3.17)$$

3.3.2 Autocorrelation of the interferometric noise

Previously the spectral density of the interferometric noise was determined for the case of mixed CW waveforms using the statistics of the phase noise itself, under the assumption of a Lorentzian linewidth. An analogous approach may be followed for modulated waveforms derived from the same source [7]. The time average of the statistical ensemble noise photocurrent autocorrelation is:

$$\begin{aligned} R_N(t, \tau) &= \langle \overline{i_N(t_1, \tau) i_N(t_1 + t, \tau)} \rangle \\ &= 16\Re^2 P_d P_x \left\langle \overline{\sqrt{a(t_1) a(t_1 - \tau) a(t_1 + t) a(t_1 + t - \tau)}} \right\rangle \cdot \\ &\quad \overline{\cos(\omega_0 \tau + \phi(t_1) - \phi(t_1 - \tau)) \cos(\omega_0 \tau + \phi(t_1 + t) - \phi(t_1 + t - \tau))} \end{aligned} \quad (3.18)$$

where as before $\langle \dots \rangle$ and $\overline{\dots}$ denote time and statistical averaging respectively.

3.3.3 Interferometric noise power spectrum

The ensemble (statistical) average above is identical to that calculated in Section 3.1.1 viz. its Fourier Transform is Lorentzian in nature of width $\Delta\nu$. The time average term R_{dd} has a spectrum $S_{dd}(f)$ of bandwidth B equal to the bandwidth of $a(t)$ [7]. Consequently the power spectrum of the noise into resistance R is:

$$S_N(f) = 16\Re^2 P_d P_x R S_{dd}(f) \otimes \text{Lorentzian (width} = \Delta\nu) \quad (3.19)$$

where \otimes denotes the convolution¹.

Thus the noise spectral bandwidth is approximately $B+\Delta\nu$ and negligible filtering occurs if $\Delta\nu \ll B$ (as for a typical externally modulated DFB transmitter ($\Delta\nu \sim 30$ MHz, $B \sim 1$ GHz)). As an example, the convolution of a rectangular function of half-width B , representing $S_{dd}(f)$, with a Lorentzian shape gives (Fig. 3.5):

$$S_N(f) = 16\mathfrak{R}^2 P_d P_x R S_{dd}(f) \otimes \text{Lorentzian (width} = \Delta\nu) \\ = 16\mathfrak{R}^2 P_d P_x R G(f) \otimes \left[\frac{\Delta\nu}{f^2 + \Delta\nu^2} \right] \frac{1}{\pi} \quad (3.20)$$

where $G(f) = 1/(2B) \quad -B \leq f \leq B$
 $0 \quad \text{else}$

$$S_N(f) = \frac{8\mathfrak{R}^2 P_d P_x R}{\pi B} \left\{ \tan^{-1} \left(\frac{B+f}{\Delta\nu} \right) + \tan^{-1} \left(\frac{B-f}{\Delta\nu} \right) \right\} \quad (3.21)$$

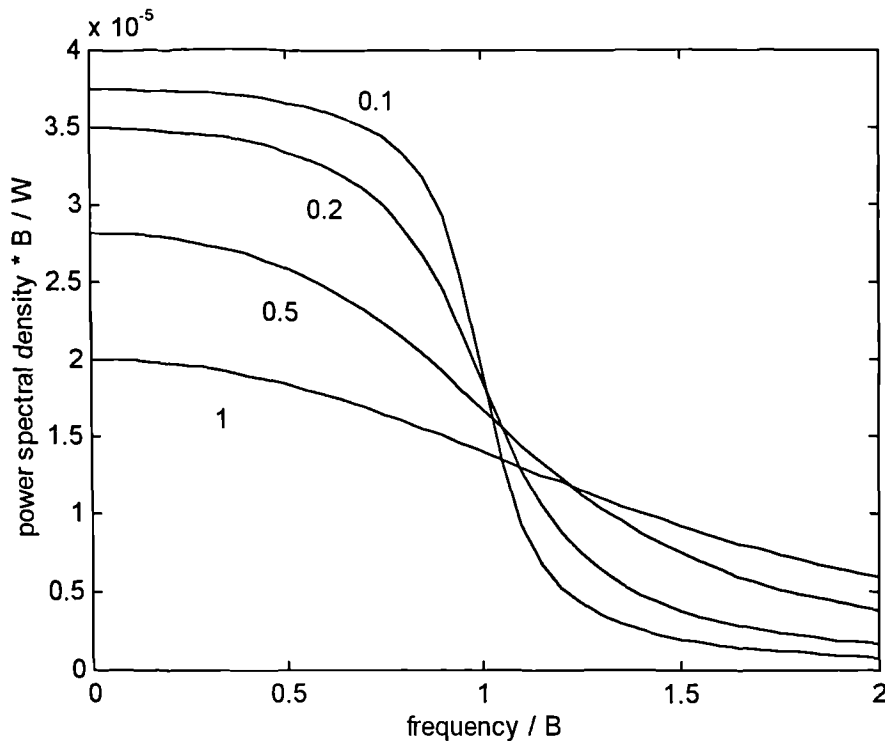


Figure 3.5. Power spectrum of interferometric noise arising from an externally modulated single source for different values of $\Delta\nu / B$ (using Eqn. (3.21)). Data power= $1mW$, crosstalk level= $-10dB$, responsivity of diode= $1A/W$, load resistance= 50Ω , and polarisations are equal.

¹the convolution is defined by - $A(f) \otimes B(f) = \int_{-\infty}^{\infty} A(f_1)B(f - f_1)df_1$

The 3dB bandwidth of the noise is approximately B for small values of $\Delta\nu / B$, e.g. it equals 1.12 B when $\Delta\nu / B=0.5$, but approximates to $\Delta\nu$ when $\Delta\nu$ exceeds B , e.g. it equals 2.24 B when $\Delta\nu / B=2.0$.

3.3.4 Signal-to-interferometric-noise-ratio (SINR)

The SINR (from Eqn. (3.21)) is:

$$\text{SINR} = \left(\frac{1}{2\xi} \right) 2\pi \left\{ 4 \tan^{-1} \left(\frac{2B}{\Delta\nu} \right) - \left(\frac{\Delta\nu}{B} \right) \ln \left(\frac{\Delta\nu^2 + 4B^2}{\Delta\nu^2} \right) \right\}^{-1} \quad (3.22)$$

It is clear from this dependency (Fig. 3.6) that the SINR improves rapidly once the linewidth is more than a few times the receiver bandwidth. However, given an externally modulated DFB source, no noise-filtering will exist.

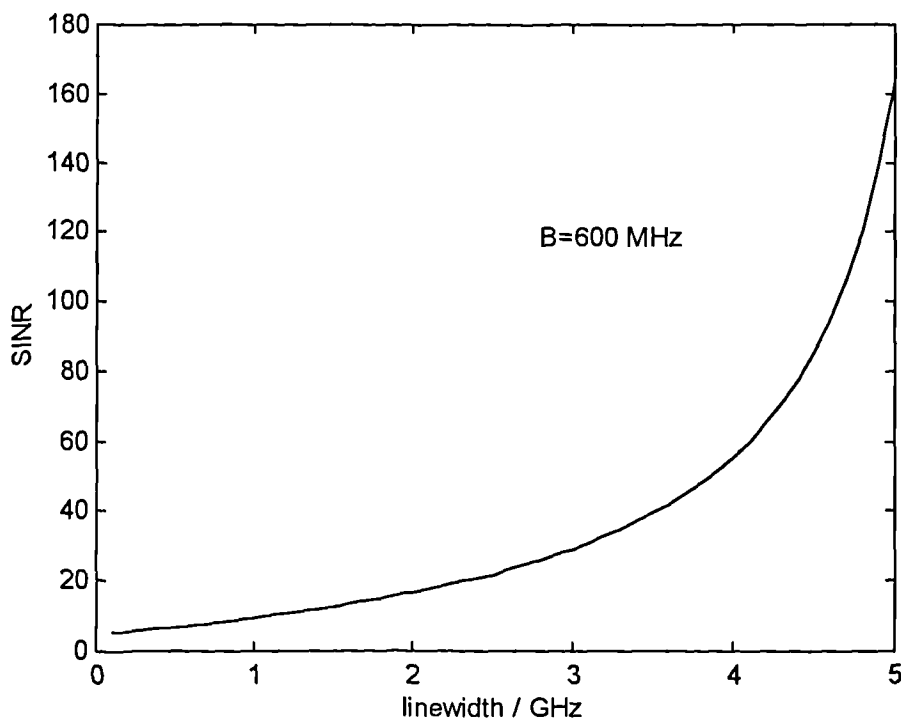


Figure 3.6. Plot of SINR against source linewidth for noise due to an externally modulated single source according to Eqn. (3.22). Data power=1mW, crosstalk level=-10dB, responsivity of diode=1A/W, load resistance=50Ω

In the coherent limit the interferometric noise spectrum will have bandwidth $\sim B$ since the phase fluctuation is narrowband. No noise will be filtered.

When the crosstalk and data derive from two sources the Lorentzian spectrum (width= $\Delta\nu_m$) centred at the beat frequency is convolved with the spectrum due to the modulation ($S_{dd}(f)$) to give the noise spectrum. This remains centred at the beat frequency and, using the previous method, the half-spectrum is shown in Fig. 3.5. If the beat frequency $< B$ then the SINR will vary in a similar fashion to Fig. 3.6; otherwise the SINR will fall as the linewidth is increased (cf. Fig. 3.4).

3.4 Properties of interferometric noise from ASK directly modulated waveforms

In practise, unless dispersion is the performance limiting parameter in the optical link, direct modulation of the laser is simpler and cheaper than external modulation. Although the pdf of (unfiltered) interferometric noise is unchanged from Eqn. 3.17, the noise power spectrum differs because direct modulation adds unwanted phase modulation to the amplitude modulated waveform. The data is encoded onto the optical medium by modulation of the free carrier density (via the injection current) and this in turn modulates the refractive index of the lasing medium, and hence the emission phase / frequency, according to the Kramers-Kronig relation [8], referred to as chirp [9,10].

Transient chirp (often called simply chirp) at the rising and falling edges of pulses, has a magnitude proportional to the rate of change of the modulation current (0.2 to 0.8 nm has been reported in the literature [9]), and a duration of approximately half of the laser relaxation period - hence the label 'transient'. Adiabatic chirp [11] arising because the equilibrated carrier density differs for 'ones' and 'zeros', being constant over a bit interval, is typically far smaller. Measurements of these forms of chirp are reported in Chapter 7.

A rigorous analysis of interferometric noise for directly modulated lasers is impractical since the influence on the laser phase is not well understood. Undoubtedly direct modulation leads to a reduction in the laser coherence time. One description takes the coherence of the modulated source to be the same as that of a CW source of linewidth equal to the modulated laser spectral width. The coherence

time is the reciprocal of the modulated linewidth. Hence, the coherence time is expected to fall as the modulation depth and transient chirp is increased.

An alternative approach considers the phase change during the transient chirp frequency oscillations. The frequency evolution is thought to vary in some random fashion from one bit to another so that the phase information is lost after every transition. Certainly if the laser is switched off there is no light to transfer the phase information from one 'one' bit to another. This implies a coherence time equal to the bit period, and therefore a noise spectrum $\sim 2B$, independent of the modulation depth or linewidth measurement. Experiment should support one explanation or the other.

A novel approach has been proposed by Nazarathy [12] which makes no assumptions on the phase noise or the laser lineshape but is only applicable to mutually incoherent signals. This method is valid for the mixing of signals from 1) two different sources or 2) from a single source in the incoherent limit. The expressions for the power spectrum of the interferometric noise are summarised in Table 3.1.

		power spectrum of the interferometric noise
PIIN incoherent limit	CW waveforms	autocorrelation of laser lineshape (the lineshape is the power spectrum of the complex E field down-shifted to baseband)
	NRZ modulated	self-convolution of the power spectra of the real E field
two lasers	CW waveforms	convolution of the power spectra of the real E fields
	NRZ modulated	convolution of the power spectra of the real E fields ²

Table 3.1. Nature of the power spectrum of the interferometric noise according to Nazarathy [12].

These results predict the following:

²Assuming that the time integral of the product of the autocorrelations of the two E fields is separable [12].

- for PIIN with CW waveforms of Lorentzian spectra of FWHM $=\Delta\nu$ the noise spectrum is also Lorentzian with HWHM of $\Delta\nu$ (as in Eqn. 3.8).
- for PIIN with NRZ modulated optical spectra of FWHM= Y the noise spectrum has HWHM of
 - Y taking the optical spectrum to be Lorentzian in shape
 - $(1/\sqrt{2}) Y$, taking the optical spectrum to be Gaussian in shape.
- for two CW sources of Lorentzian lineshapes of width $\Delta\nu_d$ and $\Delta\nu_x$, the Lorentzian noise spectrum is centred at the beat frequency and has a HWHM= $\frac{1}{2} (\Delta\nu_d + \Delta\nu_x)$ (as in Eqn. 3.9).
- for two modulated sources with optical spectra of FWHM= Y_d and Y_x the noise spectrum is centred at the beat frequency and has a HWHM of
 - $\frac{1}{2} (Y_d + Y_x)$ taking the optical spectrum to be Lorentzian in shape
 - $\frac{1}{2} \sqrt{(Y_d^2 + Y_x^2)}$ taking the optical spectrum to be Gaussian in shape.

The latter leads to an important conclusion: since chirp broadens the optical spectrum of the directly modulated laser, it also broadens the interferometric noise spectrum implying better performance compared to external modulation [13,14]. If the spectral width of the laser is equal to the transient chirp, typically several 10's of GHz, no degradation owing to interferometric noise would ever be expected, in contradiction to many observations [3,11,12]. Instead the spectral width must be rather smaller than the chirp: little power is carried during the short-lived transient oscillations. In experiment (Chapter 7) pattern dependent noise filtering has been observed for direct modulation and has been successfully explained by intra-bit frequency changes (that are not transient or adiabatic chirp). Bits of the pattern which show the most noise still show less than theory predicts, thought to be due to noise spectral broadening due to transient chirp.

3.5 Estimation of BER, power penalty and error floor

3.5.1 Preliminaries

The objective of this section is to accurately estimate the system performance degradation due to interferometric noise from the single interferer in the absence of noise filtering. The results are therefore applicable to externally modulated and low-chirp directly modulated sources. Performance is measured by the bit-error-rate (BER), the optical power penalty (relative to a system free of crosstalk), and the

position of the error floor. Estimation of the BER permits calculation of the other two parameters.

The BER is determined by integration of the probability density function (pdf) of the photocurrent of the transmitted bits between the limits of the decision threshold and $\pm \infty$, for 'zeros' and 'ones', respectively. The pdf of the interferometric noise is assumed to be either the theoretical bounded form determined in Section 3.2, or to be Gaussian. The latter is only applicable to the single interferer problem when the interferometric noise is strongly filtered at the receiver. However, the treatment offers an introduction to the later description of multiple interferers and serves to illustrate the importance of noise statistics in BER calculation. The Gaussian pdf of the thermal receiver noise is convolved with that of the interferometric noise to give the pdf of the net photocurrent noise.

The following assumptions (for nomenclature see Table 3.3) are made:

bit alignment - the message and crosstalk waveforms shall be taken to be perfectly bit-aligned, i.e. their bit boundaries are matched, although their sequences will differ in general.

pulse shape - the optical pulses shall be assumed to be perfectly rectangular.

bit classification - the bit-alignment assumption above leads to a consideration of four different types of bits present in the message signal (Table 3.2, Fig. 3.7).

optical contrast ratio - the laser diode is taken to be biased precisely at threshold so that the 'zeros' have zero intensity (the general case is addressed in Section 3.5.7).

These assumptions reduce the complexity of the BER calculation. If the pulse shape is indeed rectangular, the method below accurately predicts the performance in the absence of bit alignment - the crosstalk power at the decision point takes the same values with the same probability as in the bit-aligned case. However, if the pulse shape is non-rectangular the noise variance at the decision point is maximised under bit-alignment (peak of data bit aligns with peak of crosstalk bit) - the analysis below therefore represents the worst-case in this respect.

symbol	data	crosstalk	result
<u>a</u>	'one'	'one'	interferometric noise
<u>b</u>	'one'	'zero'	no corruption, perfect 'one' bit
<u>c</u>	'zero'	'one'	crosstalk 'one' bit, no interferometric noise
<u>d</u>	'zero'	'zero'	zero photocurrent

Table 3.2. The bit classification.

All photocurrents are normalised (without loss of generality) to that induced by a (crosstalk-free) 'one' bit:

Data signal

data 'one' (no crosstalk) $i=1$
data 'zero' (no crosstalk) $i=0$

Crosstalk signal

crosstalk 'one' (no data) $i=\xi$
crosstalk 'zero' (no data) $i=0$

Noise

thermal noise variance(i_{rms}^2)= σ_0^2
thermal noise variance+
interferometric noise variance on a bits= σ_1^2
signal to thermal noise ratio (STNR)= $1 / \sigma_0^2$

Receiver

decision threshold, D $0 \leq D \leq 1$
optical power penalty= ΔP

$$erfc(x) = 1 - erf(x) = 1 - 2\pi^{-0.5} \int_0^x e^{-i^2} di \quad (3.23)$$

Table 3.3. Nomenclature for BER calculation given a single interferer

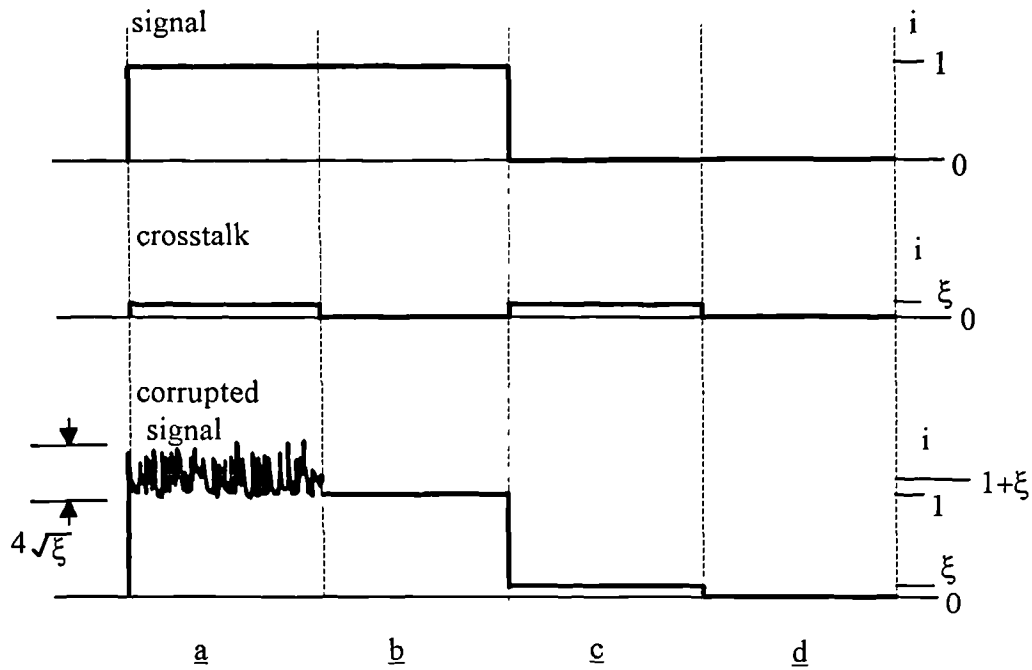


Figure 3.7. The bit classification¹

The error probabilities for each of the four cases must be determined and they are likely to be very different in magnitude, the greatest being for a and c bits.

probability density function - the pdf of the interferometric noise may take one of two forms:

$$i) \quad p(i) = \frac{1}{\pi\sqrt{4\xi - i^2}} \quad (3.24) \text{ (cf. Eqn. 3.17)}$$

this is applicable in the coherent and incoherent limits with no noise filtering;

$$ii) \quad p(i) = e^{-i^2/4\xi} / \sqrt{4\pi\xi} \quad (3.25)$$

a zero mean Gaussian with $\sigma^2 = 2\xi$. This pdf greatly simplifies the

¹the intensity noise on bit a is representative of that which would be seen on an oscilloscope given a repeating bit sequence. If individual a bits could be examined the intensity would be approximately constant over the bit duration but would differ from one a bit to the next - the bandwidth of this intensity noise is only approximately $B + \Delta\nu$, not $20B$ as the figure may suggest.

mathematics (because the convolution with the Gaussian thermal noise remains Gaussian of $\sigma^2 = \sigma_0^2 + 2\xi$) but overestimates the error count unless the averaging effects discussed in Section 3.2.1 are present.

decision level setting - this may be chosen according to

- i) given a balanced binary sequence, zero crosstalk and photodiode detection, D is set half way between 'zero' and 'one' levels, at 0.5, to minimise the BER (shot noise is neglected). If this setting is maintained in the presence of crosstalk then the error probability of a bits is dominant. This approximates to an AC-coupled receiver whose threshold would wander slightly about a mean photocurrent of zero, or $0.5(1+\xi)$ in the above.

or

- ii) D is optimised to minimise the overall BER - the approach employed in the experiments.

photodetector - a PIN photodiode with negligible shot noise was assumed.

thermal noise - this has a Gaussian pdf :

$$p_{th}(i) = \frac{e^{-i^2/2\sigma_0^2}}{\sqrt{2\pi\sigma_0^2}} \quad (3.26)$$

3.5.2 BER calculation employing bounded pdf

In this calculation the pdf of the photocurrent noise on the a bits is determined by convolving the bound interferometric noise pdf Eqn. 3.24 with the Gaussian pdf of the thermal noise (the two noise sources are independent [1]), extending previous work [15]. Assuming a random balanced bit sequence, the BER may be written as a (equally) weighted sum of the error probabilities of the bits in the classification:

$$BER = 1/4(P_{e_a} + P_{e_b} + P_{e_c} + P_{e_d}) \quad (3.27)$$

bit class a

$p_{\text{net}}(i)$ = thermal noise pdf \otimes interferometric noise pdf

$$= p_{\text{th}}(i) \otimes p(i-1-\xi)$$

$$P_{\text{ea}} = \int_{-\infty}^D p_{\text{net}}(i) di$$

$$= 1 - \int_{-\infty}^{1+\xi-D} p_{\text{th}}(i) \otimes p(i) di$$

$$= 1 - F_{\text{a}}(D) \quad (3.28)$$

$$F_{\text{a}}(D) = \int_{-\infty}^{i=1+\xi-D} \int_{-\infty}^{i_1=\infty} p(i_1) p_{\text{th}}(i-i_1) di_1 di$$

$$= \int_{-\infty}^{i=1+\xi-D} \int_{-2\sqrt{\xi}}^{i_1=2\sqrt{\xi}} \frac{1}{\pi\sqrt{4\xi-i_1^2}} \frac{1}{\sqrt{2\pi\sigma_0^2}} \exp\left(\frac{-(i-i_1)^2}{2\sigma_0^2}\right) di_1 di \quad (3.29)$$

Substituting $s=(i-i_1)/(2\sigma_0)$ and performing the i integral first -

$$F_{\text{a}}(D) = \frac{\sqrt{2}\sigma_0}{\sqrt{2\pi^3\sigma_0^2}} \int_{-2\sqrt{\xi}}^{i_1=2\sqrt{\xi}} \frac{1}{\sqrt{4\xi-i_1^2}} \int_{-\infty}^{\frac{1+\xi-D-i_1}{\sqrt{2}\sigma_0}} \exp(-s^2) ds di_1$$

$$= \frac{1}{2\pi} \int_{-2\sqrt{\xi}}^{i_1=2\sqrt{\xi}} \frac{1}{\sqrt{4\xi-i_1^2}} \left\{ \text{erf}\left(\frac{1+\xi-D-i_1}{\sqrt{2}\sigma_0}\right) + 1 \right\} di_1 \quad (3.30)$$

substituting $t = i_1/2\sqrt{\xi}$

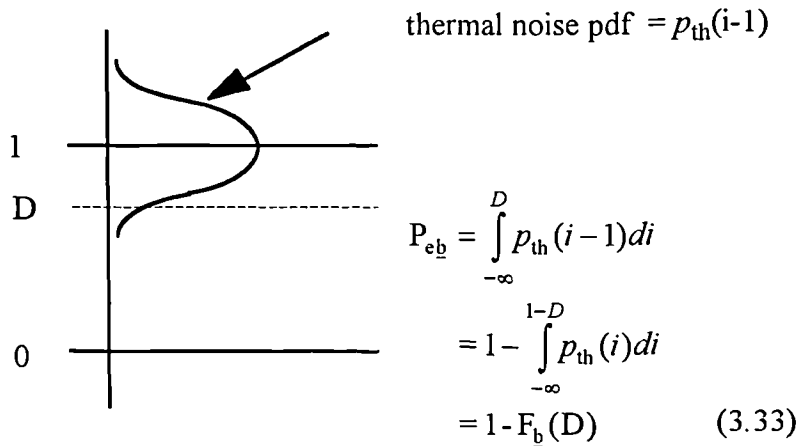
$$F_{\text{a}}(D) = \frac{1}{2\pi} \int_{-1}^1 \frac{1}{\sqrt{1-t^2}} \left\{ \text{erf}\left(\frac{1+\xi-D-2t\sqrt{\xi}}{\sqrt{2}\sigma_0}\right) + 1 \right\} dt \quad (3.31)$$

substituting $t = \sin\theta$

$$\begin{aligned}
 F_a(D) &= \frac{1}{2\pi} \int_{-\pi/2}^{\pi/2} \frac{1}{\sqrt{1-\sin^2\theta}} \left\{ \operatorname{erf}\left(\frac{1+\xi-D-2\sqrt{\xi}\sin\theta}{\sqrt{2}\sigma_0}\right) + 1 \right\} \cos\theta d\theta \\
 &= \frac{1}{2\pi} \int_{-\pi/2}^{\pi/2} \operatorname{erf}\left(\frac{1+\xi-D-2\sqrt{\xi}\sin\theta}{\sqrt{2}\sigma_0}\right) + 1 d\theta \\
 &= 1/2 + \frac{1}{2\pi} \int_{-\pi/2}^{\pi/2} \operatorname{erf}\left(\frac{1+\xi-D-2\sqrt{\xi}\sin\theta}{\sqrt{2}\sigma_0}\right) d\theta \quad (3.32)
 \end{aligned}$$

This expression can be evaluated numerically .

bit class b



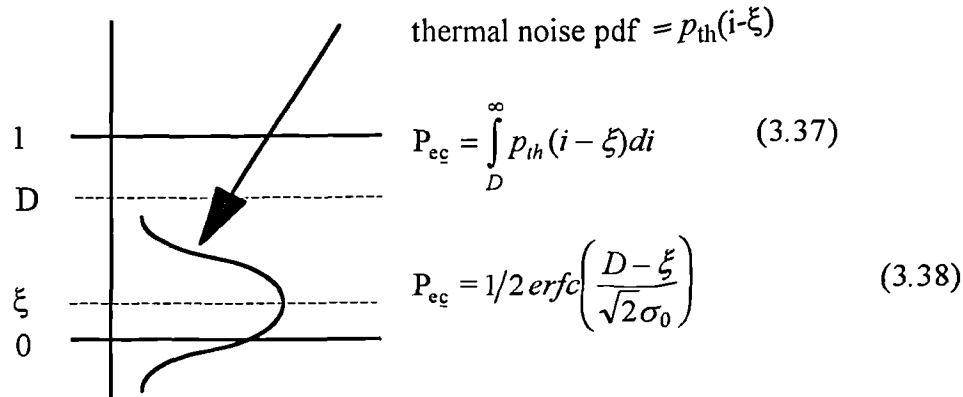
$$F_b(D) = \int_{-\infty}^{1-D} \frac{1}{\sqrt{2\pi\sigma_0^2}} \exp\left(\frac{-i^2}{2\sigma_0^2}\right) di \quad (3.34)$$

substituting $s = i / (\sqrt{2}\sigma_0)$

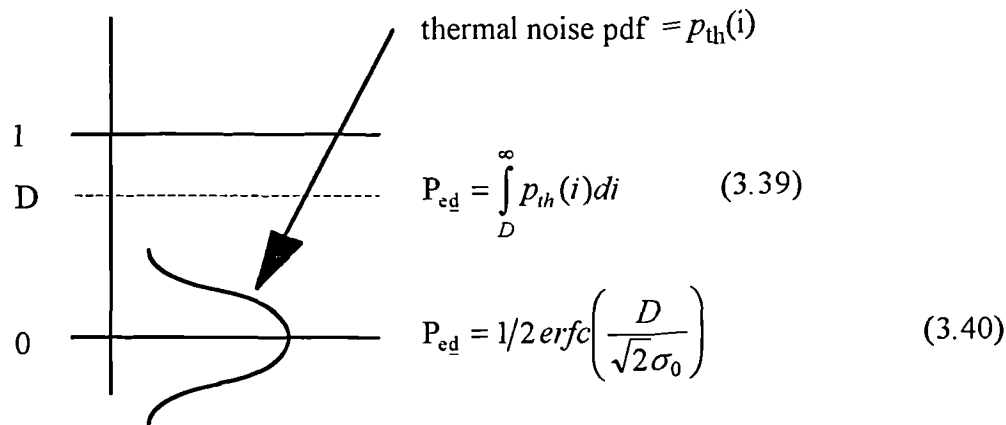
$$\begin{aligned}
 F_b(D) &= \int_{-\infty}^{(1-D)/(\sqrt{2}\sigma_0)} \frac{1}{\sqrt{\pi}} \exp(-s^2) ds \\
 &= 1/2 + 1/2 \operatorname{erf}\left(\frac{1-D}{\sqrt{2}\sigma_0}\right) \quad (3.35)
 \end{aligned}$$

$$P_{eb} = 1/2 \operatorname{erfc}\left(\frac{1-D}{\sqrt{2}\sigma_0}\right) \quad (3.36)$$

bit class c



bit class d



Thus

$$\text{BER} = 1/4 \left\{ 1 - F_a(D) + 1/2 \operatorname{erfc}\left(\frac{1-D}{\sqrt{2}\sigma_0}\right) + 1/2 \operatorname{erfc}\left(\frac{D-\xi}{\sqrt{2}\sigma_0}\right) + 1/2 \operatorname{erfc}\left(\frac{D}{\sqrt{2}\sigma_0}\right) \right\} \quad (3.41)$$

The expression Eqn. (3.36) was evaluated by a FORTRAN program - the integral within $F_a(D)$ was determined numerically using a NAG routine. The program output was carefully checked against known results (e.g. the 'back-to-back' curve, $\xi=0$, was compared against $1/2 \operatorname{erfc}(1/(2\sigma_0\sqrt{2}))$) and the predictions of Tur [15]. The calculated BER is plotted against the STNR ($=1/\sigma_0^2$) in Fig. 3.8. The STNR was chosen instead

of the received optical power, as would be employed in an experimental BER characterisation, for several reasons. The plot is independent of the sensitivity of the receiver (this equals the required optical power to give a BER=10⁻⁹ when there is no crosstalk). In a BER characterisation, the thermal noise variance is fixed so that the STNR is proportional to the data optical power squared - the theoretical curve is therefore very similar to the experimental plot but differs because the contribution to the mean optical power from the crosstalk is not included. The additional optical power required to recover a BER=10⁻⁹ when crosstalk is present is simply the horizontal separation of the zero crosstalk ('back-to-back') and non-zero crosstalk theoretical curves measured at BER=10⁻⁹; this is the power penalty of interest. In contrast, measurements taken from the experimental curves must be corrected for contribution of the crosstalk to the received power.

The BER curves (Fig. 3.8) show a pronounced improvement in performance when D is optimised. No error floors are apparent. The imbalance between the noise corrupting the \underline{a} and \underline{c} bits (which dominate the BER expression) leads to an optimum threshold of less than 0.5.

3.5.3 BER calculation employing a Gaussian interferometric noise pdf

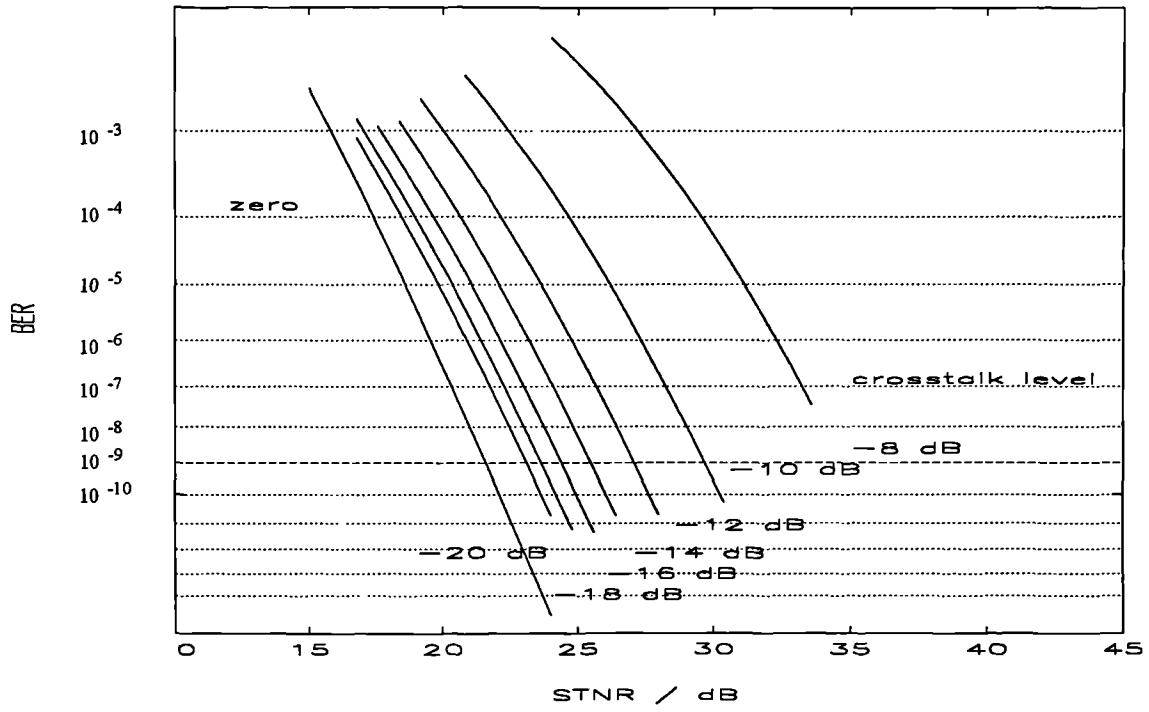
The BER is given by:

$$\text{BER} = 1/4 (P_{e\underline{a}} + P_{e\underline{b}} + P_{e\underline{c}} + P_{e\underline{d}})$$

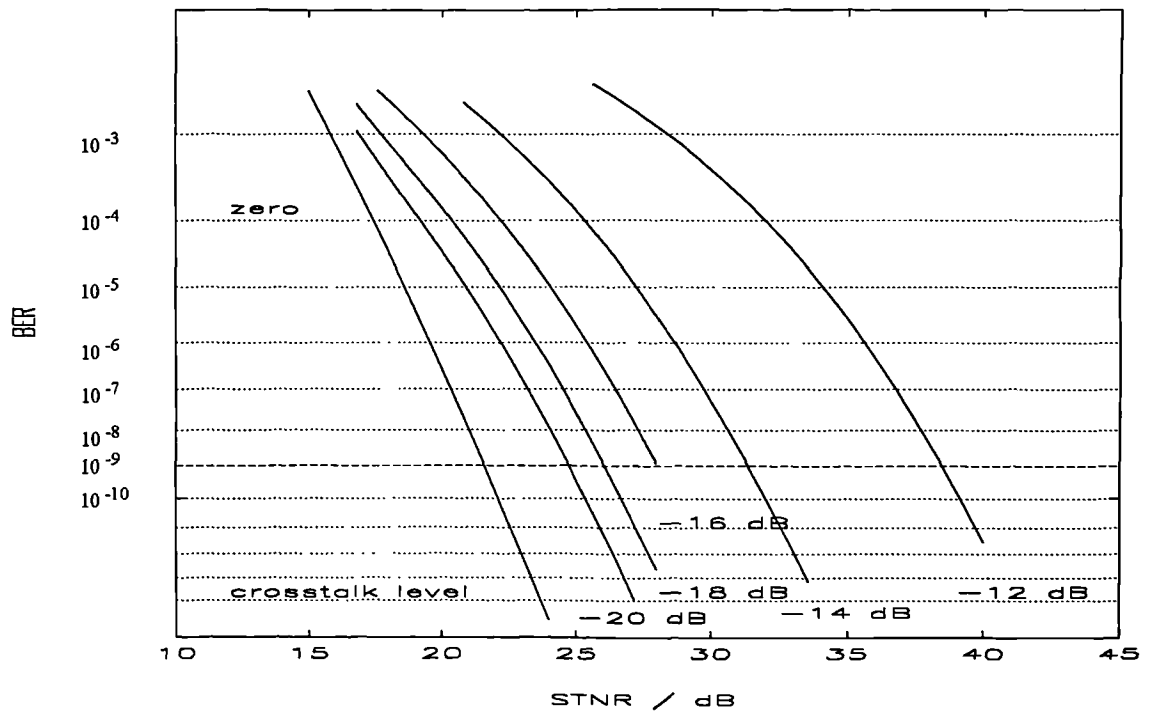
$$= 1/8 \left\{ \text{erfc} \left(\frac{1 + \xi - D}{\sqrt{2}\sigma_1} \right) + \text{erfc} \left(\frac{1 - D}{\sqrt{2}\sigma_0} \right) + \text{erfc} \left(\frac{D - \xi}{\sqrt{2}\sigma_0} \right) + \text{erfc} \left(\frac{D}{\sqrt{2}\sigma_0} \right) \right\} \quad (3.42)$$

$$\sigma_1^2 = \sigma_0^2 + 2\xi$$

The curvature of the BER lines (Fig. 3.9) may be understood by considering the contribution of the crosstalk induced interferometric noise relative to the (fixed) thermal noise as the data power is varied. At low signal levels, low STNR, high BER, the interferometric noise is also low (the SINR=1/(2ξ) is fixed) and the thermal noise is dominant - the BER curve is similar to the back-to-back (zero crosstalk) line. However, as the signal power is increased the thermal noise remains unchanged whilst the interferometric noise grows and dominates; since the SINR is independent of the signal level the curve becomes increasingly flat as it approaches the error floor. Again error performance is better when the threshold is optimised.

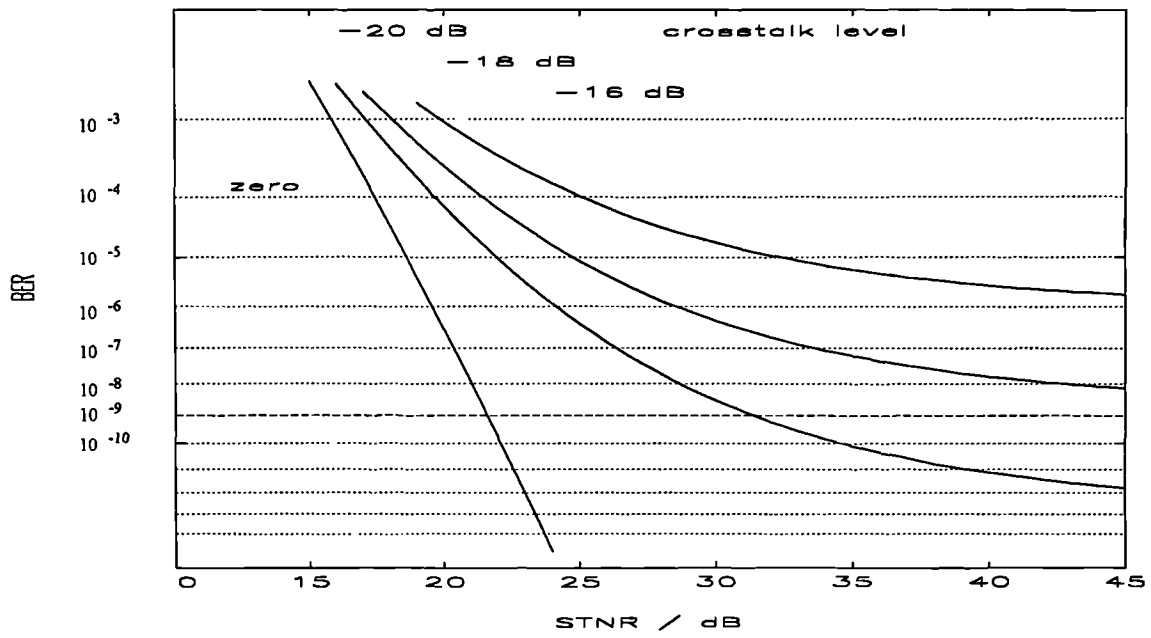


(a)

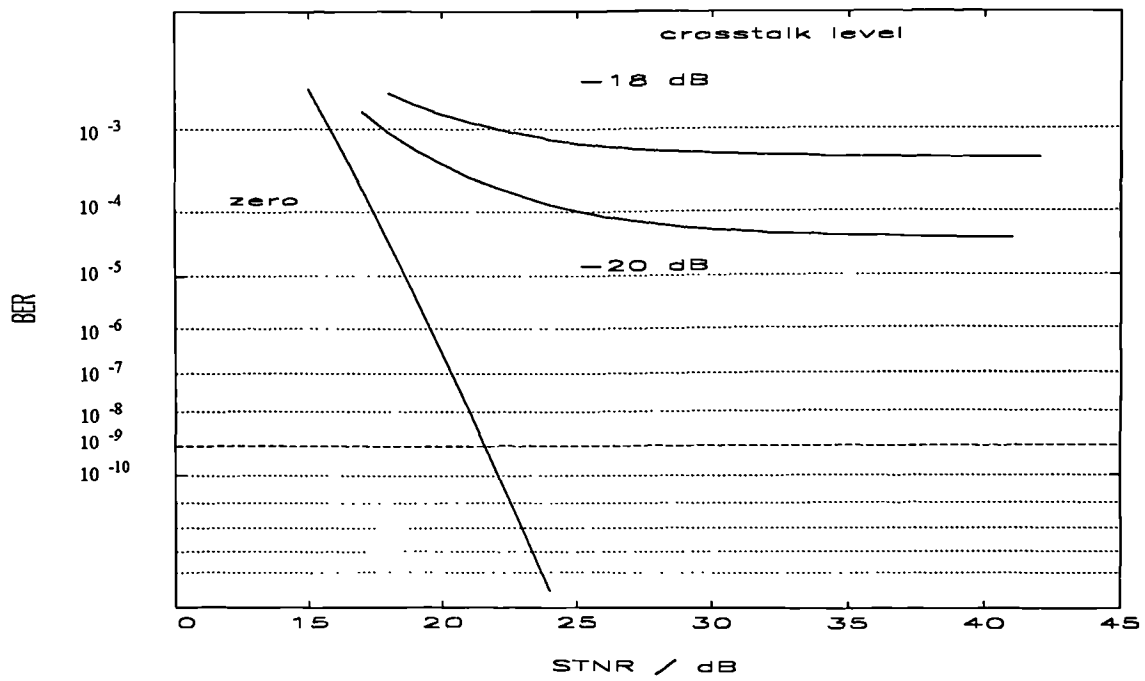


(b)

Figure 3.8. BER curves for a single interferer calculated assuming bounded interferometric noise: (a) D optimised, (b) $D=0.5$.



(a)



(b)

Figure 3.9. BER curves for a single interferer calculated assuming Gaussian interferometric noise: (a) D optimised, (b) $D=0.5$.

The differences between the behaviour shown in Fig. 3.8 and Fig. 3.9 may be better understood by examining Fig. 3.10 where the net pdf of the \underline{a} bits is plotted for a crosstalk level of -16 dB for several values of STNR. The curves were calculated by convolving the interferometric noise, taken to be (a) bounded, and (b) Gaussian, with Gaussian thermal noise. The bounded noise gives a smaller power penalty because the pdf is more tightly bound to the mean value. Increasing the signal-to-thermal noise-ratio (STNR) draws in the 'skirt' of the pdf and reduces the BER; for Gaussian interferometric noise this occurs most rapidly at small STNR whilst little improvement is attained at large STNR, in agreement with Fig. 3.9. However, for bounded noise the skirt draws in more slowly, but the BER continues to fall without limit. No error floor will exist provided that the threshold falls outside the limits of the bounded pdf.

3.5.4 BER for incoherent noise-free crosstalk

The BER performance of a data signal corrupted by crosstalk that generates no in-band interferometric noise (i.e. incoherent noise-free crosstalk, cf. Section 2.22), may be determined from Eqn. 3.42 by setting the interferometric noise variance to zero:

$$\text{BER} = \frac{1}{8} \left\{ \text{erfc} \left(\frac{1 + \xi - D}{\sqrt{2}\sigma_0} \right) + \text{erfc} \left(\frac{1 - D}{\sqrt{2}\sigma_0} \right) + \text{erfc} \left(\frac{D - \xi}{\sqrt{2}\sigma_0} \right) + \text{erfc} \left(\frac{D}{\sqrt{2}\sigma_0} \right) \right\} \quad (3.43)$$

The optimum value of D equalises the error probabilities of \underline{b} and \underline{c} bits since they dominate the BER. Thus $D = (1 + \xi)/2$. Substituting into Eqn. 3.43 gives:

$$\text{BER} = \frac{1}{4} \left\{ \text{erfc} \left(\frac{1 + \xi}{2\sqrt{2}\sigma_0} \right) + \text{erfc} \left(\frac{1 - \xi}{2\sqrt{2}\sigma_0} \right) \right\} \quad (3.44)$$

If $D = 0.5$ then substitution into Eqn. 3.43 gives:

$$\text{BER} = \frac{1}{8} \left\{ \text{erfc} \left(\frac{0.5 + \xi}{\sqrt{2}\sigma_0} \right) + \text{erfc} \left(\frac{0.5}{\sqrt{2}\sigma_0} \right) + \text{erfc} \left(\frac{0.5 - \xi}{\sqrt{2}\sigma_0} \right) + \text{erfc} \left(\frac{0.5}{\sqrt{2}\sigma_0} \right) \right\} \quad (3.45)$$

The BER is plotted against STNR for different values of crosstalk in Fig. 3.11.

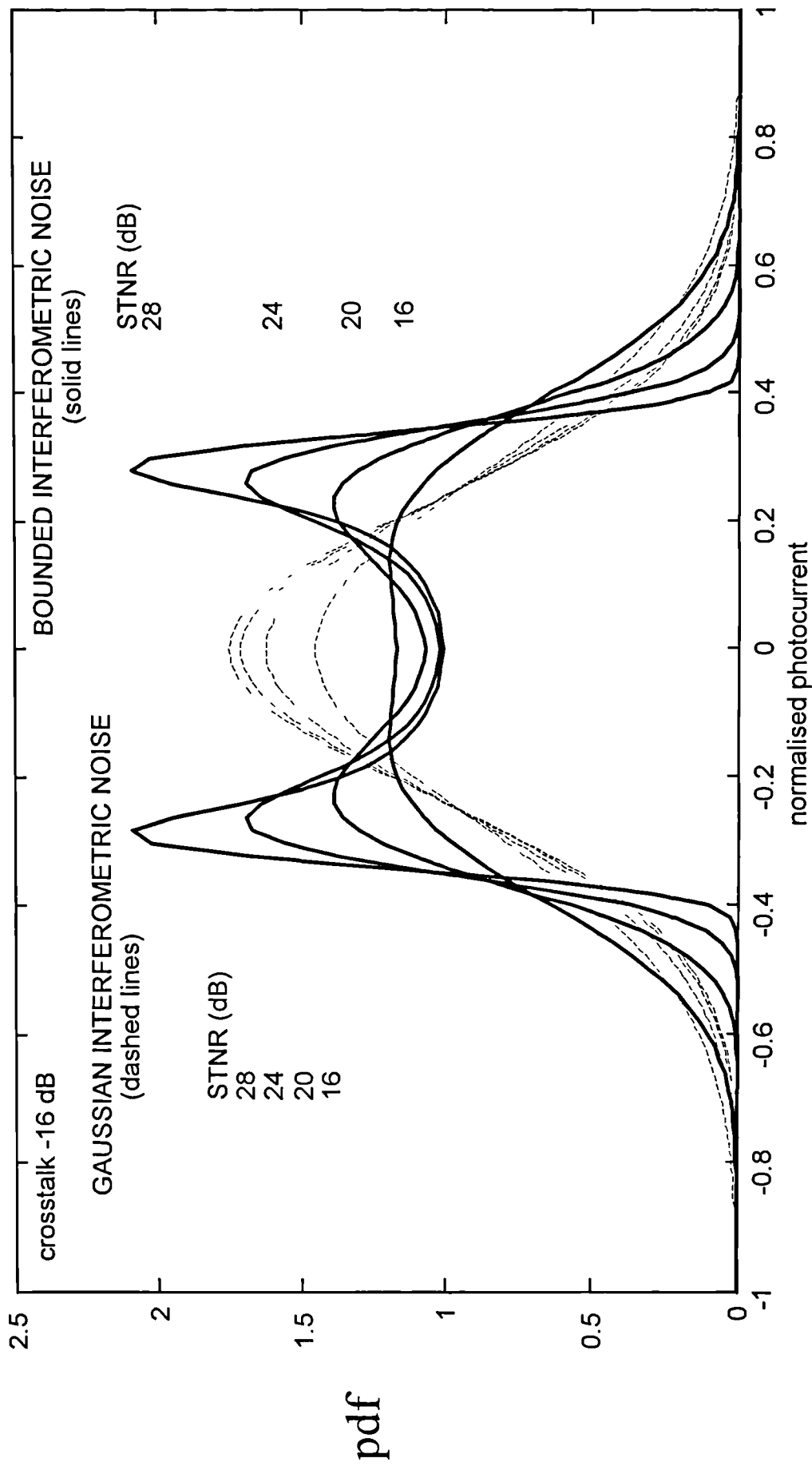
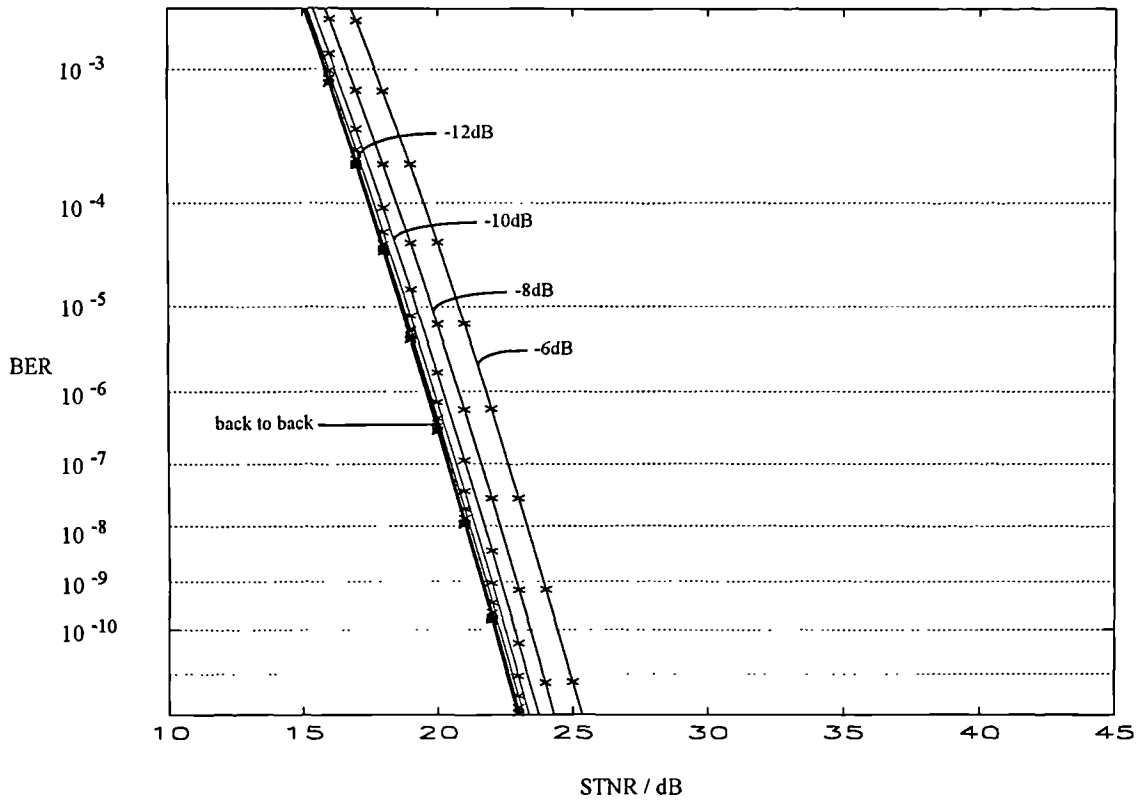
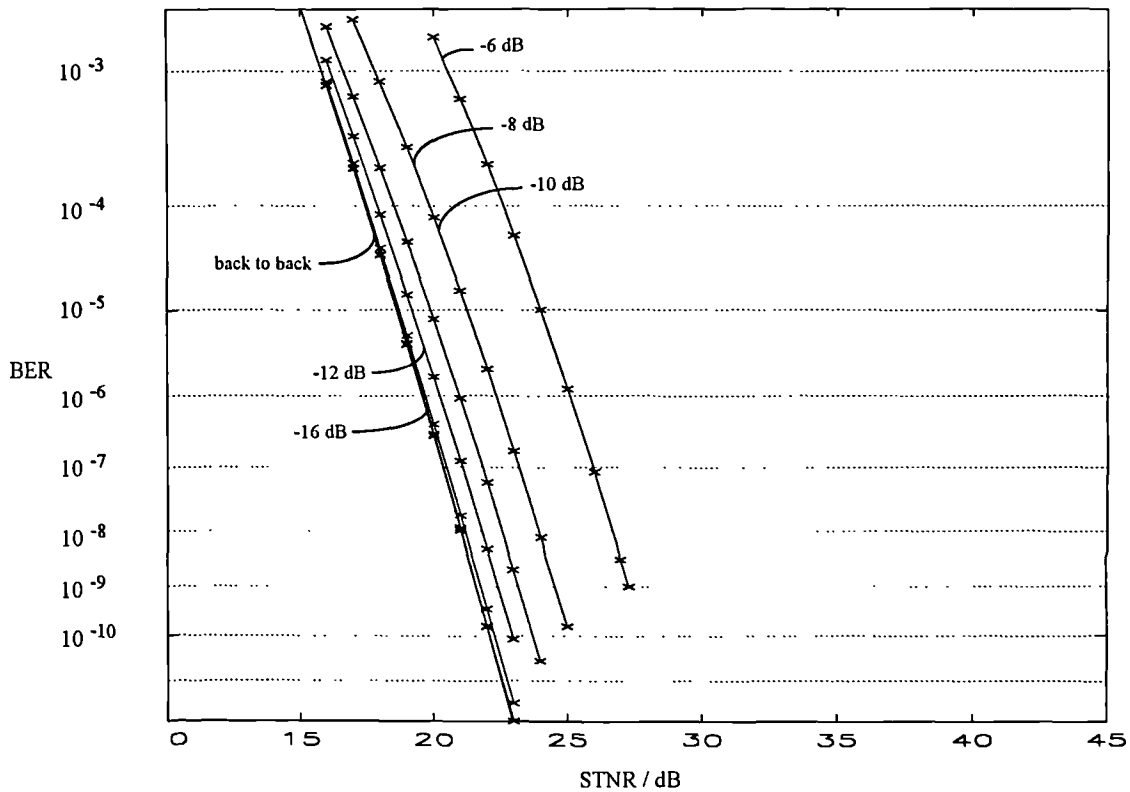


Figure 3.10. Calculated probability density functions of a bits: (a) bounded interferometric noise, (b) Gaussian interferometric noise.



(a)



(b)

Figure 3.11. BER curves for a single interferer calculated for incoherent noise-free crosstalk: (a) D optimised, (b) $D=0.5$.

In the absence of interferometric noise the data transmission is tolerant to very large amounts of crosstalk. If optimum thresholding is employed, no error flooring will occur since D can always be placed between ξ and 1 (provided $\xi < 1$). If D is fixed at 0.5, error flooring will be present for $\xi > 0.5$ (-3 dB). The eye-closure method [$\Delta P = -10 \log(1-\xi)$ (3.46) [16]) gives very similar results to the D optimised calculation Eqn. 3.44.

3.5.5 Optical power penalties

The optical power penalty represents the increase in optical power required to recover the same error rate that would exist in the absence of crosstalk (cf. Section 3.5.2).

The dependence of the optical power penalty at $\text{BER} = 10^{-9}$ on the crosstalk level is depicted in Fig. 3.12. All interferometric noise curves demonstrate an asymptote where the power penalty goes rapidly to infinity, corresponding to the existence of an error floor at $\text{BER} = 10^{-9}$. If the crosstalk is increased beyond the asymptotic value, the data may still be recovered but with a BER exceeding 10^{-9} . The models employing the Gaussian approximation predict a greater penalty than the bounded approach. Surprisingly the apparently simplistic eye-closure method ($\Delta P = -10 \log(1-2\sqrt{\xi})$ (3.47) [16,17]) closely follows the calculation assuming a bounded pdf and optimised threshold. In contrast, the curves for incoherent noise-free crosstalk demonstrate little performance degradation.

3.5.6. Error floors

Error floors are characterised by a minimum value of the BER which cannot be improved upon no matter how great the optical power incident upon the detector. In the single interferer scenario, as the incident optical power is increased the interferometric noise also increases (their ratio is invariant, cf. Section 2.6) whilst the thermal noise is unchanged - the BER falls. Eventually thermal noise may be neglected - if the BER is non-zero an error floor exists.

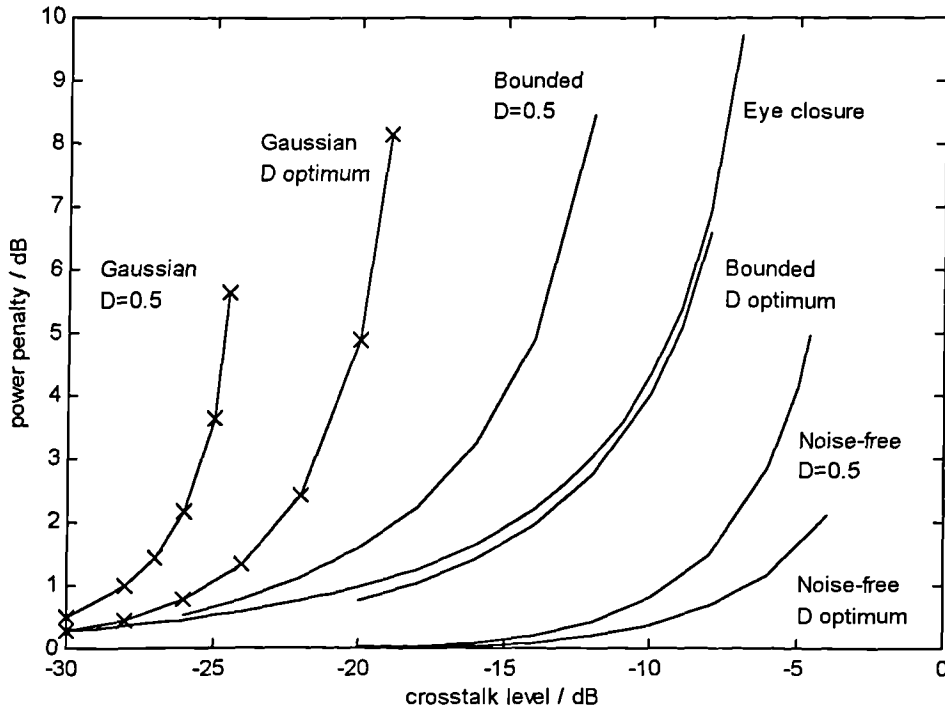


Figure 3.12. Theoretical dependence of optical power penalty (at BER=10⁻⁹) owing to a single interferer on crosstalk level (ξ).

i) Bounded interferometric noise

In the coherent and incoherent limits the intensity noise is bound to a $\pm 2\sqrt{\xi}$ variation about the signal power of $1+\xi$. Under the limiting condition of no thermal noise the error probability of b, c and d bits is zero. Thus considering a bits alone:

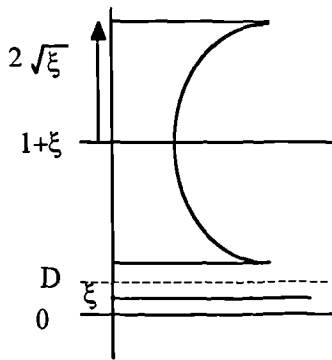
$$\begin{aligned}
 \text{BER} &= 0.25 \int_{-\infty}^D p(i-1-\xi) di \\
 &= 0.25 \int_{1+\xi-D}^{2\sqrt{\xi}} p(i) di \\
 &= 0.25 \int_{1+\xi-D}^{2\sqrt{\xi}} \frac{1}{\pi\sqrt{4\xi-i^2}} di \quad (3.47)
 \end{aligned}$$

substituting $i = 2\sqrt{\xi} \sin \theta$

$$\begin{aligned} \text{BER} &= \int_{\sin^{-1}((1+\xi-D)/2\sqrt{\xi})}^{\pi/2} \frac{1}{4\pi\sqrt{4\xi} \cos \theta} 2\sqrt{\xi} \cos \theta d\theta \\ &= \frac{\pi/2 - \sin^{-1}((1+\xi-D)/2\sqrt{\xi})}{4\pi} \end{aligned} \quad (3.48)$$

Considering the two decision level approaches -

a) D set to minimise the BER (optimised)



The setting of D is governed by minimising the error probability for a bits (whilst avoiding errors on c bits).

$$1 + \xi - 2\sqrt{\xi} > D > \xi$$

is required to prevent error flooring. Error flooring will occur when

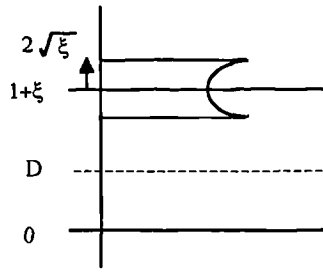
$$\begin{aligned} 1 + \xi - 2\sqrt{\xi} < \xi \\ \text{i.e. } \xi > 1/4 \quad (-6 \text{ dB}) \end{aligned} \quad (3.49)$$

For $\xi > -6$ dB the BER is minimised by setting $D=\xi$. Substitution into Eqn. 3.48 gives

$$\text{error floor} = \frac{\pi/2 - \sin^{-1}(1/(2\sqrt{\xi}))}{4\pi} \quad (3.50)$$

This is plotted in Fig. 3.13(a).

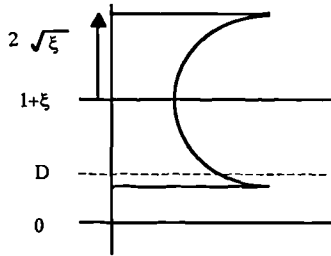
b) $D=0.5$



The error probability of a bits dominates for $D=0.5$. If

$$2\sqrt{\xi} - \xi < 0.5$$

the noise fluctuation (in the absence of thermal noise) does not cross D and no error flooring occurs.



If $2\sqrt{\xi} - \xi > 0.5$, i.e.

$$\xi > \frac{3 - 2\sqrt{2}}{2} \quad (-10.6 \text{ dB}) \quad (3.51)$$

then error flooring will occur. Substituting $D=0.5$ into Eqn. 3.48 gives (Fig. 3.13(b)):

$$\text{error floor} = \frac{\pi/2 - \sin^{-1}((0.5 + \xi)/2\sqrt{\xi})}{4\pi} \quad (3.52)$$

In conclusion, an error floor only exists at high crosstalk when the BER rises rapidly.

ii) Gaussian intensity noise

If the intensity noise is assumed to be Gaussian, there will always be an error floor because the pdf is unbounded. Under the limiting condition of no thermal noise the error probability of b, c and d bits is zero. Thus considering a bits alone -

$$\text{BER} = 1/4 [1/2 \text{erfc}((1+\xi-D)/\sqrt{(2)\sigma})] \quad (3.53)$$

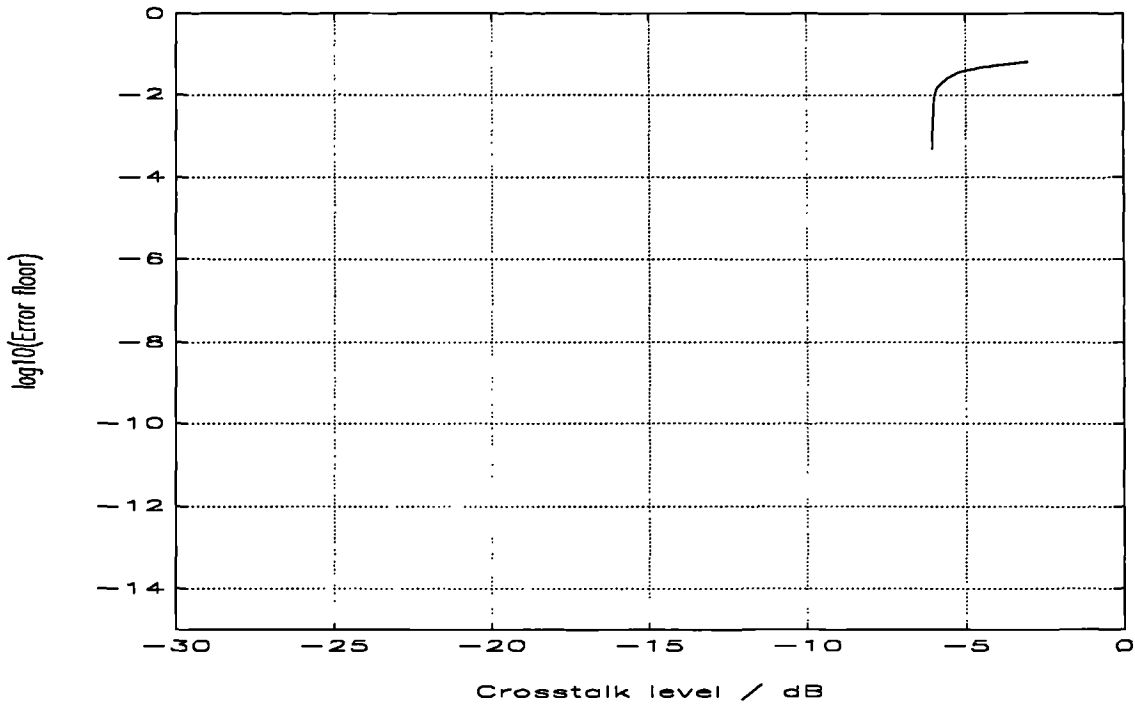
where σ is the standard deviation of the intensity noise,
 $= \sqrt{(2\xi)}$

Considering the two decision level approaches, the BER is minimised by setting $D=\xi$ giving (Fig. 3.14(a)):

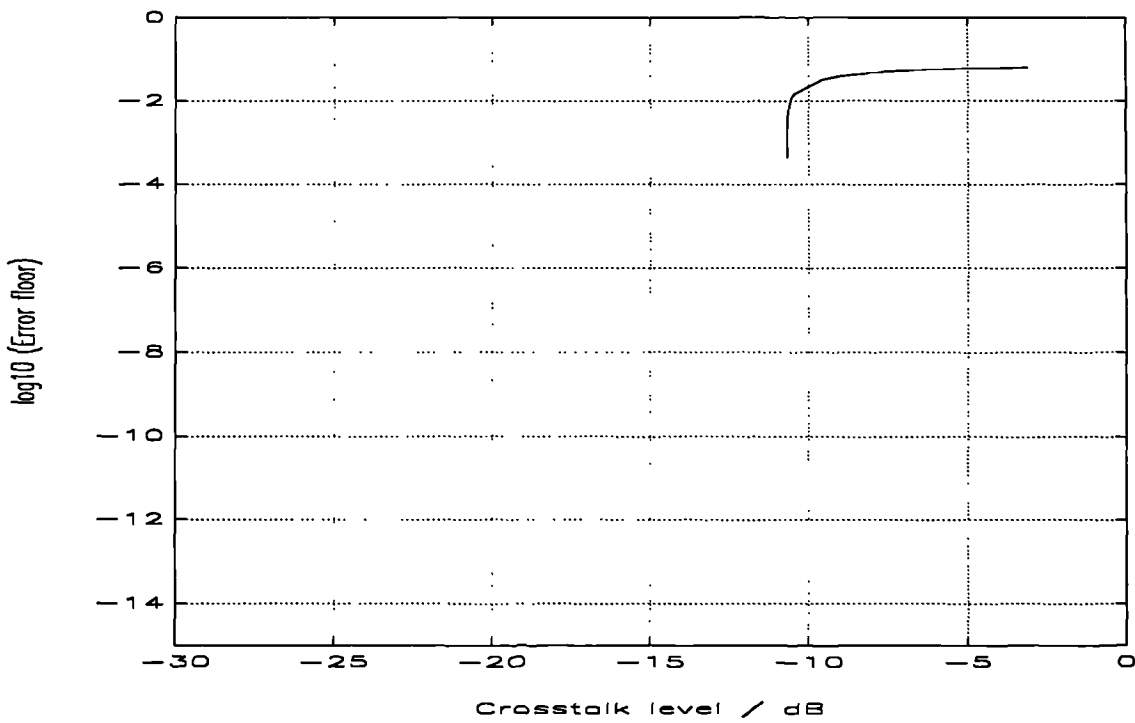
$$\text{error floor} = 1/8 \text{erfc}(1/\sqrt{(2)\sigma}) \quad (3.54)$$

For $D=0.5$ (Fig. 3.14(b)):

$$\text{error floor} = 1/8 \text{erfc}((0.5+\xi)/(2\sqrt{\xi})) \quad (3.55)$$

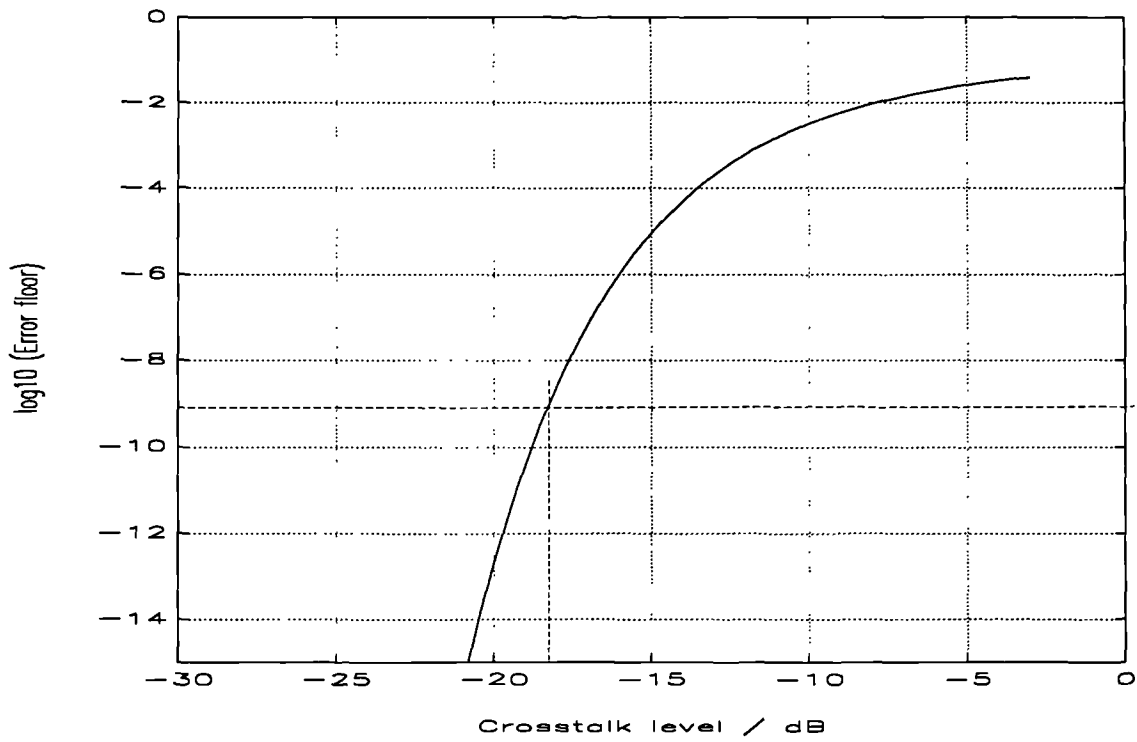


(a)

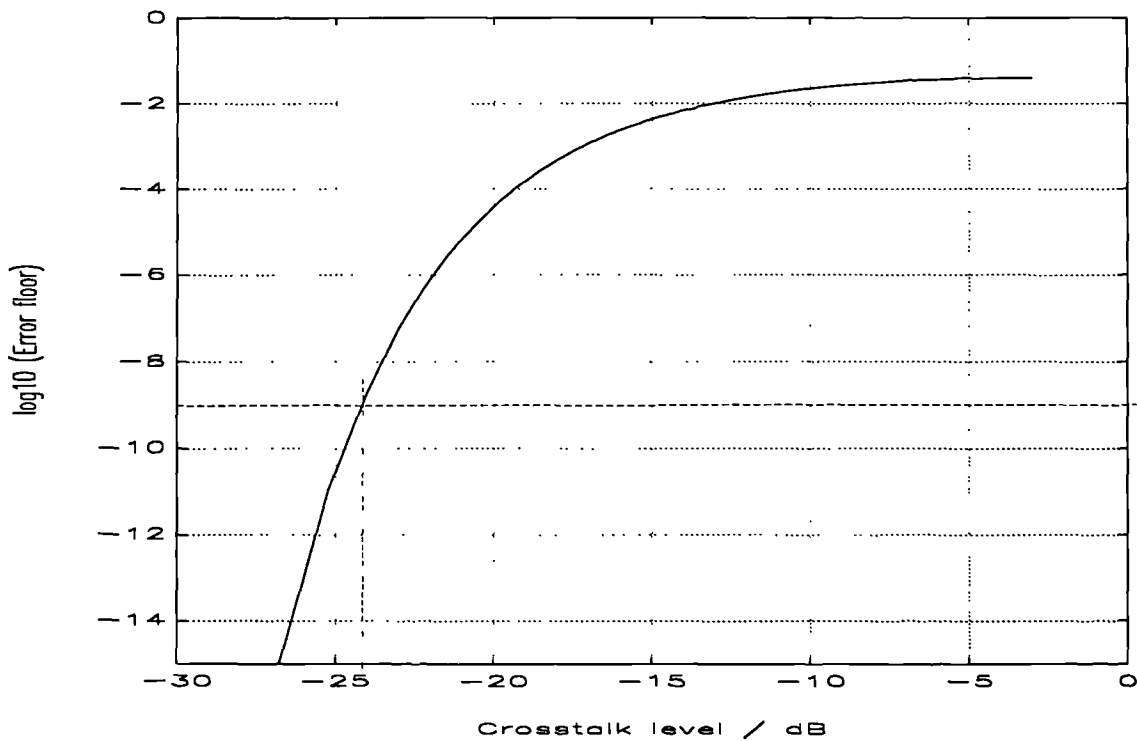


(b)

Figure 3.13. Theoretical dependence of error floor on crosstalk level under the assumption of bounded interferometric noise: (a) D optimised, (b) $D=0.5$.



(a)



(b)

Figure 3.14. Theoretical dependence of error floor on crosstalk level under the assumption of Gaussian interferometric noise: (a) D optimised, (b) $D=0.5$.

3.5.7 Performance with finite modulation depth

If the directly modulated laser is biased above threshold or the external modulator has a poor extinction ratio between on and off states, then the 'zero' bits will carry optical power. In the absence of crosstalk, this results in an increase in BER compared to the ideal case considered previously, given the same mean power - the eye opening is smaller. If crosstalk is present then interferometric noise will be generated on all four bits of the classification and the performance is degraded further. Therefore performance degrades markedly as a greater share of the mean power is carried by the 'zeros'.

The nomenclature is modified as follows: the normalised current owing to a data 'one' remains equal to 1, but that owing to a 'zero' now equals α ; the crosstalk signal has the same modulation depth as the data but its mean power is smaller by the crosstalk level ξ . The power penalty due to the addition of the crosstalk and the (bounded) interferometric noise thus generated for D optimised is estimated by the eye-closure method [16]:

$$\Delta P = -10 \log \left(1 - \frac{2\sqrt{\xi}(1+\sqrt{\alpha})}{1-\alpha} \right) \quad (3.56)$$

This dependency is depicted in Fig. 3.15. The penalty increases with an increase in α ; the crosstalk value at the asymptote is 10.7 dB greater for $\alpha=0.5$ than for $\alpha=0$. The position of the asymptote is given by:

$$\text{crosstalk at asymptote (dB)} = \left(\frac{1-\alpha}{2(1+\sqrt{\alpha})} \right)^2 \quad (3.57)$$

If the receiver is AC-coupled, the decision threshold D is set to $(1+\alpha)/2$. The larger α becomes, the smaller the separation of the means of the noise on a and c bits from D, and therefore the greater the penalty. In fact, as before, the error probability of the a bits dominates the BER even if α is large. The ratio of the interferometric noise standard deviation on the a bits to the c bits is equal to $1/\sqrt{\alpha}$. Given a large value of α , 0.5, the error contribution of the c bits is approximately that given by the a bit expression but with a crosstalk level reduction of 3 dB. Looking at Fig. 3.8(b) it is

clear that the \underline{a} bits dominate unless the crosstalk is small (< -20 dB). The penalty may be quantified using Eqn. 3.32 but here it will be sufficient to conclude that the penalty will exceed that for D optimised, which increases rapidly with α , and it is very important to maximise the modulation depth.

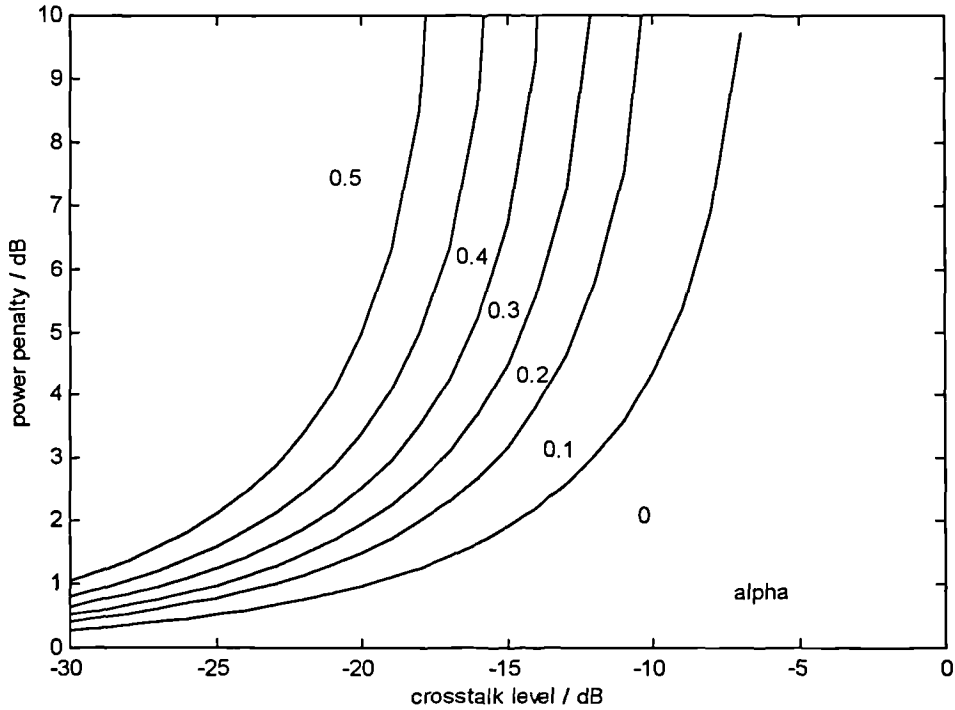


Figure 3.15. Power penalty versus crosstalk level owing to bounded interferometric noise from a single interferer by the eye-closure method. D is optimised and α is the ratio of optical power in the 'zero' to that in the 'one'.

3.6 Partial coherence

Interferometric noise may be described as partially coherent when the data and crosstalk arise from the same source with a differential delay that lies between the extremes of the coherent and incoherent limits. The pdf depends upon $\omega_0\tau$, being asymmetric (Fig. 3.16) except when the data and crosstalk are in quadrature [2]. This greatly assists identification, but implies a performance dependency on the exact value of $\omega_0\tau$.

Two factors imply that the partially coherent interferometric noise may be smaller and therefore less problematic than incoherent beat noise:

- the phase noise change is smaller giving a smaller photocurrent variation and a smaller noise power spectral density (in the absence of environmental fluctuation).
- the interferometric noise spectral width is approximately $= 1/\tau$, which is greater than that for incoherent beat noise ($=\text{linewidth } \Delta\nu$). As τ increases, the cut-off draws in until $\Delta\nu$ is reached (CW case [10]).

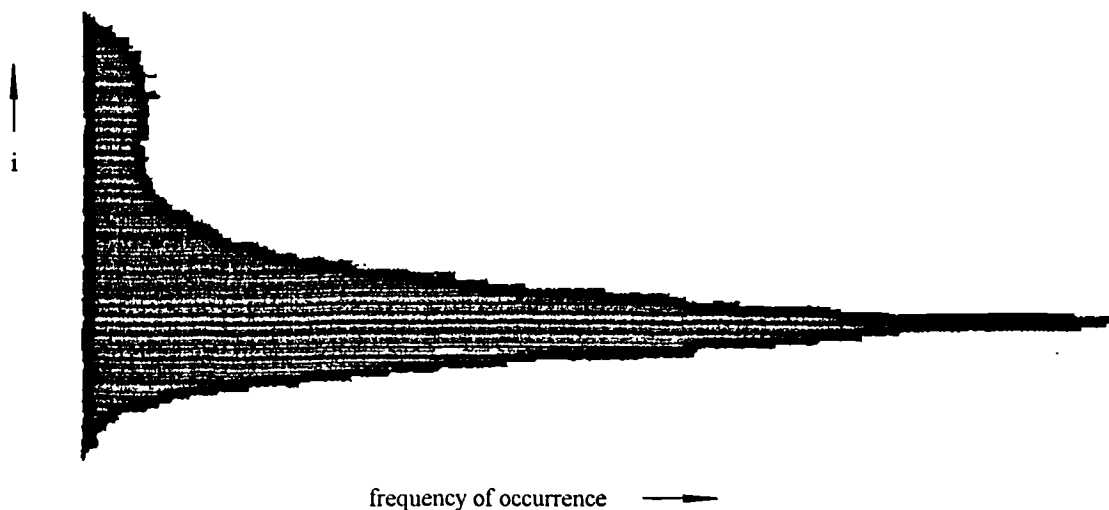


Figure 3.16. Measured noise histogram (probability density function) of partially coherent crosstalk.

3.8 Conclusions

This chapter has derived a number of key characteristics of interferometric noise owing to a single interferer. These are summarised in Table 3.4 for incoherent beat noise crosstalk. The modulation method will influence the system performance; the spectral broadening under direct modulation implies less in-band noise than for external modulation for PIIN, but more when there are two sources. In the latter case the degradation may be reduced by increasing the frequency separation of the sources.

Coherent crosstalk, given sufficient environmental phase fluctuation, has the same pdf as for incoherent beat noise crosstalk. The narrow spectrum implies no noise filtering.

The link performance in the presence of interferometric noise of (a) bounded and (b) Gaussian pdf is summarised in Table 3.5. Calculations with the Gaussian pdf overestimate the BER; results are only applicable (with suitable scaling of the crosstalk) to noise that has been strongly filtered. When the modulation depth is non-infinite, i.e. when the 'zeros' carry optical power, all bits in the classification display some interferometric noise and performance degrades markedly: even a seemingly innocuous $\alpha=0.1$ moves the asymptote by 3dB. It is therefore crucial to bias the laser at threshold (or below) if directly modulating, although other performance aspects such as dispersion may suffer, or to employ a high extinction external modulator.

Systems are far more tolerant to incoherent noise-free crosstalk than to coherent or incoherent beat noise crosstalk.

3.7 References

1. A. Papoulis, *Probability and Statistics*, Prentice Hall, Englewood Cliffs, NJ, 1990.
2. A. Arie, M. Tur and E.L. Goldstein, "Probability-density function of noise at the output of a two beam interferometer", *J. Opt. Soc. Am. A*, 8(12), pp. 1936-1942, 1991.
3. J.W. Goodman, *Statistical Optics*, J. Wiley, New York, 1985.
4. J.A. Armstrong, 'Theory of interferometric analysis of laser phase noise', *J. Opt. Soc. Am.*, 56(8), pp. 1024-1031, 1966.
5. P.J. Legg, "A theoretical description of incoherent beat noise crosstalk arising in a single directional coupler", *University of Strathclyde Memorandum*, August 1993.
6. J.L. Gimlett and N.K. Cheung, "Effects of phase-to-intensity noise conversion by multiple reflections on gigabit-per-second DFB laser transmission systems", *J. Lightwave Technol.*, 7(6), pp. 888-895, 1989.
7. P.K. Pepeljugoski and K.Y. Lau, "Interferometric noise reduction in fiber-optic links by superposition of high frequency modulation", *J. Lightwave Technol.*, 10(7), pp. 957-963, 1992.
8. L.D. Landau and E.M. Lifshitz: *Electrodynamics of continuous media*, Pergamon Press, pp. 256 ff., 1960.
9. R.A. Linke, "Modulation induced transient chirping in single frequency lasers", *IEEE J. Quantum Electron.*, 21(6), pp. 593-597, 1985.

10. K. Petermann, *Laser diode modulation and noise*, Kluwer Academic Publishers, New York, 1993.
11. B.W. Hakki, "Evaluation of transmission characteristics of chirped DFB lasers in dispersive optical fiber", *J. Lightwave Technol.*, 10(7), pp. 964-970, 1992.
12. M. Nazarathy, W.V. Sorin, D.M. Baney and S.A. Newton, "Spectral analysis of optical mixing measurements", *J. Lightwave Technol.*, 7(7), pp. 1083-1096, 1989.
13. E.L. Goldstein, L. Eskildsen and A.F. Elrefaie, "Performance implications of component crosstalk in transparent lightwave networks", *IEEE Photon. Tech. Lett.*, 6(5), pp. 657-660, 1994.
14. L. Eskildsen, E.L. Goldstein, M. Andrejco, L. Curtis, V. Shah, D. Mahoney, C.E. Zah and C. Lin, "Interferometric noise limitations in fiber-amplifier cascades", *Elect. Lett.*, 29(23), pp. 2040-2041, 1993.
15. M. Tur and E.L. Goldstein, "Dependence of error rate on signal-to-noise-ratio in fiber-optic communication systems with phase-induced intensity noise", *J. Lightwave Technol.*, 7(12), pp. 2055-2058, 1989.
16. A.M. Hill and D.B. Payne, "Linear crosstalk in Wavelength Division Multiplexed optical-fiber transmission systems", *J. Lightwave Technol.*, 3(3), pp. 643-650, 1985.
17. D.A. Fishman, D.G. Duff and J.A. Nagel, "Measurements and simulation of multipath interference for 1.7 Gb/s lightwave transmission systems using single and multifrequency lasers", *J. Lightwave Technol.*, 8(6), pp. 894-905, 1990.

		interferometric noise pdf	interferometric noise power spectrum	signal-to-interferometric-noise-ratio (SINR)
		noise filtered	noise unfiltered	noise filtered
single source (PIIN)	CW	zero mean	Baseband Lorentzian, HWHM= $\Delta\nu$	SINR= $1/\xi$ if $\Delta\nu=B$ increases rapidly $\Delta\nu>B$
	external modulation	bounded (by $\pm 2\sqrt{\xi}$ in nomenclature of Table 3.3)	HWHM $\sim B$ if $\Delta\nu<<B$ $\sim \Delta\nu$ if $\Delta\nu>B$	SINR increases rapidly $\Delta\nu>B$ (no filtering in practise)
	direct modulation		HWHM $\sim Y$ (Lorentzian spectrum) HWHM $\sim 0.7Y$ (Gaussian spectrum)	SINR= $\frac{1}{2 \text{ crosstalk level } \xi}$
two sources	CW	becomes unbounded	Centred at beat frequency Lorentzian, HWHM= $\Delta\nu_m$	SINR increases as Δf increases. If $\Delta f<B$ the SINR is greatest for large $\Delta\nu$ ($\Delta\nu_m$ or Y_d+Y_x). If $\Delta f>B$ then reverse applies
	external modulation	thermal noise is added	HWHM $\sim B$ if $\Delta\nu_m<<B$ $\sim \Delta\nu_m$ if $\Delta\nu_m>B$	
	direct modulation		HWHM $\sim 0.5(Y_d^2+Y_x^2)$ (Lorentzian spectrum) HWHM $\sim 0.5\sqrt{Y_d^2+Y_x^2}$ (Gaussian spectrum)	

Table 3.4. Properties of incoherent beat noise owing to a single interferer. ($\Delta\nu=CW$ linewidth, $\Delta\nu_m = \text{mean CW linewidth of two sources}$, $Y = \text{modulated spectral width}$, $B = \text{receiver bandwidth}$)

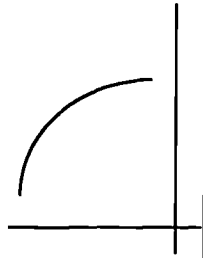

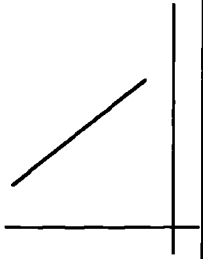
interferometric noise pdf	BER characteristic (-log(-log(BER)) vs STNR)	Crosstalk ξ (dB) for power penalty asymptote (BER=10 ⁻⁹)		Error floor condition	
		D optimised	D=0.5	D optimised	D=0.5
bounded		-6	-10.6	$\xi > -6$ dB	$\xi > 10.6$ dB
Gaussian		-18.2	-24.2	always a floor	always a floor
zero (incoherent noise-free crosstalk)		0	-3	$\xi > 0$ dB	$\xi > -3$ dB

Table 3.5. Performance given a single crosstalk interferer, aligned polarisations and no noise filtering. D is the decision threshold level.

Chapter 4

Theoretical modelling: multiple interferers

4.1 Introduction

In the previous chapter properties of interferometric noise were derived for the special case of a single interferer. In practical optical networks, as discussed in Chapter 2, the data will be corrupted by a number of crosstalk terms, and it is likely that more than one of these will give rise to in-band interferometric noise. The objective of this chapter is to analyse this general situation without reference to specific network configurations.

An expression is derived for the photocurrent when N crosstalk terms are present: there are N primary beat terms arising between each crosstalk term and the data signal, and $N(N-1)/2$ secondary crosstalk-crosstalk beating terms. It shall be shown in Chapter 6 that secondary terms may be often neglected. The aggregation of the many noise components is intractable unless conditions of mutual statistical independence are satisfied, giving a net interferometric noise variance proportional to the sum of the crosstalk power (neglecting secondary beat terms). Additionally, the noise pdf may also be calculated by convolving the (N_b) pdfs of the in-band beating terms.

If N is large, the convolution approach is impractical but the Central Limit Theorem may then be invoked (subject to certain conditions) giving a (net) Gaussian pdf that facilitates BER computation. It is shown that the total crosstalk level of the N_b noise-generating terms must not exceed -25 dB. It is assumed throughout the chapter that all polarisations are aligned (worst-case) and that interferometric noise between signals of the same optical frequency is unattenuated by the receiver filter (worst-case).

4.2 General formulation of optical mixing at the photodetector

In the following analysis it is assumed that all signals are of the ASK (NRZ) format, have the same polarisation, and are generated by chirp-free external modulation. The nomenclature of Chapter 2 & Chapter 3 is generalised as follows:

the data signal

optical frequency= ω_d
 phase noise= $\phi_d(t)$
 instantaneous optical power = $\underline{P}_d(t)$
 coherence time= τ_c

the N crosstalk terms

optical frequency= ω_i
 phase noise= $\phi_i(t)$
 network transit delay relative to that of the data = τ_i
 instantaneous optical power = $\underline{P}_i(t)$
 coherence time= τ_{ci}

where $i= 1\dots N$.

The instantaneous optical power is introduced to permit signals whose 'zeros' contain light. If a laser is (completely) switched off by the modulator the instantaneous power varies from zero ('zero' bit) to twice the mean power level ('one' bit).

The total optical electric field is

$$E(t) \propto \sqrt{\underline{P}_d(t)} \exp j(\omega_d t + \phi_d(t)) + \sum_{i=1}^N \sqrt{\underline{P}_i(t)} \exp j(\omega_i(t - \tau_i) + \phi_i(t - \tau_i)) \quad (4.1)$$

data signal
N crosstalk terms

The photocurrent on detection (responsivity= \mathfrak{R}) is :

$$\begin{aligned}
i/\mathfrak{R} = & \underbrace{\underline{P}_d(t)}_{\text{data}} + \underbrace{\sum_{i=1}^N \underline{P}_i(t)}_{\text{crosstalk}} + \\
& \sqrt{\underline{P}_d(t)} \left\{ 2 \sum_{i=1}^N \sqrt{\underline{P}_i(t)} \cos((\omega_i - \omega_d)t - \omega_i \tau_i + \phi_i(t - \tau_i) - \phi_d(t)) \right\} + \\
& \text{N primary data - crosstalk beating terms} \\
& \left\{ 2 \sum_{j=i+1}^N \sum_{i=1}^{N-1} \sqrt{\underline{P}_i(t) \underline{P}_j(t)} \cos((\omega_i - \omega_j)t - \omega_i \tau_i + \omega_j \tau_j + \phi_i(t - \tau_i) - \phi_j(t - \tau_j)) \right\} \quad (4.2) \\
& \text{N(N-1)/2 secondary crosstalk - crosstalk beating terms}
\end{aligned}$$

Note that the secondary crosstalk-crosstalk beat terms are smaller by $O(\sqrt{\xi})$ than the primary beating terms (ξ is the crosstalk level). If all crosstalk terms are of level ξ and all beating terms are in-band, the ratio of the variances of primary and secondary beat noise is $2/(N\xi)$. Since, as will be shown below (Section 4.6), considering the primary terms alone, $N\xi < 3 \times 10^{-3}$ for satisfactory performance, the secondary terms may be neglected in this case. However, secondary terms may be significant if there is greater RF filtering of the primary terms than the secondary. For example, if all the crosstalk terms arise from a single source at a different wavelength from that of the data, all primary terms, but not the secondary terms, will be RF rejected.

4.3 Conditions for statistical independence of beating terms

4.3.1 Identification of beating terms according to the crosstalk classification

It is assumed that all beating terms are examples of incoherent noise-free crosstalk, incoherent beat-noise crosstalk or coherent crosstalk according to the crosstalk classification (Section 2.2.2). The receiver bandwidth is B .

Incoherent noise-free crosstalk

Primary beating terms satisfying

$$|\omega_i - \omega_d| > 2\pi B \quad (4.3)$$

and secondary beat terms satisfying

$$|\omega_i - \omega_j| > 2\pi B \quad (4.4)$$

constitute incoherent noise-free crosstalk and add no noise to the data.

Incoherent beat noise crosstalk

Primary beating terms represent incoherent beat noise crosstalk if:

$$|\omega_i - \omega_d| < 2\pi B \quad (4.5)$$

Additionally, if $\omega_i = \omega_d$ and $\phi_i(t) = \phi_d(t)$ (data and crosstalk from same source) then $\tau_i \gg \tau_c$ (incoherent limit).

The former condition implies very closely wavelength matched sources (at the wavelength of 1.55 μm two lasers of 1 GHz beat frequency are separated by approximately 0.02 nm).

Secondary beat terms constitute incoherent beat noise crosstalk if:

$$|\omega_i - \omega_j| < 2\pi B \quad (4.6)$$

Additionally, if $\omega_i = \omega_j$ and $\phi_i(t) = \phi_j(t)$ (both crosstalk terms from the same source) then $|\tau_i - \tau_j| \gg \tau_c$ (incoherent limit).

Coherent crosstalk

All remaining terms constitute coherent crosstalk.

4.3.2 Statistical independence

Statistical independence of two noise components, a and b , requires that the joint probability density function separates into a product of individual marginal pdfs [1,2]; the probability of b having a certain value is independent of the value of a at that moment of time. For example, consider a data term and two crosstalk terms, all derived from the same laser. If the relative delays (τ_i) are all (nominally) zero, the

two primary beat terms will generate coherent crosstalk, and environmental drift over a path common to both data-crosstalk phase differences will change both primary noise currents similarly; the noise terms are not independent. However, if there is environmental drift in a path traversed by one crosstalk term but not the other, the former primary noise term will vary whilst the other is static - this is independence.

Incoherent beat noise terms cannot be statistically dependent on coherent crosstalk terms but two incoherent crosstalk terms, comprising waveform a beating with waveform b , and waveform c beating with waveform b , will be dependent if the phases of a and c are correlated to some degree. This implies that a and c arise from the same laser and the difference in their transit times is not much greater than the coherence time of that laser:

$$\phi_a(t) = \phi_c(t), \text{ and } |\tau_a - \tau_c| \text{ is not } \gg \tau_{ca} \quad (4.7)$$

For example, if there is a data term corrupted by two crosstalk terms from the same laser which have both suffered the same delay through the network, the two primary beat terms are incoherent beat noise crosstalk but are not independent of each other.

Independence of coherent crosstalk terms, as hinted to above, is more complex. Two limiting scenarios may be identified:

a) If the coherent crosstalk is shed and then added to the data on its route across a large integrated-optical space switch, the intra-substrate crosspoint interconnects are necessarily short, and the temperature differences across the substrate will be small (particularly if mounted in a temperature controlled package). Consequently, optical path length fluctuations will be small, $\ll 2\pi$. Coherent crosstalk terms which arise from different paths within the substrate will have a constant time invariant phase relationship and statistically dependent data-crosstalk beat terms.

The optical path lengths will not be matched to an accuracy greater than the optical wavelength ($\sim 0.75 \mu\text{m}$ in lithium niobate) and the relative phases are therefore random. Consequently, it is impossible to predict the precise sum of the coherent crosstalk components, since their relative phases are unknown, but the statistics of the distribution can be calculated.

Since the phases are random, when there are many terms, the Central Limit Theorem (cf. Section 4.5) may be invoked giving a Gaussian pdf with:

$$\text{mean current} = \Re(\underline{P}_d(t) + \sum_{\text{coherent crosstalk}} \underline{P}_i(t)) \quad (4.8)$$

and photocurrent variance,

$$\sigma_N^2 = \Re^2 \left(\underbrace{2 \underline{P}_d \sum \underline{P}_i}_{\text{primary beating terms}} + \underbrace{2 \sum \underline{P}_i \underline{P}_j}_{\text{secondary beating terms}} \right) \quad (4.9)$$

To obtain an estimate of the expected BER, this photocurrent will be treated as a noise source, and may be too high or too low depending upon the true values of the relative phases. The estimate will improve if the crosstalk conditions change over the bit sequence which is being tested (for example, in an optical TDM crossconnect (cf. Section 2.3.8); if the switch fabric assignment changes frequently over the duration of a channel being assessed or if several TDM channels are assessed by one receiver (implying electronic demultiplexing)).

b) In contrast, if the coherent crosstalk terms transit different optical fibre paths then path length (and hence phase) fluctuations will arise. If these are uncorrelated and persistent the beating terms may be taken to be independent.

4.3.3 Interferometric noise variance for independent beating terms

The variance of the sum of many independent noise variables is equal to the sum of the variances of each individual noise term [2]. Thus the variance of the photocurrent noise is given by (cf. Eqn. 3.10):

$$\sigma_N^2 = \Re^2 \left(\underbrace{2 \underline{P}_d \sum \underline{P}_i}_{\text{in-band primary beating terms}} + \underbrace{2 \sum \underline{P}_i \underline{P}_j}_{\text{in-band secondary beating terms}} \right) \quad (4.10)$$

and the signal-to-interferometric-noise-ratio (SINR) is

$$SINR = \underline{P}_d^2 / \left(\underbrace{2 \underline{P}_d \sum \underline{P}_i}_{\text{in-band primary beating terms}} + \underbrace{2 \sum \underline{P}_i \underline{P}_j}_{\text{in-band secondary beating terms}} \right) \quad (4.11)$$

4.4 BER calculation for independent terms by the convolution method

The probability density function of the net interferometric noise may be determined by convolving the individual pdfs of every contributing beating term, all beating terms being independent [2]. The individual pdfs take the bounded form of Eqn. 3.3 (Fig. 3.1). The error probability may then be calculated by integration of the total photocurrent noise pdf, this itself being the convolution of the net interferometric noise pdf and the Gaussian thermal noise pdf, between the decision threshold and + or - infinity, for 'zeros' and 'ones', respectively.

The convolution of the individual bounded pdfs was performed using a piece-wise representation of the bounded function

$$p(i)=1/(\pi\sqrt{4\xi-i^2}) \quad (4.12)$$

defined at 800 points¹ between the extremes of $\pm 2 f\sqrt{\xi}$, where the pre-factor f is chosen to be slightly smaller than one to avoid calculation at the asymptotes. The aggregate pdf develops towards a Gaussian-like shape as more crosstalk terms are added. This is illustrated for $f=0.999$ in Fig. 4.1.

The shape of the calculated net interferometric noise pdf for five equal crosstalk terms giving a total crosstalk level of -25 dB was found to depend critically on the value of the pre-factor, f . When $(1-f)$ is relatively large, 10^{-3} ($f=0.999$), the net pdf is Gaussian-like, Fig 4.2(d) (as in Fig. 4.1) but for smaller values of $(1-f)$, the net pdf has several sharp peaks, Fig. 4.2(e), Fig. 4.2(f). The number of peaks may be easily shown to equal the number of crosstalk terms plus one. On the addition of Gaussian thermal noise the peaky nature is lost, Fig. 4.2(h), Fig. 4.2(k), Fig. 4.2(l), unless the thermal noise magnitude is small (the STNR is large, Fig. 4.2(i)).

¹ the calculated value of the BER increased with the number of definition points until no change was noted for more than 800 points.

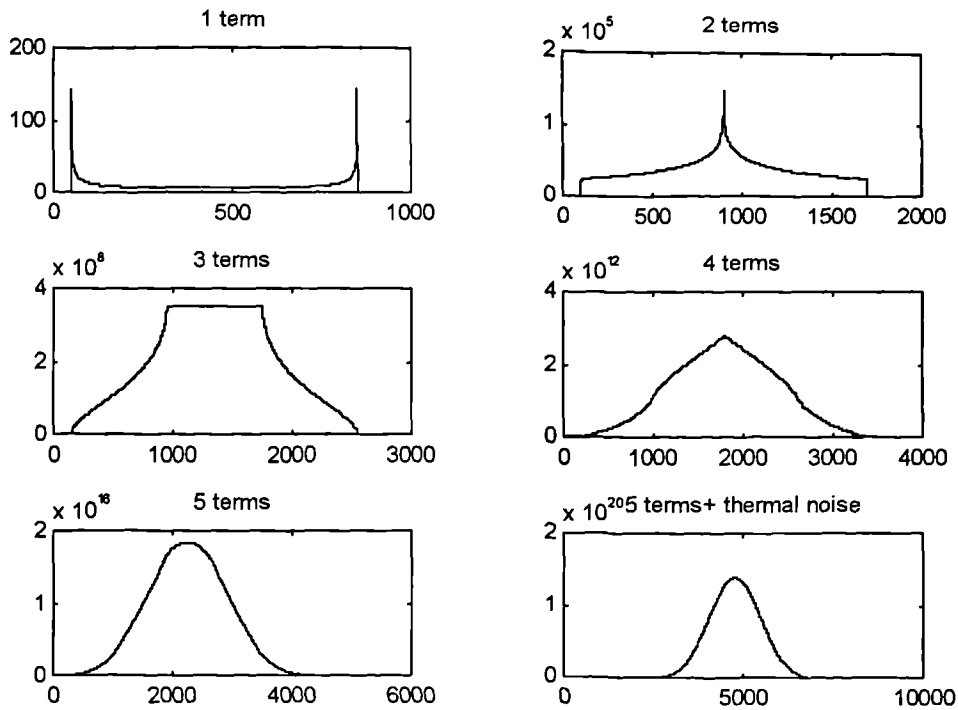


Figure 4.1. Probability density function calculated by convolution of equal crosstalk terms. The pre-factor $f=0.999$, the five terms constitute a total crosstalk level of -25dB , and the $STNR=30\text{ dB}$.

Calculation of the BER of a data bit corrupted by one and five (equal) 'high' crosstalk terms with pre-factor $f=0.999999999999$ permitted the estimation of the signal-to-thermal-noise-ratio required for an error probability of 10^{-9} (Fig. 4.3). The performance assuming a Gaussian distributed net interferometric noise of the same variance is also drawn (Central Limit Theorem). The pdf of a single interferer is more tightly bound than a Gaussian of the same variance and thus offers much superior performance. When there are five interferers the pdf is more spread, although rather peaky, cf. Fig 4.2(f), giving similar performance to the Gaussian except for large values of crosstalk when there is no error floor - the convolution of multiple bounded pdfs is itself bounded.

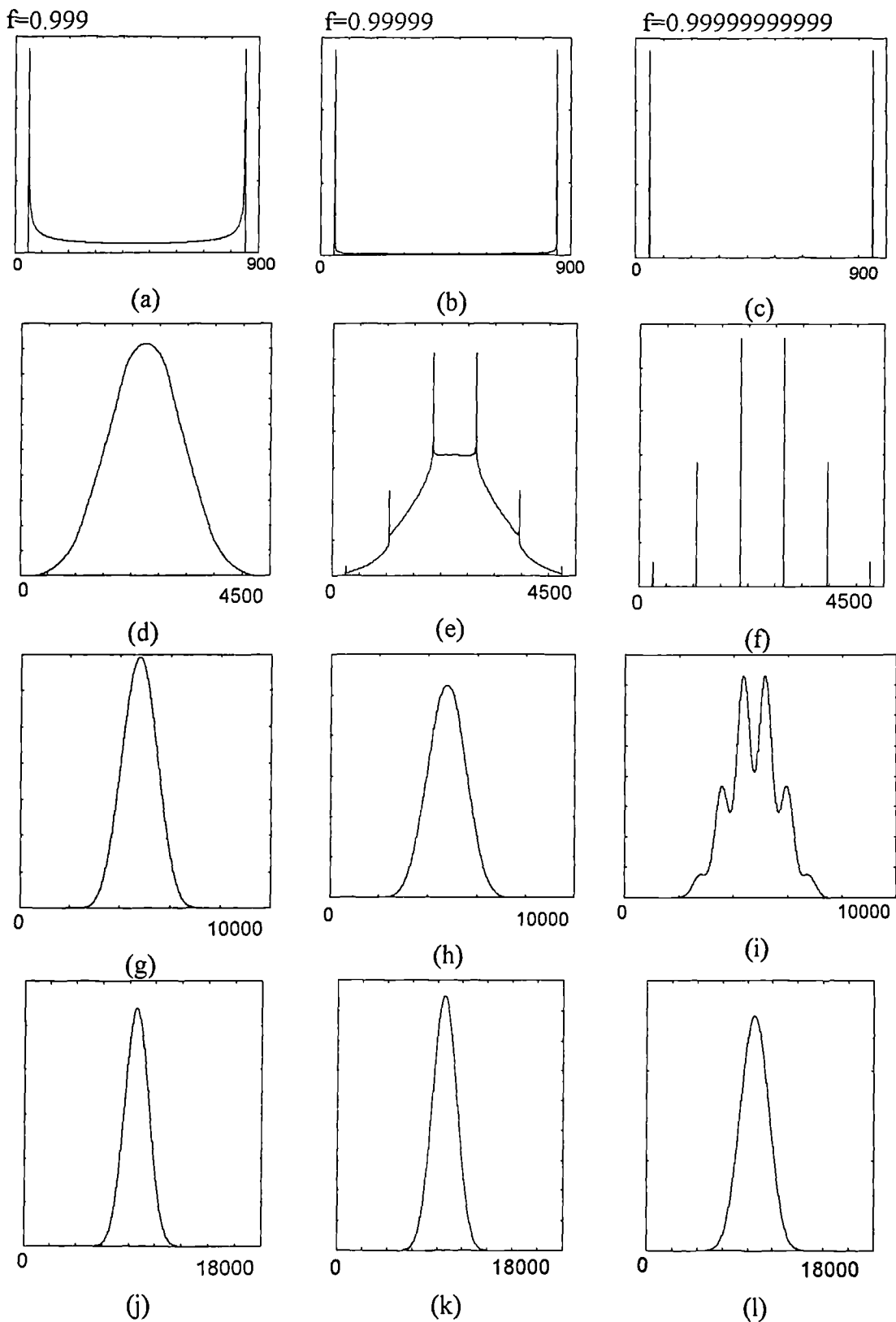


Figure 4.2. Calculated pdfs for different values of pre-factor, f . Rows from the top represent a single term (a-c), five bounded terms(d-f), five bounded terms with thermal noise, $STNR=30dB$ (g-i), and five bounded terms with thermal noise, $STNR=22 dB$ (j-l).

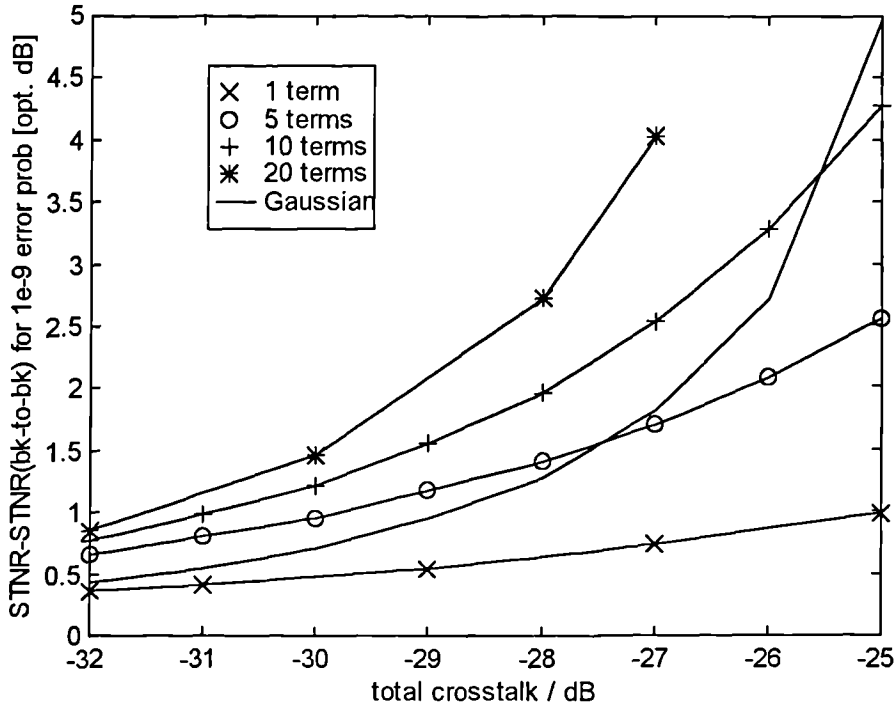


Figure 4.3. Convolution method calculated performance of data bit corrupted by different numbers of 'high' crosstalk terms, $f=0.9999999999$.

When 10 and 20 crosstalk terms are considered, again with $f=0.9999999999$, the performance, and the agreement with the Gaussian plot, deteriorate (Fig. 4.3). This is attributed to the aphysical peaky nature of the convolved pdf. The Central Limit Theorem does not accurately describe the convolution of the ideal bounded pdf, except, perhaps, for an infinite number of terms when the infinite number of peaks join to form a continuum. However, in a real system with a finite bandwidth receiver, some filtering of the noise must take place giving a pdf due to a single term that is finite at $\pm 2\sqrt{f}\xi$. Experimental measurements in Chapter 5 support this. The pre-factor $f=0.999$ gives a single interferer pdf of credible proportions and a Gaussian-like net pdf, Fig. 4.2(d); STNR calculations for this value are depicted in Fig. 4.4.

The Gaussian approximation now agrees well with the convolution method for small (<1.5 dB) values of STNR difference from the back-to-back case given 5 or more 'high' crosstalk terms. Agreement improves as the number of crosstalk terms is increased, as expected from the Central Limit Theorem. In network analysis, it is valid to

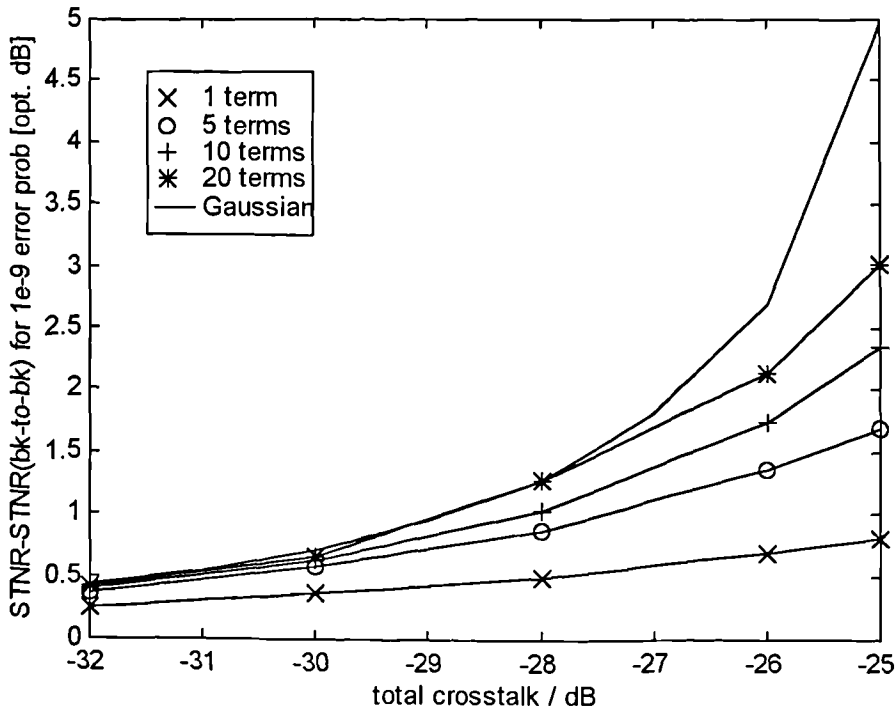


Figure 4.4. Convolution method calculated performance of data bit corrupted by different numbers of 'high' crosstalk terms, $f=0.999$.

employ the Gaussian approximation when 5 or more crosstalk terms are typically 'high', i.e. when 10 or more crosstalk terms are present; the Gaussian prediction overestimates the true power penalty - small penalties of $< 2\text{dB}$ may be recovered by increasing the transmitter power level (assuming crosstalk levels increase by the same amount) but network operation is unlikely to be reliable for higher values since small crosstalk changes may induce catastrophic failure at the asymptote (error floor for $\text{BER} > 10^{-9}$).

If $f < 0.999$ then the net pdf will develop more rapidly to the Gaussian form as more terms are added. Increasing the RF filtering of the baseband noise improves the agreement of the Gaussian approximation to the form of the net noise pdf (and thus to the shape of the BER characteristic) but the penalty will be overestimated if significant noise power is lost.

4.5 BER calculation for independent terms by the Central Limit Theorem

4.5.1 Conditions for application of the Central Limit Theorem

If the Central Limit Theorem is to be applied to the summation of the N_b in-band beating terms (these are termed u_i and have variance σ_i^2) the following conditions must be met [3]:

- i. u_i are independent random variables
- ii. N_b is 'large'
- iii. $\sigma_i^2 > r > 0$

iv. $E\left[|u_i - \bar{u}_i|^3\right] < s$

where r and s are positive numbers.

Condition (i) was considered in Section 4.3.2. The number of terms N_b required was addressed in Section 4.4; $N_b=10$ gives reasonable agreement and $N_b=20$ gives good agreement.

Employing the pdf for u_i of $p(u_i)=1/(\pi\sqrt{4\xi_i-u_i^2})$

iii) implies that $2\xi_i > r > 0$

iv) implies that $32 \xi_i^{3/2} / (3\pi) < s$,

r and s may be chosen to satisfy these criteria.

Thus the Central Limit Theorem may be applied to a good approximation if

- a) the beating terms fall into coherent or incoherent limits.
- b) the number and magnitude of incoherent beat noise statistically dependent terms are small in comparison with those that are independent.
- c) N_b is large (>10).

4.5.2. Application of the Central Limit Theorem

The Central Limit Theorem aggregates all random noise components to give a resultant Gaussian distributed noise whose mean is the sum of the mean of the

individual contributions and whose variance is the sum of the individual variances. Thus:

$$\text{mean current} = \bar{i} = \Re(\underline{P}_d(t) + \sum_{i=1}^N \underline{P}_i(t)) \quad (4.13)$$

and photocurrent variance,

$$\sigma_N^2 = \Re^2 \left(\underbrace{2 \underline{P}_d \sum \underline{P}_i}_{\text{in-band primary beating terms}} + \underbrace{2 \sum \underline{P}_i \underline{P}_j}_{\text{in-band secondary beating terms}} \right) \quad (4.14).$$

4.5.3 BER calculation

The calculation of the mean BER from the net Gaussian variable is given below. It is important to note that although some worse-case conditions have been assumed, namely no filtering of the beat noise from waveforms of equal wavelength and aligned polarisations, the BER will fluctuate below and above the mean value. Since the bandwidth of the phase fluctuation of the interferometric noise is typically much smaller than the data bandwidth, errors will tend to occur in bursts that hinder error correction. This is particularly true for the slowly varying coherent crosstalk but in the scenario that the crosstalk terms are unchanged¹ over a time period exceeding the fluctuation period, there may be sufficient time to adjust the threshold and minimise the degradation. These factors must be born in mind when the net Gaussian variable is employed in BER calculations.

The error probability for each bit may be determined given the following at the decision point-

- mean photocurrent, \bar{i}
- interferometric noise variance, σ_N^2
- thermal noise current variance, σ_0^2
- decision level threshold, D.
- responsivity, \Re .

¹ as discussed above this depends critically on the nature of the network, its operation and the detected signal (one or multiple channels).

Shot noise shall be neglected - a valid assumption for typical PIN receivers.

a) Error probabilities for 'one' bits

The photocurrent pdf for a 'one' bit is drawn schematically below (Fig. 4.5).

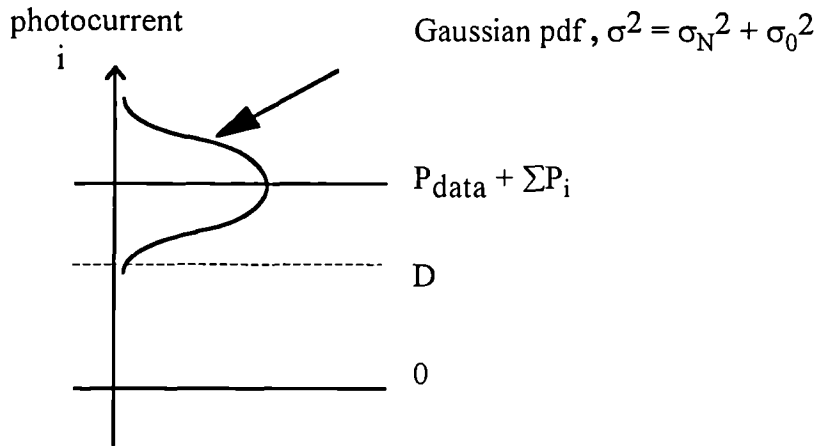


Figure 4.5. Probability density function for 'one' bit

$$\begin{aligned} \text{error probability} &= \int_{-\infty}^D \frac{1}{\sqrt{2\pi\sigma^2}} \exp\left(-\frac{(i-\bar{i})^2}{2\sigma^2}\right) di \\ &= \frac{1}{2} \operatorname{erfc}\left(\frac{\bar{i}-D}{\sqrt{2}\sigma}\right) \end{aligned} \quad (4.15)$$

b) Error probabilities for 'zero' bits

$$\text{error probability} = \frac{1}{2} \operatorname{erfc}\left(\frac{D-\bar{i}}{\sqrt{2}\sigma}\right) \quad (4.16)$$

Giving the general expression:

$$\text{error probability} = \frac{1}{2} \operatorname{erfc}\left(\frac{|\bar{i}-D|}{\sqrt{2}\sigma}\right) \quad (4.17)$$

4.6 Application of the Central Limit Theorem: statistical model.

An analytical model has been developed to estimate the power penalty due to interferometric noise. The assumptions made are:

- there are N_b crosstalk terms, each of crosstalk level ξ , with the same polarisation, which all generate unfiltered interferometric noise when they beat with the data.
- secondary crosstalk-crosstalk beating is neglected (see comment in Section 4.2).
- all 'zero' bits have zero optical power.
- the probability that m of the N_b number of crosstalk terms are simultaneously 'ones' is given by the binomial distribution:

$$p(m) = \frac{N_b!}{(N_b - m)!m!2^{N_b}} \quad (4.18)$$

- the noise is aggregated according to the Central Limit Theorem.
- the decision threshold $D=0.5$.
- the BER is calculated by a statistical average of the error probability for each value of m .

The calculated BER curves shows a similar behaviour to the calculations for a single interferer with Gaussian interferometric noise (cf. Fig. 3.9). The optical power penalty at $\text{BER}=10^{-9}$ is plotted in Fig. 4.6. The curve for a single crosstalk term (this is identical to the $D=0.5$ curve of Fig. 3.12) in addition represents the worst-case for multiple interferers when all crosstalk bit sequences are identical. The system may tolerate more total crosstalk when the crosstalk is distributed over more terms; however, a limit is approached as the binomial distribution becomes narrower, and ultimately single-valued at $m=N_b/2$. Hence, the $N_b = \infty$ curve is 3dB displaced from the worst-case curve. In conclusion, for a penalty of <1dB the total crosstalk level of noise generating terms in the network must be held below -25 dB; a further 2 to 4 dB of total crosstalk may lead to network failure at the asymptote (error floor at $\text{BER}=10^{-9}$).

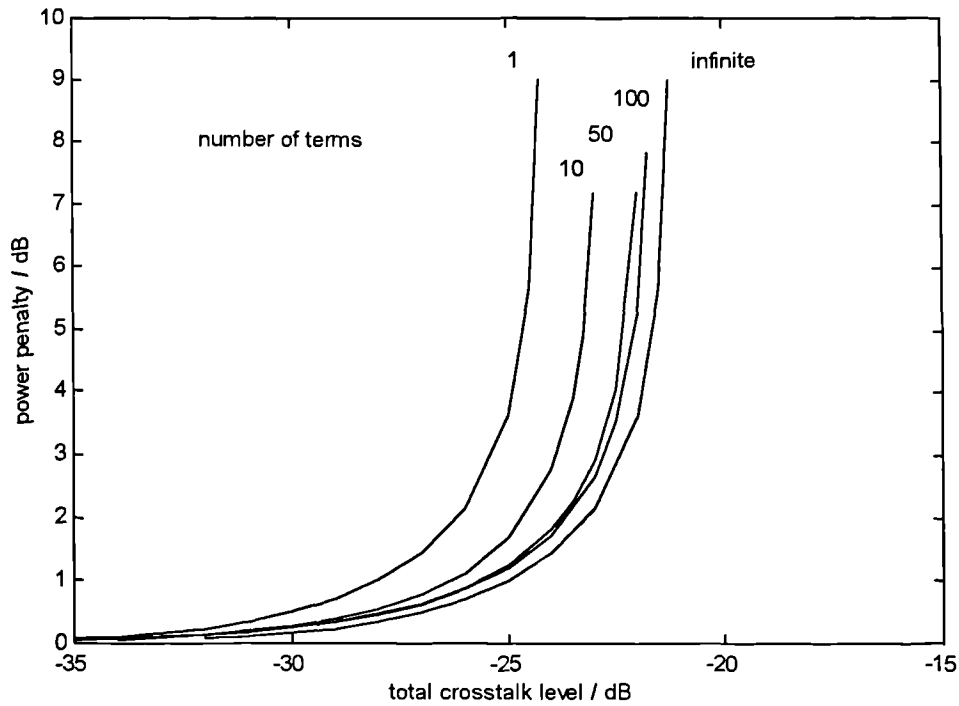


Figure 4.6. Optical power penalty at $BER=10^{-9}$ versus total crosstalk level for different numbers of noise-generating crosstalk terms.

4.7 Conclusions

When the data signal is corrupted by N crosstalk terms, photodetection generates N primary and $N(N-1)/2$ secondary beating terms. The terms giving in-band interferometric noise may be identified according to the crosstalk classification. Under the assumption of statistical independence, the net interferometric noise variance is proportional to the total crosstalk power of the in-band terms (neglecting secondary terms and any RF filtering).

The bit-error-rate in the presence of the interferometric noise may be computed given the form of the probability density function. A rigorous approach determines the probability density function by convolving the bounded 'two-pronged' pdfs of all in-band terms. A second approach invokes the Central Limit Theorem to give a Gaussian pdf. The Gaussian approximation overestimates the BER determined by the convolution method but agreement is good when there are 5 or more in-band components typically 'high'. Agreement improves with more terms.

A statistical model employing the Gaussian approximation indicates that the total crosstalk level of noise generating terms in a network should be held below -25dB for a penalty of <1dB (assuming no RF filtering of base-band noise, AC-coupled receiver, and infinite modulation depth). A further 2 to 4 dB may lead to network failure. The crosstalk tolerance is 3dB less in the worst-case than in the typical case.

4.8 References

1. J.W. Goodman, *Statistical Optics*, J. Wiley, New York, 1985.
2. A. Papoulis, *Probability and Statistics*, Prentice Hall, Englewood Cliffs, NJ, 1990.
3. G. Grimmett and D. Stirzaker, *Probability and Random Processes*, Oxford University Press, New York, 1992.

Chapter 5

Experimental investigation

5.1 Introduction

Much of the impetus behind the research reported in this thesis followed the observation of unidentifiable noise in an optical TDM switching network (cf. Section 2.3.8) test-bed. This noise level increased as more crosspoints were added to the switch fabric until the bit sequence could only be observed by multiple averaging. The noise was identified as interferometric noise; this chapter summarises the subsequent experimental investigation.

The addition of a single interferer is considered first of all. Several properties of the resulting interferometric noise, its appearance on an oscilloscope, the magnitude and the probability density function (pdf), and the impact on the bit-error-rate (BER) are reported for incoherent noise-free, coherent and incoherent beat-noise classes (cf. Section 2.2.2). In the latter case comparison is made between the use of direct and external modulation. DFB sources were employed exclusively.

Demonstration optical TDM switching networks constructed from several 2x2 crosspoints interconnected by fibre delay lines suffer from multiple crosstalk interferers and the resultant interferometric noise. This noise is characterised, all of the above classes are identified, and it is shown that the network size is thus limited to three or four crosspoints of isolation = -15 dB. Multiple interferers may also be generated by a recirculating delay-line structure; this experiment elegantly demonstrates the convergence of the noise pdf towards a Gaussian function as more interferers are present.

5.2 Single Interferer

5.2.1 Incoherent noise-free crosstalk

A lithium niobate integrated-optical 2x2 directional coupler [1] held in the 'cross' state and fed by modulated data at 622 Mb/s from two directly modulated lasers (1535 nm and 1548 nm) formed the heart of the test-bed to investigate incoherent noise-free crosstalk, (Fig. 5.1). Both lasers were driven by the same 64-bit NRZ word pattern but that of the crosstalk (1548nm) lagged by 16 bits. The second directional coupler permitted adjustment of the crosstalk level.

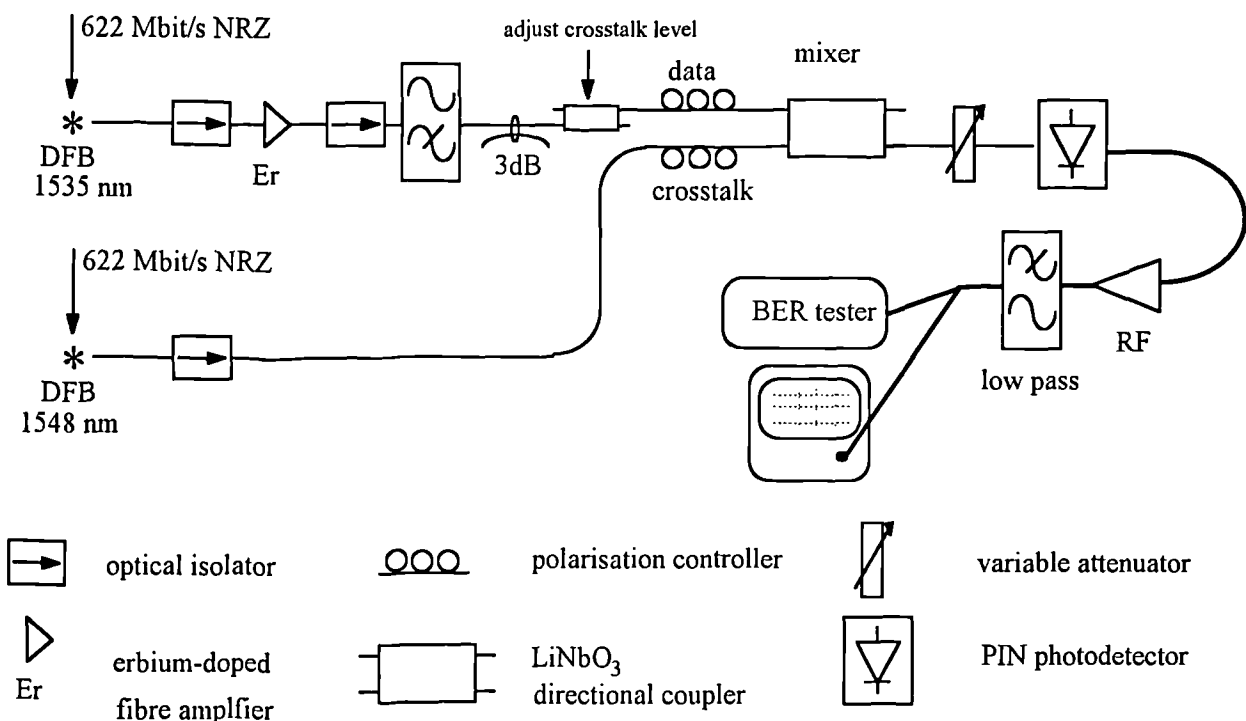
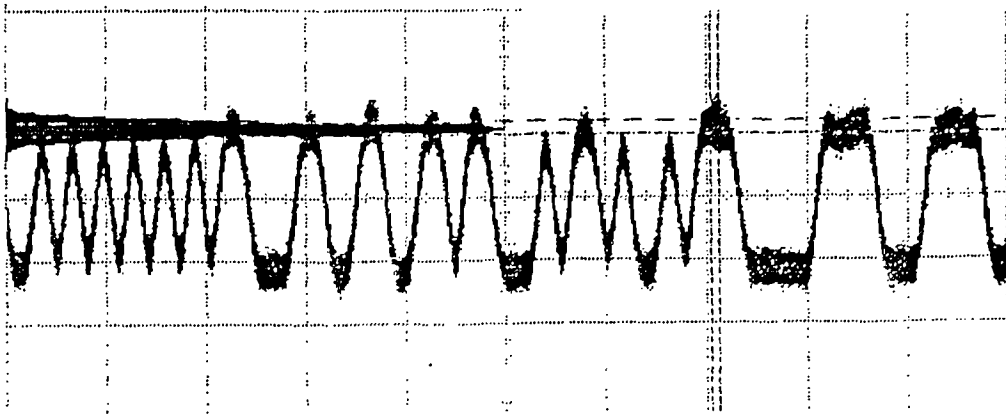
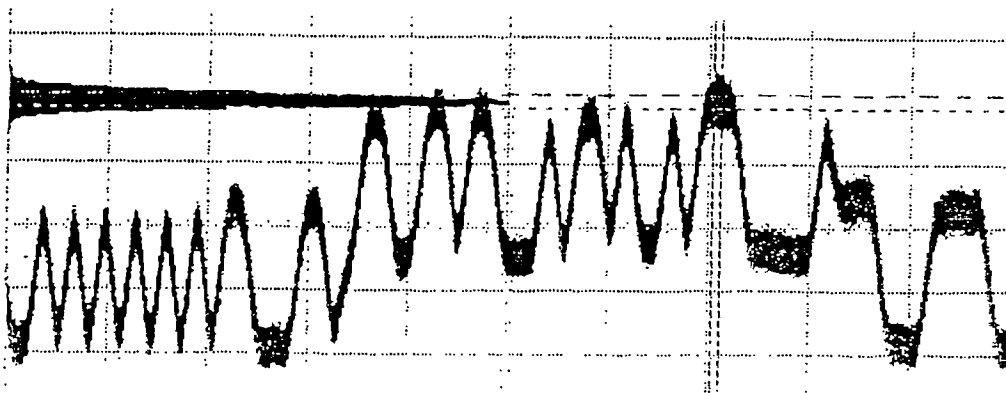


Figure 5.1. Test-bed arrangement for characterisation of incoherent noise-free crosstalk.

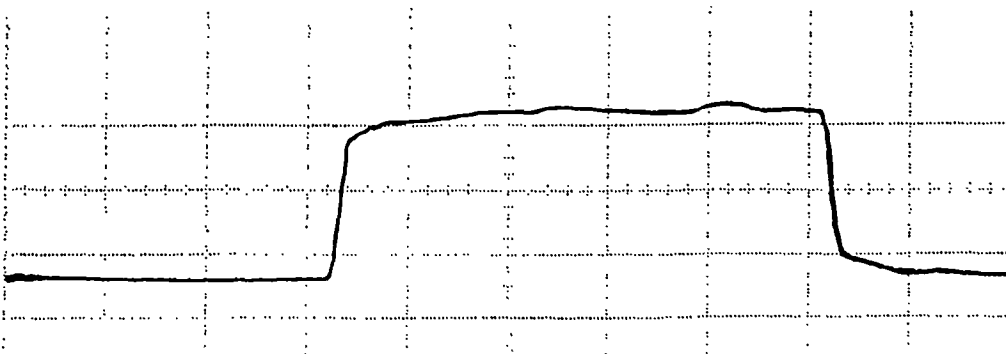
Oscilloscope traces (Fig. 5.2) demonstrate that the crosstalk simply translates the optical power level and adds no noise. The horizontal peak-like traces on Fig. 5.2(a) and Fig. 5.2(b) are histograms of the noise within the time window defined by the dashed vertical lines. The two histograms represent the Gaussian thermal noise, no interferometric noise being present.



(a)



(b)



(c)

Figure 5.2. Incoherent noise-free crosstalk addition. (a) crosstalk-free signal (1548 nm laser disconnected); (b) signal with crosstalk shown in (c) added. Scale 10.5 ns/div. The horizontal peak-like traces on (a) and (b) are noise histograms.

The BER was measured against the received optical power for different values of crosstalk level (altered via the control voltage to the first directional coupler) under optimum thresholding (Fig. 5.3). There is no change in line-gradient as the crosstalk is added, in agreement with theory (Section 3.5.4).

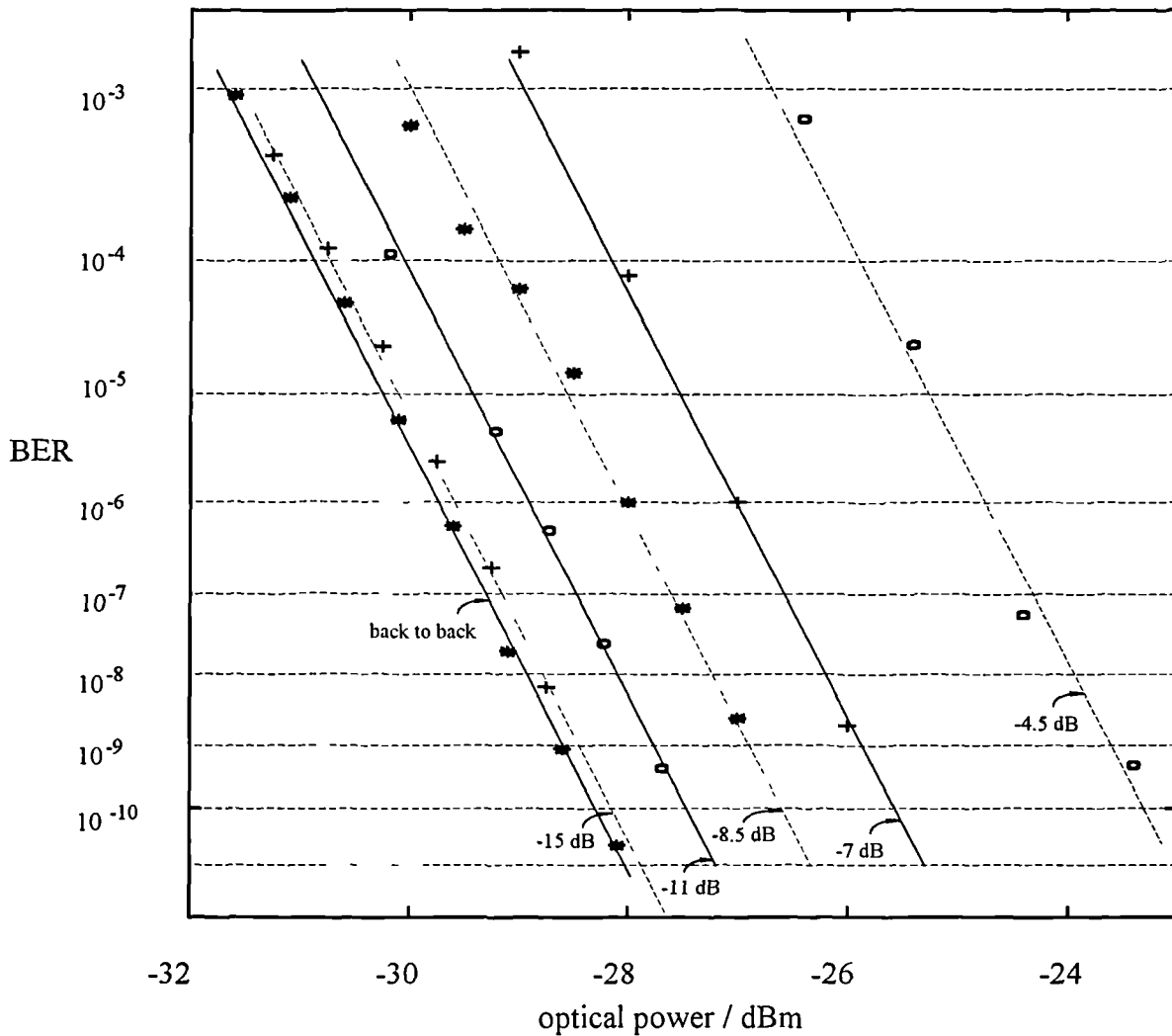


Figure 5.3. BER characterisation of incoherent noise-free crosstalk for different values of crosstalk level.

The optical power penalty, at $BER=10^{-9}$, corrected for the contribution of the crosstalk waveform to the received power (cf. discussion in Section 3.5.2), is plotted in Fig. 5.4. This demonstrates the resilience of the system to noise-free crosstalk but agreement with theory is disappointing. It appears that the optimisation of the decision threshold was unsuccessful. Signal-spontaneous beat noise between the crosstalk and the spontaneous emission of the erbium amplifier may also contribute to the error.

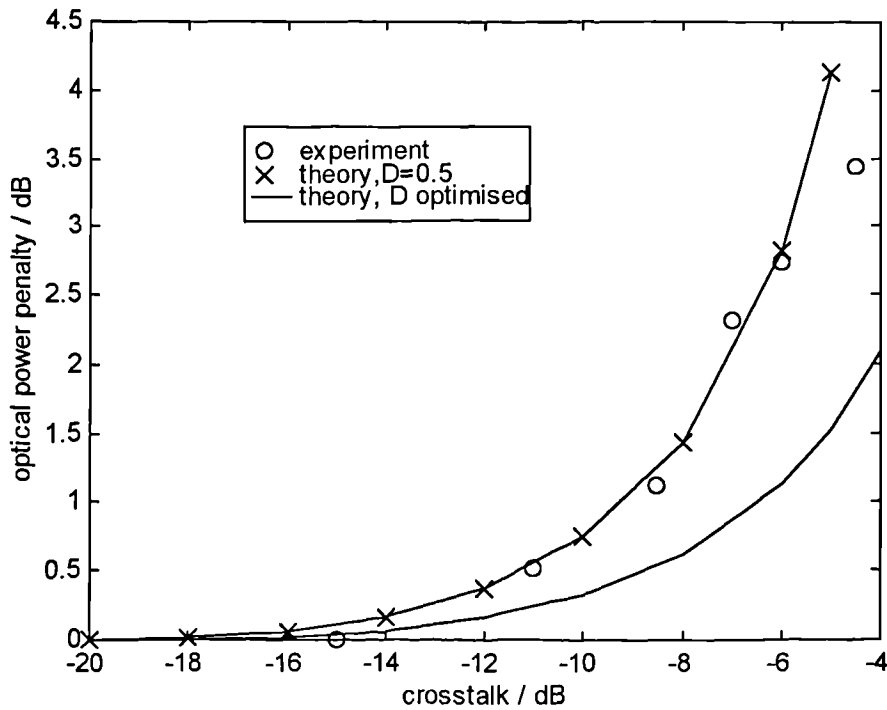


Figure 5.4. Power penalty versus crosstalk level for incoherent noise-free crosstalk

5.2.2 Coherent crosstalk

The configuration depicted in Fig. 5.5 was employed in the investigation of coherent crosstalk. Initially τ was set to 'zero' ($<100\text{ps}$), the polarisations were aligned (to TM), and the output was fed to an optical power meter. The reading was observed to fluctuate randomly with a frequency that increased to the order of 10 Hz when a hand was held in close proximity to the fibre linkage. This fluctuation arises from the variation in the optical path difference of data and crosstalk owing to phonon excitation and temperature micro-changes in the few metres of fibre [2]. When τ was increased the power fluctuation magnitude decreased; when the laser was operated CW, fluctuations were still present with a path length difference of the order of 100m; when modulated at 1.244Gb/s, however, a delay difference of only 2.6m ($\tau=12.85\text{ns}$) eliminated all fluctuation. In the latter, the modulation of the laser reduces its coherence time and the incoherent limit is reached. Although the environmental phase fluctuations are still present they are masked by the (averaged) phase-to-intensity noise.

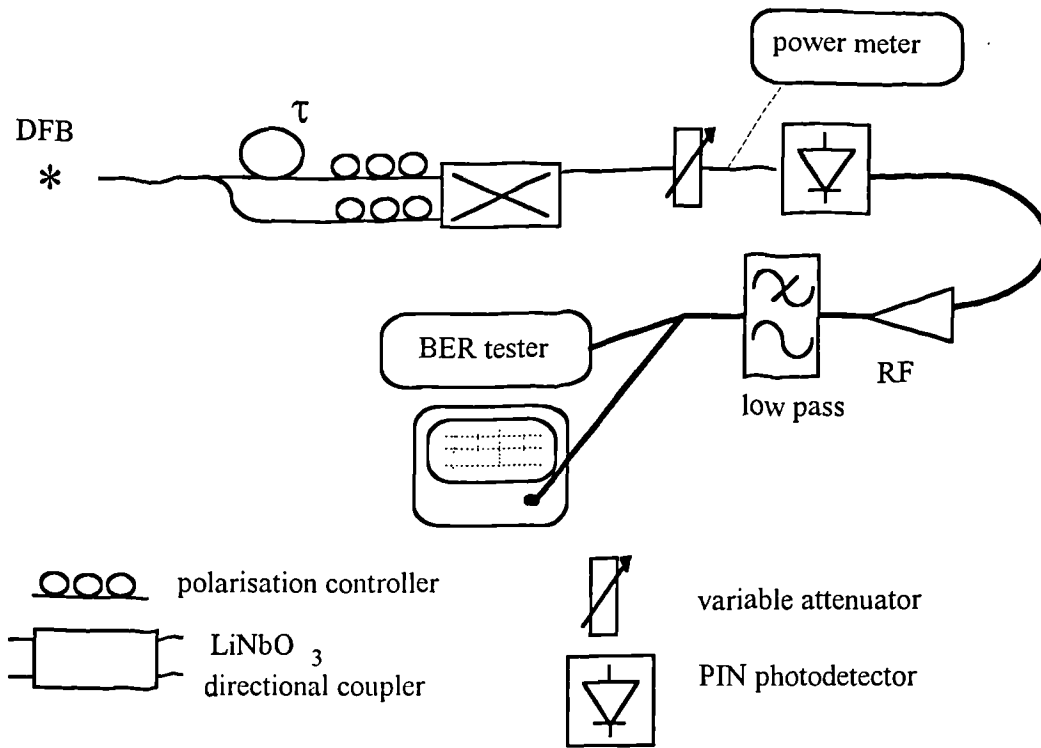


Figure 5.5. Test-bed arrangement for characterisation of coherent crosstalk.

Measurements of the noise pdf at 622 Mb/s were made using a histogram capture function on a digitising oscilloscope (Fig. 5.6). When both inputs are TM polarised, (Fig. 5.6(a)), the pdf agrees well with theory (cf. Section 3.2.1 and Section 3.5.3, note that receiver noise is also present). If one input is now set to approximately TE (Fig. 5.6(b)), the interferometric noise is reduced in magnitude but is not eliminated completely, being of similar size to the thermal noise alone; this is attributed to imperfect polarisation orthogonality.

The low bandwidth of the coherent crosstalk induced noise results in errors that occur in bursts. This behaviour is illustrated by a histogram of the error count recorded over a one second interval (Fig. 5.7). Although it is most likely that the error count will be less than 100, counts of over 1000 were also measured. A similar measurement for the faster incoherent beat noise crosstalk would give a distribution of much smaller range. The burstiness over a one second interval makes BER measurement impractical.

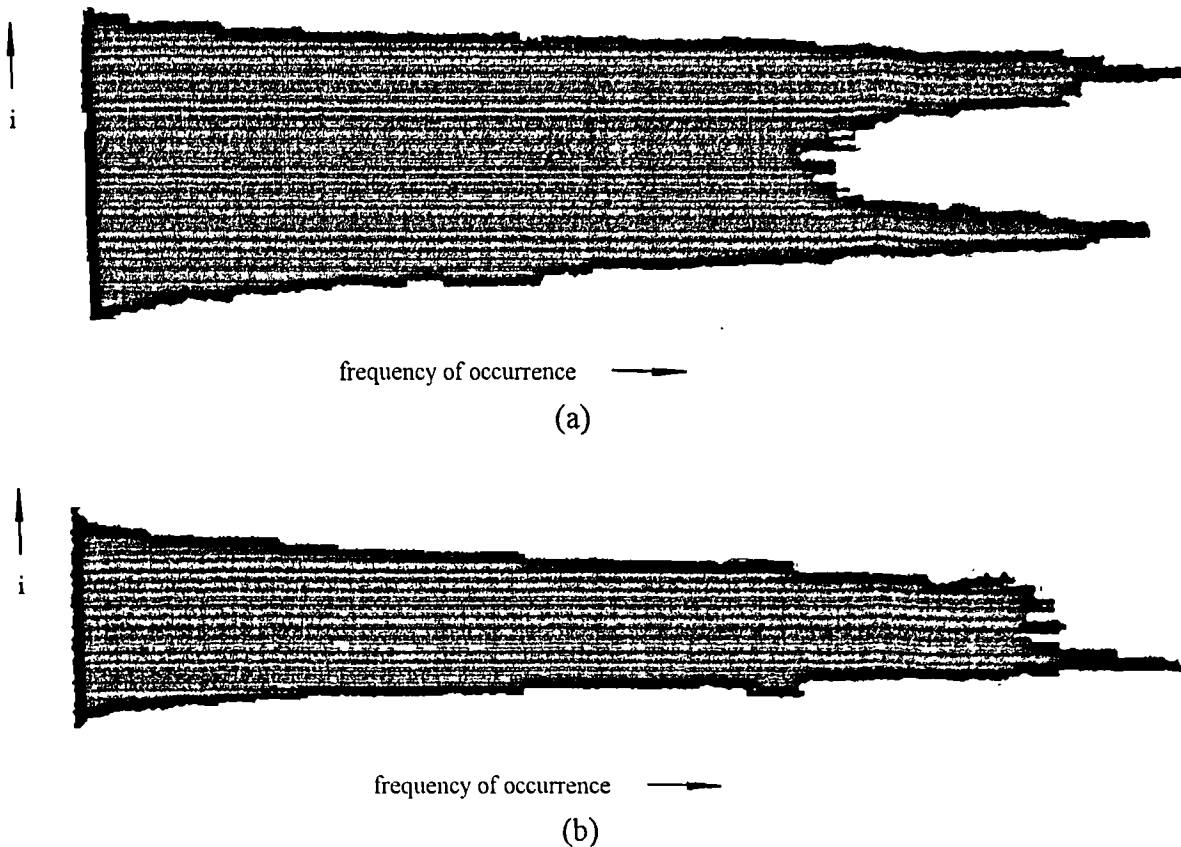


Figure 5.6. Coherent interferometric noise histograms. (a) both inputs TM polarised, (b) input polarisations approximately orthogonal.

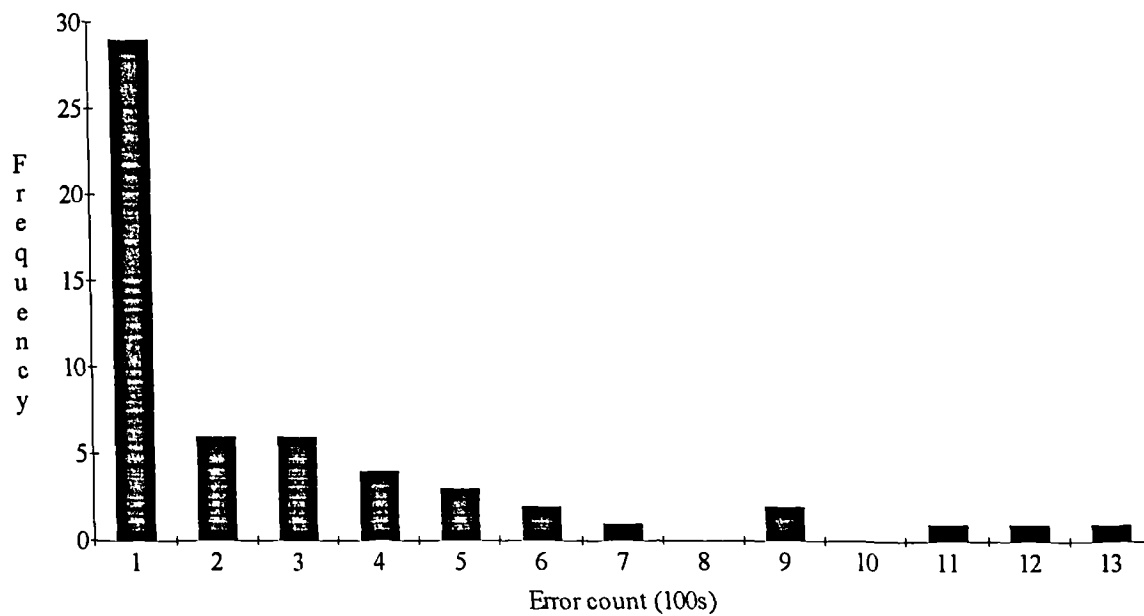


Figure 5.7. Histogram of coherent crosstalk error count, measured over one second at 622 Mb/s.

5.2.3 Incoherent beat noise crosstalk - direct modulation

Incoherent beat noise crosstalk was generated from a single directly modulated source (this is phase-induced intensity noise, PIIN) (Fig. 5.8). The delay of 25.7 ns (16 bits at 622 Mb/s) was sufficient to satisfy the incoherent limit for the chirped source (biased 2mA below the threshold and modulated by 40 mA). The configuration employs a 10 dB fibre coupler, rather than a LiNbO₃ directional coupler, to mix the data and crosstalk. This eliminates the drifting of the crosstalk level and the optical amplifier is no longer required. The optical power meter permits monitoring of the received optical power during the BER characterisation.

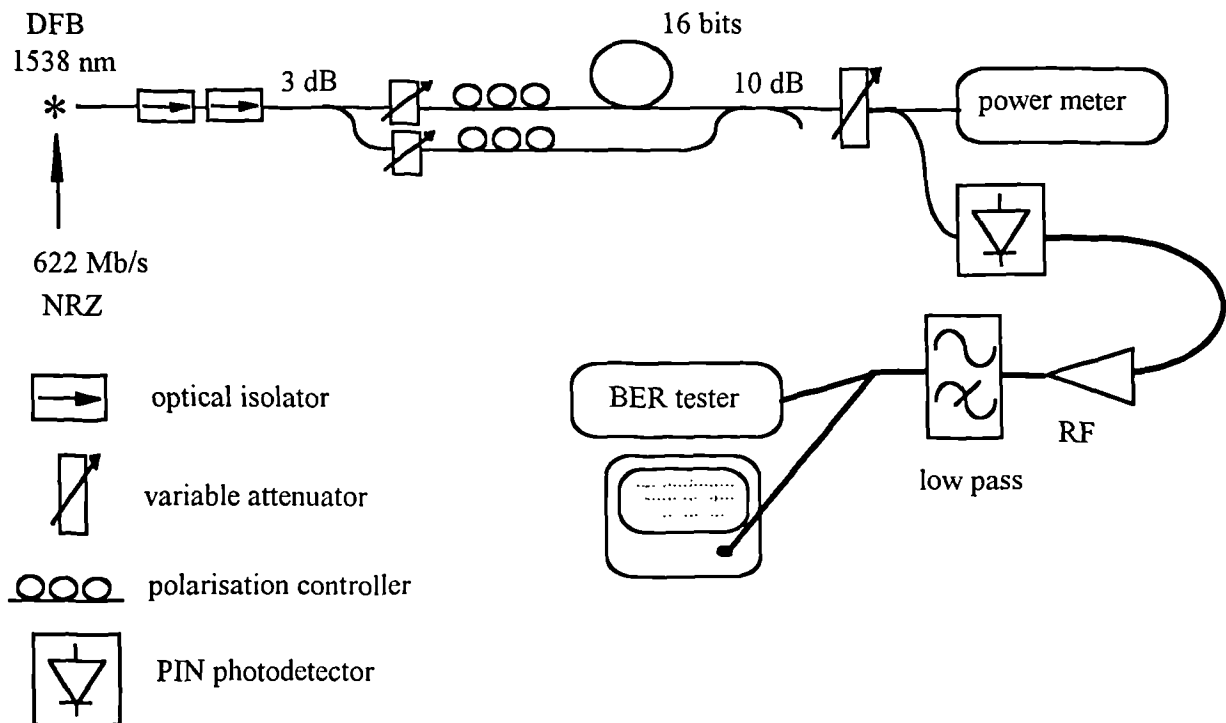


Figure 5.8. Test-bed arrangement for characterisation of incoherent beat noise crosstalk.

'Flame-like' interferometric noise is easily observed on an oscilloscope trace. It displays the anticipated polarisation dependence, arising only when both data and crosstalk are 'one', and has the expected pdf. However, on closer inspection of many bits, the noise pdf took either a bounded form (Fig. 5.9(a)), a Gaussian-like form (of smaller variance) (Fig. 5.9(b)), or some intermediate state. This demonstrates that the interferometric noise is being RF filtered to different degrees on different bits. It is shown in Chapter 7 that the filtering results from a change in the centre frequency of

the laser during an individual bit, leading to a centre frequency variation along the bit sequence. This may be predicted given the modulation sequence and the parameters of the underlying physical mechanism.

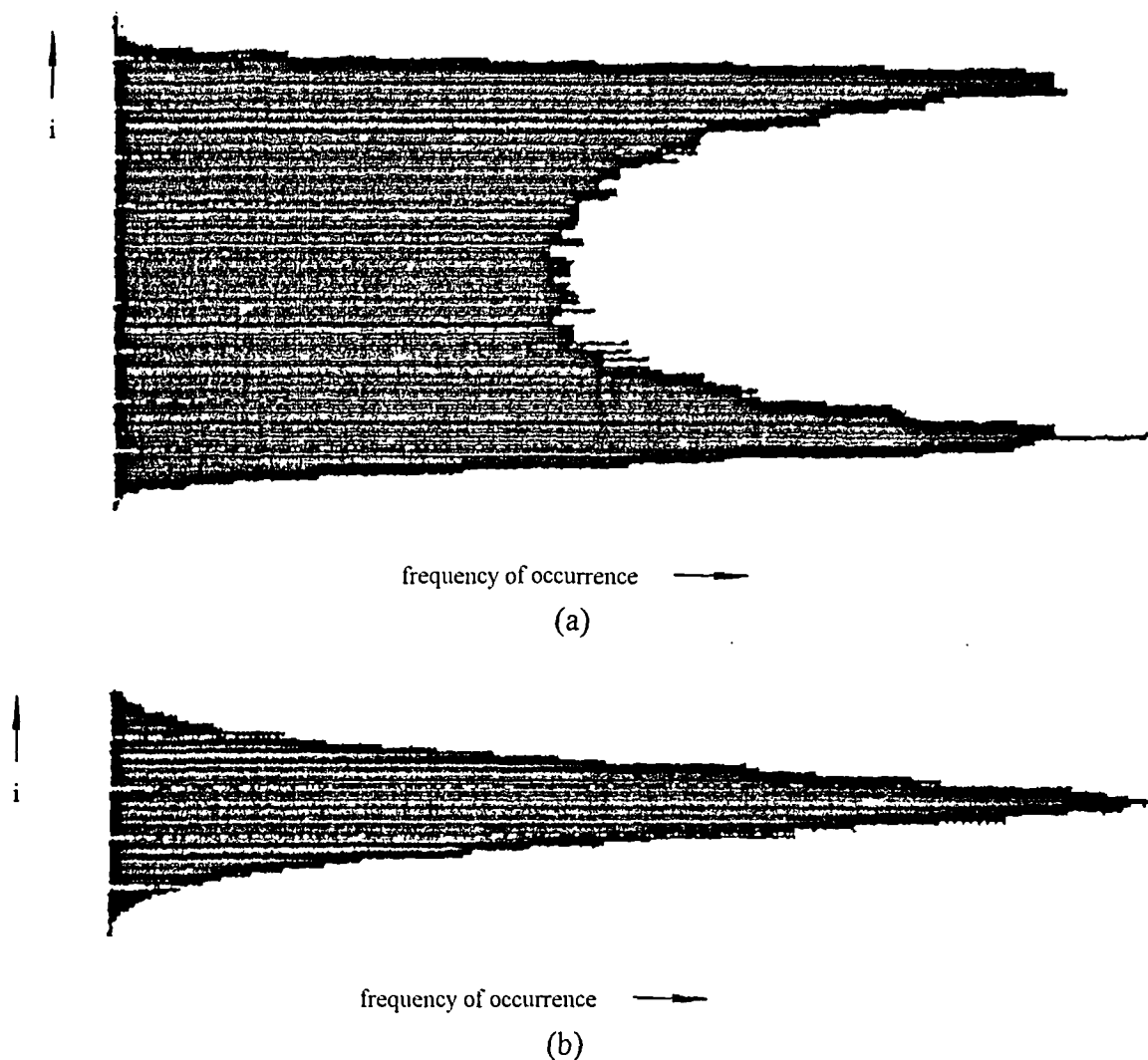


Figure 5.9. Histograms of incoherent beat noise at two different 'one' bits of a 622 Mb/s word subject to crosstalk, (a) bounded form (as expected), and (b) Gaussian-like due to filtering.

Estimations of the interferometric noise range for bits with bounded histograms gave values of approximately 70% of the theory. Although the centre frequencies of interfering bits are identical at such points, RF filtering of the baseband noise still occurs.

In a delayed¹ self-homodyne measurement [3] of the laser CW linewidth, a series of sharp peaks in the RF spectrum, regularly spaced 34 MHz apart, were noted. These are consistent with a reflection from the (first) external isolator at 2.94m (cf. Section 2.3.3).

The BER was measured with a 622 Mb/s 2^{15} -1 pseudo-random bit sequence (PRBS) for different values of crosstalk (Fig. 5.10). The threshold was optimised and the receiver bandwidth was measured to be 530 MHz (6dB electrical) - this approximates to the ideal value of $0.7 \times \text{bit rate} = 435$ MHz. The gradient of the BER curve becomes shallower as the crosstalk level is increased, an indication that unbounded interferometric noise is present (cf. theoretical plots with Gaussian interferometric noise, Section 3.5.3). It is postulated that the RF filtering, present to some extent on all bits, renders the noise unbounded. An error floor of greater than 10^{-9} occurs for crosstalk > -9 dB.

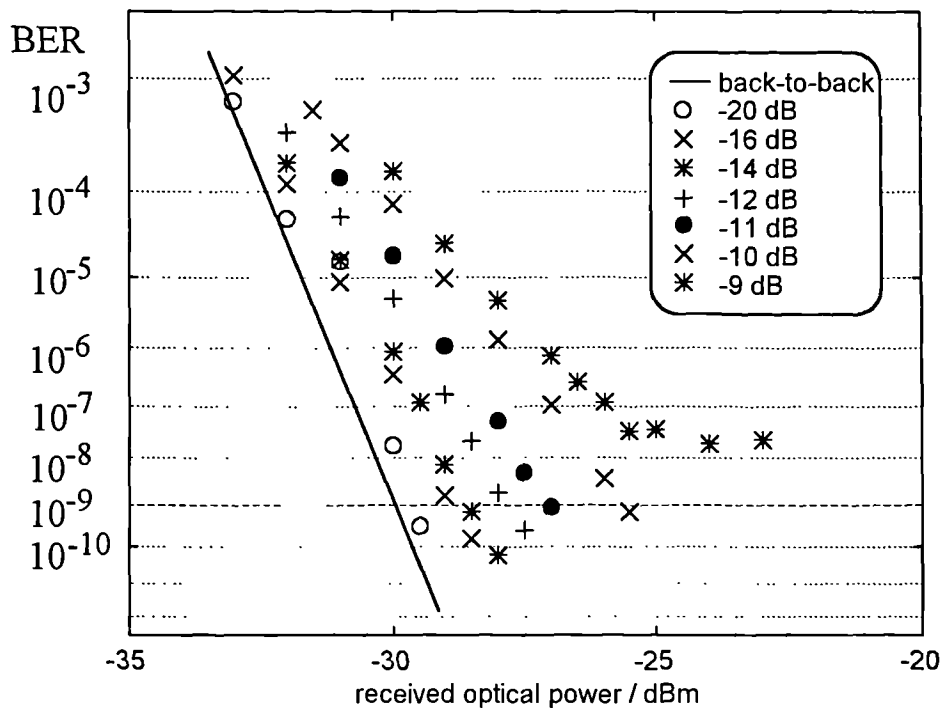


Figure 5.10. BER characterisation of phase-induced intensity noise for different values of crosstalk level. The DFB laser was biased 2 mA below threshold and was directly modulated by a 622 Mb s 2^{15} -1 PRBS NRZ pattern. The receiver bandwidth was 530 MHz.

¹many kms of fibre were required to establish the incoherent limit

The measured power penalty (Fig. 5.11) is in good agreement with theory. The discrepancy is attributed to RF filtering of the baseband interferometric noise, and not to the filtering of the non-baseband noise of bits with Gaussian-like pdfs (explained in Chapter 7). Further BER characterisations using a 64-bit word with receiver bandwidths of 530 and 900 MHz showed similar trends and penalties.

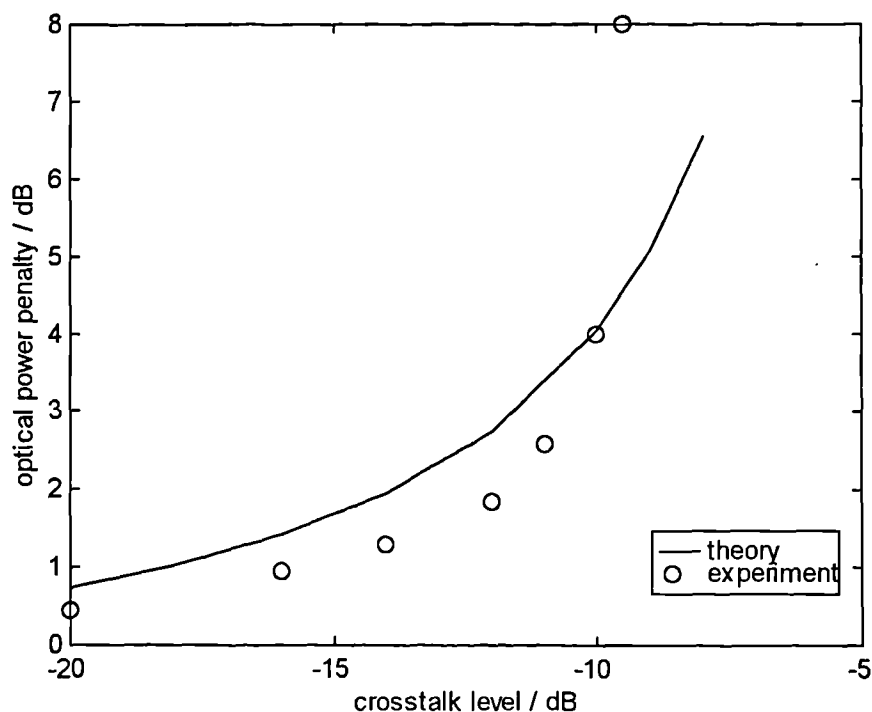


Figure 5.11. Power penalty versus crosstalk level for phase-induced intensity noise with a directly modulated DFB laser.

5.2.4 Incoherent beat noise crosstalk - external modulation

In order to investigate the properties of phase-induced intensity noise in the absence of chirp, the DFB laser of Fig. 5.8 was run CW, and data was encoded by a lithium niobate Mach-Zehnder external modulator. The differential path was increased to the order of 10 km to establish the incoherent limit. It proved difficult to achieve a clean and undistorted RF modulation signal with sufficient amplitude to fully modulate the light; the compromise value 2.0V p-to-p was approximately half of the switching voltage. The DC bias and polarisation were then tuned to maximise the extinction ratio of 'zeros' and 'ones'; approximately 10:1 was realised but this deteriorated owing to drift.

Coherent interferometric noise due to multiple reflections induced a continuous slow fluctuation in the mean received optical power and its influence on the BER made threshold optimisation difficult. Under direct modulation this noise would be incoherent and would pass unnoticed. The BER was measured at 622 Mb/s with a 64-bit word (Fig. 5.12). In contrast to direct modulation the histograms of all bits corrupted by interferometric noise were very similar, showing the expected two-pronged bounded form (cf. Fig. 5.9(a)).

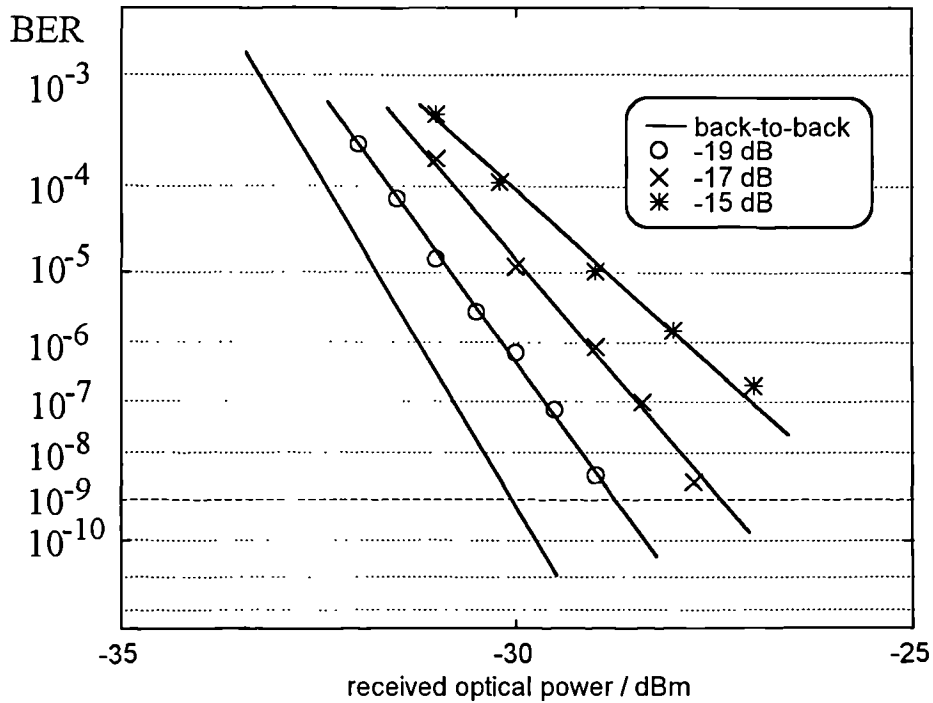


Figure 5.12. BER characterisation of phase-induced intensity noise for different value of crosstalk level. The DFB laser was externally modulated at 622 Mb/s by a 64 bit-word. The receiver bandwidth was 530 MHz.

The power penalties are far worse than for the direct modulation case (Fig. 5.13). It is suggested that this is largely due to the imperfect extinction ratio, α . Comparison with the theory of Section 3.5.7 supports an extinction ratio of 0.1 to 0.2 (Fig. 5.13).

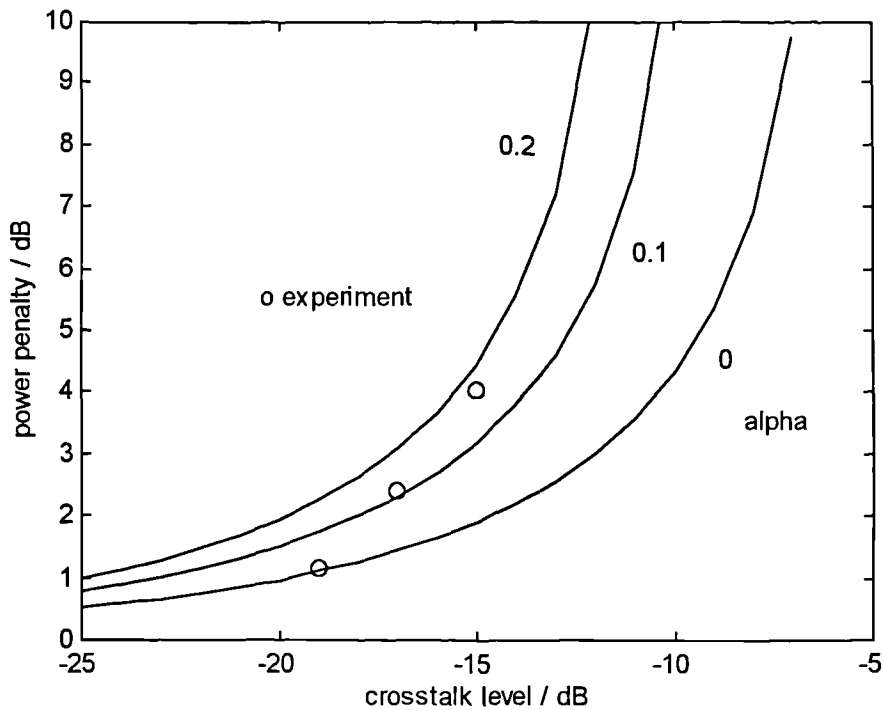


Figure 5.13. Power penalty versus crosstalk level for phase-induced intensity noise with an externally modulated laser. The theoretical curves are reproduced from Section 3.5.7, α is the reciprocal modulation depth.

5.3 Multiple Interferers

5.3.1 Case-study optical TDM switching networks

Optical TDM switching networks were introduced in Section 2.3.8. Small examples of these networks are suitable for demonstration on an experimental test-bed [4-6]. The building blocks are 2x2 directional coupler switches, as employed in the investigation of the single interferer, and accurately cut fibre delay lines. At each of the m spatial inputs the TDM frame is subdivided into an integer number of time-slots, denoted n . Each time-slot may contain a block of bits that may be independently routed to any available time-slot in the output frames. The delays are in multiples of the time-slot and the crosspoints are toggled between 'cross' and 'bar' states every time-slot, as required. The switch fabric is denoted $T(m,n)$, and an example, $T(1,4)$, is depicted below in Fig. 5.14.

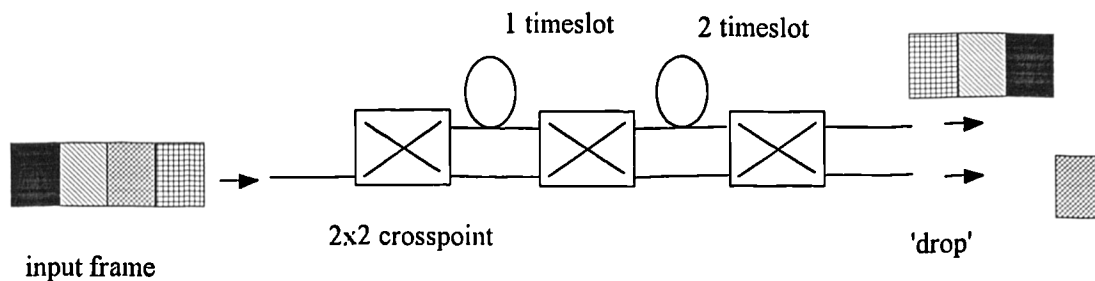


Figure 5.14. $T(1,4)$ optical TDM switching network with 1 input and 4 time-slots per frame.

$T(1,4)$ has only one spatial input ($m=1$) and therefore is also known as a time-slot interchanger - blocks in the four time-slots in each frame may be interchanged in time. In addition, the network possesses frame integrity - blocks entering in the same time frame will exit in the same time frame; this is essential to avoid block loss on reconfiguration of the network. The network operation may be understood by plotting a time-space diagram that tracks individual blocks as they traverse the network in space (drawn horizontally) and in time (drawn vertically). Successive rows represent the network as if photographed every time-slot. In the example (Fig. 5.15) the input blocks $abcd$ occupying input time-slots 1234 respectively are mapped to output time-slots 3241. Block c is dropped to the 'spare' lower output.

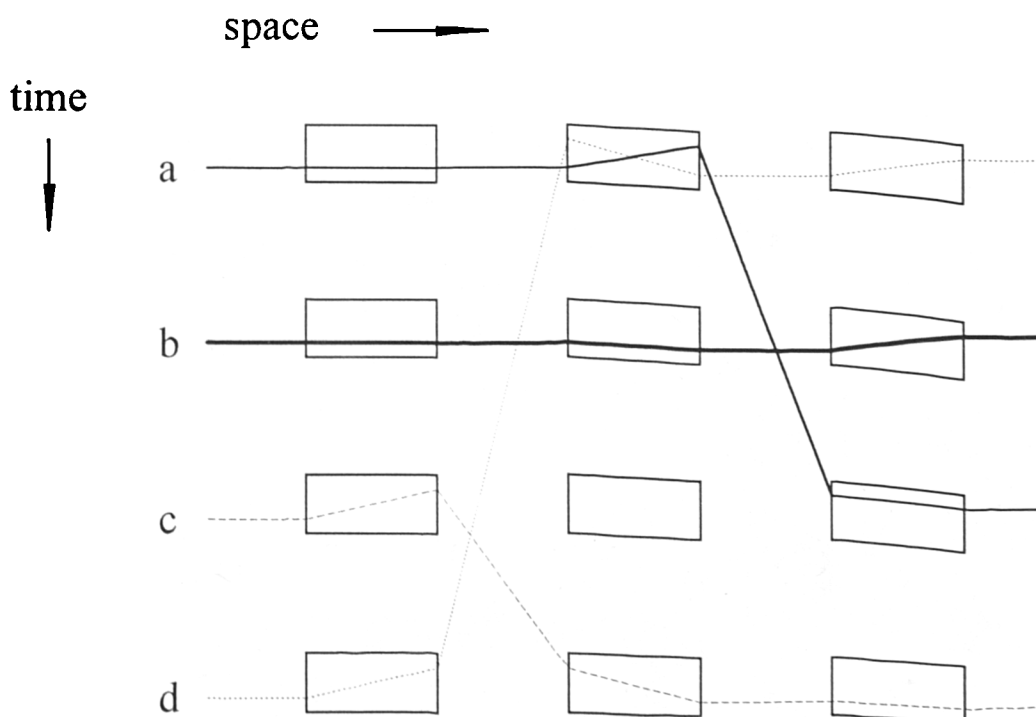


Figure 5.15. Space-time diagram of $T(1,4)$ for a particular routing assignment.

In previous work, the T(1,4) network was realised from 2x2 lithium niobate directional couplers of isolation ~ -15 dB and single mode fibre delay lines [4,6]. The individual crosspoints were set by a data generator running at the block-rate according to computer control. Oscilloscope traces for the above assignment are reproduced in Fig. 5.16.

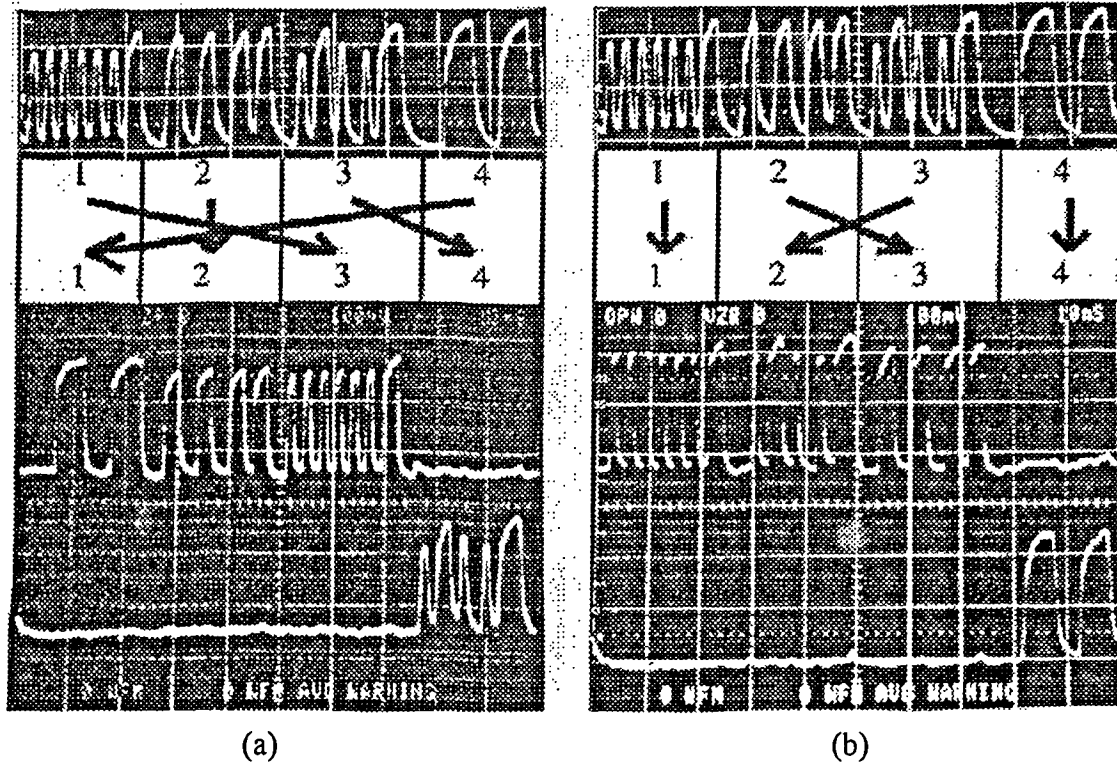


Figure 5.16. Oscilloscope trace of T(1,4) input and output for the assignments. (a) the assignment of Fig. 5.15, (b) another assignment. The bit-rate=720 Mb/s and there are 16 bits per block (from [3]).

BER measurements undertaken on the single dropped block showed an improvement in sensitivity for assignment (a) compared to the back-to-back with no switches. This results from the rerouting of the amplifier noise by the switches. If the assignment is set so that the dropped block meets another block at the central crosspoint, then more crosstalk is exchanged and the sensitivity falls by about 1 dB. Note that since all crosstalk is derived from the same laser, interferometric noise is always generated; coherent crosstalk is impossible - there are no two routes through the network with the same delay; for a directly modulated DFB, whose coherence time is much less than the time-slot, all crosstalk is incoherent beat noise.

Another time-slot interchanger, $T(1,2)$, was constructed on the test-bed from three - 15dB isolated directional couplers and was fed by the 1538nm DFB directly modulated by a 64-bit word representing two frames of two blocks each (Fig. 5.17).

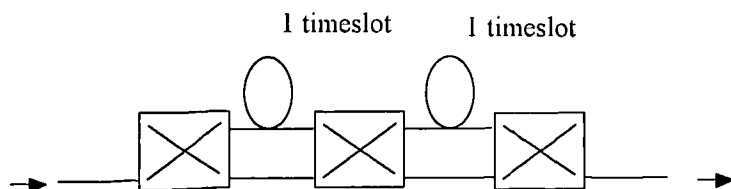
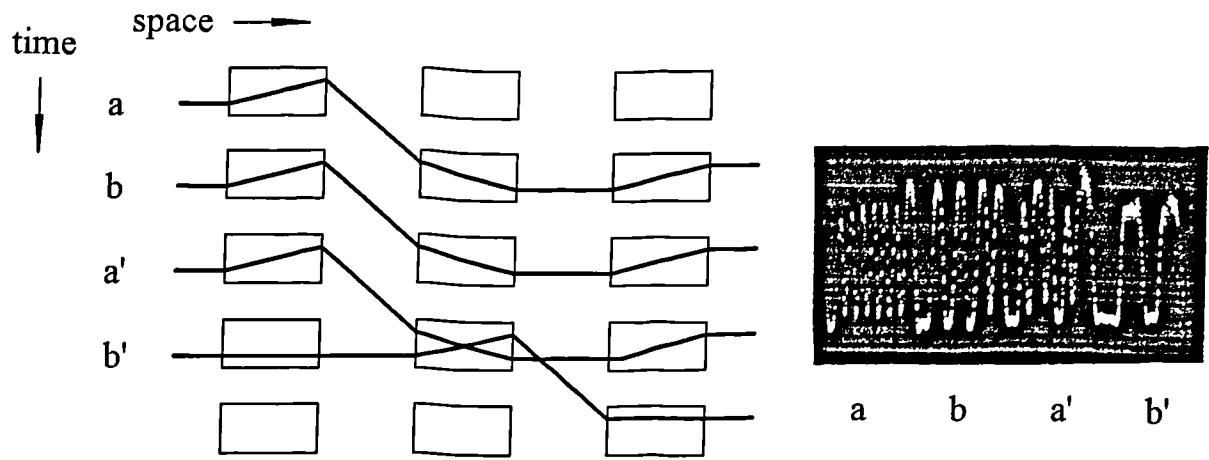


Figure 5.17. Time-slot interchanger formed from three crosspoints.

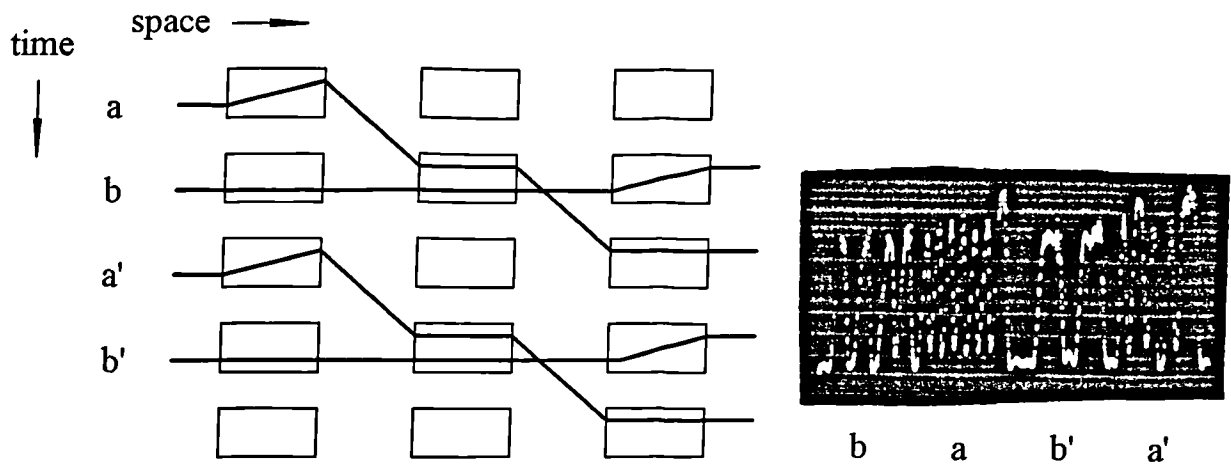
This network possesses multiple delays of delay length=1 time-slot from input to output and is therefore expected to demonstrate coherent crosstalk. Two assignments, A and B, were studied (Fig. 5.18). In assignment A, blocks b and a' suffer coherent crosstalk. This is termed 'second order' since the crosstalk level is of the order of the crosspoint isolation squared; blocks a' and b' suffer 'first order' incoherent beat noise crosstalk since they meet at the centre crosspoint. In assignment B, all blocks suffer first order incoherent beat noise crosstalk but no coherent crosstalk.

BER characterisation of assignment B gave a power penalty of 3.75 dB at $BER=10^{-9}$ (Fig. 5.19). However, approximately 2dB of this is attributed to eye-closure owing to differential path loss (not visible in Fig. 5.18) giving an interferometric noise penalty typical of a single interferer of crosstalk ~ -15 dB. The change in line-gradient is indicative of the optical interferometric noise (cf. Fig. 5.10 & Fig. 5.12).

Finally, a $T(2,2)$ network with frame integrity was constructed (Fig. 5.20). The DFB laser fed both inputs via zero and half time-slot delays to permit block identification. However, each block suffers first order incoherent beat noise crosstalk at each crosspoint (together with some coherent crosstalk - this is less significant being at most second-order). The BER could not be measured in the presence of such noise. However, if two lasers had been employed the incoherent beat noise power would be halved on average, and of course performance would also benefit from better crosspoint isolation.



Assignment A. Note incoherent beat noise crosstalk for blocks a' and b'; b and a' also show coherent effects but these are difficult to capture on photographs.



Assignment B. Note the incoherent beat noise on all blocks.

Figure 5.18. Space-time diagrams and oscilloscope traces for $T(1,2)$ time-slot interchanger.

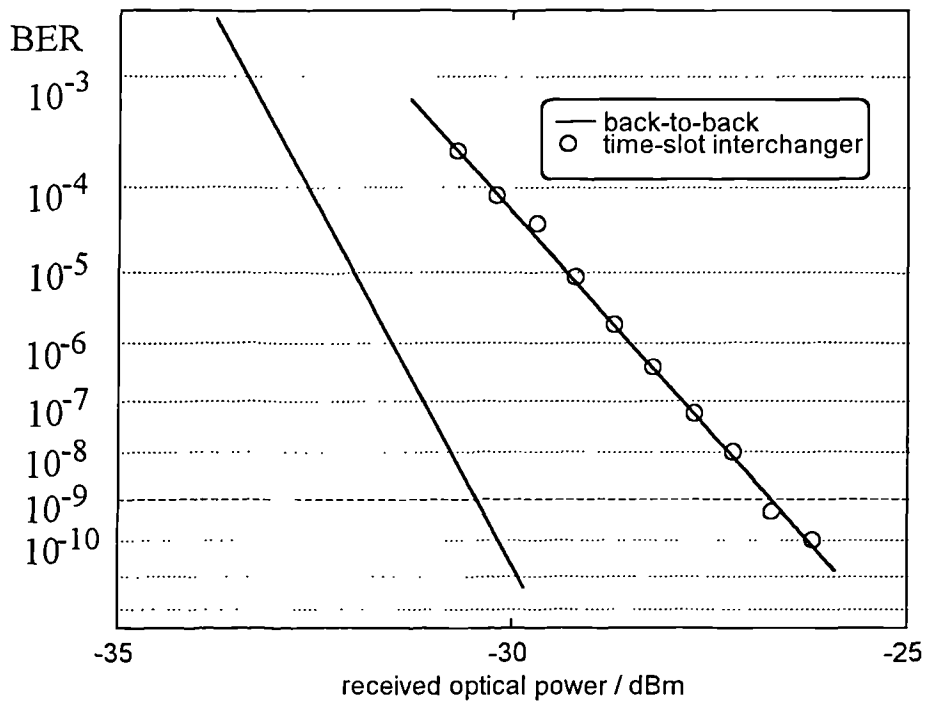


Figure 5.19. BER characterisation of $T(1,2)$ time-slot interchanger of Fig. 5.17. Data comprised four 16 bit blocks at 622Mb/s routed according to assignment B.

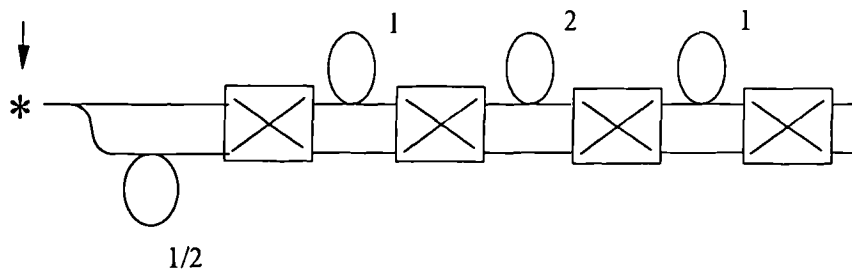


Figure 5.20. $T(2,2)$ with frame integrity fed from a single laser.

5.3.2 Recirculating delay-line

Multiple crosstalk terms may be generated without the complexity of active componentry by utilising a fibre coupler and a recirculating delay line (Fig. 5.21). The principle of operation is as follows: a repeating 64 bit word sequence is fed to a 10:90 fibre coupler with a feedback loop delay equal to the word length. The first word enters the coupler and 90% of the signal is routed to the photodetector. Additionally, 10% of the signal is routed back to the coupler input and on subsequent passage through the coupler 10% of this feedback waveform is added (as crosstalk) to the second data word. The second word also sheds light into the loop but the majority reaches the detector together with the single added crosstalk term.

Light shed into the loop continues to circulate, its power falls due to splitting and propagation losses giving crosstalk addition of ever decreasing amounts to successive data words. Thus, for example, word number three suffers from two crosstalk terms, one due to light shed from word one (after two circulations) and one due to light shed from word two (after one circulation). In general the number of crosstalk terms that corrupt word number n is equal to $n-1$. After many words the total crosstalk power saturates.

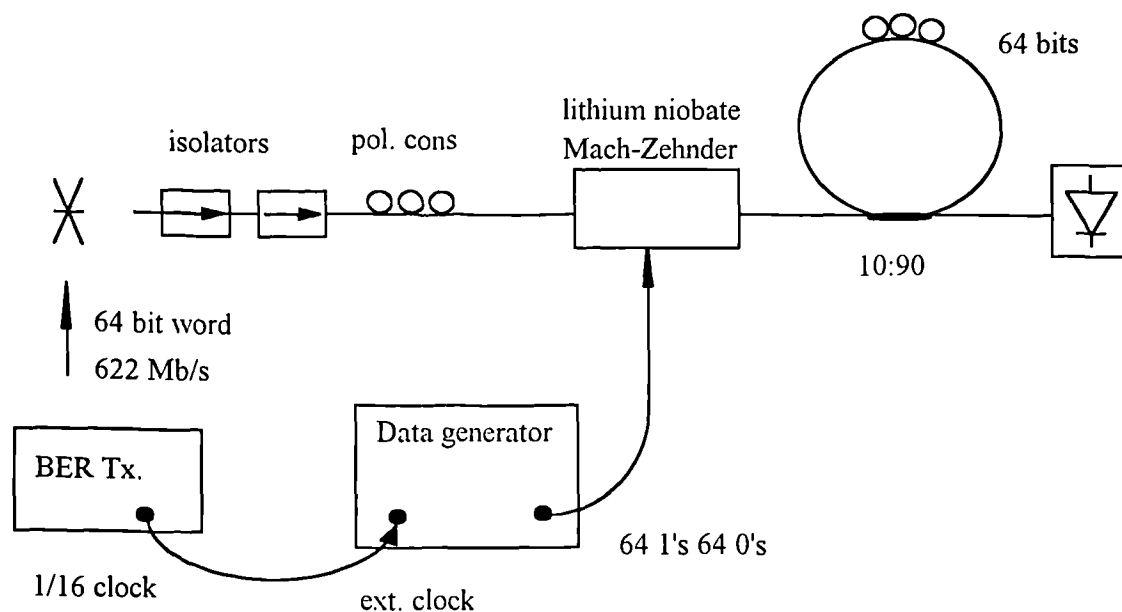


Figure 5.21. Recirculating delay-line experiment.

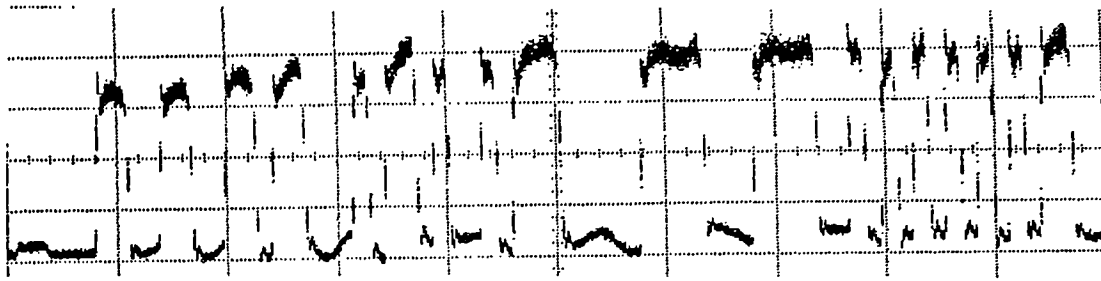
The loop delay greatly exceeds the coherence time of the directly modulated DFB implying that all crosstalk terms are independent and constitute incoherent beat noise crosstalk. Interferometric noise is maximised by alignment of data and crosstalk polarisations. Measurements of the loop patchcord loss (0.50dB), the coupler excess loss (0.27dB) and splitting ratio (9.57:1), imply the crosstalk levels in Table 5.1.

The lithium niobate modulator was gated every 16 words to permit the study of the development of interferometric noise. Fig. 5.22 shows the oscilloscope traces for the first four words whilst Fig. 5.23 shows the change in the noise pdf from the bounded form (one crosstalk term) towards the Gaussian form (fifteen crosstalk terms).

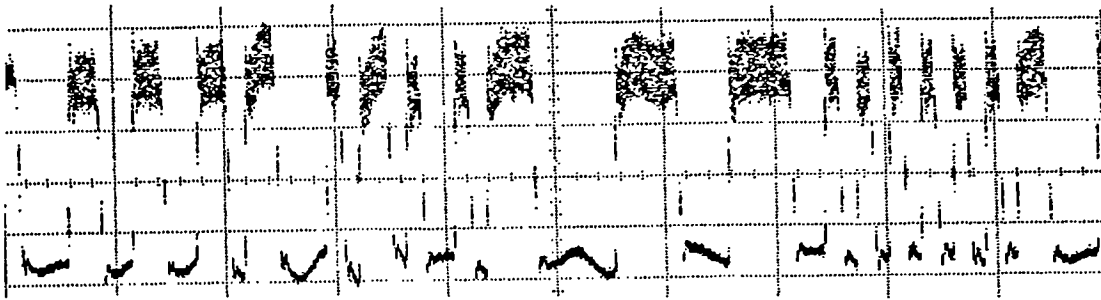
Word number	Crosstalk level of corrupting crosstalk terms (dB)							Total crosstalk (dB)
1	none							-
2	-20.83							-20.83
3	-20.83	-22.04						-18.38
4	-20.83	-22.04	-23.25					-17.15
5	-20.83	-22.04	-23.25	-24.46				-16.41
6	-20.83	-22.04	-23.25	-24.46	-25.67			-15.93
7	-20.83	-22.04	-23.25	-24.46	-25.67	-26.88		-15.59
8	-20.83	-22.04	-23.25	-24.46	-25.67	-26.88	-28.09	-15.36
∞								-14.69

Table 5.1. Detail of crosstalk corruption of successive words in recirculating loop experiment.

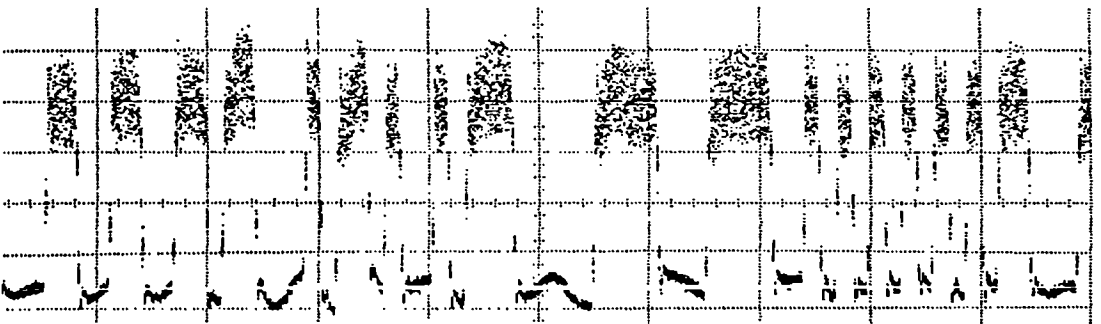
The BER characteristic (Fig. 5.24) is similar to that of the time-slot interchanger of the previous section (Fig. 5.19). The power penalty at BER= 10^{-9} , corrected for the contribution of the crosstalk to the mean optical power, is 2.8dB. This value lies below that expected for Gaussian distributed noise of crosstalk= -14.7dB (error floor above 10^{-9}), but is much higher than that of a single interferer (1.7 dB). The number of significant crosstalk terms, 4 - 5, is not sufficient to satisfy the Central Limit Theorem (cf. section 4.4).



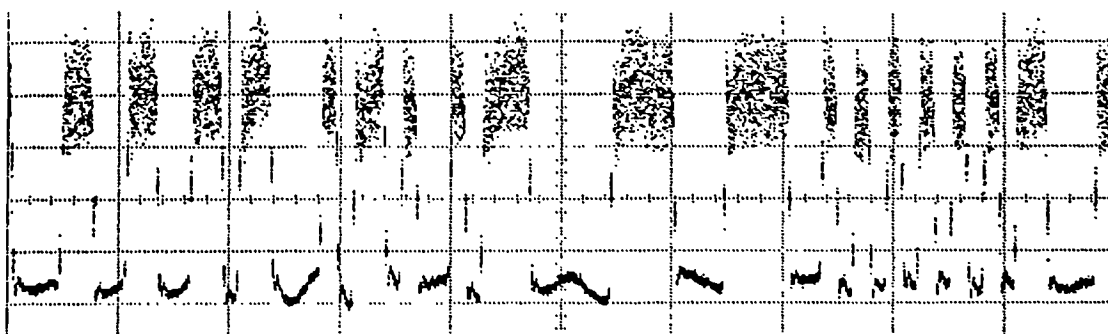
Word number 1.



Word number 2.



Word number 3.



Word number 4.

Figure 5.22. Oscilloscope traces of words 1 to 4.

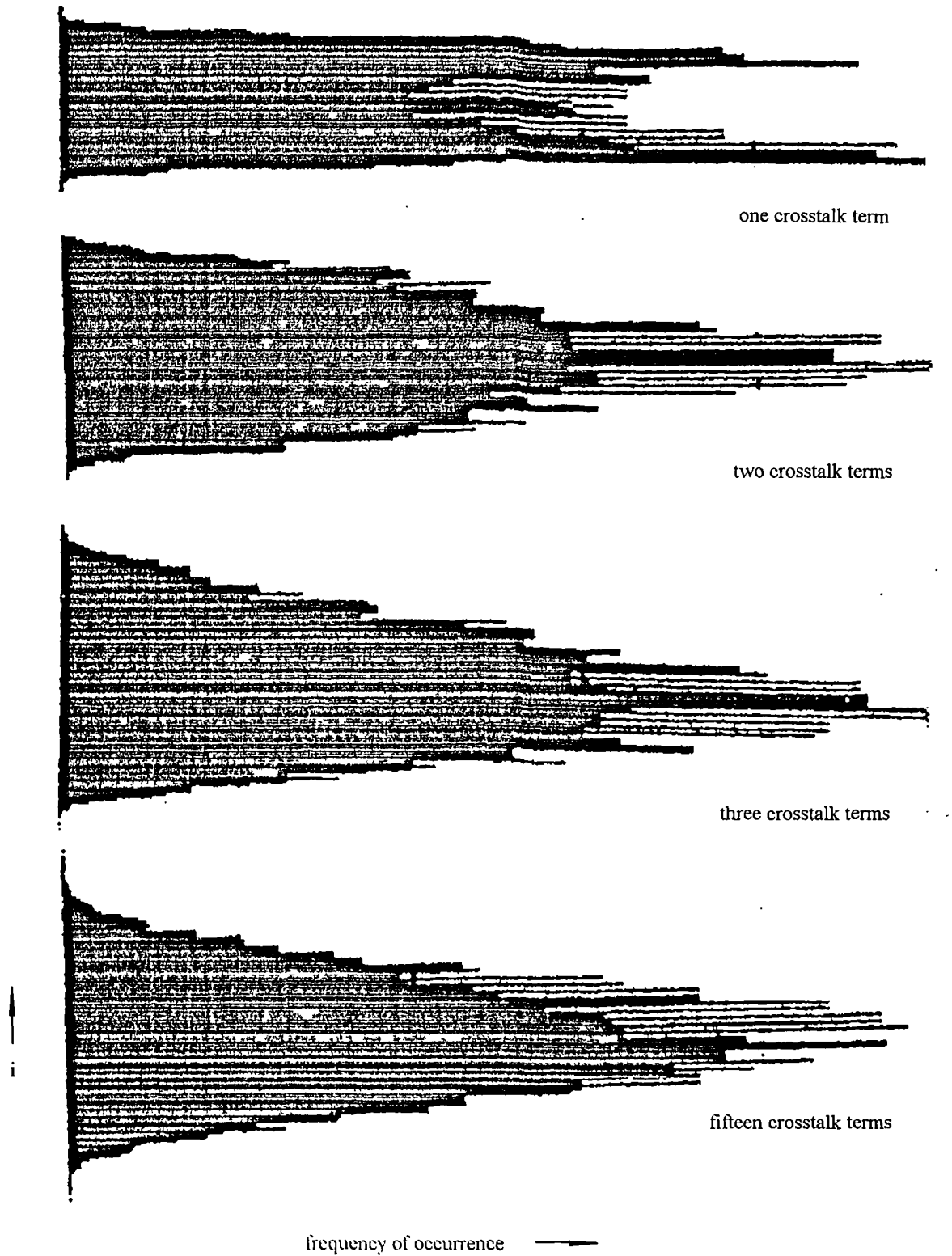


Figure 5.23. Histograms of interferometric noise for words 2,3,4 and 16.

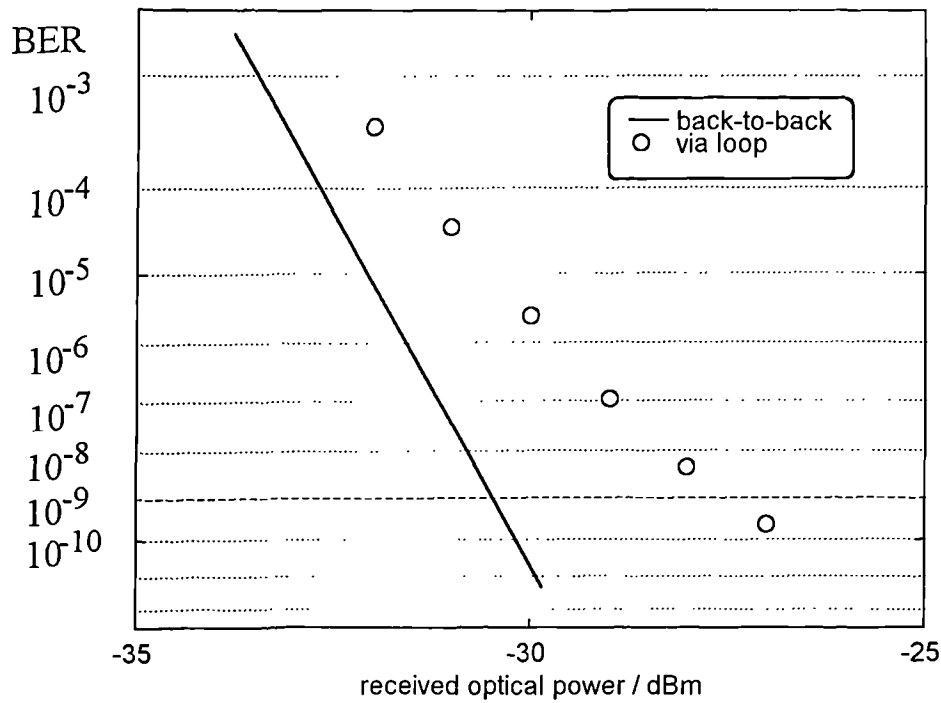


Figure 5.24. BER characterisation of the recirculating loop experiment.

5.4 Conclusions

The experimental study of a single interferer has confirmed many of the predictions of Chapter 3. In particular the importance of maximising the modulation depth is illustrated by the poor BER performance experienced with the external modulator. Unexpectedly, with direct modulation, the noise pdf was found to vary in a seemingly random way between the extremes of bounded and Gaussian forms along the bit sequence. The underlying mechanism for this behaviour may be exploited to suppress interferometric noise, as shall be discussed in Chapter 7. Table 5.2 summarises the key findings for a single interferer.

Optical TDM switching networks comprising -15dB isolated lithium niobate directional couplers and delay lines have been constructed on a test-bed. These networks are prone to all classes of crosstalk but particularly to incoherent beat noise crosstalk that may be of first order magnitude. Coherent crosstalk requires multiple paths of equal delay through the fabric and is at most second order.

Time-slot interchangers requiring three crosspoints, T(1,4) and T(1,2), suffered worst-case penalties of approximately 1.0 and 1.75 dB respectively. A four

crosspoint T(2,2) network whose two inputs were fed by the same laser suffered from too much noise to permit BER measurement.

A recirculating delay-line experiment has demonstrated the evolution of the interferometric noise pdf from the bounded towards the Gaussian form as more crosstalk terms are aggregated. However, the number of significant crosstalk terms (4-5) in the steady state is too small to satisfy the Central Limit Theorem; a penalty of 2.8dB was measured for an aggregate crosstalk of -14.8dB.

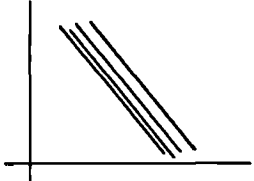
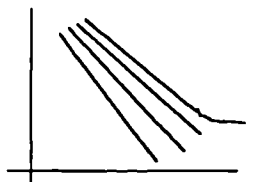
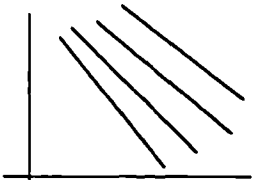
class of interferometric noise	pdf	BER and power penalty	Notes
incoherent noise-free	N/A	 <p>penalty small agrees well with $D=0.5$</p>	
coherent	bounded 'two-prong'	very slow noise \Rightarrow very bursty BER impractical	fibre lengths a few m long
incoherent beat noise - direct modulation	varies from bounded 'two-prong' to Gaussian	 <p>penalty agrees well with theory asymptote at -9.5 dB (D optimised)</p>	baseband noise is slightly filtered
incoherent beat noise - external modulation	bounded 'two-prong'	 <p>penalty \gg theory attributed to poor modulation depth</p>	

Table 5.2. Summary of investigation of a single interferer.

5.5 References

1. A. Selvarajan and J.E. Midwinter, "Photonic switches and arrays on LiNbO₃", *Optical and Quantum Electronics*, 21(1), pp. 1-15, 1989.
2. K. Bløtekjær, "Thermal noise in optical fibers and its influence on long-distance coherent communication systems", *J. Lightwave Technol.*, 10(1), pp. 36-41, 1992.
3. K. Petermann, *Laser diode modulation and noise*, Kluwer Academic Publishers, New York, 1993.
4. D.K. Hunter, P.E. Barnsley, I. Andonovic, and B. Culshaw, "Architectures for optical TDM switching", *OE/Fibers '92*, Paper 1787-18, SPIE, Boston, 1992.
5. D.K. Hunter, I. Andonovic, B. Culshaw, and P.E. Barnsley, "Experimental test bed for optical time-domain switching fabrics", *Optical Fiber Communication OFC/IOOC '93*, paper TuO2, OSA/IEEE, San Jose, 1993.
6. D.K. Hunter, I. Andonovic and P.E. Barnsley, "Demonstration of optical time-slot interchanging through 2x2 crosspoints and feedforward delay lines", *Elect. Lett.*, 30(11), pp. 875-876, 1994.

Chapter 6

Network modelling by the XHatch computer simulator

6.1 Introduction

A computer-aided optical network design tool (XHatch) [1] has been extensively modified to offer new optical components and BER estimation [2]. XHatch is able to track all the optical signals in the simulated network and to determine the crosstalk, interferometric noise and optical amplifier induced noise that corrupt the data at the receiver.

An example of XHatch's user-interface is drawn in Fig. 6.1. The optical network (here a T(1,4) optical TDM switch fabric, cf. Section 5.3.1) is formed from components, selected from the palette on the left hand side of the window, interconnected by fibre or coax as appropriate. Data of binary ASK (NRZ) format is encoded onto the optical medium at laser transmitters. The simulator is digital in nature, it determines the events, i.e. 'one'-'zero' transitions, of all signals that are generated in the network and ultimately fall upon the photodetector. The mean BER is calculated from the error probability of each bit using the crosstalk classification (Section 4.3.1) and the Central Limit Theorem (Section 4.5). Noise due to in-line optical amplifiers is Gaussian distributed and is therefore easily added [3]. The program output takes three forms; an oscilloscope plot of the photocurrent with bars denoting the noise standard deviation; a plot of BER versus signal-to-thermal-noise ratio; and a bit-by-bit listing of the noise contributions.

Examining Fig. 6.1 more closely, in the upper window a T(1,4) optical TDM switching network (cf. Section 5.3.1), formed from three 2x2 switches and delay lines of 16 and 32 ns, is under test. The laser is modulated by a 512-bit PRBS sequence (trace Scp1 in the lower graph window) at a bit rate set by oscillator Os1 (1 Gb/s). The switches are toggled at the block-rate (every 16 bits) set by oscillator Os2 according to the binary sequences stored in pattern generators Pa2-4 - in this case the assignment of Fig. 5.15 and Fig. 5.16(a) has been chosen. The network output is

detected and displayed in the graph window (traces Scp2-3). Note that in every frame of four blocks two blocks suffer large noise (as indicated by the dotted 'error bars') - these correspond to blocks 'a' and 'd' of Fig. 5.15 that traverse the central switch simultaneously and exchange first-order crosstalk.

The remainder of this chapter is devoted to the crosstalk simulation of optical TDM switching networks (cf. Section 2.3.8 and Section 5.3.1 [4-6]). In the next section, the relative magnitude of primary and secondary beating terms (c.f. Section 4.2) for crosstalk of different orders (cf. Section 5.3.1), is addressed for TDM switching networks obtained by time-space transformation of classical Benes space switches [7,8] - networks which are particularly suitable for economic integrated-optical implementation. The network performance with respect to interferometric noise may be improved by transmitting different channels at slightly different wavelengths (such that beating is out-of-band); guidelines are derived for the minimum value of crosspoint isolation as function of the number of different optical frequencies employed.

Results from the simulation of such networks (Section 6.3) highlight the importance of parameters other than the crosspoint isolation on the network performance.

6.2 Comparative magnitude of different beating terms in optical TDM switching networks

Many optical TDM switching network architectures may be obtained by space-time mapping of suitable space switch designs¹ (cf. Sections 2.3.8 and 5.3.1 [4,5]). In this chapter, switching networks derived from the Benes [7,8] architecture are considered [6]. Denoted $T(m,n)$, where m equals the number of spatial inputs and n the number of time-slots per frame, the switch fabrics are rearrangeably non-blocking, suitable for fabrication using large integrated-optical switch arrays giving hardware economy, and offer tremendous capacity. The impact of crosstalk and interferometric noise can be combated by dilation of the architecture [9]. An architecture is dilated by, firstly, replacing a 2x2 crosspoint by four 2x2 crosspoints (Fig. 6.2(a)) such that only a single

¹they may also be obtained by modifying existing results in switching theory [10,11], which is outside the scope of this thesis.

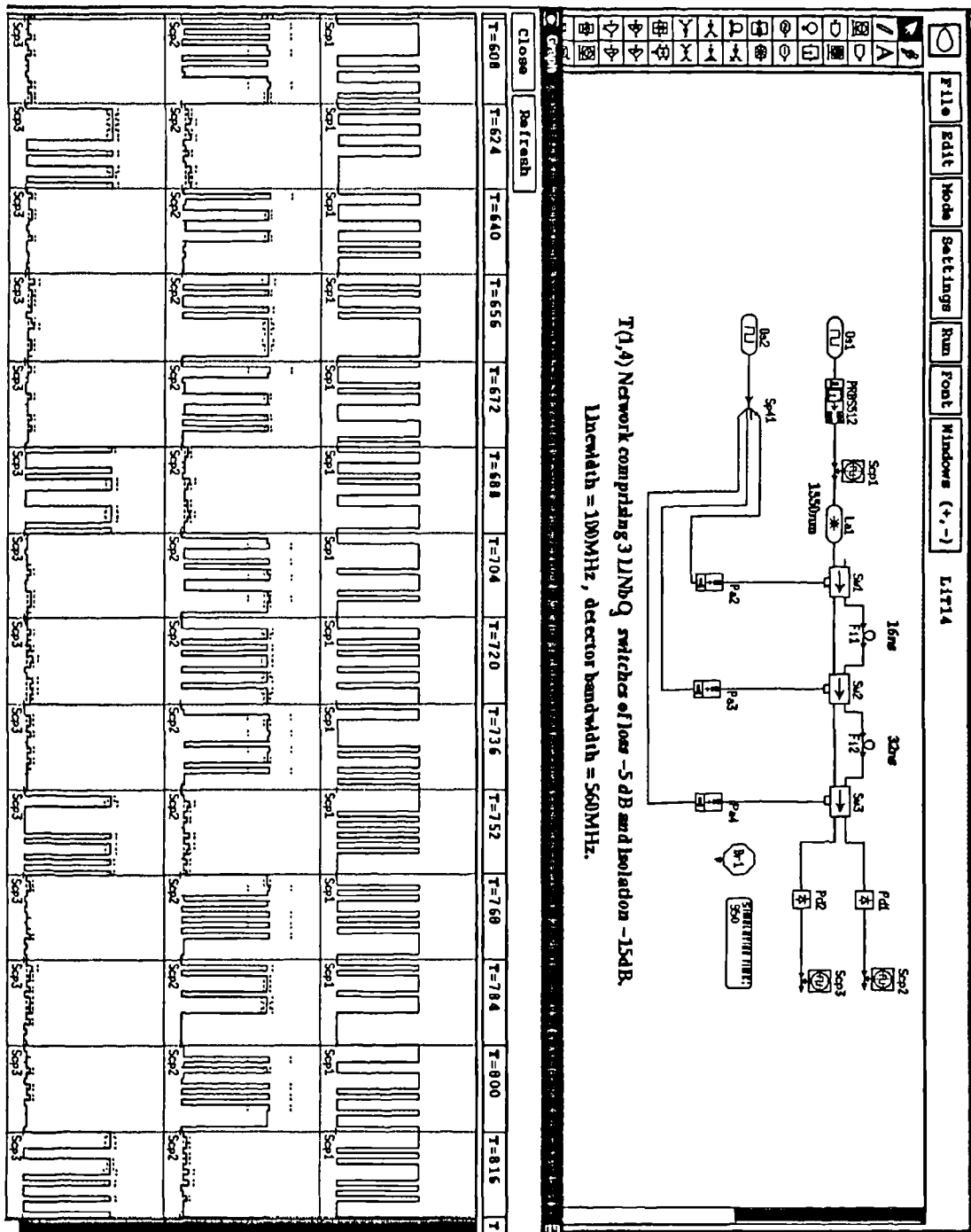


Figure 6.1. The XHatch computer network design tool. In the upper window a T(1,4) network is under test. The lower graph window displays the input sequence (Scp1) and the output sequences (Scp2-3). The dotted lines indicate a single standard deviation of the interferometric noise from the mean.

input of any crosspoint is used at any one time¹, thereby eliminating the possibility of first order crosstalk addition to the data. The number of crosspoints is rationalised (many are redundant, Fig. 6.2(b)), resulting in a total crosspoint count approximately twice that of the original undilated structure. A dilated T(4,4) network, for example, comprises 40 crosspoints arranged in 10 columns (Fig. 6.3).

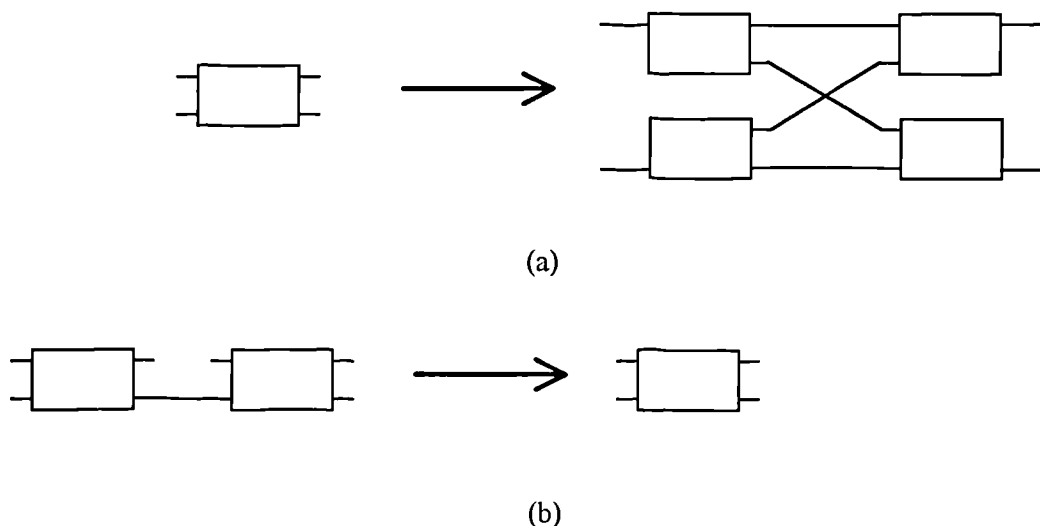


Figure 6.2. Dilation of a space switch. (a) step one - every crosspoint is replaced by four crosspoints; (b) step two - redundant crosspoints are removed.

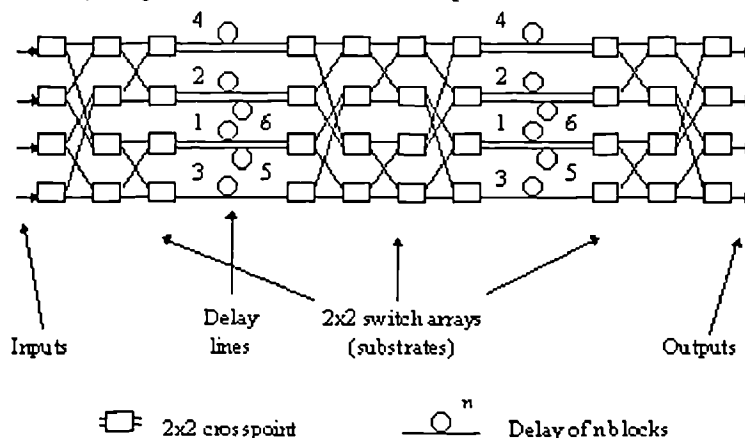


Figure 6.3. Dilated T(4,4) optical TDM switching architecture.

The number of crosspoint stages s (i.e. columns of switches) required to construct T(m,n) when $n=m^2$ is given by:

¹ this does not imply that calls be broken if new calls are added to the system.

$$s = 6 \log_2 m - 1 \quad \text{undilated} \quad (6.1)$$

$$s = 6 \log_2 m + 4 \quad \text{dilated} \quad (6.2)$$

The number of crosstalk terms at every output of the network is dependent upon the number of stages s , equalling $2^s - 1$ and $2^{s-1} - 1$, for undilated and dilated fabrics, respectively. Large fabrics therefore suffer very many terms - for example, a dilated T(16,256) has 134 million. However, it shall be shown that only the second-order crosstalk terms are significant for dilated fabrics; T(16,256) has 378 of these. The number of terms of order p is also determined by the number of stages (Table 6.1). Note that odd-ordered terms do arise in dilated fabrics but exit by the unused ports of the final switch rank and do not corrupt the data.

Order of crosstalk	Number of crosstalk terms	
	undilated T(m,n) s stages	dilated T(m,n) s stages
1 st	s	0
2 nd	$s(s-1)/2$	$s(s-1)/2$
3 rd	$s(s-1)(s-2)/6$	0
4 th	$s(s-1)(s-2)(s-3)/24$	$s(s-1)(s-2)(s-3)/24$
p	$\binom{s}{p} = \frac{s!}{p!(s-p)!}$	$\binom{s}{p} = \frac{s!}{p!(s-p)!}$ p even else zero

Table 6.1. Number of crosstalk terms of different order corrupting data in T(m,n) switching network.

The advantage of dilation may be illustrated by considering the minimum crosspoint isolation required to give a total crosstalk level of less than -25dB - this guideline having been established in Section 4.6 (the receiver is AC-coupled, modulation depth is infinite, secondary beating is neglected and all primary beating components have aligned polarisations, are in-band and unfiltered, Fig. 6.4). The dilated structure can tolerate crosspoints with 13dB worse isolation than the undilated. Larger networks require better crosspoint isolation - dilated T(4,4) and dilated T(16,256) require -20.8dB and -25.4dB, respectively.

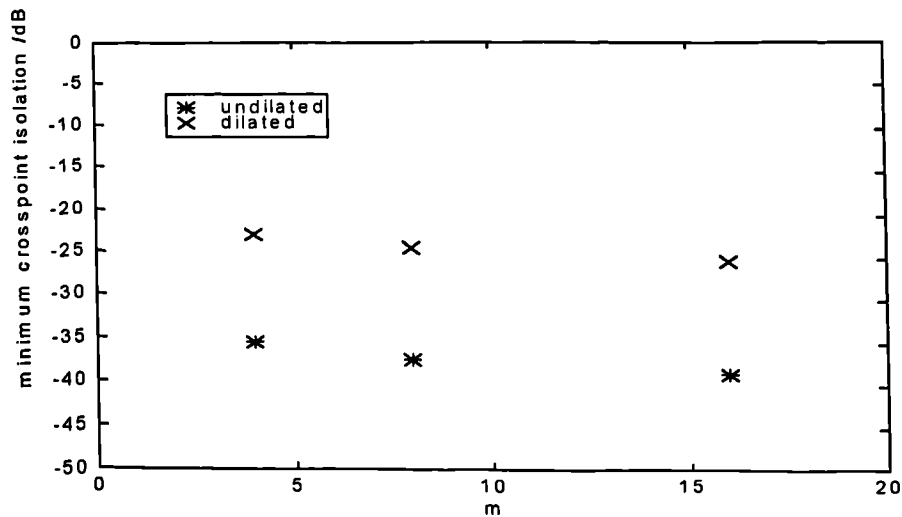


Figure 6.4. Crosspoint isolation required for satisfactory performance of $T(m,n)$ (with $n=m^2$).

When the inputs to the switching network comprise lasers of different wavelengths, and it is assumed that beating between different lasers is outside the receiver bandwidth, the crosspoint isolation specification is relaxed. It is assumed that the input traffic is uniformly distributed over k wavelengths - the probability that any two waveforms at the output generate in-band noise $=1/k$. The minimum crosspoint isolation (dB) increases as $5 \log(k)$ (Fig. 6.5). For example, the isolation is relaxed by 5dB when the number of wavelengths is increased by $\times 10$, e.g. from 1 to 10. Only primary beating of data and second-order crosstalk is included for these dilated architectures. This shall now be justified.

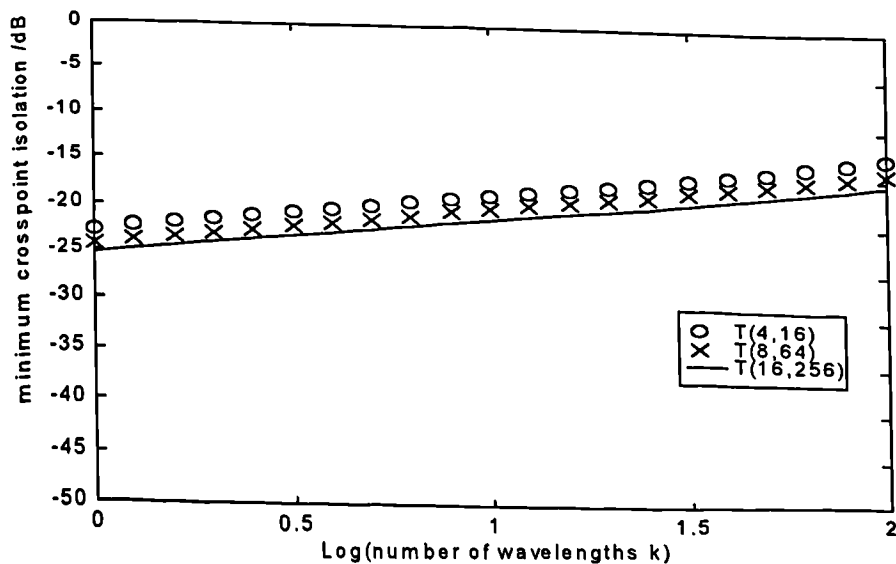


Figure 6.5. Crosspoint isolation required for satisfactory performance of dilated $T(m,n)$ as a function of the number of wavelengths k .

In a *dilated* network the ratio of the interferometric noise power from primary beating of data and second order crosstalk, to that of data and fourth order crosstalk is given by:

$$\Gamma_{2/4} = \frac{\sigma^2(\text{data} - \text{second} - \text{order crosstalk})}{\sigma^2(\text{data} - \text{fourth} - \text{order crosstalk})} = \frac{12}{(s-2)(s-3)\eta^2} \quad (6.3)$$

where s = the number of stages, and η = the crosspoint isolation.

The minimum value of this ratio, occurring when the crosspoint isolation is only just sufficient for satisfactory performance given k wavelengths, varies little with the fabric dimension, falls with the number of wavelengths as the isolation is relaxed, but remains very much greater than one (Fig. 6.6). The fourth-order crosstalk may be neglected given $k < 100$ ($\Gamma_{2/4} \geq 20$).

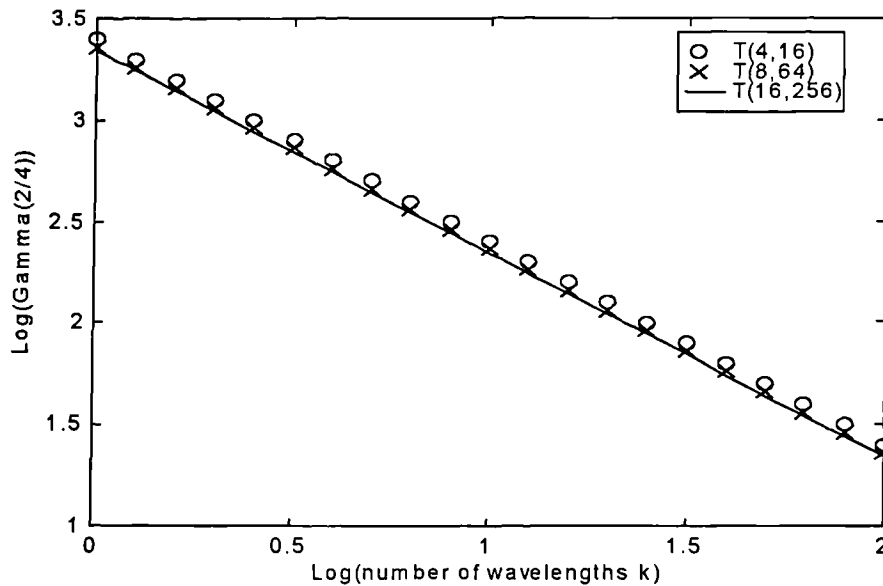


Figure 6.6. Dependence of the ratio of the interferometric noise power from primary beating of data and second order crosstalk, to that of data and fourth order crosstalk, on the number of wavelengths.

Finally, the ratio of the noise variance of primary data - second-order crosstalk beating, to secondary second-order - second-order is given by:

$$\Gamma_{p/s} = \frac{\sigma^2(\text{data} - \text{second-order crosstalk})}{\sigma^2(\text{second-order crosstalk} - \text{second-order crosstalk})} = \frac{4}{(s(s-1) - 2k)\eta^2} \quad (6.4)$$

where s = the number of stages, k = the number of wavelengths and η = the crosspoint isolation.

The ratio is very much greater than one, falling with the number of wavelengths as the isolation is relaxed; secondary beating terms may be neglected given $k < 100$ ($\Gamma_{p/s} \geq 10$). Although secondary crosstalk-crosstalk beating terms are significant for data 'zero' bits, the BER is dominated by the data 'one' bits when the receiver is AC-coupled (as assumed above).

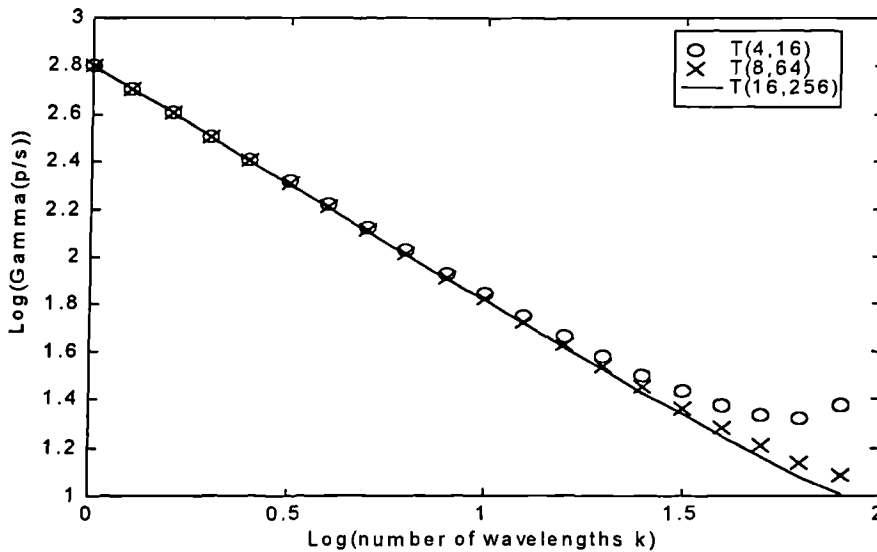


Figure 6.7. Dependence of the ratio of the noise variance of primary data - second-order crosstalk beating, to secondary second-order crosstalk - second-order crosstalk, on the number of wavelengths.

6.3 Simulation of optical TDM switching networks

Simulation of optical TDM switching networks by XHatch employed the following conditions [2]:

- dilated T(4,4), T(4,16) and T(8,64) modelled.

- one laser feeding each input.
- laser wavelengths separated by 1nm so that beating between different lasers is out-of-band.
- 32 bits/block.
- $2^{10}-1$ PRBS sequence.
- all crosspoints possess the same loss and isolation.
- all polarisations aligned.
- crosstalk classification invoked (partial coherence forbidden, cf. Section 4.3.1).
- no filtering of base-band noise.
- secondary beating neglected (justified above, Section 6.2).
- net interferometric noise is Gaussian distributed (Central Limit Theorem, cf. Section 4.5).
- BER determined by averaging over one complete bit sequence (cf. Section 4.5).
- decision threshold, D , was optimised or held midway between 'zero' and 'one' levels ($D=0.5$, similar to AC-coupled receiver).

All networks suffer sufficient noise-generating crosstalk terms ($T(4,4)$ has the fewest at 11 (on average)) for the Gaussian approximation to be accurate, assuming some slight filtering of the baseband noise (cf. Section 4.4). The results are applicable to directly modulated DFB sources which satisfy this criterion; the laser employed in the experimental studies is such an example. However, the restriction on partial coherence excludes externally modulated DFBs whose coherence time is far greater.

Examination of the crosstalk components at the output of the dilated $T(4,4)$ indicated that only 60% of incoherent beat noise crosstalk terms had a unique delay value not shared by any other, and could therefore be added as statistically independent variables. The influence of the statistical dependence remains to be studied.

The power penalty at $BER=10^{-9}$ was determined (Fig. 6.8 and Fig. 6.9). The following conclusions can be drawn:

1. The power penalty characteristic displays a very rapid rise towards an asymptote representing an error floor at $BER>10^{-9}$. Such behaviour has been observed in experiment (Chapter 5) and statistical simulation (Chapter 4).
2. Optimisation of the decision threshold gives a performance improvement that falls with increasing network size; for example, for $T(4,4)$, the asymptote occurs

at an isolation of -15dB compared to -17dB for the AC-coupled receiver (cf. a single interferer where the difference is 4.6 dB).

3. The performance varies markedly between different channels and is assignment dependent (Fig. 6.8). Near the asymptote this variation is greater and periods of error flooring are likely - the crosspoint isolation should be held several dB better than the asymptote.
4. Performance, as measured by the position of the asymptote, degrades with increasing network size. For T(8,64) the isolation should be better than -20dB to give a mean penalty of less than 1dB (using Fig. 6.5 an isolation of -19.8dB is required).

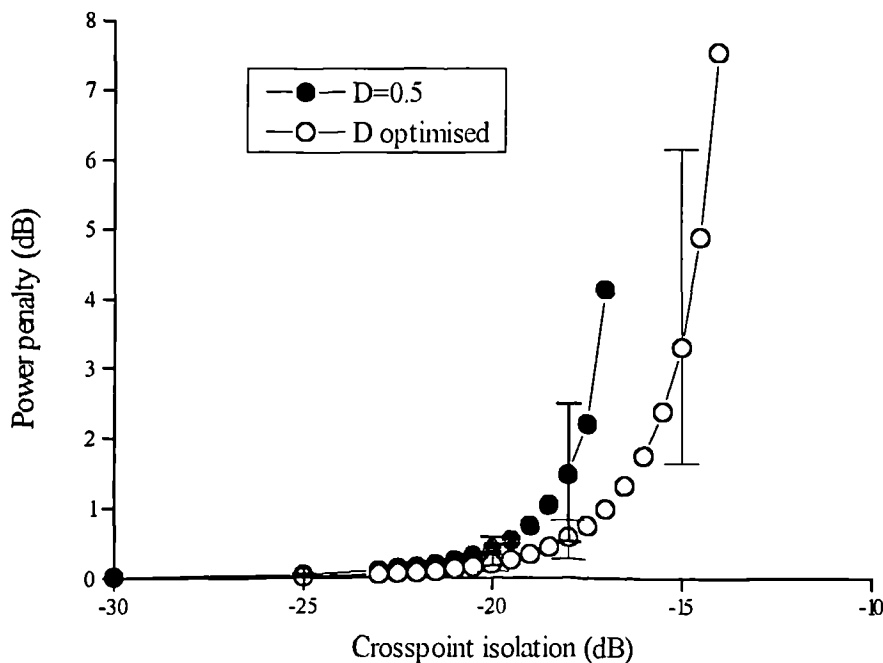


Figure 6.8. Power penalty versus switch isolation for a dilated T(4,4) network fed by four lasers. The decision threshold D is both optimised or set mid-way between 'zero' and 'one' levels ($D=0.5$). Bars signify best and worst case performance as channel number and assignment was varied.

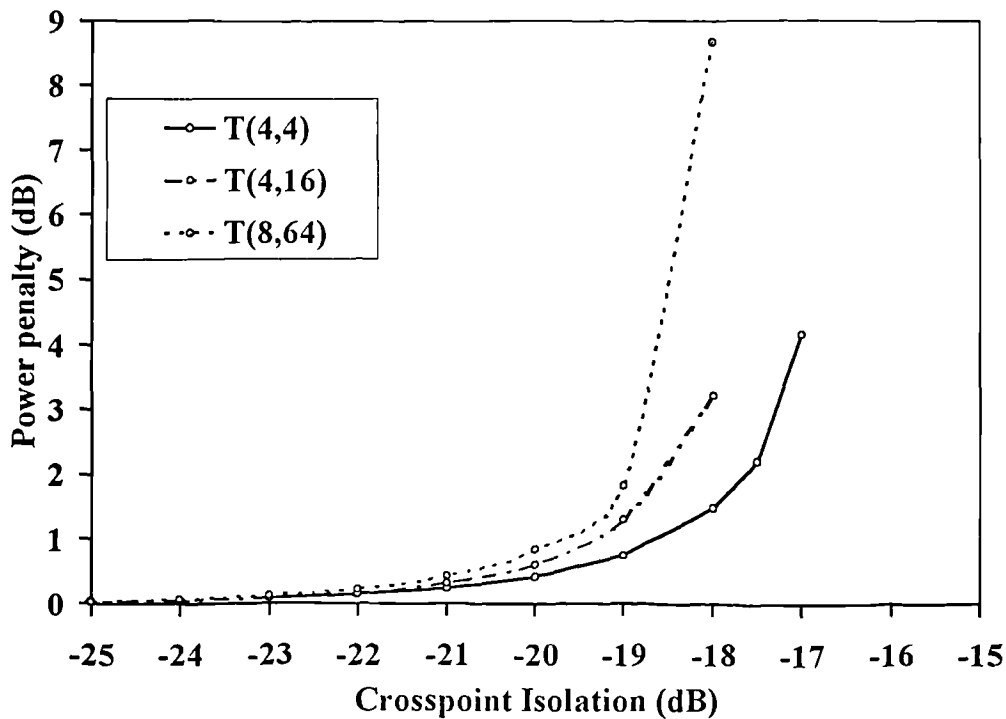


Figure 6.9. Typical performance of $T(4,4)$, $T(4,16)$ and $T(8,64)$ architectures for AC-coupled receivers.

6.4 Conclusions

Optical TDM switching networks are prone to interferometric noise owing to switch crosstalk. Dilation of the architecture approximately doubles the crosspoint count but eliminates first-order crosstalk, thereby relaxing the crosspoint isolation specification for every fabric by 13 dB. The (minimum) isolation required with an AC-coupled receiver may be estimated using the criterion that the total crosstalk level of noise generating terms < -25 dB, considering only primary data-second order crosstalk beating. For example, in the worst-case of a single wavelength for all inputs, dilated $T(4,4)$ and $T(16,256)$ require -20.8 dB and -25.4 dB, respectively. Using k wavelengths the isolation is relaxed by $5\log(k)$ dB.

Simulation using the customised computer design tool (XHatch) considers primary (but not secondary) beating with all crosstalk terms. Isolation specification is in good agreement with the above, and, in addition, the performance variation with channel number, routing assignment and threshold choice is revealed. Crosspoint isolation must be several dB better than the value at the penalty asymptote.

6.5 References

1. M. Salerno, *XHatch User's Manual*, Optoelectronic Computing Systems, University of Colorado, Boulder, USA.
2. T.H. Gilfedder, P.J. Legg, D.K. Hunter, I. Andonovic and M. Shabeer, "Modelling of the performance of optical TDM switching networks in the presence of interferometric noise due to inter-channel crosstalk", Proceedings of *Advanced Networks and Services*, vol. 2450, European Optical Society, Amsterdam, March 1995.
3. J. Yao and M.J. O'Mahony, "Experimental-study of semiconductor-laser amplifiers for photonic time and space switching systems", *Int. J of Optoelectronics*, 9(3), pp. 219-226, 1994.
4. D.K. Hunter, P.E. Barnsley, I. Andonovic, and B. Culshaw, "Architectures for optical TDM switching", *OE Fibers '92*, Paper 1787-18, SPIE, Boston, 1992.
5. D.K. Hunter, I. Andonovic, B. Culshaw, and P.E. Barnsley, "Experimental test bed for optical time-domain switching fabrics", *Optical Fiber Communication OFC/IOOC '93*, paper TuO2, OSA/IEEE, San Jose, 1993.
6. D.K. Hunter, P.J. Legg and I. Andonovic, "Architecture for large dilated optical TDM switching networks", *IEE Proceedings-J*, 140(5), pp. 337-343, 1993.
7. F.K. Hwang, "On Benes rearrangeable networks", *Bell Syst. Tech. J.*, 50(1), pp. 201-207, 1971.
8. V.E. Benes, "Mathematical theory of connecting networks and telephone traffic", *Academic Press*, 1965.
9. K. Padmanabhan and A.N. Netravali, "Dilated networks for photonic switching", *IEEE Trans. Commun.*, 35(12), pp. 1357-1365, 1987.
10. D.K. Hunter and D.G. Smith, "An architecture for frame integrity optical TDM switching", *J. Lightwave Technol.*, 11(5/6), pp. 914-924, 1993.
11. D.K. Hunter and D.G. Smith, "New architectures for optical TDM switching", *J. Lightwave Technol.*, 11(3), pp. 495-511, 1993.

Chapter 7

Interferometric noise suppression through intra-bit frequency evolution of directly modulated lasers

7.1 Introduction

Considerable efforts are underway to find practical solutions to the problem of interferometric noise. In this chapter, a new technique is demonstrated, and in Chapter 8 all methods are critically appraised.

In the new strategy, every transmitter comprises a DFB laser that is NRZ ASK directly modulated with a large modulation depth [1]. Under modulation, the centre frequency of the DFB laser varies over the duration of each bit, falling during 'one' bits and rising during 'zero' bits with an exponential-like dependency of characteristic time constant ≈ 20 ns). The optical frequency at the midpoint of each bit interval is not constant, but depends upon the sequence of the preceding bits. Therefore, on the interference of a delayed-replica parasitic crosstalk waveform, the interferometric noise generated on detection may be reduced by RF filtering according to the difference in centre frequency of the interfering bits. This noise suppression, which requires no additional hardware, has been successfully modelled and experiment demonstrates little performance gain for a single interferer, as predicted. However, in the presence of multiple interferers significant improvement is predicted at sub-Gb/s rates.

Under direct NRZ modulation, the carrier density and the temperature within the active region of a DFB laser change with time, thereby inducing a sympathetic refractive index and length (only due to temperature) variation, resulting in an evolution of the laser centre frequency along the waveform. At 'one'-'zero' transitions, short-lived frequency oscillations - transient chirp - arise as a consequence of carrier-photon relaxation oscillations [2]. Once the laser is equilibrated, the carrier density remains constant during the bit but differs in magnitude for 'ones' and 'zeros' - this results in adiabatic chirp [3]. In addition, the frequency has been observed to

vary during a bit interval, a phenomenon that has been attributed to temperature evolution within the active region in response to the injection heating [4-8]. This intra-bit frequency evolution is the origin of the interferometric noise suppression method described in this chapter.

On the injection of carriers into the active region heat is generated by three mechanisms [9]; non-radiative recombination - this involves an Auger process by which an excited electron loses energy to optical phonons - proportional to iV is the biggest; electron scattering, the normal resistive mechanism, given by $i^2 R_s$ ($R_s \sim 2\Omega$); radiative absorption - this is principally non-axial spontaneous emission. The explanation through a thermal mechanism is supported by the observation of a decrease in optical frequency with injection current (the dependence is typically -10 GHz / $^\circ\text{C}$) with an exponential-like time dependence of characteristic time constant $\sim 20 - 40$ ns [8]. This is in good agreement with thermal diffusion modelling [9], but a definitive confirmation remains to be established.

Section 7.2 summarises the initial experimental investigation [7,8]. Further experimental studies addressing the bit-rate dependency of the noise suppression, the laser FM response, and the BER performance for the case of a single interferer are then presented. A simple theoretical model of the frequency evolution explaining the noise suppression and the observed bit-rate dependency is described in Section 7.3. The small performance gain for a single interferer is justified. In the scenario when there exist multiple interferers (Section 7.4) significant performance gain is predicted.

7.2 Experimental characterisation

7.2.1 Initial investigation

A p-side up buried-heterostructure (BH) DFB laser¹ biased at 20 mA (2mA below the threshold) was directly modulated by a repetitive 32-bit NRZ word pattern at 622 Mb/s with magnitude 40mA. The laser fed an imbalanced fibre interferometer which generated an undelayed sequence and an attenuated 16 bit (25.72ns) delayed sequence of the same polarisation, representing the main signal and the parasitic

¹ 1538 nm laser described in Chapter 5.

crosstalk, respectively (Fig. 7.1). The interferometer output was detected, RF filtered and displayed on a digital oscilloscope.

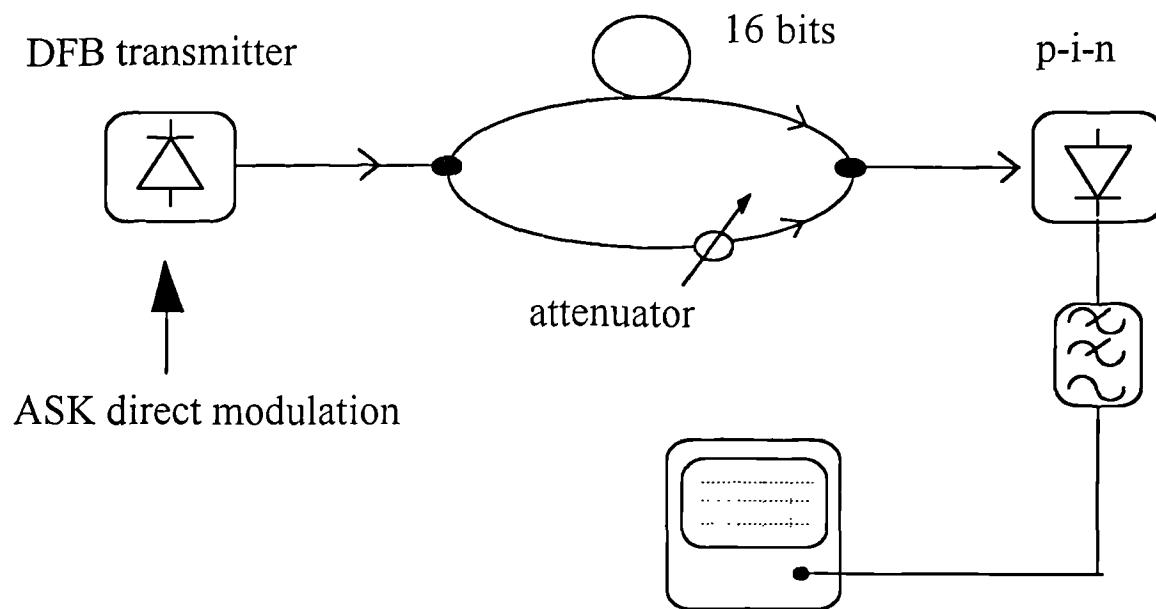


Figure 7.1. Experimental configuration.

PIIN is expected to be present only when both the main signal and crosstalk are 'one' bits (identified with x's in Fig. 7.2(a)), and this was found to be the case for a receiver bandwidth of 2.0 GHz (Fig. 7.2(b)). However, when the receiver bandwidth is reduced to 615 MHz (\sim data bandwidth) only selected bits are subject to noise (Fig. 7.2(c), arrows indicate bits without the expected PIIN) - the interferometric noise has been (partially) suppressed (cf. Fig. 5.9). The noise suppression was dependent on both the word pattern and the differential delay, and fell with a reduction in the modulation depth; in all cases only selected bits lacked the expected interferometric noise.

To gain further insight into the history dependence, the laser was driven by a special bit sequence consisting of an isolated sequence of 'ones' and 'zeros'; the attenuation was removed and the receiver bandwidth was fixed at 2.0 GHz. The results (Fig. 7.3) clearly show that the PIIN grows in magnitude with time and the probability density function (pdf) evolves from a Gaussian-like shape at the beginning of the interference (Fig. 7.3(c)) to the standard [11,12] two-pronged shape for fully developed PIIN (Fig. 7.3(e)).

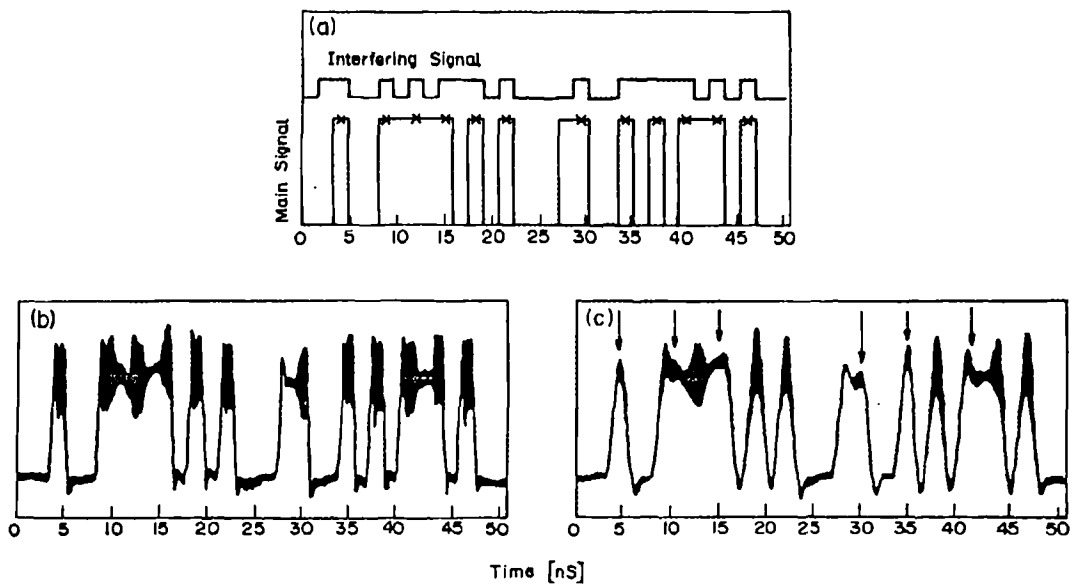


Figure 7.2. (a) 32-bit word at 622 Mb/s together with a 16-bit delayed interferer; bits marked by x's are prone to PIIN. Experimental results for (b) 2.0 GHz and (c) 615 MHz receiver bandwidths. Noise is suppressed on the arrowed bits.

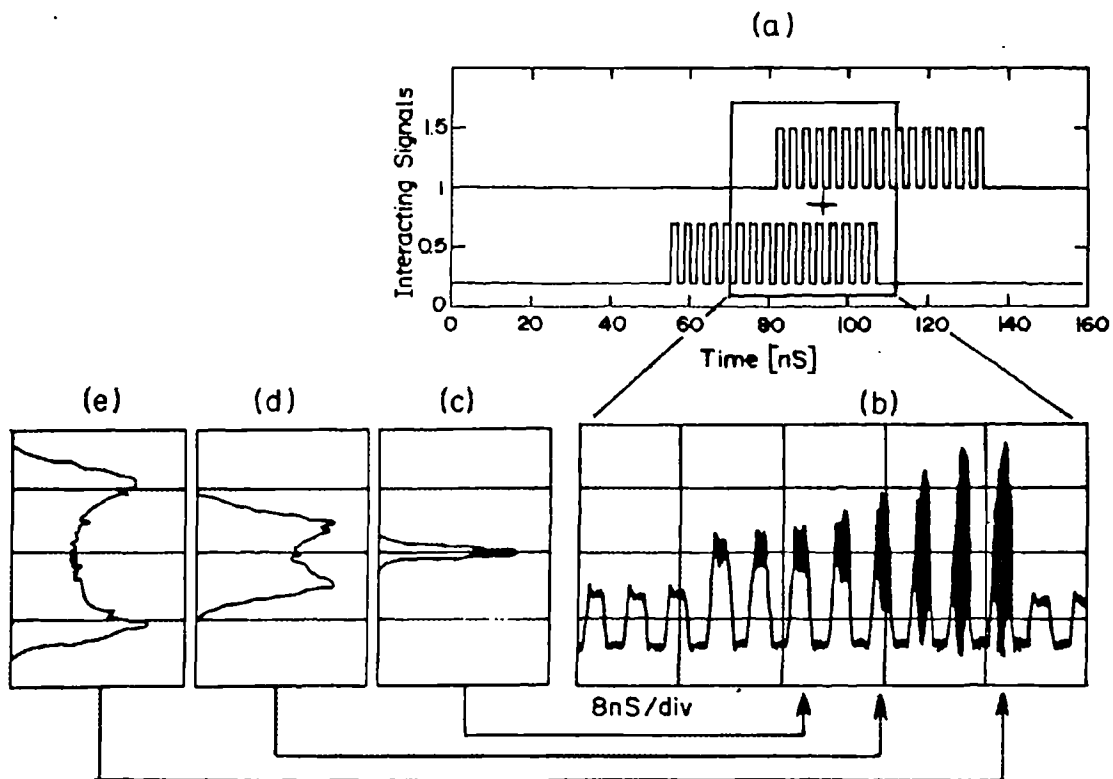


Figure 7.3. Experimental results (622 Mb/s) obtained with a receiver bandwidth of 2.0 GHz; signal and crosstalk are equal in power: (a) 32-bit long 1010... pattern and

a 16-bit delayed interferer, (b) PIIN on the interfering bits. Noise (voltage) histograms are also shown at the middle of (c) the third, (d) the fifth, and (e) the last interfering bits.

From the above observations the following explanation was proposed [6]. In response to the modulation, the laser centre frequency changes during each bit interval (experimental evidence of this is presented below). During 'ones' the frequency falls, and during 'zeros' the frequency rises. Therefore, the frequency at a particular 'one' bit in the sequence depends upon on how many 'ones' and 'zeros' preceded it, as measured over the duration of the memory time of the phenomenon. On the interference of a 'one' bit from a delayed crosstalk replica, it is possible that the centre frequencies of the two 'one' bits differ since they were emitted at different points in the sequence. In this case, the power spectrum of the interferometric noise thus generated is translated from baseband by the difference in the respective centre frequencies; if this is greater than or equal to the receiver bandwidth the noise is filtered and reduced in power by at least one half, as for the arrowed bits of Fig. 7.2(c). Bits which display full noise result from the interference of bits of (approximately) equal centre frequency. The sequence dependence of the waveform centre frequency implies the sequence dependence of the PIIN.

In the second experiment (Fig. 7.3), after the first 'one' bit the frequencies of the successive 'ones' fall with time until an equilibrium is established. At the first interfering bit, the crosstalk bit has a high frequency whilst that of the main signal is lower being close to equilibrium; thus little PIIN falls within the receiver bandwidth and the pdf shows the influence of the filtering [12]. As time progresses, the frequency difference falls as the crosstalk waveform frequency approaches the same equilibrium state enjoyed by the main signal. Hence, the noise grows in size until the last interfering bit shows full noise.

The variation in the centre optical frequency along the modulated waveform was measured using a fibre etalon of 0.09 nm bandwidth and a 12 GHz analog receiver linked to a digital sampling oscilloscope (Fig. 7.4 [6,13]). The transmitted power was measured as the etalon passband was scanned in 0.02nm steps, and the 'wavelength' at each point along the bit sequence was determined from the centre of gravity of the power produced at every filter wavelength [6].

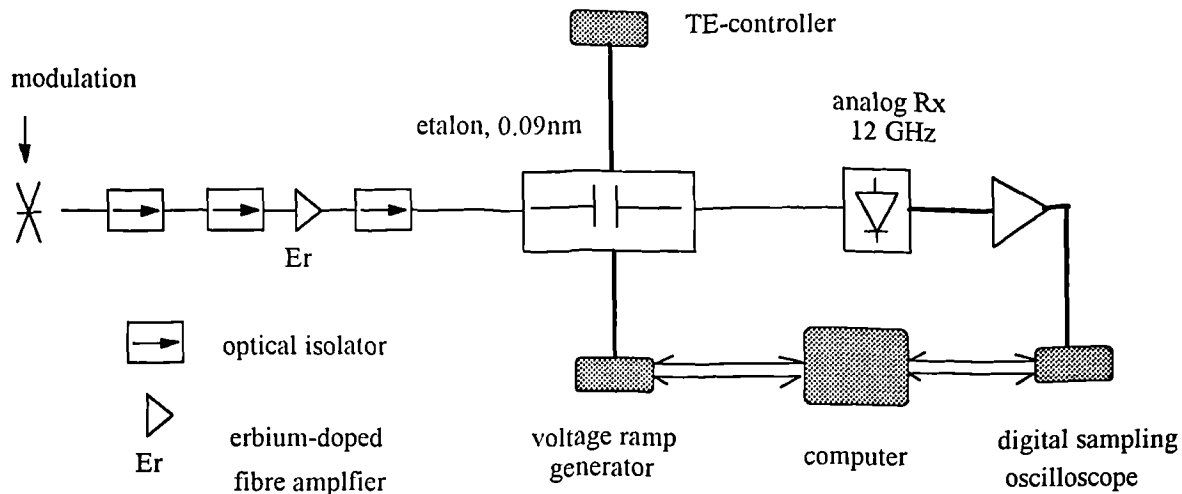


Figure 7.4. Time-resolved spectroscopy of modulated optical waveforms: experimental set-up.

Examination of the trace for the 622 Mb/s word of Fig. 7.2 (Fig. 7.5(a)), shows the transient chirp [2] at the bit transitions and also an increase in wavelength (fall in frequency) *during* 'one' bits - this is most apparent over five successive 'ones' where 2.25 GHz of chirp accumulates. Using this trace the frequency differences of the interfering 'ones' can be estimated - values of greater than 0.5 GHz are found only for the arrowed (filtered) bits of Fig. 7.2(c); the maximum frequency difference is 0.9 GHz.

When the laser is modulated more slowly, at 9.72 Mb/s, and is biased above threshold (modulation=20mA), the complimentary frequency change during 'one' and 'zero' bits is revealed (Fig. 7.5(b)). The exponential-like time dependence has a time constant of ~ 22.5 ns. The frequency change over a bit (103ns), 6.2 GHz, results from a temperature change of $\sim 0.6^\circ\text{C}$ (the dependency for the laser under test is -10 GHz/ $^\circ\text{C}$ [14]). Furthermore, the adiabatic chirp [3] can now be measured to equal $+200$ MHz/mA. Adiabatic chirp may also be measured on a high resolution optical spectrum analyser - two peaks are observed representing 'ones' and 'zeros' for a laser biased above threshold [15].

In order to establish that the above behaviour was not peculiar to the laser six further DFB chips, constructed from both bulk and MQW material, in both ridge and BH structures, and mounted both p-up and p-down, were assessed by the dynamic chirp measurement. All chips showed the same exponential-like behaviour, with time constants of 35-38 ns, while p-up mounted chips showed a greater frequency change.

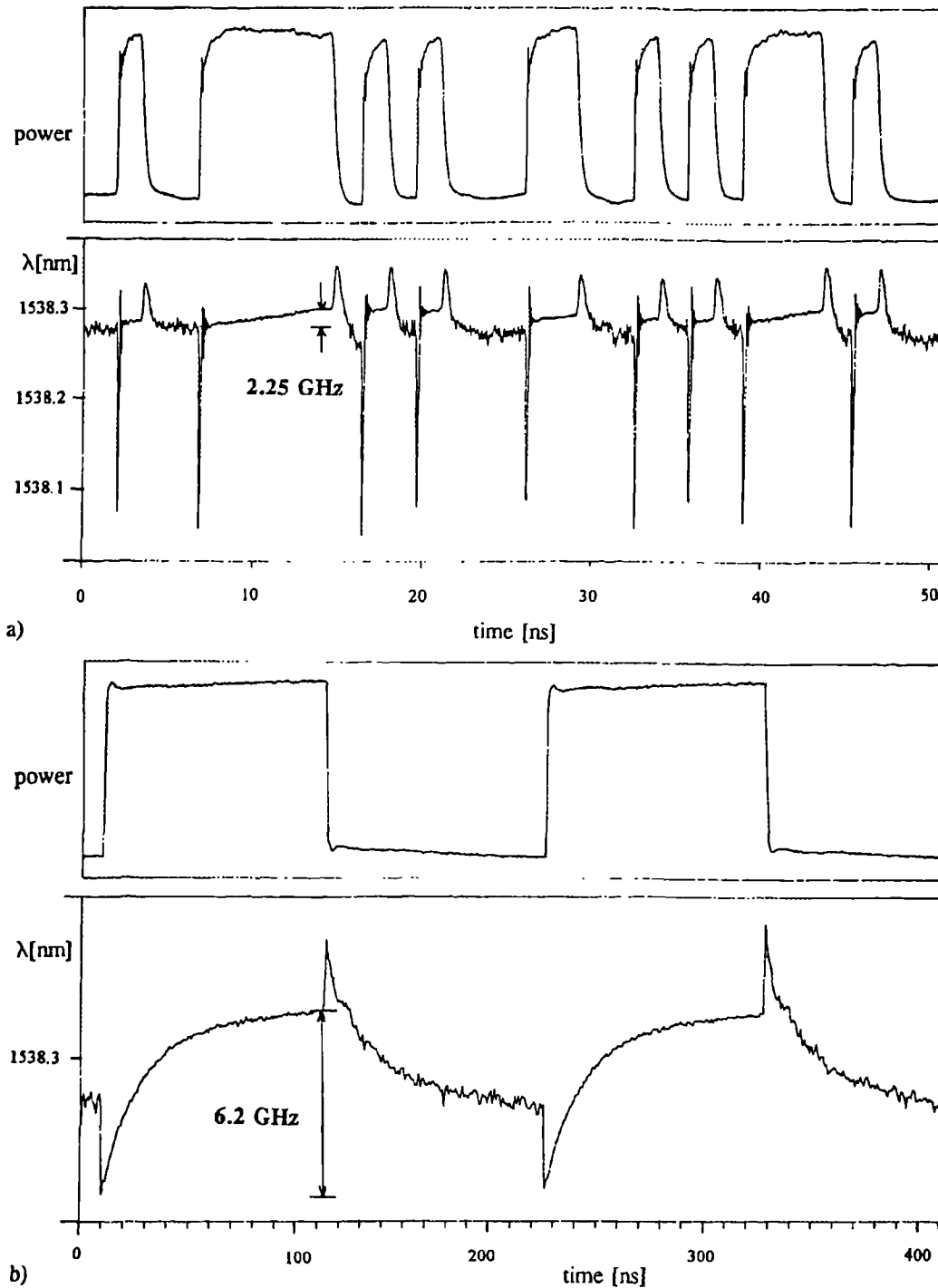


Figure 7.5. Time-resolved spectroscopy of modulated optical waveforms. (a) 622 Mb/s 32-bit word (as Fig. 7.2); (b) 9.72 Mb/s 0101... sequence.

7.2.2 Further investigation

The degree of interferometric noise suppression was predicted to be dependent upon the bit-rate of the modulation in the following way: at high bit rates (greater than ~ 1

Gb/s) the bit period is too short to allow significant frequency change within a bit period; all 'one' bits will possess approximately the same optical frequency, and therefore noise suppression will be slight. At low frequencies (less than ~ 1 Mb/s), the bit-period is much greater than the time constant (~ 20 ns) which implies that all 'one' bits will have the same equilibrium frequency, again giving poor noise suppression. At intermediate frequencies, a maximum in the noise suppression is expected (assuming a fixed receiver bandwidth) for a bit period \sim time constant - here the frequencies of the 'ones' bits are distributed over their maximum range.

Another description considers the 'memory' of the optical centre frequency - the frequency of a given bit is influenced by the sequence of bits that may be 'remembered', i.e. those emitted up to a time constant previously [16]. At very low bit-rates, the memory only spans one or two bits, eliminating the pattern dependence; at very high bit rates the memory spans so many bits that the pattern itself is averaged out. Both these give low noise filtering.

These predictions were tested using the configuration of Fig. 7.1 for a fixed receiver bandwidth of 2.0 GHz. The fraction of bits that remained corrupted by interferometric noise, termed the *noise reduction factor* γ , was measured from the oscilloscope traces (Fig. 7.6). The trend predicted above is visible and the 'optimum bit-rate' lies within 20 - 80 Mb/s, accurate estimation being impossible because the pattern length employed (32 bits) is too short.

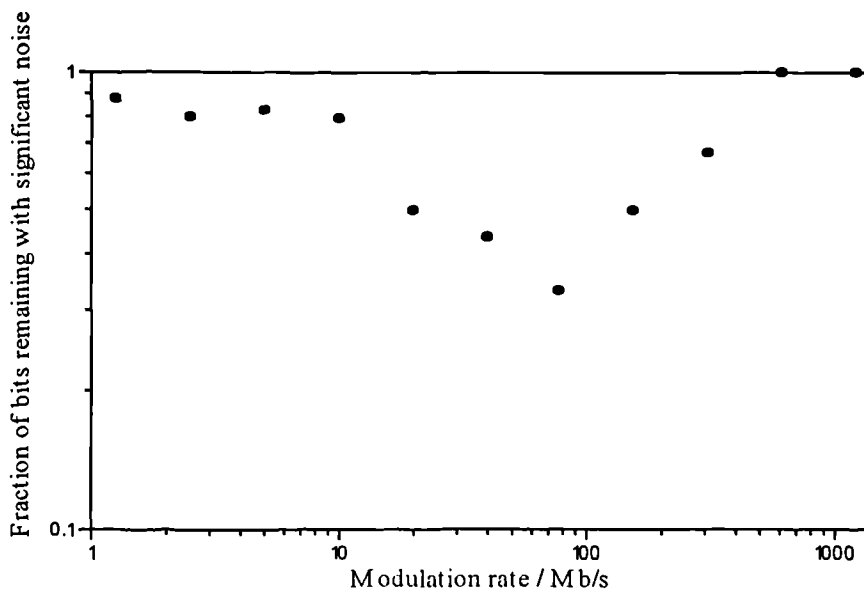


Figure 7.6. Experimental assessment of the bit-rate dependency of the interferometric noise suppression.

The interferometric noise suppression was also investigated with return-to-zero (RZ) modulation. The RZ format restricts the continuous heating time to only (approximately) a half-bit duration, resulting in little temperature or frequency variation along the bit sequence. Indeed, more noise was observed for RZ than NRZ for 77.76 and 622 Mb/s $2^7 - 1$ PRBS sequences.

The laser FM response to low frequencies, an indicator of the laser thermal response, was also measured (Fig. 7.7). The slow roll-off (compared to, for example, [17]) suggests that the laser has a short thermal time constant (<100ns).

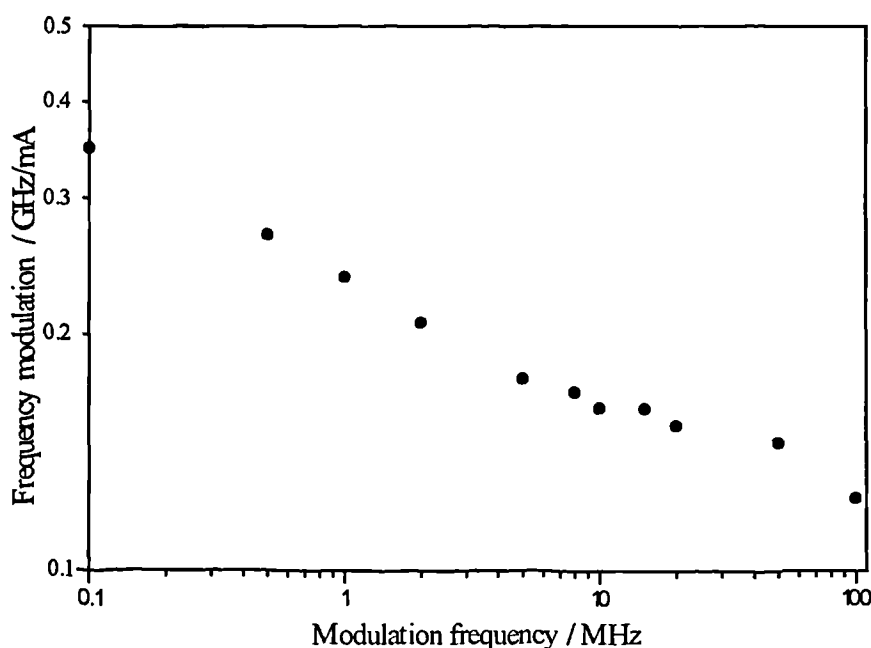


Figure 7.7. FM response of the DFB laser at low frequencies.

The BER performance in the presence of PIIN owing to an identically polarised single interferer was assessed at 77.76 and 622 Mb/s (Fig. 7.1). A $2^{15} - 1$ PRBS sequence was employed and the (fixed) receiver bandwidth was 530 MHz. The oscilloscope revealed that approximately one in two bits remained corrupted by noise at 622 Mb/s (cf. Fig 7.2(c)); this fell to about one in four at 77.76 Mb/s. The optical power penalty at BER= 10^{-9} , with an optimised decision threshold (always set to minimise the BER), was determined for several values of crosstalk level (the ratio of main signal and crosstalk optical powers, Fig. 7.8). The theoretical curve was determined from the theoretical noise pdf, calculated by convolving the bounded and Gaussian pdfs of the interferometric and thermal receiver noise, respectively (cf. Section 3.5.2

[18]). The experimental curves demonstrate that only a small improvement in power penalty, of approximately 0.1 dB, is attainable by operation at 77.76 Mb/s rather than 622 Mb/s. The agreement with the theoretical curve is good; differences are not due to the mechanism under discussion here but are attributed to a small amount of noise filtering that exists even when interfering bits have equal frequencies.

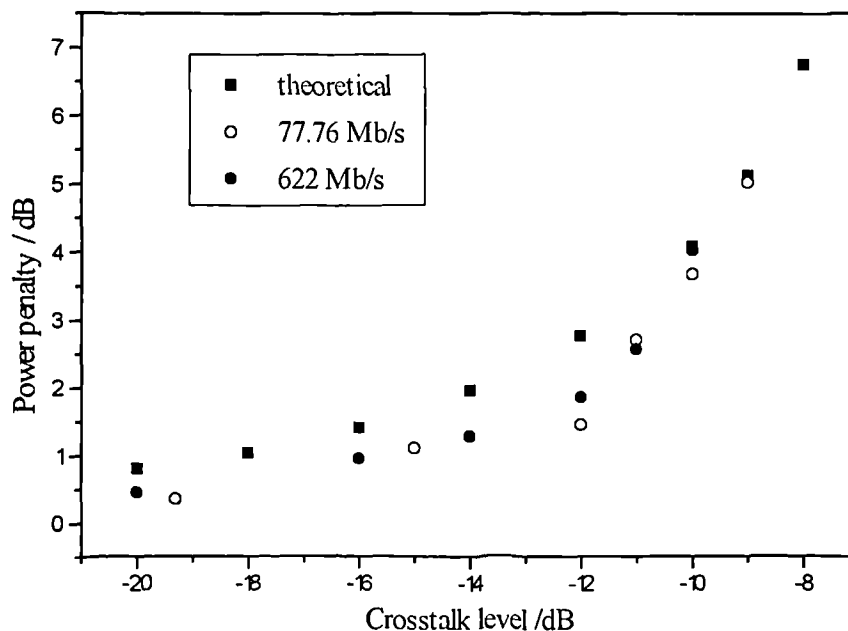


Figure 7.8. Optical power penalty at $BER=10^{-9}$ plotted against crosstalk level for a single interferer.

7.3 Theoretical model for a single interferer

In the simplest thermal analysis, the lasing region is treated as a lumped thermal capacitance C_T linked to the ambient surroundings (principally the heat sink), at temperature T_0 , by a thermal resistance R_T [17,19]. It is assumed that all heating occurs in the active region, the temperature of which remains uniform throughout its volume (i.e. it has an infinite thermal conductivity), with the heat flow to the surroundings proportional to the temperature difference of the active region and the surroundings (only strictly true in the steady-state). Applying the conservation of energy, the temperature of the active region, T , is given by the following differential equation:

$$\frac{Q(t)}{C_T} = \frac{dT}{dt} + \frac{(T - T_0)}{\tau} \quad (7.1)$$

where $Q(t)$ is the heat input, C_T is the thermal capacitance, T and T_0 are the temperatures of the active region and ambience, respectively, and τ is the thermal time constant ($=R_T C_T$, R_T being the thermal resistance). The response is analogous to the voltage across a capacitor in a RC series electrical circuit.

If the active region has area A , depth h and specific heat capacity c_p , and all heat flows towards the heat sink through a semiconductor of thermal conductivity κ and of height z (Fig. 7.9), the thermal resistance and capacitance are:

$$R_T = \frac{z}{\kappa A} \quad (7.2)$$

$$C_T = \rho A h c_p \quad (7.3)$$

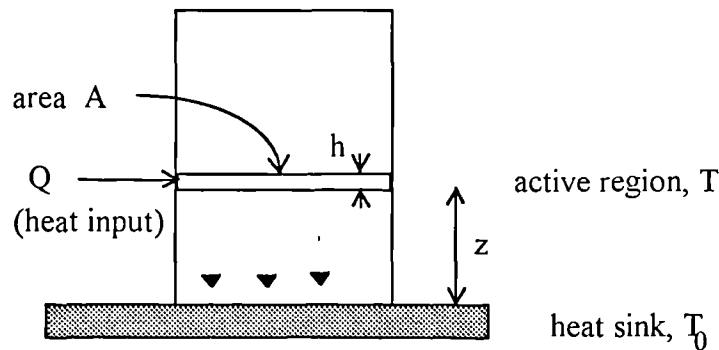


Figure 7.9. Simple thermal model of a semiconductor laser.

Solution of Eqn. 7.1 with a time constant of 22.5 ns (chosen to match that measured from Fig. 7.5(b)) shows the exponential-like dependency of temperature (or frequency) on time as observed in experiment (Fig. 7.5(b)). The temperature dependence for the 32-bit pattern of Fig. 7.2 together with its delayed copy (Fig. 7.10(a)) permits calculation of the temperature difference of data and crosstalk (Fig. 7.10(c)). Full PIIN should be observed when the interfering 'one' bits have near zero temperature (i.e. optical frequency) difference (marked by stars in Fig. 7.10(b)). The agreement between the predictions (Fig. 7.10(b)) and the experimental results (Fig. 7.2(c)) is excellent.

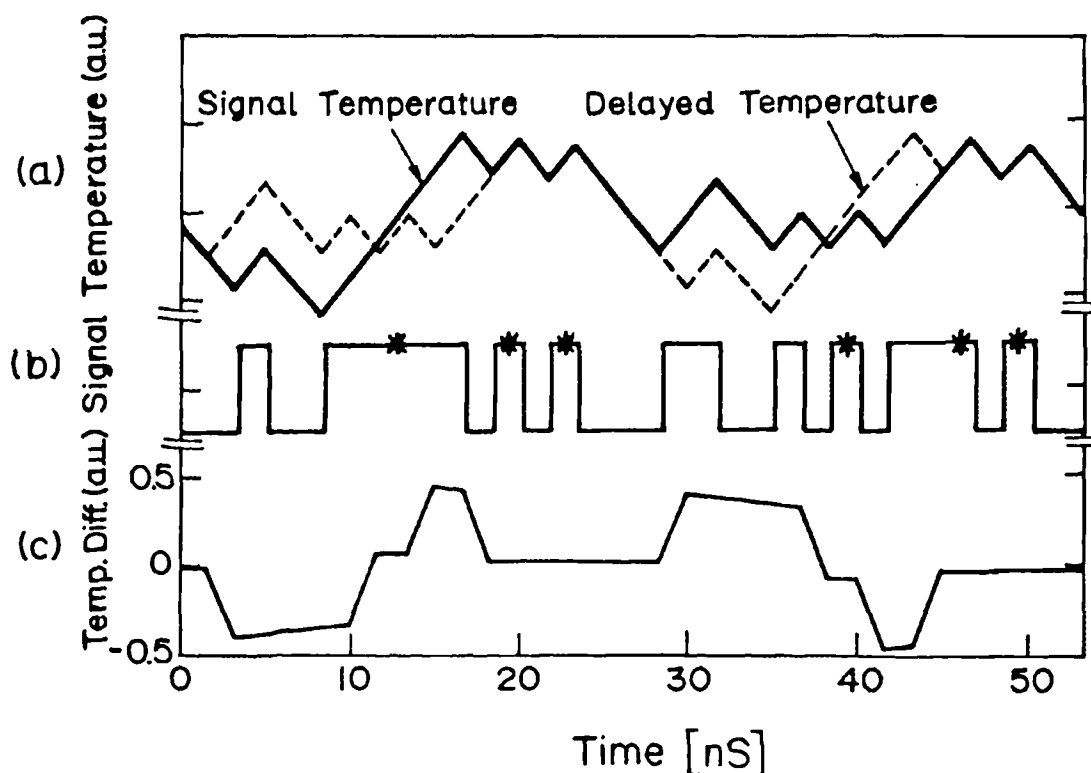


Figure 7.10. (a) The active region temperature as a function of bit position within the sequence. (b) The bit sequence: stars denote bits which should exhibit PIIN even for a relatively narrowband receiver (cf. the noisy bits of Fig. 7.2(c)). (c) The temperature difference between the interfering bits.

To simplify the calculation of the BER for many interferers (Section 7.4), it is assumed that on the interference of data and crosstalk 'one' bits, a beat frequency less than the receiver bandwidth constitutes a data bit that is corrupted by fully developed noise, otherwise the noise is insignificant. The fraction of bits that satisfy the former is the *noise reduction factor*, γ , as defined above (see Fig. 7.6 for experimentally determined values), and equals the probability of full noise generation on the interference of data and crosstalk 'one' bits.

The noise reduction factor γ was determined from Eqn. 7.1 as a function of the bit duration to time constant ratio, for a 512-bit pseudo-random-bit-sequence [20]. The optical frequency at the centre of each bit, and thus the probability histogram of the appearance of each optical frequency, were calculated. Subsequently, the probability for different beat frequencies between all possible data 'one' - crosstalk 'one'

coincidences was calculated by autocorrelating the histogram. Finally, γ was found by integration of the autocorrelation over the bandwidth of the receiver.

Simulation of γ as a function of bit-rate, for a time constant of 20ns and a (fixed) RF bandwidth of 2.0 GHz (Fig. 7.11), shows good agreement with the experimental results (Fig. 7.6), indicating an optimal value of about 80Mb/s (where the value of $\gamma = 0.35$). Moreover, the results show that bit-rates as great as 100Mb/s give values of γ that are smaller than 0.4. The same simulation was repeated for RF bandwidth matched to the bit rate (Fig. 7.11). Using the matched filter gives a γ improvement of 2-10 times; the optimal bit rate is still 80Mb/s which brings the value of γ to 0.04. γ is less than 0.1 for bit-rates of 40 to 300 Mb/s.

The thermally-governed low frequency FM response of a laser has been accurately modelled [20]. The response falls from dc until bit-rates exceeding $10/(\text{thermal time constant})$, where it becomes constant. This flattening is not apparent in the experimental FM response (Fig. 7.7) because the modulation rate was limited to 100 MHz; it may only be concluded that the time constant is less than 100ns.

The simple model of the laser temperature evolution described above, based upon a single layer assumption, although offering excellent qualitative description of the interferometric noise suppression, failed to accurately predict the frequency variation of Fig. 7.5 [20]. An improved model was developed assuming multiple layers between active region and heat sink, described by multiple time constants, one per layer. Excellent fit of the optical frequency deviation Δf evolution was achieved with three layers (Fig. 7.12):

$$\Delta F(t) = 0.25 \cdot \exp\left(-\frac{t}{16.8}\right) + 0.34 \cdot \exp\left(-\frac{t}{366}\right) + 0.95 \cdot \exp\left(-\frac{t}{4100}\right) \quad (7.4)$$

$$[t]=\text{ns} \quad [\Delta F]=\text{GHz/mA}$$

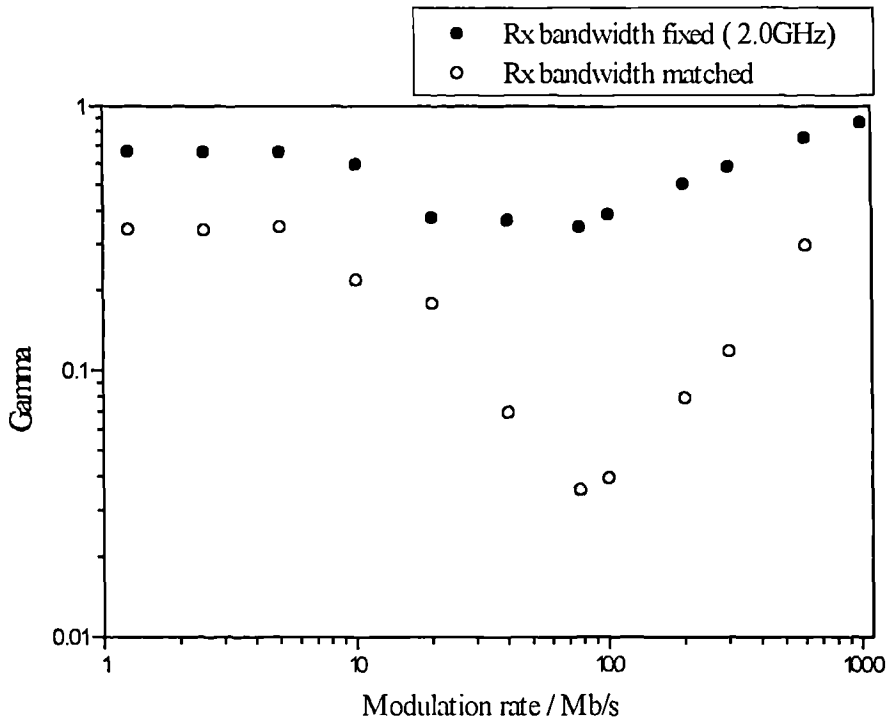


Figure 7.11. Simulated bit-rate dependence of the interferometric noise reduction factor γ for fixed (2.0 GHz) and matched receiver bandwidths. The thermal time constant of the laser is 20ns.

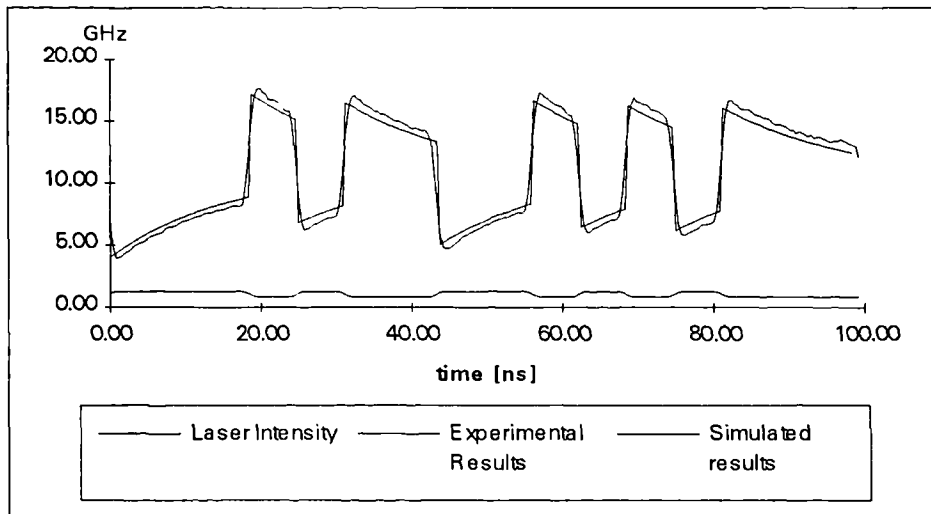


Figure 7.12. Comparison of improved thermal model employing three time constants with experiment. Adiabatic chirp is included in the model.

The BER in the scenario of a single interferer and an optimised decision threshold is dominated by the error probabilities of the 'one' bits which remain corrupted by full (unfiltered) interferometric noise (referred to as 'a' bits, cf. Table 3.2) and by the 'zero'

bits which are corrupted by crosstalk (but no interferometric noise - there is no optical power in the 'zero' bits since the laser is assumed to be biased at or below threshold, these bits are 'c' bits). The BER is minimised when the contributions to the BER from these two sources are equalised. When there is no noise suppression the BER is given by:

$$\begin{aligned} BER &= \frac{1}{4}(P_a + P_c) \\ &= \frac{1}{2}P_a \end{aligned} \quad (7.5)$$

where P_a and P_c are the probability of error for 'a' and 'c' bits respectively when the threshold is optimised.

If the direct modulation induces a noise reduction factor γ , although the optimum threshold level is now slightly higher, the error probabilities of 'a' and 'c' bits are unchanged, and the BER is given by (to a good approximation)-

$$\begin{aligned} BER &\cong \frac{1}{4}(\gamma P_a + P_c) \\ &= \frac{1}{4}(\gamma + 1)P_a \end{aligned} \quad (7.6)$$

The BER falls by $(1+\gamma)/2$. Even if γ is very small, the BER only falls by 1/2 which corresponds to a power penalty improvement of 0.1 dB at a BER= 10^{-9} . This explains the small gain observed in the experiment (Fig. 7.8).

If the decision threshold is set midway between 'one' and 'zero' levels, as in an AC-coupled receiver, the BER is dominated by the 'a' bits.

$$BER = \frac{1}{4}\gamma P_a' \quad (7.9)$$

where P_a' is the error probability of an 'a' bit with a midway threshold. The power penalty improvement is now greater; for example, with $\gamma=0.1$ it equals 0.4 dB for a crosstalk level of -20dB (there is a small increase in power penalty improvement with increasing crosstalk level).

7.4 Theoretical model for multiple interferers

Although the noise suppression method gives little improvement for a single interferer, significant performance gains arise in the more practical scenario of multiple interferers. In the single interferer case the BER is reduced by, at most, a factor of γ (for an AC-coupled receiver) which makes little difference to the power penalty because of the rapid complementary error function dependence of BER on the received optical power. If there are n (>1) parasitic interferers which may all add interferometric noise to the main data signal (it is assumed that they arise from the same laser as the data, or from distinct lasers that are nominally identical (same optical frequency evolution) to that of the data), the probability that a particular interferer generates full noise is equal to γ . A probability analysis that considers all states between every interferer being simultaneously a 'zero' and every interferer being simultaneously a 'one', assuming random and uncorrelated bit sequences, and equal optical powers of all crosstalk terms, shows that the mean number of full noise terms is reduced by γ , implying a performance equal to that of a network with no noise suppression and total crosstalk reduced by γ . For example, if $\gamma=0.1$ a reduction in the effective total crosstalk of 10 dB is expected, dramatically improving the performance of an interferometric noise limited network.

Calculation of the BER was undertaken with the further assumption that the addition of many full noise terms results in a Gaussian distributed net noise component (Central Limit Theorem [21]). If there are very many interferers (1000's) crosstalk reduction of $-10 \log(\gamma)$ is realised, but for practical numbers the gain is somewhat smaller. This may be understood by careful consideration of the contribution to the BER of different numbers of full noise terms. For example, if $n=10$ the greatest contribution arises from 8 and 5 full noise terms, for $\gamma=1$ and $\gamma=.25$ respectively. The ratio of 1.6 falls short of the value of 4 expected. When there are many interferers, only the contributions from a number of full noise terms close to the mean are significant giving the reduction by γ .

However, the performance for a small number of interferers will be better than that predicted by the above calculation because the pdf of the interferometric noise will, in practise, be more tightly bound than the assumed Gaussian function (cf. Section 4.4). Calculations of the minimum reduction in effective total crosstalk (measured by the

position of the asymptote of the power penalty versus crosstalk characteristic (cf. Fig. 7.8) as a function of γ and n are drawn in Fig. 7.13.

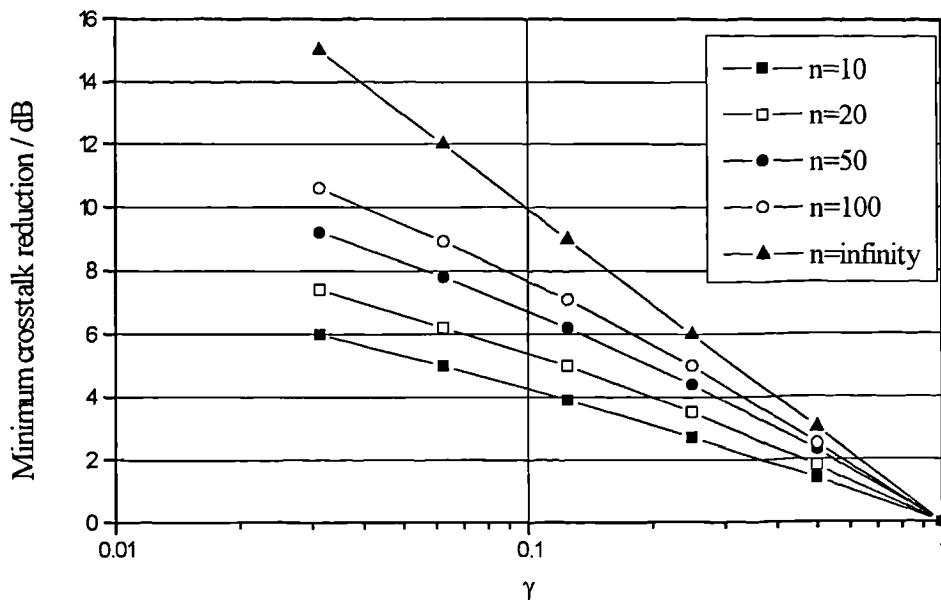


Fig. 7.13. Dependence of the minimum effective crosstalk reduction on γ for different numbers of crosstalk terms, n .

7.5 Discussion

Study of Fig. 7.11 and Fig. 7.13 predicts an effective crosstalk reduction of >5 dB for 20 interferers at transmission rates of 40 to 300 Mb/s. Significant performance gains at higher bit-rates necessitates many more interferers or a DFB laser with better characteristics (for noise suppression). Simple analysis, based on the solution to Eqn. 7.1, indicates that the value of γ is dependent upon the thermal resistance and capacitance, not simply on their product, the thermal time constant. If the thermal capacitance is held fixed, changes in thermal resistance, by varying z , for example, have little influence on γ . Thus similar performance is expected of a chip in p-up and p-down configurations (the p-up chip should have a slightly greater thermal resistance giving a longer time constant and a greater frequency change, as observed experimentally, Section 7.2.1). If, in contrast, the thermal resistance is fixed, γ is reduced dramatically by reducing the thermal capacitance. Thus, an optimum laser structure should possess minimum thermal capacitance (minimum active-region volume) whilst the thermal resistance is less important. Note, however, that the

engineering of large temperature (frequency) changes may upset other aspects of the laser performance, the threshold current, for example [22].

The suppression technique is applicable to PIIN given a data-crosstalk differential delay greater than a few bit periods, and to interference of two sources of near identical wavelength. It is important to maximise the modulation depth - this gives not only the greatest frequency variation but eliminates light from the 'zero' bits (cf. Section 3.5.7). Noise suppression comes for 'free' since there are no added hardware cost or dispersion penalties.

Techniques that mirror the frequency variation along the bit-sequence, but do so at higher bit-rates, may be conceived. For example, an external frequency (or phase) modulator may be driven to vary the frequency of successive bits according to some algorithm. Since the frequency difference required for noise suppression need only slightly exceed the bit-rate, the additional frequency spread will be smaller than the existing transient chirp, so added dispersion should be slight. Multi-section lasers [23] may be AM modulated through one contact and FM modulated, as above, through another.

7.6 Conclusions

Interferometric noise may be suppressed by exploitation of the intra-bit optical frequency evolution of directly modulated DFB lasers. This frequency variation, with exponential time dependence of time constant ~ 20 ns and thought to derive from a thermal mechanism, implies interfering bits of different optical frequencies giving interferometric noise translated from baseband and thereby RF rejected.

The noise suppression for a single interferer is sequence and delay dependent (only selected bits show noise), increases with modulation depth and is bit-rate dependent, being significant for transmission rates of 40 to 300 Mb/s. BER characterisation demonstrates little performance gain, as predicted. However, given multiple interferers, worthwhile gains are predicted for the above bit-rates; for example, the effective crosstalk is reduced by >5 dB for 20 interferers at 300 Mb/s. Furthermore, the technique uses a commercially available source driven with a deep modulation, there are no additional hardware cost nor dispersion penalties.

7.7 References

1. International Patent No. PCT/GB94/01149, 'Inter-channel crosstalk', British Telecommunications PLC, 1994.
2. R.A. Linke, "Modulation induced transient chirping in single frequency lasers", *IEEE J. Quantum Electron.*, 21(6), pp. 593-597, 1985.
3. B.W. Hakki, "Evaluation of transmission characteristics of chirped DFB lasers in dispersive optical fiber", *J. Lightwave Technol.*, 10(7), pp. 964-970, 1992.
4. N.S. Bergano, "Wavelength discriminator method for measuring dynamic chirp in DFB lasers", *Elect. Lett.*, 24(20), pp. 1296-1297, 1988.
5. S. Yamazaki, K. Emura, M. Shikada, M. Yamaguchi and I. Mito, "Realization of flat FM response by directly modulating a phase tunable DFB laser diode", *Elect. Lett.*, 21(7), pp. 283-285, 1985.
6. S.J. Pycock, "Modelling and measurement of wavelength chirp for the prediction of transmission performance", MSc Thesis, University of Essex, UK, 1992.
7. M. Tur, P.J. Legg, M. Shabeer and I. Andonovic, "Sequence dependence of phase induced intensity noise in optical networks that employ direct modulation", *Optics Letters*, 20(4), pp. 359-361, 1995.
8. M. Tur, P.J. Legg and I. Andonovic, "Novel suppression of interferometric noise in optical networks by employing direct modulation", *Optical Fiber Communication OFC'95*, paper WQ8 IEEE/OSA, San Diego, February 1995.
9. R.F. Broom, "Transient temperature distribution in diode lasers and the time duration of the output pulse at 300K", *IEEE J. Quantum Electron.*, 4(4), pp. 135-140, 1968.
10. W. Nakwaski, "Dynamical thermal properties of stripe-geometry laser diodes", *IEE Proceedings Part-I*, 131(3), pp. 94-102, 1984.
11. J.L. Gimlett and N.K. Cheung, "Effects of phase-to-intensity noise conversion by multiple reflections on gigabit-per-second DFB laser transmission systems", *J. Lightwave Technol.*, 7(6), pp. 888-895, 1989.
12. A. Arie, M. Tur and E.L. Goldstein, "Probability-density function of noise at the output of a two beam interferometer", *J. Opt. Soc. Am. A*, 8(12), pp. 1936-1942, 1991.
13. S.J. Pycock and S.F. Carter, "Measurement of wavelength chirp in advanced electro-optic devices", *4th Bangor Communications Symposium*, University of Bangor, UK, May 1992.
14. Hitachi, *Optodevice Data Book*, September 1993.
15. P.E. Barnsley, *Personal Communication*.

16. A.M. Hill, *Personal Communication*.
17. S. Kobayashi, Y. Yamamoto, M. Ito, and T. Kimura, "Direct frequency modulation in AlGaAs semiconductor lasers", *IEEE J. Quant. Electron.*, 18(4), pp. 582-595, 1982.
18. M. Tur and E.L. Goldstein, "Dependence of error rate on signal-to-noise-ratio in fiber-optic communication systems with phase-induced intensity noise", *J. Lightwave Technol.*, 7(12), pp. 2055-2058, 1989.
19. F.P. Incropera and D.P. Witt, *Fundamentals of heat and mass transfer*, Wiley, New York, 1985.
20. H. Regev, *M Sc Thesis*, Tel Aviv University, 1995.
21. G. Grimmett and D. Stirzaker, *Probability and Random Processes*, Oxford University Press, New York, 1992.
22. K. Petermann, *Laser diode modulation and noise*, Kluwer Academic Publishers, New York, 1993.
23. S. Murata, I. Mito and K. Kobayashi, "Spectral characteristics of a 1.5 μ m DBR laser with frequency-tuning region", *IEEE J. Quantum Electron.*, 23(6), pp. 835-838, 1987.

Chapter 8

Solution paths to combat crosstalk and interferometric Noise

8.1 Introduction

The multitude of methods to combat crosstalk and interferometric noise are summarised and critically appraised in this chapter. All methods are applicable to the proposed bilateral strategy comprising, firstly, minimisation of the crosstalk optical power (Section 8.2) and, secondly, suppression of the interferometric noise owing to the remaining crosstalk (Section 8.3).

8.2 Minimisation of the crosstalk optical power

Effective means of optical crosstalk power reduction in a network are summarised in Table 8.1. Most methods incur an additional hardware cost; the sparse coding and time compression techniques, requiring greater symbol-rates, are prone to dispersion.

Crosstalk source	Method to reduce crosstalk
space switch	<ul style="list-style-type: none">• crosspoints with better isolation• dilation of architecture (cf. Section 6.2 [1])
WDM MUX/DMUX filter	<ul style="list-style-type: none">• lower crosstalk components• WDM dilation [2]
discrete reflections	<ul style="list-style-type: none">• low reflectivity components (super PC connectors, angled or anti-reflection coated solid state devices)• termination of <i>all</i> fibres, e.g. unused coupler output ports• in-line isolators
Rayleigh backscatter	<ul style="list-style-type: none">• minimise fibre lengths (to less than half-attenuation length)• in-line isolators
non-specific	<ul style="list-style-type: none">• sparse coding (cf. Section 2.4, [3])• time compression of TDM blocks [4]

Table 8.1. Means of reducing optical crosstalk power.

In the time compression technique [4], blocks of TDM data (i.e. many (p) successive bits from the same communication channel) are compressed in time at the network input, and suitably delayed to occupy a chosen subchannel within the original block period (Fig. 8.1). The compressed block is then transmitted through the network and crosstalk from other channels is added. However, crosstalk from channels that were time-compressed into different, non-overlapping, (termed 'orthogonal'), subchannels does not induce degradation and is eliminated by the time decompression circuitry that re-establishes an uncompressed block at the network output.

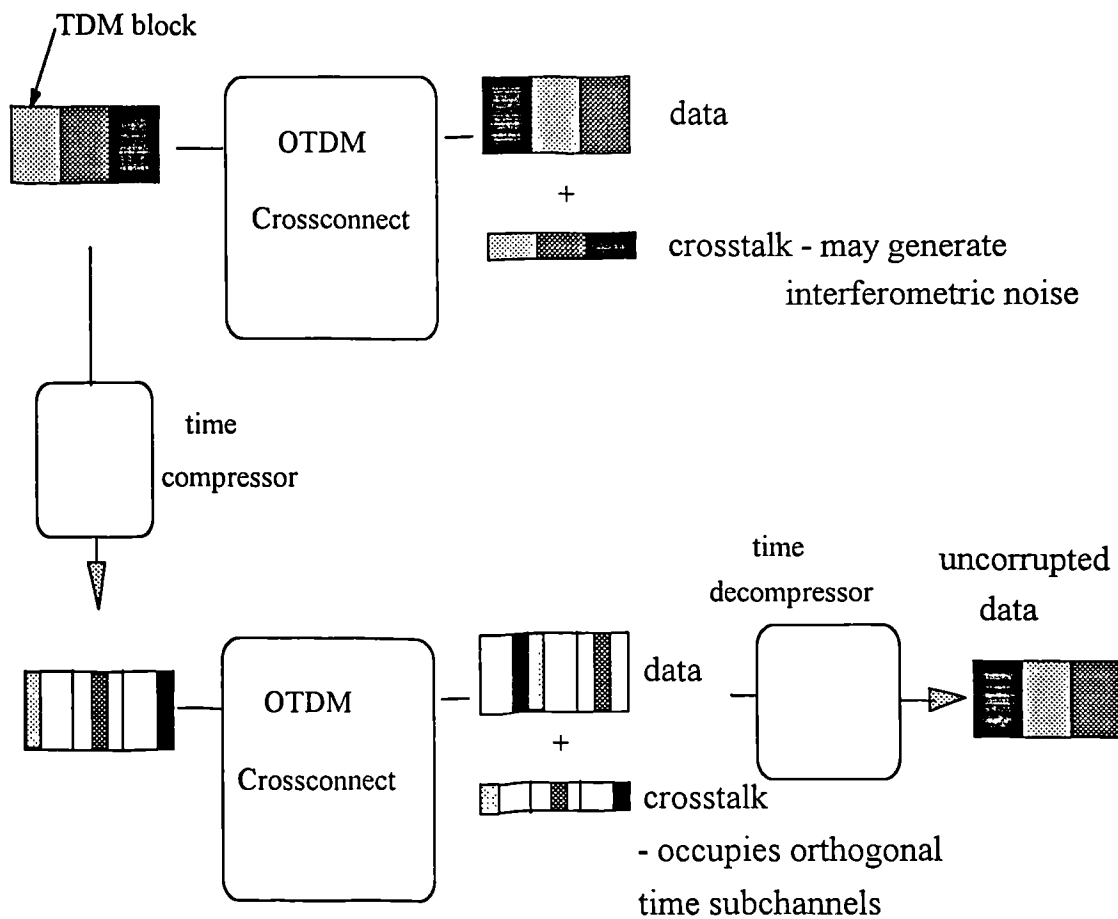


Figure 8.1. Crosstalk elimination by the time compression method. Crosstalk is added, in this example, by an OTDM crossconnect; the method is applicable to other crosstalk sources too.

In one practical realisation of the time compressor, the input block modulates a mode-locked optical pulse train (via an all-optical AND gate, or by detection and external modulation) which is fed into a compression circuit comprising fibre asymmetric

Mach-Zehnder interferometers and $\log_2(N_T)$ integrated-optical switches, where N_T is the compression ratio (Fig. 8.2, [5]). The block is folded and compressed by each interferometer, unwanted pulses being rejected by the following switch. Switch speed must increase along the chain; the last switch needs a rise-time much shorter than the final compressed bit period. Optical power losses are offset by the use of the powerful mode-locked source. NRZ data is converted to RZ format which may be undesirable, and bit order is not maintained (although it may be restored on decompression).

An alternative approach is to employ a parallel array of p switches and delay lines (Fig. 8.3, [6]). The compression ratio, N_T , is dependent upon the switching speed of the gates and the length tolerance of the delays. Switch costs will exceed those of the folding circuit (Fig. 8.2) unless N_T is large and p is small. However, no additional source is required, the bit-sequence is maintained, and both NRZ and RZ may be handled without format conversion.

Time decompression requires a parallel arrangement of all-optical AND gates and delays (Fig. 8.4, [5]). A semiconductor amplifier may function as an all-optical AND gate with an inverted output (i.e. a NAND gate, [5]). The number of gates is equal to N_T and conversion to the electrical domain is unavoidable. If successive blocks occupy different time subchannels then some buffering is also essential.

As an example, the x2 time compression/decompression according to [5] would require in total six switching elements (electro-optic or all-optical), a distributed mode-locked train of repetition-rate equal to the uncompressed bit period and additional components for pulse integration. The implementation of time compression for high data rates is hindered by the speed and synchronisation limitations of the componentry.

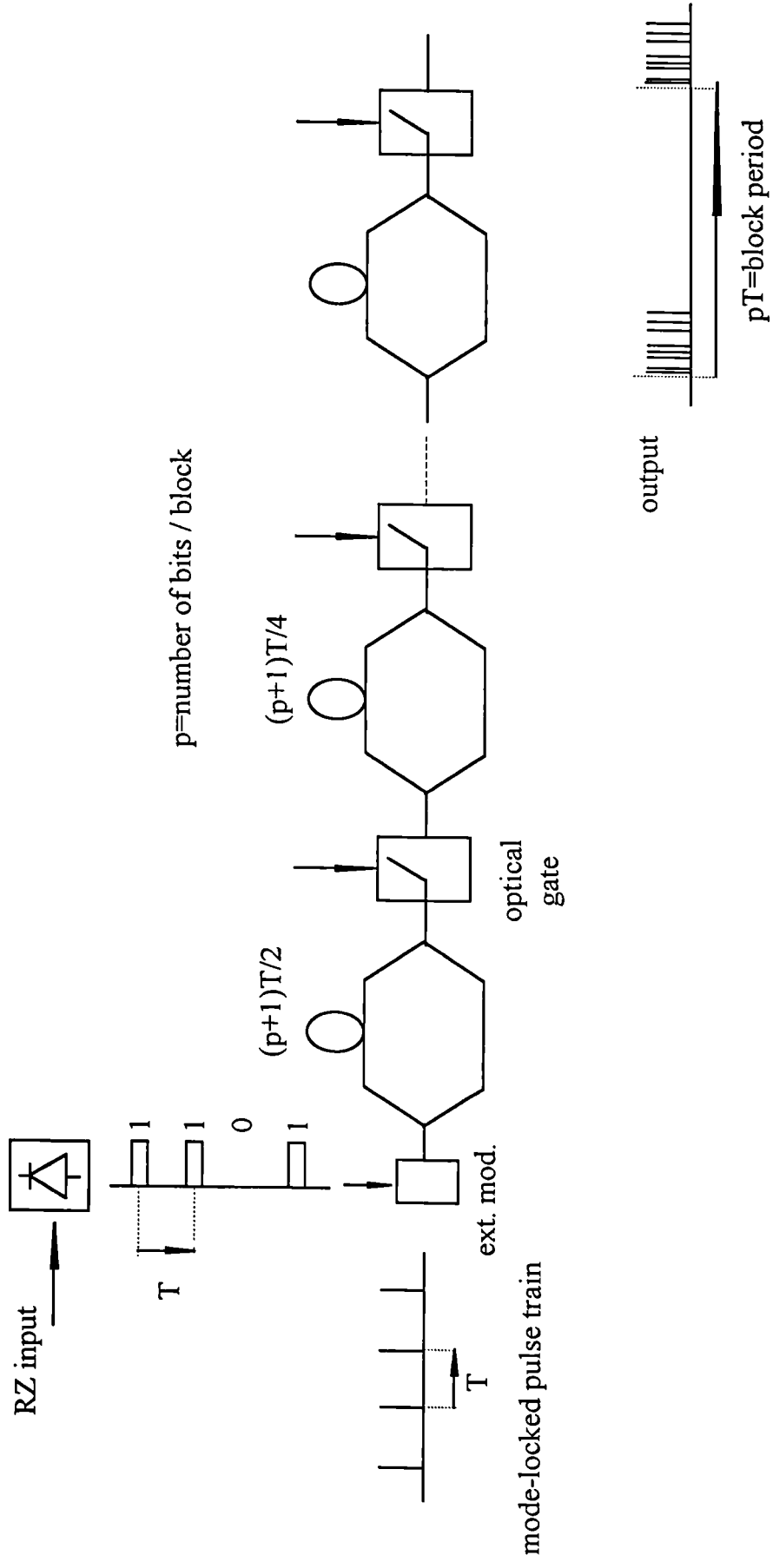


Figure 8.2. Time compression by a folding circuit according to [5].

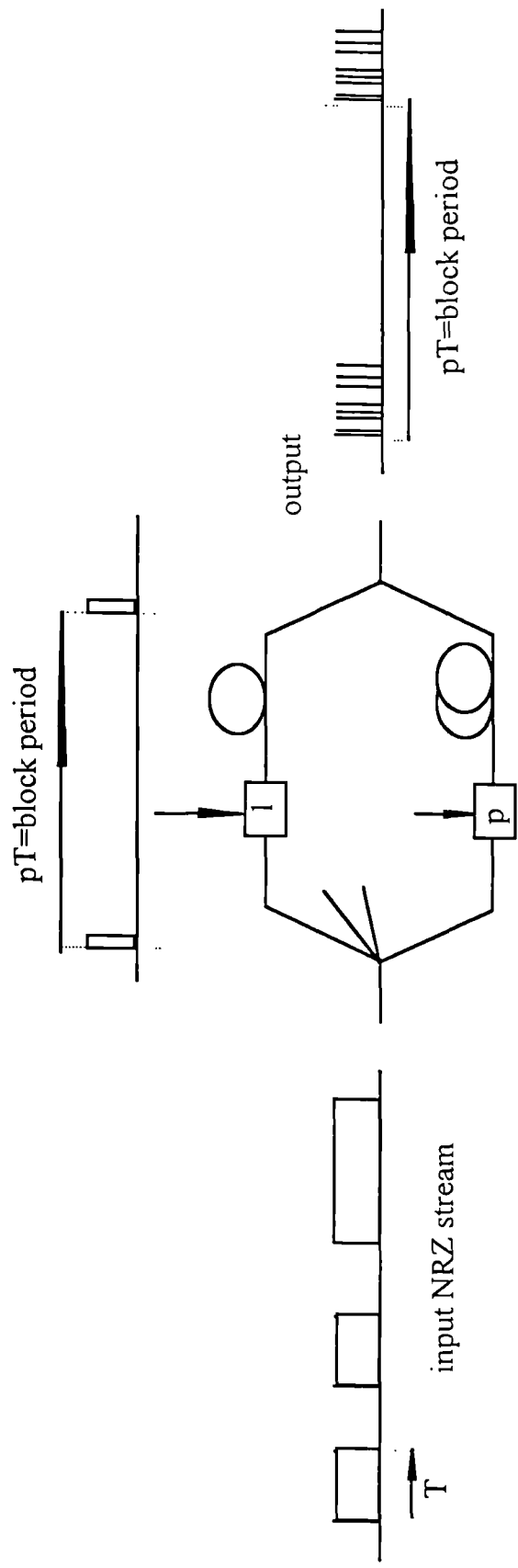


Figure 8.3. Time compression by parallel circuit according to [6].

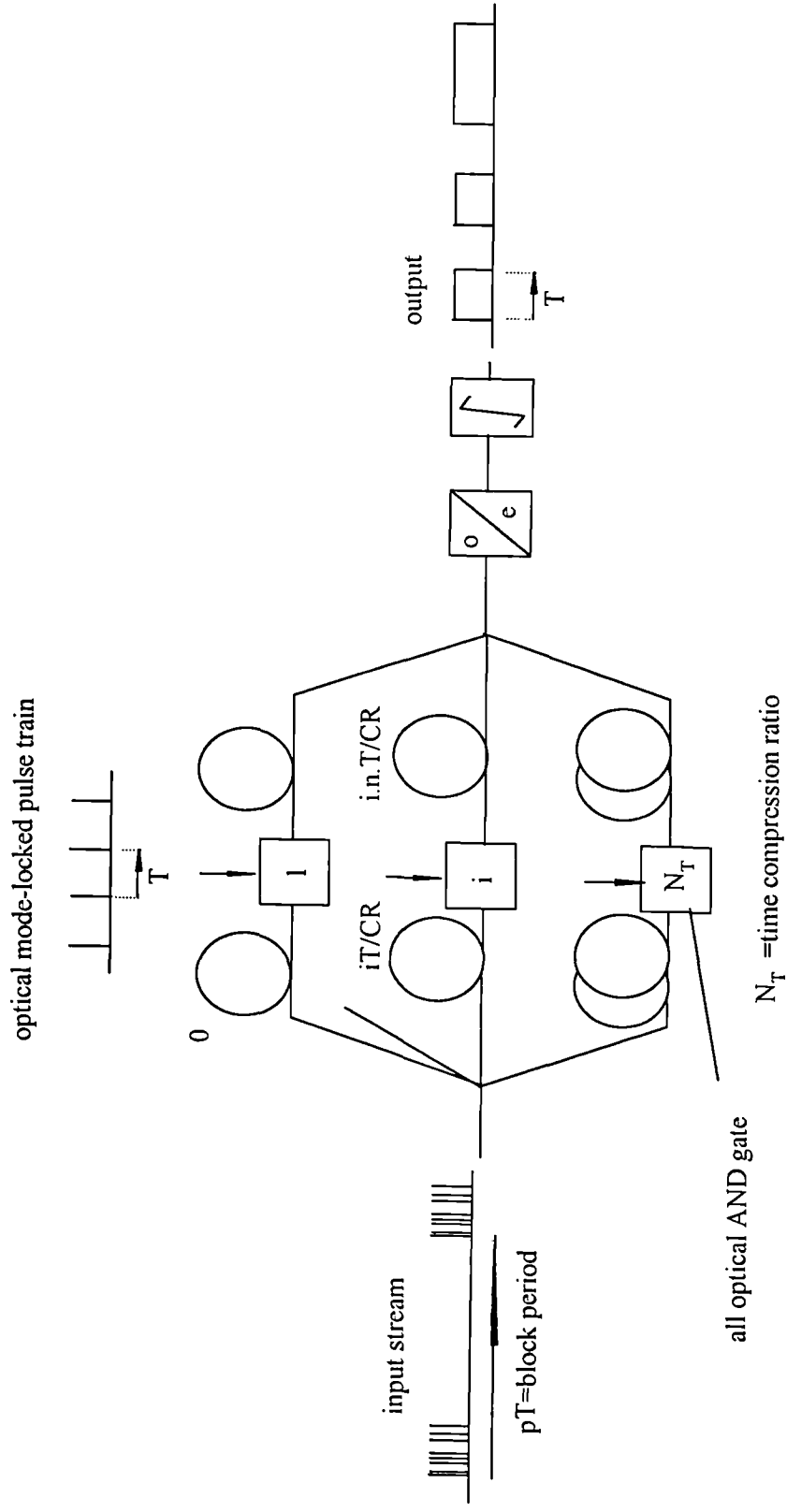


Figure 8.4. Time decompression circuit according to [5].

8.3 Suppression of interferometric noise

The magnitude of the interferometric noise that corrupts the detected data bit-sequence may be minimised by control of the polarisation of the incident data and crosstalk waveforms, by minimisation of the phase noise difference, and by RF rejection (Table 8.2).

Methods that exploit the polarisation dependence of the interference are only applicable to networks comprising polarisation independent components; many integrated-optical switching technologies, the lithium niobate directional coupler described in Chapter 5, for example, are polarisation sensitive. The state of polarisation of each laser may be 'scrambled', i.e. made to follow a circle on the Poincaré sphere, by a lithium niobate integrated-optical device placed external to the source [7]. On the interference of crosstalk and data from two such scrambled sources, the scalar product of their polarisations, and the interferometric noise magnitude, will vary at a rate determined by the modulation rate of the scrambler. If lumped element electrodes are employed on the scrambler this is limited to about 1 MHz but may be extended to as great as 10 GHz by a coplanar travelling-wave electrode geometry [7]. The slow-speed scrambler is easy to drive and will give an effective crosstalk improvement of 3dB in the above example with two sources.

If data and crosstalk arise from the same source, the modulation period must be smaller than the multipath differential delay. Slow scramblers are therefore suitable for managing interferometric noise due reflections in long haul links but not for an OTDM crossconnect, for example. High speed scramblers are suitable for small differential delays and, in addition, may be driven at rates exceeding the data bandwidth, thereby eliminating all interferometric noise by RF filtering. The drive signal must ensure that the polarisation scalar product varies more rapidly than the transmission rate. Although expensive, and requiring large drive powers ($\sim 2W$), high speed scramblers also combat polarisation-dependent gain due to polarisation hole burning in fibre amplified links [7]. The phase is also modulated although no dispersion penalty is found in practise [7].

The phase noise variation of phase-induced intensity noise (PIIN) may be reduced by selecting a source whose coherence time is larger than the delays incurred by multipath crosstalk waveforms. The crosstalk becomes partially coherent (cf. Section

3.6). In typical optical networks, spanning many kms, sources developed for coherent communication, for example, the external cavity semiconductor laser, and low-chirp external modulation would be required. However, even if all laser phase noise is eliminated there remains coherent crosstalk, potentially problematic with or without environmental phase noise (cf. Section 4.3.2). In the baseband ASK modulation considered in this thesis, the coherent crosstalk falls in-band and is problematic; however, in subcarrier networks this is not necessarily the case and improvements are possible with highly coherent sources [8].

Techniques that exploit RF filtering of the noise at the incoherent limit truly eliminate all interferometric noise, and are therefore preferred to the above coherent limit approach. Several methods engineer a modulated optical spectrum that is either broad or translated from baseband thereby suppressing the noise, albeit at the expense of increased dispersion. Low coherence sources [9-13], as described in Section 2.4, suffer less from interferometric noise than single frequency lasers (e.g. DFB). Phase modulation is a proven suppression technique [14-19] but requires additional hardware, comprising, in the simplest realisation, a high frequency single tone laser driver.

The exploitation of the thermally-induced intra-bit frequency evolution in directly modulated lasers (cf. Chapter 7) requires no additional hardware and adds no dispersion penalty [20]. However, the suitability for high speed (Gbit) transmission is limited by the small temperature change over a bit duration. Lasers with superior thermal characteristics or analog techniques that vary the frequency in a similar way, via an external phase modulator or additional laser tuning region, are required.

Interference between NRZ waveforms, of bit-rate B bit/s separated by at least $2B$ Hz in optical frequency, may be eliminated by either optical filtering of the crosstalk, or by baseband RF filtering of the interferometric noise at the receiver. This suggests a technique for noise reduction whereby different optical channels are transmitted at different 'orthogonal' wavelengths (Fig. 8.5). For example, in an OTDM crossconnect (cf. Chapter 6) every input may be fed by a different laser; alternatively, wavelength converters may be placed at each input to tune the wavelength as appropriate [4]. The method is compatible with the time compression described in Section 8.2, and offers a 'bolt-on' upgrade strategy to combat ageing of the crossconnect components (Fig. 8.6). In the MWTN crossconnect (cf. Section 2.3.7 [21]), wavelength converters could be located at the inputs (and outputs - to restore the correct

wavelength) to the space switches. Note (as for time compression) coherent crosstalk is not suppressed.

In a similar strategy, with channels transmitted at a single wavelength but with different subcarriers located within a non-baseband octave of frequency, for example, 2 to 4 GHz [22], interferometric noise generated between any two signals (including signals from the same channel) falls into the 0 to 2 GHz region of the RF spectrum and thus causes no degradation.

Finally, other approaches may be considered, including spread spectrum transmission [23,24] and conventional error correction (hindered by the bursty nature of the noise). Modulation depth must also be maximised.

Method	Noise suppression mechanism	Comments	Ref.
Polarisation			
polarisation scrambling	exploits polarisation dependence, $p_1 \cdot p_2$ varies (randomly) between 0 and 1	noise power reduced by 3dB; need pol. independent components	[7]
rapid random polarisation modulation (>>bit rate)	$p_1 \cdot p_2$ varies rapidly, >> bit-rate, noise RF filtered (spectrum translated from baseband)	need polarisation independent components; adds phase modulation too	[7]
Suppress phase noise			
employ source of coherence time >> multipath delays	phase noise change $\phi(t) - \phi(t - \tau) \ll 2\pi$	environmental phase noise still potentially problematic; only applicable to PIIN	[8]
Low coherence sources			
LED	noise RF filtered (spectrum very broad)	only suitable for short links	[9]
Fabry-Perot and self-pulsating laser (multi-mode)	noise RF filtered (beating of non-identical modes out-of-band)	only suitable for short links	[10-12]
chirped DFB	noise RF filtered (spectrum broadened)	dispersion difficulties	[13]
Phase modulation			
phase modulation at $f >$ bit-rate	noise RF filtered (spectrum translated to multiple harmonics of f)	dispersion difficulties; additional hardware	[14-19]
Carrier frequency manipulation			
direct modulation of DFB	thermally-induced intra-bit frequency evolution, noise RF filtered (translated from baseband)	no additional hardware; currently ineffective at Gbit rates	[20]
employ multiple wavelengths	crosstalk optically filtered or noise RF filtered (beating between different wavelengths out-of-band)		[4]
employ subcarriers centred within an octave	noise RF filtered (beating components fall out of subcarrier passbands)		[22]

Table 8.2. Means of interferometric noise suppression

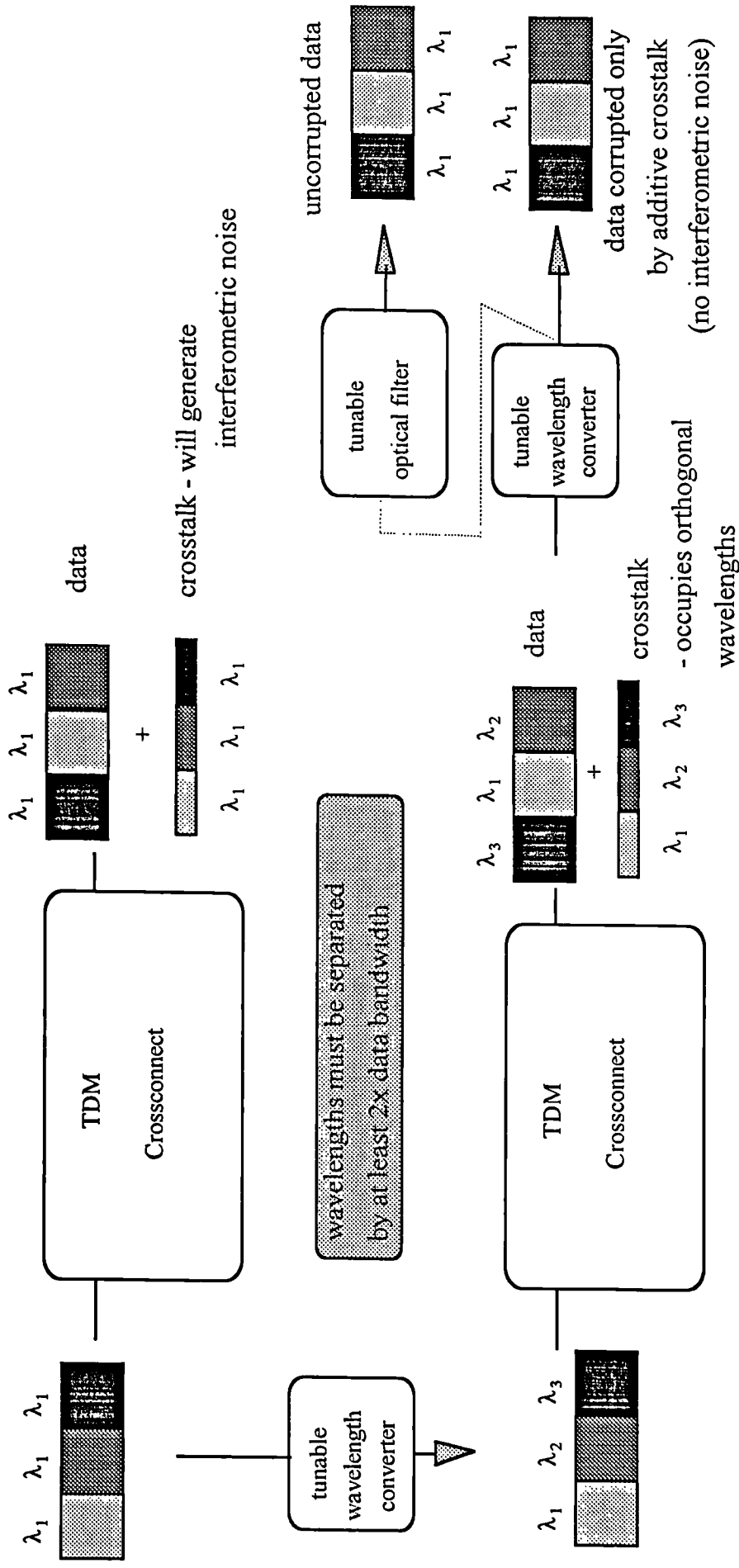


Figure 8.5. Interferometric noise suppression by wavelength manipulation.

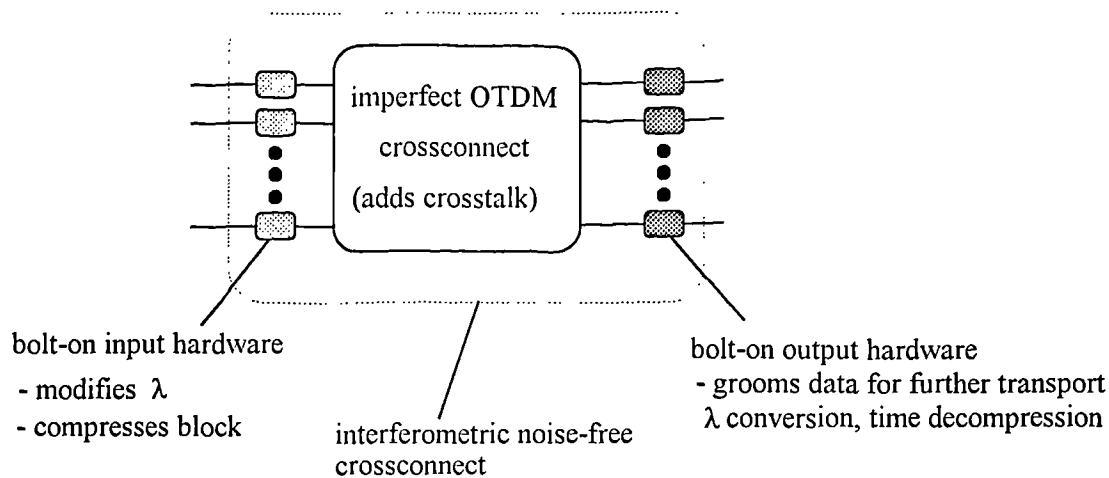


Figure 8.6. Interferometric noise suppression in OTDM crossconnects via time compression and/or wavelength manipulation.

8.4 Conclusions

A bilateral strategy has been proposed to combat crosstalk and interferometric noise: the crosstalk power should be minimised, and interferometric noise owing to the remaining crosstalk should be suppressed. Crosstalk may only be reduced by spending more on optical hardware; state-of-the-art components, in-line isolators and dilated space switches are suitable candidates. Sparse coding and time-compression are highly complex and should only be employed if other strategies fail.

Interferometric noise may be suppressed by RF rejection. Data and crosstalk may be separated in optical frequency by transmission at different wavelengths or on different subcarriers at the same wavelength. Low coherence sources, LED, multimode Fabry-Perot laser, self-pulsating lasers, and chirped DFBs, are less prone to interferometric noise but are unsuitable for long links. The novel direct modulation method exploiting the thermal effect (Chapter 7) has no known drawbacks but is currently unproven at high bit-rates. High speed phase and polarisation modulation are highly effective but require additional hardware. Phase modulation additionally increases dispersion.

8.5 References

1. K. Padmanabhan and A.N. Netravali, "Dilated networks for photonic switching", *IEEE Trans. Commun.*, 35(12), pp. 1357-1365, 1987.
2. J. Sharony, K.W. Cheung and T.E. Stern, "Wavelength dilated switches (WDS) - a new class of high density, suppressed crosstalk, dynamic wavelength-routing crossconnects", *IEEE Photon. Tech. Lett.*, 4(8), pp. 933-935, 1992.
3. C-J.L. Van Driel and A.N. Sinha, "How to beat the beat-noise in an SCMA-PON", *20th European Conference on Optical Communication ECOC '94*, pp. 809-812, 1994.
4. P.J. Legg, L. Tancevski, M. Tur and I. Andonovic, "Elimination of interferometric noise in crosstalk corrupted optical TDM crossconnects", *10th International Conference on Integrated Optics and Optical Fibre Communication (IOOC'95)*, Hong Kong, 1995.
5. B. Bostica, P. Cinato, A. de Bosio, E. Garetti and E. Vezzoni, "Electro-Optical ATM digital cross-connect system based on cell aggregation and compression", *Proceedings XIV International Switching Symposium, ISS'92*, pp. 422-426, Yokohama, Japan, 1992.
6. P.J. Legg, *unpublished*.
7. F. Heismann, D.A. Gray, B.H. Lee and R.W. Smith, "Electrooptic polarization scramblers for optically amplified long-haul transmission systems", *IEEE Photon. Tech. Lett.*, 6(9), pp. 1156-1158, 1994.
8. S. Ovidia, L. Eskildsen, C. Lin and W.T. Anderson, "BER degradation due to optical reflections in multichannel AM/16-QAM video lightwave transmission systems", *Optical Fiber Communication OFC'95*, IEEE/OSA, San Diego, U.S.A., February 1995.
9. C. Desem, "Optical interference in subcarrier multiplexed systems with multiple optical carriers", *IEEE J. Selected Areas Commun.*, 8(7), pp. 1290-1295, 1990.
10. M. Fujiwara, "Optical cross-connect system using photonic switch matrices", paper Th12, *Optical Fiber Communication OFC'94*, IEEE/OSA, San Jose, U.S.A., February 1994.
11. K. Petermann, *Laser diode modulation and noise*, Kluwer Academic Publishers, New York, 1993.
12. S. Yamashita, A. Ohishi, T. Kajimura, M. Inoue and Y. Fukui, "Low-noise AlGaAs lasers grown by organo-metallic vapor phase epitaxy", *IEEE J. Quantum. Electron.*, 25(6), pp. 1483-1488, 1989.

13. T.H.Wood and N.K.Shankaranayanan: "Measurements of the effect of optical beat interference on the bit error rate of a subcarrier-based passive optical network", *Optical Fiber Communication OFC '93*, paper ThM3, OSA/IEEE, San Jose, 1993.
14. P.K. Pepeljugoski and K.Y. Lau, "Interferometric noise reduction in fiber-optic links by superposition of high frequency modulation", *IEEE J. Lightwave Technol.*, 10(7), pp. 957-963, 1992.
15. A. Yariv, H. Blauvelt and S-W. Wu, "A reduction of interferometric phase-to-intensity conversion noise in fiber links by large index phase modulation of the optical beam", *IEEE J. Lightwave Technol.*, 10(7), pp. 978-981, 1992.
16. A. Yariv, *Personal communication*.
17. P.J .Duthie, *Personal communication*.
18. F.W. Willems and W. Muys, "Suppression of interferometric noise in externally modulated lightwave AM-CATV systems by phase modulation", *Elect. Lett.*, 19(23), pp. 2062-2063, 1993.
19. T.H. Wood, E.C. Carr, B.L. Kasper, R.A. Linke and C.A. Burrus, "Bidirectional fibre-optical transmission using a multiple-quantum-well (MQW) modulator/detector", *Elect. Lett.*, 22(10), pp. 528-529, 1986.
20. M. Tur, P.J. Legg, M. Shabeer and I.Andonovic, "Sequence dependence of phase induced intensity noise in optical networks that employ direct modulation", *Optics Letters*, 20(4), pp. 359-361, 1995.
21. P.J. Chidgey, "Multi-wavelength transport networks", *IEEE Comms. Mag.*, 32(12), pp. 28-35, 1994.
22. N. Karafolas, *Personal communication*.
23. N. Karafolas, "Fiber optic CDMA (Code Division Multiple Access) networks using serial correlation of bipolar codes", *PhD Thesis*, University of Strathclyde, 1995.
24. T. O'Farrell and S.I. Lochmann, "An indoor wireless infrared CDMA network using unipolar-bipolar correlation techniques", *Second Communication Networks Symposium*, Manchester Metropolitan University, pp. 178-181, July 1995.

Chapter 9

Conclusions and further work

9.1 Conclusions

Interferometric noise, arising on the interference of data and parasitic crosstalk at the receiver, corrupts the detected data in many digital optical communication networks employing single frequency DFB transmitters and ASK (amplitude shift keying). Seemingly harmless levels of crosstalk generate significant noise on the square-law detection. Crosstalk may arise from component imperfection (space switches, WDM components), from reflections (Rayleigh backscatter and Fresnel reflections), and from other communication channels in subcarrier FDMA (Frequency Division Multiple Access).

The optical mixing or interference of data and crosstalk results in three photocurrent components, the data (as desired), the crosstalk (undesired but relatively harmless) and the interferometric (or beat) noise (undesired and potentially damaging). The latter is proportional to the scalar product of the individual polarisation vectors and varies as the cosine of the relative optical phase - the form of the noise is therefore dependent upon the origin of the data and crosstalk waveforms.

If the data and crosstalk derive from the same laser, the interferometric noise may be classified as coherent, partially coherent or incoherent, depending upon the relative coherence of the data and crosstalk. 'Coherent crosstalk', driven by environmental phase noise alone, is much slower than the typical data rate, thereby inducing bursts of many consecutive errors. 'Incoherent beat noise crosstalk' (also called phase-induced intensity noise (PIIN)), is dominated by the accumulation of source phase noise over the source to receiver transit delay difference of data and crosstalk (much greater than the source coherence time). Errors arise in shorter bursts (approximately the reciprocal of the source linewidth). Partially coherent crosstalk is an intermediate state for which both environmental and source phase noise are significant.

Only the interference of data and crosstalk from distinct lasers with near identical wavelengths generates interferometric noise within the baseband of the receiver ('incoherent beat noise crosstalk', a difference of less than 0.02 nm for 1 Gb/s @ 1.55 μ m) - otherwise the noise is RF rejected and only slight eye-closure results ('incoherent noise-free crosstalk').

In the case of a single crosstalk interferer, with aligned polarisations and no RF filtering of the interferometric noise, analysis predicts the probability density function (pdf) of the interferometric noise to be bounded, and the signal-to-interferometric noise ratio to equal the reciprocal of twice the crosstalk level (i.e. it depends upon the ratio of the data and crosstalk optical powers, not on their absolute values). If the interferometric noise RF spectrum extends beyond the receiver bandwidth the noise power is reduced and the pdf is no longer bounded (it approaches a Gaussian form with increasing rejection). In baseband ASK transmission with DFB lasers, no filtering will arise for coherent crosstalk nor for PIIN given an externally modulated source. However, directly modulated lasers suffer spectral broadening and some filtering is to be expected. When data and crosstalk arise from distinct lasers the noise spectrum is centred at the optical beat frequency which must be comparable with the receiver bandwidth for any noise to fall within the baseband.

The optical power penalty at bit-error-rate (BER) = 10^{-9} is predicted to increase with crosstalk level, slowly to equal 1 dB for a crosstalk level of -18.2dB (-22.7dB), and then very rapidly to hit an asymptote (error floor) at a crosstalk level of -6 dB (-10.6dB), for a threshold-optimised receiver (AC-coupled receiver). In experiment, for PIIN generated with a directly modulated DFB laser biased just below threshold, some noise is filtered and the respective crosstalk figures, for a decision-optimised receiver, are -16dB and -9dB. A Gaussian pdf greatly overestimates the degradation owing to a single interferer.

Under external modulation the BER performance was found to be far worse; this was attributed to the limited modulation depth achievable with the lithium niobate Mach-Zehnder modulator. Analysis has shown the importance of maintaining a large modulation depth. For example, if the optical power in the 'zero' bits is increased from zero to one-tenth of that carried in the 'one' bits, the power penalty asymptote is translated to a 3dB smaller crosstalk. Other workers [1] have found improved performance with external modulation, accredited to RF rejection under direct modulation resulting from spectral broadening (chirp).

Systems are far more tolerant to incoherent noise-free crosstalk than to coherent or incoherent beat noise crosstalk. A crosstalk level of -6.8 dB gives a 1 dB power penalty (threshold optimised).

When the data is corrupted by N crosstalk terms photodetection results in N primary, and $N(N-1)/2$ secondary, interferometric noise terms. Those terms that generate in-band interferometric noise may be identified according to the above crosstalk classification. Under the assumption of statistical independence, the net interferometric noise variance is proportional to the total crosstalk power of the in-band terms (neglecting secondary terms (typically a valid assumption) and in-band noise filtering). Calculation of the pdf of the net noise by multiple convolutions supports the use of a Gaussian (Central Limit Theorem) aggregate pdf if there are five or more in-band terms typically 'high' (i.e. ten binary in-band crosstalk bit streams). This Gaussian approximation gives a lower bound on performance and is widely quoted in the literature [1-4].

Analysis predicts the total crosstalk level of noise generating terms should be held below -25 dB for a penalty of less than 1 dB - a further 2 to 4 dB may lead to network failure. Computer simulation (XHatch) of optical TDM crossconnects supports this conclusion and, additionally, highlights the variation in performance with channels number and assignment. The gain in performance over an AC-coupled receiver by decision threshold optimisation diminishes with increasing network size.

Optical TDM switching networks, comprising -15dB isolated lithium niobate directional couplers and delay lines, are prone to all the above classes of crosstalk but particularly to incoherent beat noise crosstalk which may be first-order in magnitude. Time-slot interchangers requiring three crosspoints suffered from worst-case penalties of 1.0 and 1.75dB; a two input/four crosspoint network fed by the same laser at both inputs was uncharacterisable owing to interferometric noise. A recirculating delay-line has demonstrated the evolution of the interferometric noise pdf from bounded to Gaussian form as more crosstalk terms are added. In common with the TDM switch fabrics, the number of significant crosstalk terms (4-5) in the steady state is too small to satisfy the Central Limit Theorem; a penalty of 2.8dB was measured for an aggregate crosstalk of -14.8 dB.

Crosstalk and interferometric noise may be managed by a bilateral approach that minimises the crosstalk power and suppresses the noise owing to the remaining crosstalk. The former requires greater hardware expenditure on state-of-the-art components, in-line isolators and dilated space switches. Sparse coding and time-compression are highly complex and should only be employed if other strategies fail.

Interferometric noise may be suppressed by RF rejection at the receiver. Data and crosstalk may be separated in optical frequency by transmission at different wavelengths or on different subcarriers at the same wavelength. Low coherence sources may be deployed, but are unsuitable for long links, or high speed phase or polarisation modulation may be added at the transmitter. Phase modulation increases dispersion. Finally, a novel method, exploiting the intra-bit frequency evolution of a directly modulated DFB laser in response to injection heating has been demonstrated. This offers potential noise suppression for 'free', suffers no known drawbacks, but is currently limited to sub-Gb/s modulation. In all cases the ASK modulation depth must be maximised.

In conclusion, the performance of many current and proposed optical communication networks will be limited by interferometric noise unless measures are taken to minimise parasitic crosstalk and/or to suppress the noise itself. Such measures increase the hardware cost, and may compromise other performance criteria, such as dispersion, but will largely maintain the flexibility and transparency that only an optical network can provide.

9.2 Further work

The scope for further study into a phenomenon as complex as interferometric noise is almost unlimited. Those avenues considered to be of most importance are highlighted below.

9.2.1 Experimental

In the investigation of a single interferer the poor performance with external modulation was attributed to a small modulation depth. This dependency on modulation depth, as theoretically analysed (Section 3.5.7), may be investigated with a high extinction-ratio external modulator or, alternatively, under directly modulation

the modulation depth may be simply varied through the bias point (although small differences owing to the variation in noise suppression from injection heating and chirp will also arise).

Multiple interferers may be generated using a many-arm Mach-Zehnder fibre interferometer - a nine-arm configuration (Fig. 9.1) as previously reported [5] is a practical proposition. The convergence of the noise statistics towards the Gaussian form may be studied by adding from one to eight crosstalk terms to the data. The delays are chosen so that crosstalk addition gives rise to incoherent beat noise crosstalk. Correlated beating terms may be generated by matching delays in the network. Additionally, significant performance gains with direct modulation from injection heating (cf. Section 7.4) may be demonstrated.

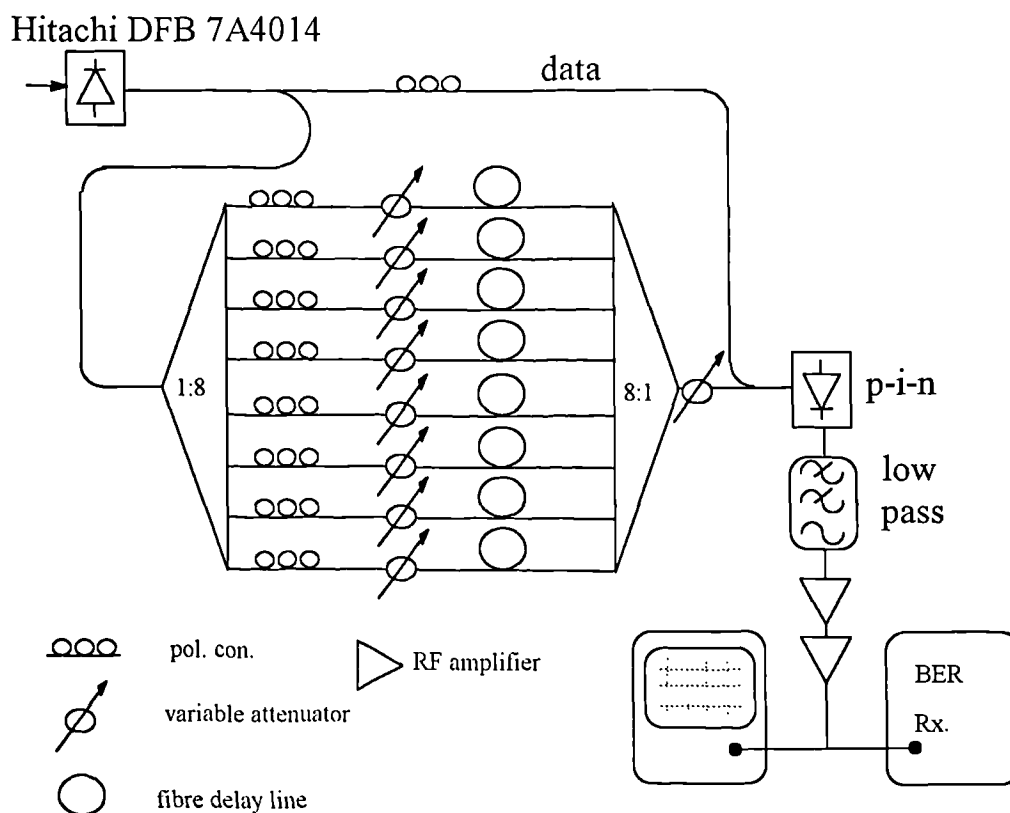


Figure 9.1. Proposed multiple interferer experiment in which the data is corrupted by up to eight crosstalk terms.

Interferometric noise suppression techniques, high speed phase and polarisation modulation, and frequency control in multi-section lasers, may be tested. Polarisation

modulation would require a lithium niobate travelling-wave polarisation controller and a high-speed drive signals. The form of the drive signal must be determined.

Partial coherence is particularly relevant to networks employing highly coherent sources, for example, externally modulated DFB lasers; but current understanding is limited. Experimental results will be essential to generate confidence in theoretical work that will undoubtedly be extremely complex. Examination of the pdf, noise spectrum and BER using the above test-bed would constitute a worthy initial investigation.

In future ultra-fast optical transmission, sources of very short optical pulses will be employed, including mode-locked and externally electro-absorption modulated lasers. The broad spectra of such sources suggest broad interferometric noise spectra, and thus greater tolerance to crosstalk. Coherence between pulses is not well understood. Experiment in these areas would be of value.

9.2.2 Theoretical

Further theoretical analysis, tackling chirped sources (cf. Section 3.4), correlated beating terms (cf. Section 4.3.2.), partial coherence (cf. Section 3.6), and the influence of filtering on the interferometric noise pdf and RF spectrum appear very challenging.

The simulator package (XHatch) may be developed to offer new functionality, addressing noise filtering, partial coherence, polarisation, and a more sophisticated BER output (including, for example, the pdf of n consecutive errors). An important question concerns the criteria for the quality of transmission service offered by a network. Should the network be designed to accommodate the worst or just the typical performance? Is the bursty nature of the noise particularly undesirable for the customer? Should error correction be added?

9.3 References

1. L. Eskildsen, E.L. Goldstein, M. Andrejco, L. Curtis, V. Shah, D. Mahoney, C.E. Zah and C. Lin, "Interferometric noise limitations in fiber-amplifier cascades", *Elect. Lett.*, 29(23), pp. 2040-2041, 1993.

2. E.L. Goldstein, L. Eskildsen and A.F. Elrefaie, "Performance implications of component crosstalk in transparent lightwave networks", *IEEE Photon. Tech. Lett.*, 6(5), pp. 657-660, 1994.
3. J.L. Gimlett and N.K. Cheung, "Effects of phase-to-intensity noise conversion by multiple reflections on gigabit-per-second DFB laser transmission systems", *J. Lightwave Technol.*, 7(6), pp. 888-895, 1989.
4. A. Ehrhardt, M. Eiselt, G. Großkopf, L. Küller, R. Ludwig, W. Pieper, R. Schnabel and H.G. Weber, "Semiconductor laser amplifier as optical switching gate", *J. Lightwave Technol.*, 11(8), pp. 1287-1295, 1993.
5. L. Eskildsen, E.L. Goldstein, "Scaling limitations in transparent optical networks due to low-level crosstalk", *IEEE Topical Meeting on Optical Networks*, 1994.

Publications resulting from this work

1. P.J. Legg, D.K. Hunter, P.E. Barnsley and I. Andonovic: "Crosstalk effects in optical time division multiplexed switching networks", IEE Colloquium on *Optical Switching*, London, June 1993.
2. D.K. Hunter, P.J. Legg and I. Andonovic, "A technology independent architecture for optical TDM switching", IEE Colloquium on *Optical Switching*, London, June 1993.
3. D.K. Hunter, P.J. Legg and I. Andonovic, "Architecture for large dilated optical TDM switching networks", *IEE Proceedings-J*, 140(5), pp. 337-343, 1993.
4. P.J. Legg, D.K. Hunter, M. Tur, P.E. Barnsley, and I. Andonovic, "Degradation of optical TDM switching networks by noise due to inter-channel crosstalk", paper WI3, *Optical Fiber Communication OFC'94*, IEEE/OSA, San Jose, USA., February 1994.
5. International Patent No. PCT/GB94/01149, 'Inter-channel crosstalk', British Telecommunications PLC, 1994.
6. P.J. Legg, D.K. Hunter, I. Andonovic and P.E. Barnsley, "Inter-channel crosstalk phenomena in optical time division multiplexed switching networks", *IEEE Photon. Tech. Lett.*, 6(5), pp. 661-663, 1994.
7. M. Tur, P.J. Legg and I. Andonovic, "Sequence dependence of phase induced intensity noise in optical networks that employ direct modulation", *Optics Letters*, 20(4), 1995.
8. P.J. Legg, T.H. Gilfedder, D.K. Hunter, I. Andonovic and M. Shabeer, "Modelling of the performance of optical TDM switching networks in the presence of interferometric noise due to inter-channel crosstalk", Proceedings of *Advanced Networks and Services*, vol. 2450, European Optical Society, Amsterdam, March 1995.
9. M. Tur, P.J. Legg, M. Shabeer and I. Andonovic, "Novel suppression of interferometric noise in optical networks by employing direct modulation", *Optical Fiber Communication OFC'95*, paper WQ8 IEEE/OSA, San Diego, February 1995.
10. P.J. Legg, L. Tancevski, M. Tur and I. Andonovic, "Elimination of interferometric noise in crosstalk corrupted optical TDM crossconnects", *10th International Conference on Integrated Optics and Optical Fibre Communication (IOOC'95)*, Hong Kong, June 1995.
11. L. Tancevski, P.J. Legg, D.K. Hunter, I. Andonovic and M. Tur, "Interferometric noise reduction in crosstalk corrupted optical WDM and TDM switching fabrics", to be published *IEEE Photon. Tech. Lett.*